DEVELOPMENT OF PRACTICAL AND ECONOMICAL ULTRA HIGH PERFORMANCE FIBRE REINFORCED CONCRETE FOR PRESTRESSED BEAMS

by

Sharifeh Vatannia

Submitted in partial fulfilment of the requirements for the degree
Philosophiae Doctor (Civil Engineering)

in the

Department of Civil Engineering
Faculty of Engineering, Built Environment and Information Technology

UNIVERSITY OF PRETORIA

2019

DECLARATION

I, the undersigned hereby declare that:

- I understand what plagiarism is and I am aware of the university's policy in this regard;
- The work contained in this thesis is my own original work;
- I did not refer to work of current or previous students, lecture notes, handbooks, or any other study material without proper referencing;
- Where others people's work has been used this has been properly acknowledged and referenced;
- I have not allowed anyone to copy any part of my thesis;
- I have not previously in its entirely or in part submitted this thesis at any university for a degree.

Signature of student:

Name of student: Sharifeh Vatannia

Student number: 14445957

Date: January 2019

SUMMARY

DEVELOPMENT OF PRACTICAL AND ECONOMICAL ULTRA HIGH PERFORMANCE FIBRE REINFORCED CONCRETE FOR PRESTRESSED BEAMS

by

Sharifeh Vatannia

Supervisor: Prof. E. P. Kearsley

Department: Civil Engineering

University: University of Pretoria

Degree: Philosophiae Doctor (Civil Engineering)

Keywords: Ultra High Performance Concrete (UHPC), Practical, South Africa, Fibre, Shear, Prestress Beams, Bond Performance

Ultra High Performance Concrete (UHPC) is an ultra-high strength concrete with superior mechanical properties. The high compressive strength (more than 150 MPa) and high ductility make UHPC a suitable material for manufacturing pre-cast structural members. Its high compressive strength can be beneficial for high-rise buildings as well as long-span bridge decks by making lighter structures. However, manufacturing UHPC in large-scale is not appealing for industry and the main reason can be attributed to the manufacturing cost including the material and preparation cost as well as the cost of equipment required. Typical UHPC contains high cementitious materials and fine aggregate (less than 600 μm). In addition, UHPC often requires highly specific types of curing making it unpractical as well as expensive.

Although literature exists on development of UHPC and its applications, little has been published considering wider applications and practicality, particularly in South Africa. This thesis is an attempt to develop a more practical and economical UHPC utilizing local materials in South Africa while maintaining significant UHPC properties. The study

contributes toward findings a solution for increasing the use of UHPC, thus allowing industry to take advantage of its superior properties.

A comprehensive study was conducted not only on the development of an economical and practical UHPC, but also on the development of practical curing regimes. Manufacturing UHPC prestressed beams required investigation of bond performance between UHPC and high strength prestressing wires. UHPFRC prestressed I-beams were tested under flexure to determine whether shear fibres can act as shear reinforcing, thus making it possible to eliminate shear stirrups and limit the web thickness.

The results revealed that manufacturing practical and economical UHPC is achievable by utilizing local materials available in South Africa. This accomplishment is possible as a result of several modifications to the typical UHPC mix design. These modifications include: 1) increasing the aggregate content to an aggregate to cement ratio (by mass) of 2.5 resulted in the reduction of the cement content to 593 kg/m^3 ,2)increasing the aggregate size with a maximum particle size of 4.75 mm and 6.7 mm as a fine aggregate and coarse aggregate, respectively. Heat treatment in 80°C water for 2 days can be considered as a practical curing regime. During the curing procedure, the rising and falling of the water temperature should be controlled to avoid thermal shocking.

Experimental results on the bond performance between UHPC and high strength prestressing wires revealed shorter development length is required by inclusion of fibres in UHPC. In the presence of fibre, embedment lengths of 100 mm and more at the age of 7 days and older provides a sufficient development length. However, in the absence of fibre sufficient development lengths are achieved at higher embedment lengths of 125 mm and 150 mm.

Testing UHPFRC prestressed I-beams under flexure confirms that fibres can act as shear reinforcing.

ACKNOWLEDGEMENTS

After thanking God for His infinite mercies in reaching this milestone, I would like to acknowledge the following people:

- my utmost gratitude to my supervisor, Professor Elsabe P. Kearsley, for her eye for details, excellent feedbacks, technical guidance, good supervisor-student relationship and for her financial support in the attainment of this degree. The extra hours she invested in checking this work even in her personal time is deeply appreciated;

- Mr Derek Mostert for helping me with experiments and for his valuable guidance;

- my sincere appreciation to my parents and sister, for their endless love, concern, encouragement, prayer and words of advice;

- special thanks to my beloved husband Dr M. Moghimi Ardekani, for his encouragement, love and continuous moral support in the successful completion of my PhD degree;

- Thanks to all the personnel of the Department of Civil Engineering, University of Pretoria, for making me feel comfortable throughout the course of my PhD programme.

PUBLICATIONS

Parts of the study were presented in the following list of papers while the study was in progress. Therefore, some parts of this thesis have the same content as many of the articles and conference papers.

Manuscripts under review in international peer-reviewed journals

1. **Vatannia, S.,** Kearsley, E., & Mostert, D. (2017). Development of Practical Ultra-high Performance Concrete. *Proceedings of the Institution of Civil Engineers - Construction Materials,* Resubmitted after addressing reviewer comments
2. **Vatannia, S.,** Kearsley, E.P., Mostert, D. (2018). The shear behaviour of Ultra High Performance Concrete pre-stressed beams. *Journal of the South African Institution of Civil Engineering*, First submission.
3. **Vatannia, S.,** Kearsley, E.P., Mostert, D. (2019). Experimental study on effect of fibre on bond performance in ultra-high performance concrete. *Journal of the South African Institution of Civil Engineering*, First submission.

Published article in magazine (invited by editor: Dr.-Ing. Hans-Dieter Beushausen)

4. **Vatannia, S.,** Kearsley, E., & Mostert, D. (2016). An Introduction to a Practical UHPC Manufacturing in South Africa, *CPI (Concrete Plant International)*, 6, 66-69.

Conference papers in international peer-reviewed conferences

5. **Vatannia, S.,** Kearsley, E., & Mostert, D. (2016). The mechanical properties of UHPC reinforced by different types of fiber. *fib Symposium: Performance-based Approaches for Concrete Structures*, Cape Town, South Africa.
6. **Vatannia**, S., Kearsley, E. Mostert, D. (2016). The effect of curing regime on the compressive strength of ultra high performance concrete. In *Proceedings of the 9th international concrete conference on environment, efficiency and economic challenges for concrete*, Dundee, Scotland.

TABLE OF CONTENTS

LIST OF FIGURES

LIST OF TABLES

NOMENCLATURE

A	Gross cross sectional of a section (mm^2)
$A_{c,s}$	Concrete surface area (m^2)
A_{s1}	Area of the tensile reinforcement which extends beyond the section being considered by at least a full anchorage length plus one effective depth (mm^2)
A_w	Cross sectional area of prestressing wires (mm^2)
a	Shear span (m)
b	Width of a section (mm)
b_w	Width of the cross-section at the centroidal axis (mm)
$C_{L,c}$	Extra labour costs for casting (ZAR/m^3)
$C_{L,v}$	Extra labour costs for consolidating (ZAR/m^2)
$C_{M\ ,c,r}$	Total material costs (ZAR)
$C_{L,r}$	Labour costs for cutting, placing and connecting of the reinforcement bars in the concrete beam (ZAR)
c_L	Labour costs per working hour (ZAR/h)
$c_{M,c}$	Prices of the concrete (ZAR/m^3)
$c_{M,r}$	Prices of the reinforcement (ZAR/kg)
D	Fibre diameter (mm)
D_w	Diameter of prestressing wires (mm)
d	Effective depth (mm)
d'	Distance between top wires and the top fibre in a section (mm)
d_f	Bond factor
ds	Diameter of reinforcing steel (mm)
E_c	28-day modulus of elasticity (GPa)
E_{ci}	Modulus of elasticity at the time of wire releasing the prestressing wires (GPa)
E_p	Modulus of elasticity of prestressing wires (GPa)
e	Eccentricity of the bottom prestressing force with respect to the centroidal axis of the section (mm)
e_t	Eccentricity of the top prestressing force with respect to the centroidal axis of the section (mm)

f_{cdt}	Direct tensile strength (MPa)
f_{ci}	Compressive strength of cubes at the time of wire releasing the pre-stressing wires (MPa)
f_{ck}	Characteristic cylindrical compressive strength (MPa)
f_{cs}	Allowable compressive stress at the serviceability limit state (MPa)
f_{cst}	Splitting tensile strength (MPa)
f_{ct}	Allowable compressive stress at transfer (MPa)
f_{ctd}	Design value of the uni-axial (direct) tensile strength (MPa)
f_c	28- day compressive strength of cubes (MPa)
f_{pu}	Ultimate tensile strength of prestressing wires (MPa)
f_{ts}	Allowable tensile stress at the serviceability limit state (MPa)
f_{tt}	Allowable tensile stress at transfer (MPa)
f'_c	Characteristic cylindrical compressive strength (MPa)
h	Total depth of beam (mm)
I	Second moment of area of the section about the centroidal axis (mm^4)
k_b	Ratio of the final prestressing force of bottom wires to the force at the transfer
k_t	Ratio of the final prestressing force of top wires to the force at the transfer
L	Beam length (m)
L_f	Fibre length (mm)
M	Bending moment (kN.m)
M_m	Moment occurs simultaneously with the shear force to the section considered (kN.m)
M_u	Ultimate moment (kN.m)
N_{bw}	Number of wires in bottom flange
N_{tw}	Number of wires in top flange
N_u	Factored axial force normal to cross section occurring simultaneously with V_u (kN)
P	Load in four-point bending test (kN)
P_t	Prestressing force in wires of top flange (kN)
P_0	Prestressing force immediately after transfer (kN)
Pr	Precentage of prestressing (%)

S	Beam span (m)
T_c	Extra concreting time (h/m^3)
T_r	Time required for cutting, placing and connecting the reinforcement (h/kg)
T_v	Vibration time required for the consolidation of concrete (h/m^2)
V	Shear force (kN)
V_c	Volume of the concrete beam (m^3)
$V_{s,l}$	Volume of longitudinal reinforcement (m^3)
V_{sw}	Volume of shear reinforcement (m^3)
V_u	Shear force occurs simultaneously moment to the section considered (kN)
V_{Rd}	Concrete shear strength (kN)
W_D	Distributed load due to self-weight (kN/m)
Y_b	Distance from the bottom of the section to centroidal axis of gross section (mm)
Y_t	Distance from the top of the section to centroidal axis of gross section (mm)
Z_t	First moment of area above and about the centroidal axis (mm^3)
Z_b	First moment of area under and about the centroidal axis (mm^3)
α_1	A factor taking into account the bond characteristics of the longitudinal reinforcement
γ	Unit weight of concrete (kN/m^3)
γ_c	Partial safety factor for concrete
δ_L	Vertical deflection in the midspan due to loading (mm)
δ_p	Vertical deflection in the midspan due to prestressing force in bottom wires (mm)
δ_t	Vertical deflection in the midspan due to prestressing force in top wires (mm)
ε_{bot}	Strain at the bottom of a section
ε_{top}	Strain at the top of a section
ρ_f	Fibre volume fraction
ρs	Unit mass of steel (kg/m^3)
σ_{bot}	Maximum stress below the neutral axis at the bottom of a section (MPa)

σ_{bw1}	Stress in bottom wires the most furthest from the neutral axis of the section (MPa)
σ_{bw2}	Stress in bottom wires the second furthest from the neutral axis of the section (MPa)
σ_{bw3}	Stress in bottom wires the third furthest from the neutral axis of the section (MPa)
σ_{bw4}	Stress in bottom wires the forth furthest from (closest to) the neutral axis of the section (MPa)
σ_{cp}	Concrete compressive stress at the centroidal axis due to axial loading (MPa)
σ_{top}	Maximum stress above the neural axis at the top of a section (MPa)

Abbreviation

AC	Autoclave Curing
ACI	ACI 318-11
AFGC	Association Française de Génie Civil
C	Concrete
CMOD	Crack Mouth Opening Displacement
cr	Cracking
EC2	Eurocode 2
F	Fibre Factor
FA	Fly Ash
GBS	Ground Granulated Blast Furnace Slag
GGBS	Ground Granulated Blast Furnace Slag
GGBFS	Ground Granulated Blast Furnace Slag
GP	Glass Powder
HSFRC	High Strength Fibre Reinforced Concrete
HSFRC	High Strength Fibre Reinforced Concrete
HT	Heat Treatment
LP	Limestone Powder
max	Maximum
min	Minimum
M-S	Microsand

MOR	Modulus Of Rupture
nS	Nano-Silica
NSC	Normal Strength Concrete
N-S	Normal Sand
RPC	Reactive Powder Concrete
SC	Steam Curing
SF	Silica Fume
SFRC	Steel Fibre Reinforced Concrete
SP	Superplasticizer
STD	Standard Curing
test	Tested
UHPC	Ultra High Performance Concrete
UHPFRC	Ultra High Performance Fibre Reinforced Concrete
USD	Dollar (United States currency)
W	Water
ZAR	Rand (South African currency)

CHAPTER 1 INTRODUCTION

1.1 BACKGROUND

Nowadays, interest is drawn toward manufacturing very high-strength concrete and using precast elements in large-scale projects. The reasons for such increased interests are applications of high-strength concrete where reduced weight is crucial or where small support elements are called for due to architectural considerations. In addition, by carrying loads more efficiently than normal-strength concrete, high-strength concrete also reduces the total amount of material placed and lowers the overall cost (Portland Cement Associations, 2018a). Ultra High Performance Concrete (UHPC) is a type of concrete which possesses very high compressive strength (more than 150 MPa)[1], high ductility, energy absorption and durability (Association Française de Génie Civil (AFGC), 2002; Graybeal, 2006; Yang et al., 2009; Kazemi and Lubell, 2012; Wille et al., 2012; Yoo et al., 2013; Shafiefar et al., 2017; Ronanki et al., 2018). Its high compressive strength can be beneficial for high-rise buildings as well as long-span bridge decks by making lighter structures (up to 30% to 50% of the weight of normal-strength concrete structures). Impact- or blast-resistant structures can take advantage of its significant energy absorption capacity (Yoo and Banthia, 2016; Arowojolu et al., 2018). Superior durability can enhance the service life with less maintenance, particularly for bridge decks and industrial floors which are exposed to harsh conditions (Tam et al., 2012; Zhou 2018).

The basic principles of ultra-high strength concrete with ductile behaviour, known as Reactive Powder Concrete (RPC), were suggested by Richard and Cheyrezy (Richard and Cheyrezy, 1995) as following:

[1] There is not a unanimous definition for very high compressive strength in UHPCs. In literature, some researchers focus on the compressive strength range of 120-150 MPa (Lappa, 2007; Walraven, 2009; Russell and Graybeal, 2013; ASTM C1856/1856M, 2017; Portland Cement Associations, 2018b; National Precast Concrete Association, 2018). However, there are numerous studies and standards which focus on compressive strength above 150 MPa (Association Française de Génie Civil (AFGC), 2002; Graybeal, 2006; Yang et al., 2009; Kazemi and Lubell, 2012; Wille et al., 2012; Yoo et al., 2013; Shafiefar et al., 2017; Ronanki et al., 2018). This study focuses on the latter definition for compressive strength (>150MPa).

- Enhancement of homogeneity by elimination of coarse aggregates;
- Enhancement of density by optimization of the granular mixture;
- Enhancement of the microstructure by post-set heat treatment;
- Enhancement of ductility by incorporating adequate size fibres;
- Maintaining mixing and casting procedures as close as possible to existing practice.

Eliminating the coarse aggregate to increase the homogeneity of mix was one of their suggestions. In their proposed mix design, the ratio of sand to cement (by weight) was 1.1 and 600 μm was considered as the maximum size of aggregate. There are numerous studies (Voo et al., 2006; Park et al., 2008; Habel and Gauvreau, 2008; Kang and Kim, 2011; Yang et al., 2012; Yoo et al., 2013; Azmee and Shafiq, 2018) carried out to investigate the behaviour of UHPC following Richard and Cheyrezy's proposed principles.

There are several published studies on the mix composition development of UHPC employing the principals of the particle packing model of Andresean and Andersen (1930) to achieve a densely compacted cementitious matrix (Pyo et al., 2017; Ragalwar et al., 2017; Song et al., 2018; Chen et al., 2018a). The original model was developed by Andreasen and Andersen (1930), showing that a minimal porosity can theoretically be achieved by an optimal particle size distribution (PSD) of all the solid particles in the mix. A modified model was suggested by Funk and Dinger (1994) where a mix design can be developed using an integral particle size distribution approach of continuously graded mixes. Limestone powder, quartz powder and fine sands were the materials used to achieve dense matrixes (Yu et al., 2015a; Yu et al., 2015b).

1.2 PROBLEM STATEMENT

Manufacturing this type of concrete in large-scale is however not appealing for industry and the main reason can be attributed to the manufacturing cost of UHPC. The cost includes the material and preparation cost as well as the cost of equipment required in manufacturing.

Some studies can be found which considered coarser aggregate with maximum particle sizes up to 0.8mm (Wille et al., 2011; Wille et al., 2014), 1mm (Voo et al., 2006) and up to 4mm (Vejmelková et al., 2018a and 2018b), but, this still does not make this concrete practical.

Typical materials and a mix composition for UHPC are shown in **Table 1.1**. UHPC contains a high amount of cement (800-1000 kg/m^3) resulting in the higher cost of concrete. The high cement content also causes higher shrinkage as well as high emission of CO_2. Silica flour is used to not only increase the packing density of the concrete, but it also works as a cementitious material. This material is one of the most expensive materials in the mix design and it is not widely available. The ratio of aggregate to cement (Agg/c) is mostly kept at 1.1. Using very fine aggregate (less than 600 μm) is another characteristics of UHPC. The relatively low aggregate content leads to higher cost as aggregate is a cheaper material in comparison to the other materials used in manufacturing concrete. Moreover, providing aggregate in different gradings require sieving, which makes preparation expensive. All these material requirements make UHPC unpractical and too expensive for use in large-scale projects. Further costs are incurred when it is not possible to obtain the required materials locally and materials have to be imported.

Table 1.1 Materials and mix design in typical UHPFRC (Graybeal, 2006; Hung et al., 2018)*

Material	**Amount (kg/m^3)**
Portland cement	712
Fine sand	1020
Silica fume	231
Ground quartz	211
Superplasticizer	30.7
Accelerator	30
Steel fibre	156
Water	109

- It's noteworthy that Shafieifar et al. (2017) and Wang et al. (2017) also used the same materials with similar mix compositions in their UHPFRCs.

In addition, UHPC often requires highly specific types of curing making it impractical and expensive, as well. Typically, the specimens are submerged in 90°C water for several days. In order to achieve UHPC with ultra-high strength (more than 200 MPa) an autoclave is used in the manufacturing process (Yang et al., 2009; Chen et al., 2018b).

To increase the practical use of UHPC the aggregate size needs to be increased. Yang et al. (2009) achieved a compressive strength of 120 MPa (water cured in 20°C) and about 180 MPa in 90°C heat curing by using local natural sand sized less than 5 mm and Ground

Granulated Blast Furnace Slag (GGBS) as well as Silica Fume (SF) as supplementary cementitious materials. Yazici et al. (2008) concluded that in order to get ultra-high strength in RPC there is no need to only use fine aggregate. They managed to get a strength of 281 MPa by autoclaving at 210 °C under 2 MPa pressure. The maximum aggregate size was 3 mm. The possibility of utilizing Fly Ash (FA) and GGBS as a silica source was investigated.

By considering the high cost of UHPC manufacturing, UHPC can only be cost effective if the volume of concrete used is reduced. However, reduction in cross sectional areas is limited by implementing traditional shear reinforcement. In order to avoid this issue, fibres can be a replacement for shear reinforcement. In other words, in order to reduce the weight and size of structural elements, shear reinforcement can be eliminated and replaced by fibres. This thesis is an attempt to *develop a more practical and economical UHPC utilizing local materials in South Africa while maintaining significant UHPC properties*. In order to reduce the structural members' weight and size, fibres are considered to eliminate stirrups. The study contributes towards finding a solution for increasing the use of UHPC thus allowing industry to take advantage of its superior properties. Although literature exists on development of UHPC and its applications, little has been published considering wider applications and practicality, particularly in South Africa.

1.3 OBJECTIVE

Since UHPC is quite new for South Africa it is necessary to develop a mix design using local materials. The knowledge and understanding of the behaviour of UHPC in large-scale applications such as UHPC prestressed beams, will make a valuable contribution to promoting UHPC utilization. In order to be able to produce practical and economical UHPC the main objectives in this study were to:

- Develop an economical and practical mix design by using local materials;
- Investigate practical curing regimes;
- Investigate the mechanical properties of UHPC and UHPFRC affected by the use of different fibre types and curing regimes;
- Evaluate bond performance between prestressing steel wire and the surrounding concrete as a preliminary study for prestressed beams;

- Test UHPC prestressed I-beams under flexure to determine whether fibres can act as shear reinforcing, thus making it possible to eliminate shear stirrups and limit the web thickness.

1.4 METHODOLOGY

Initially it was decided to start working with small batches to investigate the mix design thus reducing experimental material costs while obtaining main trends before investigating the effect of curing regime. During the first phases of the experimental work, the compressive strength was chosen as a main indicator of material properties. Workability and consistency of the developed mixes were evaluated qualitatively. Experiments were performed in order to understand the effect of the following parameters on the strength of UHPC:

- Type of aggregate;
- Cementitious materials combination;
- Aggregate content;
- Aggregate size.

Unit cost per 7-day compressive strength was calculated for the studied mix designs as well as the proposed final mix design to evaluate their economic aspects.

During the second phase of the experimental work, further investigation of the mechanical properties of the proposed final mix design was conducted. Mechanical properties including density, compressive strength, modulus of rupture (flexural strength), direct tensile strength, splitting tensile strength and modulus of elasticity were measured. Besides, the effect of the following aspects on the mechanical properties of the proposed mix design was investigated:

- Different types of fibre (shape and ultimate tensile strength);
- Different durations of curing in heat treatment.

Supplementary studies were conducted on curing regimes, investigating the effect of heat curing temperature gradient on the compressive strength of UHPC. In the study the following parameters were considered:

- Different water temperatures for heat treatment;
- Time that samples were cured in the heat treatment;
- Curing regime after the heat treatment.

The final mix design and curing regime were chosen to satisfy economical and practical requirements.

The final phase of the experimental work, involved the design and preparation of UHPC prestressed beams. To predict prestress losses, drying shrinkage and creep were measured for UHPC and UHPFRC. Preliminary studies were performed to understand the bond performance between UHPC and high strength prestressing wires. Pull-out tests were conducted to evaluate embedment lengths, thus avoiding bond failure. The following parameters were considered:

- Embedment length;
- Concrete cover;
- Age of UHPC;
- Fibre content.

A preliminary study was conducted on one-metre long UHPC prestressed beams to investigate the possible issues that may occur during prestressing and wire releasing procedures. These tests provided an overall indication of the behaviour of prestressed beams under flexure that one may expect. The behaviour of UHPC prestressed beams under flexure was investigated in the presence and absence of steel fibre.

Large-scale UHPC prestressed I-beams were designed to fail in shear, thus making it possible to evaluate the effect of fibre on the shear strength. The use of steel fibres in the concrete mix may eliminate the necessity of stirrups, thus reducing the labour and material cost. Two I-beams were cast and four-point bending tests were conducted to investigate the behaviour of fibre reinforced UHPC prestressed beams under flexure. Besides, drying shrinkage and creep were measured for UHPFRC containing andesite and dolomite.

1.5 SCOPE OF RESEARCH

Local materials available in South Africa were employed to achieve a practical and economical UHPC mix design. It is noteworthy that the fibres were the only imported materials.

Compressive strength was the only material property evaluated during the process of investigation on mix design and curing was conducted in 80°C steam and water.

To investigate the effect of different type of fibres on the mechanical properties of UHPFRC, the following mechanical properties were investigated:

- compressive strength;
- direct tensile strength;
- splitting tensile strength;
- flexural strength;
- modulus of elasticity.

Pull-out tests were performed using 7 mm high strength prestressing steel wires (ultimate tensile strength of 1750 MPa) on UHPC and UHPFRC (2% fibre volume fraction). Pull-out tests for UHPC and UHPFRC were performed at different ages including 3, 7, 14, 28 and 56 days after casting.

One-metre long UHPC and UHPFRC beams were prestressed using two 7 mm high strength prestressing steel wires (single-wire tendon) in the bottom and top of the beams. Wires were prestressed up to 75% of ultimate tensile strength.

The two large-scale UHPFRC prestressed I-beams had a 4.4 m length with 400 mm total depth. The beams were reinforced using sixteen 7 mm high strength prestressing steel wires (single-wire tendon) in the bottom and two 7 mm high strength prestressing steel wires in the top of the I-beams. The wires were prestressed up to 75% of ultimate tensile strength. The prestressed beams were designed to not fail in flexure to make it possible to evaluate the effect of fibre on the shear strength.

As the aim of the study was to determine whether local materials could be used to manufacture UHPFRC prestressed beams, only one set of tests was conducted. Repeatability and effect of variability in materials supplied was not studied as it falls outside the scope of this study. Investigation on the following aspects in UHPC falls out of scope of this study:

- Durability;
- Fire resistance;
- Carbonation Phenomenon;
- Freeze/thaw Phenomenon;
- Actual performances of UHPC and UHPFRC structures;
- Microstructural analysis of UHPC and UHPFRC.

1.6 ORGANIZATION OF THE THESIS

- Chapter 1 serves as an introduction to the thesis.
- Chapter 2 presents an insight from literature reviewed on the development of prestressed concrete and UHPC, typical mix designs, binder types, curing regimes, as well as their effects on the mechanical properties of UHPC. In addition, studies on bond performance including bond mechanisms, bond failure, factors affecting bond strength and effect of fibre on the bond performance have been covered. Finally, different types of failure in beams as well as parameters affecting shear failure are discussed.
- Chapter 3 introduces the testing procedures used to determine the mechanical properties of UHPC and UHPFRC including compressive strength, modulus of elasticity, flexural strength, splitting tensile strength and direct tensile strength. It also covers the preliminary experiments on the mix design development and curing regime. Economical aspect of the proposed mix design is evaluated. The effect of different types of fibre on the mechanical properties of the achieved UHPC is discussed and the effects of different curing regimes for each series of UHPFRC are explained. In addition, the experimental studies to achieve an effective UHPC curing regime for optimal compressive strength are explained in detail. Eventually, the final mix design, incorporating only local materials as well as a practical curing regime are introduced.
- Chapter 4 introduces the tests conducted to predict prestress losses. The testing procedures to measure drying shrinkage and creep for UHPFRC are described in this chapter. The study programme on evaluation of the bond performance between the concrete and the prestressing wire is described in this chapter including the properties of the prestressing wire and the test set-up to perform pull-out tests. Finally, the experimental programme including the specimen specifications and ages is introduced.
- Chapter 5 contains the experimental results of not only shrinkage and creep tests but also bond performance obtained from pull-out tests for UHPC and UHPFRC, including the results for evaluation of development length and the effect of concrete cover on bond strength. Finally, summary of bond strength and tensile strength in prestressing wires are presented.

- Chapter 6 illustrates the preliminary four-point bending test set-up for the UHPC and UHPFRC prestressed beams. The behaviour of the beams under flexure is described in this chapter.
- Chapter 7 contains the design, fabrication, testing method of two simply-supported full-scale prestressed UHPFRC beams that were tested to failure.
- Chapter 8 provides the experimental results of full scale prestressed UHPFRC beams under four-point loading. Besides the mechanical properties of UHPFRC prestressed beams, a detailed analysis of the behaviour of the beams is covered, including load versus deflection relationship, crack pattern, distribution and magnitude of concrete strains in the critical shear span. Finally, the experimental results are compared to the ones calculated by code provisions.
- Chapter 9 contains the conclusion as well as recommendations for further work on UHPFRC.

CHAPTER 2 LITERATURE STUDY

2.1 INTRODUCTION

This chapter starts with an introduction into the history of prestressed concrete and the development of UHPC including its advantages and recent large-scale applications. This is followed by a literature review of previous studies on typical mix design, binder types and curing regimes considered for UHPC, as well as their effects on the mechanical properties of this type of concrete. In addition, the effect of fibre on the mechanical properties of UHPC including compressive, tensile and flexural strength is reported, based on previous studies.

Since manufacturing UHPC prestressed beams is one of the objectives in the thesis, bond performance between prestressing steel bar and the concrete surrounding it is an important factor. Therefore, in this chapter a literature review of studies regarding bond performance have been covered, including bond mechanism, bond failure, factors affecting bond strength and effect of fibre on the bond performance. Finally, different types of failure in beams as well as parameters affecting shear failure are explained based on previous studies found in literature.

2.2 DESIGN CONSIDERATION IN PRESTRESSED CONCRETE

Concrete properties (early-age and long-term) are crucial for design purposes of prestressed concrete members (Hurst, 1988; Raju and Sandeep 2017; Huang et al., 2018). The concrete modulus of elasticity is important, not only in estimating deflection of prestressed concrete members but also, in the losses of prestress force. Early-age modulus of elasticity is required for determining the short-term deflection of prestressed concrete members and initial losses of prestress force due to elastic shortening. Knowing tensile strength of concrete is necessary in prestressed concrete, since, at and after the time of wire releasing, tensile stresses are induced in the concrete in the anchorage zone that may cause longitudinal cracks at the end of the members. Knowing both early-age and long-term compressive strengths are essential for controlling required compressive strength before wire releasing and for design purposes, respectively.

Prestressing force magnitude in the prestressing bars of a prestressed concrete member is reduced (prestress loss) due to several factors including some related to the material properties of the concrete. Creep and shrinkage not only affects loss of prestress force in prestressed concrete members but also, the long-term deflections. Knowing both of their values is essential for designing prestressed concrete members.

In conclusion, a thorough investigation on UHPC prestressed beams demands preliminary studies on UHPC as well as its early-age and long term mechanical properties (modulus of elasticity, compressive strength and tensile strength), prestress loss and bond behaviour.

2.3 ULTRA HIGH PERFORMANCE CONCRETE (UHPC)

In the mid-1990s, a new generation of UHPC called Reactive Powder Concrete (RPC) was developed by researchers in France. Their mix design differed significantly from that of normal and high-strength concretes. Ultra High Performance Fibre Reinforced Concretes (UHPFRC) has high durability (mainly due to optimized particle gradation that produces a very tightly packed mixture) compressive strength over 150 MPa, tensile strength in the range of 8 to12 MPa and flexural strength of about 40 MPa (Charron et al., 2004; Habel, 2004; Rossi et al., 2005; Tsioulou et al., 2017; Singh e al. 2017). Significant ductility is provided by high strength steel fibres which are distributed throughout the matrix.

The main advantage of UHPC over normal-strength concrete is its high compressive strength. Other advantages include low porosity, improved microstructure and homogeneity, as well as high flexibility with the inclusion of fibres. As a result of its superior performance, UHPC has found application in the storage of nuclear waste, seismic-resistant structures, bridges, roofs, piers, and structures designed to resist impact loading (Mohammed, 2015; Nicolaides et al., 2015). Owing to its high compression resistance, precast structural elements can be manufactured in slender form to enhance aesthetics. For many years, durability issues of normal-strength concrete have been acknowledged and significant funds have been allocated to repair aging infrastructure. UHPC possesses good durability properties as a result of lower porosity and fewer smaller capillaries account for its endurance. UHPC requires lower maintenance costs during its service life than conventional concrete. UHPC may incorporate larger quantities of steel or synthetic fibres and has enhanced ductility, high temperature performance and improved impact resistance. This enables structural members to be built entirely from UHPFRC without the use of conventional transverse reinforcement or stirrups,

relying on the UHPC without traditional reinforcement because of the tensile strength contribution of high strength steel fibres (Zagon et al., 2016)

There are many successful applications of UHPC which have been reported, such as (Spasojevic, 2008):

- The 60 metre span Sherbrooke footbridge (see **Figure 2.1**) in Canada in 1997;
- The Shawnessy LRT station canopy in Canada 2003;
- The Cattenom power station in France in 1999;
- The 7 metre span roof panels and the 21 metre span road bridge in USA in 2001 and 2004, respectively;
- The 120 metre span Seonyu footbridge in South Korea in 2002;
- The 50 metre span Sakata Mirai footbridge in Japan in 2002;
- The 16 metre span Shepherd Gully Creek Bridge in Australia in 2004; etc.

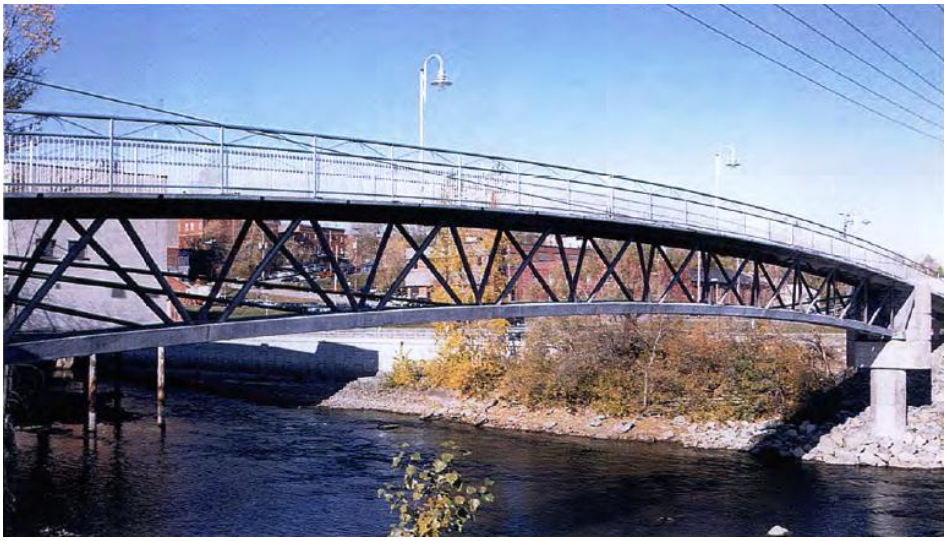

Figure 2.1 Sherbrooke footbridge with 60 metre span in Canada (Blais and Couture, 1999)

The world's first engineering structure designed with UHPC was the Sherbrooke footbridge in 1997 in Sherbrooke, Quebec. This precast, prestressed pedestrian bridge is a post-tensioned open-web space RPC truss, with 60 m span and 4 access spans made of High Performance Concrete (HPC). The main span consisted of six 10 m prefabricated match-cast segments. The cross section is made of a ribbed slab 30 mm thick, with transverse prestressing made of greased sheathed monostrands. The truss webs are made of RPC confined in stainless steel tubes, as shown in **Figure 2.2**. The structure is longitudinally

prestressed by an internal prestressing cable placed in each longitudinal flange and external prestressing cables anchored at the upper part of the end diaphragms and guided through blocks placed at the level of the lower flange. The connection between the flanges and truss diagonals is ensured by greased sheathed monostrands and miniaturized anchorage.

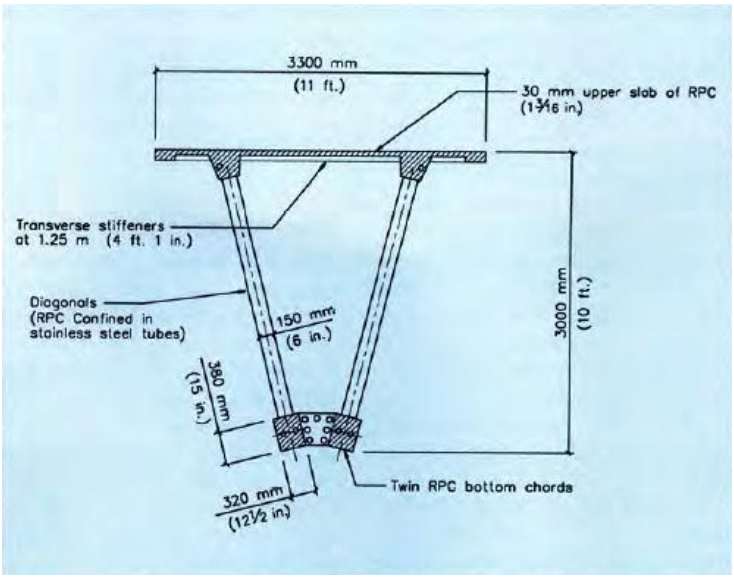

Figure 2.2 Typical cross section of Sherbrooke footbridge (Blais and Couture, 1999)

2.4 UHPC MIX DESIGN AND CURING

2.4.1 Mix design

In 1995, a study was done by Richard and Cheyrezy on RPC to achieve very high-strength concrete by introducing some basic principles. Their proposed principles (Richard and Cheyrezy, 1995) include:

- Improving homogeneity by eliminating coarse aggregate, utilizing fine aggregate limited to finer than 600µm, while reducing the sand content to 1.1 (the proportion of sand to cement by weight) in comparison to ordinary concrete.
- Optimizing the packing density of the granules (cement, silica fume, crushed quartz and fine quartz sand aggregate) in the mix by correct selection of their size ranges to fill the gaps between the particles, in order to reduce the voids caused by water demand and entrapped air.

Cement, silica fume and crushed quartz powder are the major cementitious materials. A mean compressive strength of 218 MPa was achieved through heat treatment at 90°C (without any pre-setting pressurization). Sand with particle sizes between 150 µm and 600µm was chosen

as an aggregate. In order to get ultra-high strength (about 800 MPa), steel aggregate finer than 800µm as well as heat treatment at 250-400°C and compacting pressure of 50 MPa were applied. They also managed to get compressive strengths between 490 MPa and 680 MPa by using heat treatment (at 250°C to 400°C), compacting pressure (of 50 MPa) and sand with particle diameter between 150µm and 600µm as aggregate.

The selection and proportioning of mix constituents help to achieve an optimized packing density for the granular mixture. The optimized particle gradation results in a low void ratio and thus higher compressive strength. The largest granular material in a RPC is fine sand, with a particle size ranging from 150µm to 600µm. The second largest size in the mix is cement particles, with a nominal size of 15µm. Quartz flour has a nominal diameter of 10µm and silica fume is the finest particle in the mix, with a nominal size of 1µm. Silica fume acts as micro filler, minimizing the voids in the hardened concrete, thus reducing permeability. Silica fume also reacts with calcium hydroxide resulting from cement hydration. This reaction of silica fume results in the final strength improvement. Another important effect of the silica fume is the improvement of the interfacial transition zones between binder and aggregates and between binder and steel fibres (Banthia, 1990; Bentz et al., 1992; Chung, 2002; Malier, 2018; Koutný et al. 2018).

The high cement content (about 1000-800 kg/m^3) is a disadvantage. Numerous studies have been conducted to investigate the behaviour of UHPC following the principles proposed by Richard (Voo et al., 2006; Habel and Gauvreau, 2008; Kang and Kim, 2011; Yang et al., 2012; Yoo et al., 2013). In their mix designs the maximum size of aggregate is limited to 600µm and the proportion of sand to cement was kept at 1.1 (by weight). Using aggregate with a maximum size of 600µm makes this type of concrete impractical in large applications such as bridges and high-rise buildings.

In 2008, Park et al. investigated the effect of the water to cement ratio, silica to cement ratio, type of filler as well as the size and content of aggregate. The aggregate to cement ratio was varied from 1 to 1.3. The mix design is given in **Table 2.1**. Based on the results shown in **Figure 2.3**, they concluded that in order to achieve a compressive strength of 180 MPa, an aggregate size of less than 0.5 mm and an aggregate to cement ratio of 1.1 should be used. The silica fume to cement ratio should range between 0.2 and 0.3, while the grain size of filler should be 13µm. Although, some studies can be found which considered slightly coarser

aggregate up to 0.8 mm (Wille et al., 2011; Wille et al., 2014) and 1 mm (Voo, et al., 2006), the concrete mix composition is still not practical.

Table 2.1 Mix design considered in the study by Park et al. (2008)

Item	W/B	B		S	FP	SP	STF (V_f)
		OPC	SF				
Optimum mix design	0.16~0.24	1	0~0.35	1~1.3	0~0.4	0.016	2%

OPC: Cement, SF: Silica Fume, S: Sand, FP: Filing Powder, SP: Superplasticizer, STF: Steel Fibre

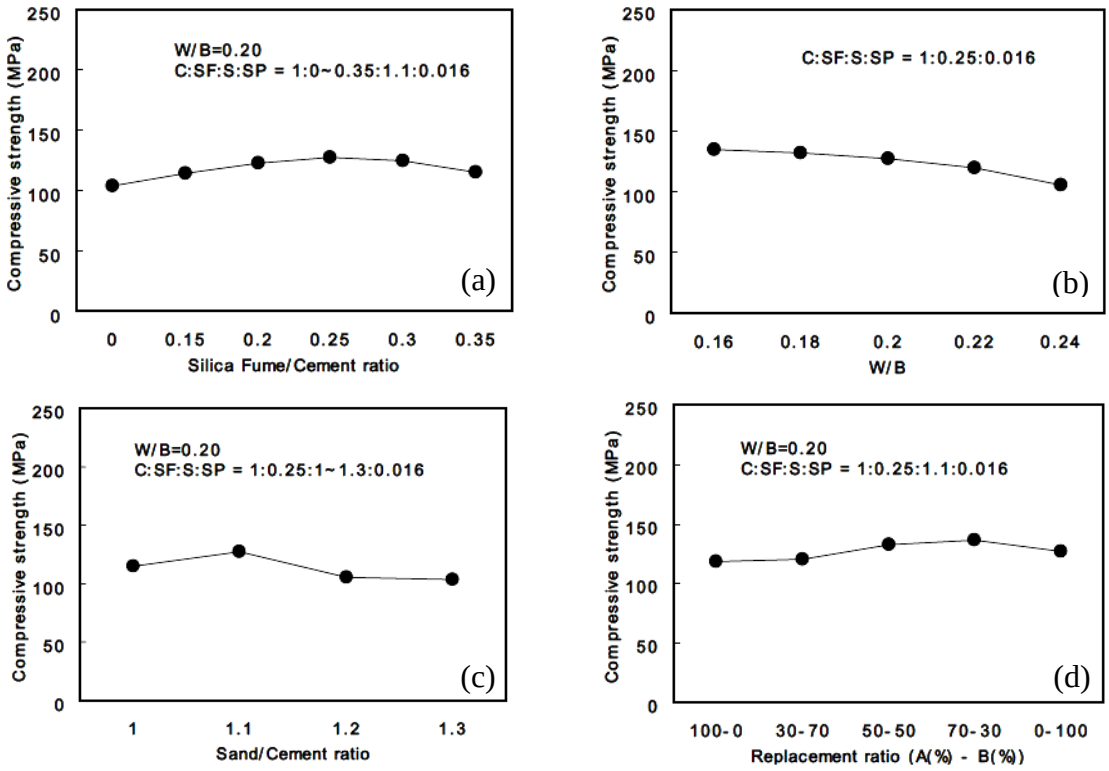

Figure 2.3 Compressive strength as affected by a) Silica fume content, b) Water content, c) Sand to cement ratio and d) Sand size (A: 0.3~0.5 mm B: 0.17~0.3 mm) (Park et al., 2008)

The cost of UHPC can be decreased by not having to process the aggregate. By using local natural sand sized less than 5 mm, GGBS and silica fume as supplementary cementitious materials, Yang et al. (2009) managed to obtain a compressive strength of 120 MPa by water curing at 20°C, and a compressive strength of about 180 MPa after using a 90°C heat-curing regime.

In 2008, Yazıcı et al. concluded that the use of very fine aggregate is not the only way to get ultra-high strength in RPC. They managed to get a compressive strength of 281 MPa by autoclaving at 210 °C under 2 MPa pressure. The maximum aggregate size was 3 mm. In this study the possibility of utilizing fly ash and GGBS as a silica source was investigated.

Ma et al. (2004) compared the results of the compressive strength, modulus of elasticity and autogenous shrinkage in UHPC containing coarse aggregates with ones obtained in UHPC containing no coarse aggregate. Both concretes (with and without coarse aggregate) had the same sand size ranges from 0.3 to 0.8 mm, while the UHPC contained coarse basalt aggregate ranged from 2 to 5 mm in diameter. The results indicated that UHPC containing coarse aggregate can achieve the same range of compressive strengths than with no coarse aggregate. Both concretes had a compressive strength of about 190 MPa after curing at 90°C. The big difference between these two concretes is the autogenous shrinkage (the macroscopic volume reduction of unloaded cementitious materials when cement hydrates after initial setting). The results show that autogenous shrinkage in UHPC with coarse aggregate is 40% lower.

2.4.2 Cementitious materials in UHPC

The cement content of UHPC should be minimized before the material will become widely used. In a study done by Yazıcı et al. (2010) the mechanical properties of RPC were measured using high volumes of ground granulated blast furnace slag as a cement replacement (20%, 40% and 60% cement replacement were considered). Granite and bauxite aggregates were used separately in the mix designs. The mix designs considered in the study are presented in **Table 2.2**. Test results indicate that consumption of high volumes of GGBFS is possible in producing RPC both with granite or bauxite aggregates. By replacing a portion of cement with GGBS (40% in RPC containing granite aggregate and 60% in RPC containing bauxite aggregate), the cement content can be considerably lower than that of conventional RPC. This is beneficial not only in reducing heat of hydration and shrinkage, but it also has environmental and economic advantages. The results also showed that by increasing GGBS content, the silica fume content can be reduced. The influence of GGBFS content on compressive strength of both bauxite aggregate RPC and granite aggregate RPC is shown in **Figure 2.4**. The compressive strengths presented in the figure were at the ages of 7, 28 and 90 days after STD curing (standard curing). Testing age of SC (steam curing) and AC (autoclave curing) cured specimens were 8 and 2 days, respectively.

Table 2.2 Mix design considered in the study by Yazıcı et al. (2010) (adapted)

Material (kg/m^3)	Bauxite				Granite			
	B-S0	B-S20	B-S40	B-S60	G-S0	G-S20	G-S40	G-S60
Cement	940	752	564	376	940	752	564	376
SF	282	282	282	282	282	226	169	113
GGBS	0	188	376	564		188	376	564
1–3 mm Bauxite	940	922	904	887	–	–	–	–
0–1 mm Bauxite	240	236	233	227	–	–	–	–
1–3 mm Granite	–	–	–	–	800	840	881	921
0.5–1 mm Quartz	–	–	–	–	100	104	109	114
0–0.4 mm Quartz	–	–	–	–	100	104	109	114
Water	125	125	125	125	125	125	125	125
Steel fiber	234	234	234	234	234	234	234	234
SP (L/m^3)	55	55	55	55	61	52.0	44.0	37.0
Water from SP (L/m^3)	33	33	33	33	37	31	26	22
Water*/cement	0.17	0.21	0.28	0.42	0.17	0.21	0.27	0.39
Water/powder	0.10	0.10	0.10	0.10	0.10	0.11	0.11	0.12
Water*/powder	0.13	0.13	0.13	0,13	0.13	0.13	0.14	0.14

* Calculated as total water (water + water from SP)/powder ratio.

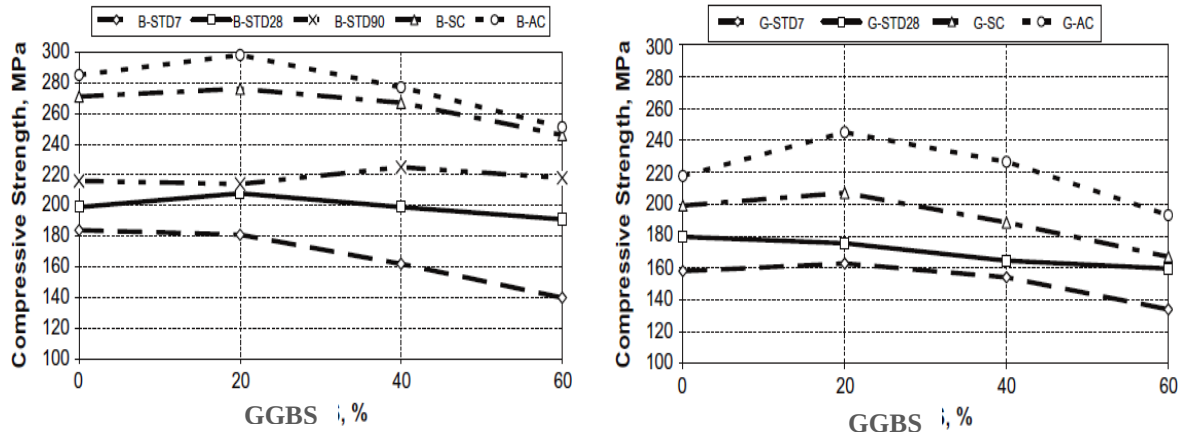

(a) (b)

Figure 2.4 The influence of GGBS content on compressive strength of a) Bauxite aggregate RPC, b) Granite aggregate RPC (STD: Standard curing, SC: Steam curing, AC: Autoclave curing) (adapted from Yazıcı et al., 2010)

In a study carried out by Wille et al. (2012) packing density was improved by optimization of material particle sizes as well as material proportions. The mix design strategy was based on the flow cone results, where the packing density is increased by either increasing the flowability of the paste, while the amount of water remains constant, or by maintaining the same flowability while the water content is reduced. The particle size of materials and their proportions were chosen to reduce the volume of water entrapped in the voids, thus resulting in a higher packing density. Cement (C), silica fume (SF) and very fine glass powder (GP) filler were considered as cementitious materials. The optimum proportions of C: SF and C: SF: GP were obtained as 1:0.25 and 1:0.25:0.25, respectively.

Yu, Spiesz and Brouwers (2015a) applied the modified Andereasen and Andersen particle packing model to develop a dense UHPFRC resulting in a relatively low binder content (about 620 kg/m^3) and low fibre content. The Particle size distributions of the ingredients used in this study are presented in **Figure 2.5**. The binder consisted of cement and nano-silica as pozzolanic materials and limestone powder as filler. The mix design is shown in **Table 2.3**. They concluded that by using a low binder content, significant mechanical properties of UHPFRC can be maintained. The studied mechanical properties included compressive strength and flexural strength. The highest 28-day compressive strength of 141.5 MPa and flexural strength of 30.8 MPa were achieved by using water curing at 21°C.

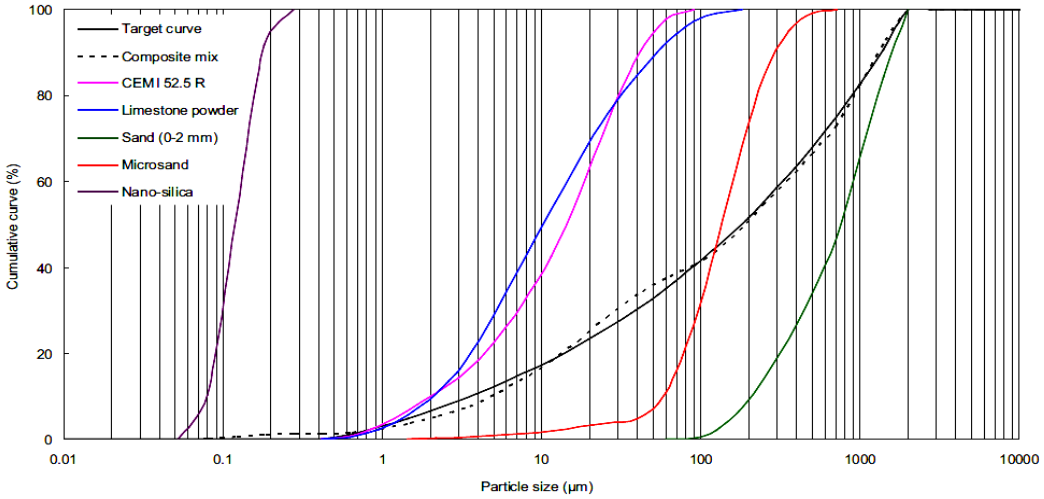

Figure 2.5 Particle size distribution of the ingredients used in the study by Yu, Spiesz and Brouwers (2015a)

Table 2.3 Mix design in the study by Yu, Spiesz and Brouwers (2015a)

C (kg/m^3)	LP (kg/m^3)	M-S (kg/m^3)	N-S (kg/m^3)	nS (kg/m^3)	W (kg/m^3)	SP (kg/m^3)
594.2	265.3	221.1	1061.2	24.8	176.9	44.2

C: cement, LP: limestone powder, M-S: microsand, N-S: normal sand, nS: nano-silica, W: water, SP: superplasticizer

In another study, Yu, Spiesz and Brouwers (2015b) investigated the production of an eco-friendly UHPC by utilizing different cement replacements. Fly ash, GGBS and lime stone powder were considered as cement replacement (about 30% of Portland cement (by mass)). Three different water to binder ratios were considered. The mix design was calculated based on the modified Andereasen and Andersen particle packing model. They reported that UHPC containing GGBS provided higher mechanical properties than UHPC with the other cement replacements. UHPC with GGBS had a compressive strength of 110 MPa and flexural

strength of 17 MPa. They believed that although the properties achieved were not as high as those reported by other researchers, the embedded CO_2 emission and environmental impact of the UHPC they developed were much less than that of UHPC with a compressive strength of 200 MPa with a high cement consumption.

Randl et al. (2014) investigated an UHPFRC mixture with a smaller environmental impact than the reference UHPFRC, while maintaining similar fresh and hardened properties. Maximum packing density of fine grains was the basis of the reference mixture proportion. In order to reduce the cement consumption, two types of GGBS (fine and extra fine) and fly ash were considered as supplementary cementitious materials. The Portland cement of the reference mix design was replaced with 45% (by weight) of the supplementary materials. The mix designs considered in this study are shown in **Table 2.4**. The highest 28-day compressive strength of 163.5 MPa was achieved by the mixture containing extra fine GGBS as a cement replacement (UM-5-GBSef) which is fairly close to the reference compressive strength of 166.1 MPa. It also showed higher workability in comparison with the reference mixture. The results of slump test and compressive strength are shown in **Figure 2.6**. The reference mixture (UM-5) is a fine grain mixture with a maximum grain size of 0.5 mm. The k-factor defines the hydraulic activity of supplementary cementitious materials which in this study is taken as k = 0.4 for FA and k = 0.8 for GBS.

Table 2.4 Mix design in the study by Randl et al. (2014)(adapted)

Components	UM-5	UM-5-FA	UM-5-GGBS (fine)	UM-5-GGBS (extra fine)
	kg/m^3			
Cement CEM I 42.5 R	729	401	401	401
Microsilica (*k*=1.0)	124	124	124	124
FA (*k*=0.4)	-	328	-	-
GGBS fine (*k*=0.8)	-	-	328	-
GGBS extra fine (*k*=0.8)	-	-	-	328
Quartz powder	397	397	397	397
Quartz sand	833	833	833	833
Total water (incl. SP)	200	200	200	200
Superplasticizer (SP)	30	30	30	30
Fibres (Stratec 0.2/15)	155	155	155	155
w/c_{eq}	0.234	0.305	0.254	0.254
w/f	0.47	0.44	0.44	0.44

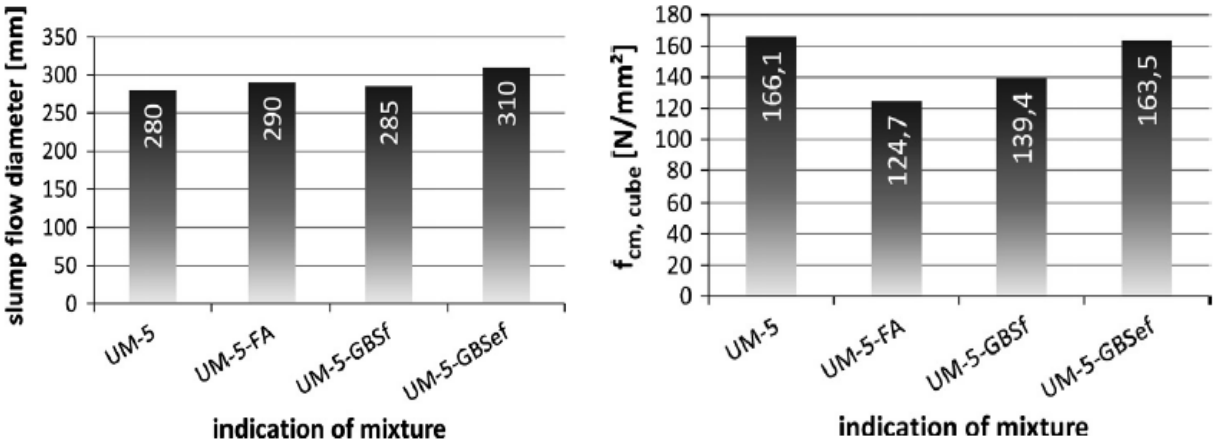

(a) (b)

Figure 2.6 Results of a) slump flow test after 2 min, b) 28- day compressive strength cured in accordance with the Austrian standard ONR 23303 (Randl et al., 2014)

2.4.3 UHPC curing regimes

Curing regime plays an important role on the properties of concrete especially on the compressive strength of UHPC. The most commonly implemented curing regime for UHPC is heat treatment which involves subjecting the specimen to 90°C under very moist conditions. As UHPC mostly contains cement extenders, there is a belief that high temperatures accelerate the pozzolanic reaction in concrete (Yazıcı et al., 2010; Zheng et al., 2012; Abid et al., 2017; Peng et al., 2018). Actually, the microstructure of the concrete is improved by the heat treatment accelerating the pozzolanic reaction of silica fume and cement modifying the structure of the hydrate. However, heat treatment is not required for all application of UHPC. Without any heat treatment, the concrete can still have superior strength and ductility characteristics compared to any previously manufactured concrete.

Various investigations have been published referring to various curing regimes with different procedures in order to reach to the highest possible compressive strength (Ay, 2004; Schachinger et al., 2008; Ahlborn et al., 2008; Yang et al., 2009; Askar et al., 2017; Peng et al., 2018). These different curing regimes include hot air curing, steam curing, water curing and autoclaving at different temperatures and durations.

Richard and Cheyrezy (1995) suggested heat treatment as one of the basic principles used to increase the compressive strength of RPC. In their study the compressive strength of concretes were enhanced from 170 MPa to 230 MPa by heating samples from 20°C to 90°C,

respectively. De Larrard and Sedran (1994) observed that the 7-day compressive strength improved from 120.6 MPa to 235.8 MPa. This improvement was achieved by changing the curing regime from normal water curing to thermal curing at 90°C for 48 hours. Heat treatment is considered as curing regime in most of the UHPC studies (Voo et al., 2006; Yang et al., 2010; Hassan et al., 2012; Yoo, 2013; Kang et al., 2017; Li et al., 2017).

Graybeal and Davis (2008) studied the compressive strength of UHPC with different size of cubes (51, 70.7 and 100 mm) and cylinders (51, 76 and 102 mm) with the aim of checking the reliability of compressive strength results obtained from other cube and cylinder sizes rather than the standard sizes. In their research, they also applied different curing regimes. Some of the specimens were kept in a laboratory environment, some were kept in 95% humidity at different temperatures (95°C, 90°C, 80°C, 60°C, 40°C and 22°C) mostly for 2 days. The results showed that by decreasing the temperature from 95°C to 22°C the average 28-day compressive strength of 100 mm cubes decrease from 198.1 MPa to 139.0 MPa. An average compressive strength of 141.5 MPa was obtained from the specimens kept in a laboratory environment for 28 days. The results revealed that the 70.7 and 51 mm cubes, as well as the 102 and 76 mm cylinders tend to show similar strengths.

In the study done by Yang et al. (2009) two types of curing were considered, 20°C and 90°C water. Some of the specimens were kept in 90°C water for 6 days (followed by storing in air at room temperature until testing) and the rest were cured in 20°C water until testing. Results revealed that at 28 days specimens cured at 90°C had 20% higher compressive strength, 10% higher flexural strength and 15% higher fracture energy than specimens cured at 20°C.

While moist curing conditions are the most common implemented conditions for UHPC, dry oven heating is also a possible treatment. This treatment is implemented mostly for 48 hours. When only heat and no moisture are applied during the heat treatment, the mechanical properties of UHPC are slightly reduced. However, the mechanical properties are still better than when no heat treatment is applied at all. In a variation to the heat treatment process, steam treating and oven drying were combined. Reda, Shrive and Gillott (1999) examined the microstructure of UHPC, in which specimens were subject to a hot water bath at 50°C and for some specimens this was followed by 48 hours oven drying at 200°C (after the hot water curing). The samples experiencing oven drying after the hot water curing showed at least

20% higher compressive strength in comparison with the cubes that experienced only hot water curing.

There are some studies in which no heat curing was applied. Wille et al. (2012) managed to get a compressive strength of 240 MPa with no heat curing and no pressure curing with the aim of facilitating the on-site applications of this type of concrete. Wang et al. (2012) tried to overcome the difficulties such as high expenses and sophisticated technologies in manufacturing UHPC. In their study, one of the aspects that were taken into consideration was the type of curing regime. The samples were exposed to a curing regime in the moist room at a temperature of (20 ± 2) °C and no less than 95% relative humidity until testing. Almost compressive strengths of 176 MPa and 183 MPa after 90 and 365 days were respectively achieved.

Ay (2004) used three different curing regimes for UHPC and UHPFRC including submerging in water until one hour before testing, water curing for five days followed by air curing before testing based on a Swedish standard and keeping the cubes sealed in plastic sheets in 80±5% RH (relative humidity) at 20±2 °C. Almost, the highest compressive strengths of 159 MPa and 180.5 MPa were achieved using the Swedish standard curing regime for UHPC and UHPFRC, respectively. For UHPC, the lowest compressive strength of 140 MPa was obtained for samples cured in water. The UHPC compressive strength differences were not negligible. Ay believed that one reason could be that more micro cracks formed in UHPC cured in water. The other reason is attributed to the impermeability of UHPC which leads to more hydration on the surface of cubes than in the inner core. The compressive strength differences in UHPFRC were not significant, which can be due to the effect of fibres on preventing micro cracks from opening.

Ahlborn et al. (2008) studied the effect of different curing regimes, as well as the influence of heat treatment timing on the compressive strength of UHPC. They considered four different curing regimes including:

1) TT: thermal steam treatment at 90°C with 100% RH for 48 hours.
2) Air: ambient air curing.
3) DTT: thermal heat steam treatment after 10 days of delay.
4) DDTT: thermal steam treatment after 24 days of delay.

No significant differences between the compressive strength obtained from the delayed thermal curing regimes were found. The compressive strength results are shown in **Table 2.5**. Modulus of elasticity as well as Poisson's ratio was measured beside the compressive strength. The results showed that UHPC cured thermally had a 4% higher modulus of elasticity than air-cured specimens, while Poisson's ratio was independent of the curing conditions. The effect of curing regime on the modulus of elasticity and Poisson's ratio are presented in **Figure 2.7**.

Table 2.5 Compressive strengths in different curing regimes (Ahlborn et al., 2008)

Curing Regime	Age	Sample Size	Sample Mean Compressive Stress (MPa)	Sample COV
Air	3	6	99.6	3.8
	7	6	137.3	1.8
	14	6	153.7	3.2
	28	6	165.0	2.2
TT	7	6	208.8	2.9
	14	6	207.4	4.6
	28	6	214.4	1.3
DTT	14	5	205.0	3.5
	28	6	206.3	2.2
DDTT	28	5	202.9	3.2

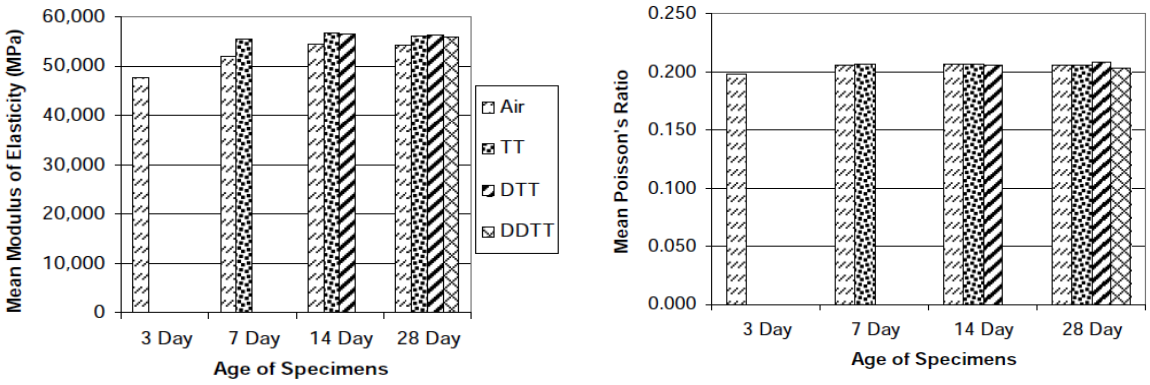

(a) (b)

Figure 2.7 Effect of curing regime on a) Modulus of elasticity, b) Poisson's ratio by Ahlborn et al. (2008)

In the literature reviewed regarding the curing regime, there is no specific indication if the specimens were tested in a dry or saturated condition. So, it is assumed that the specimens kept in a laboratory environment up to testing time were considered to be dry before testing and those kept in 95% humidity or water up to the testing time were tested in a saturated condition.

Since in the literature, heat treatments higher than 65°C have been considered for curing UHPCs, therefore, Delayed Ettringite Formation (DEF) should be considered.

2.4.4 Delayed Ettringite Formation (DEF)

DEF is a reaction that affects cementitious materials that potentially resulting in swelling and cracking of them. DEF is a type of internal sulphate attack that occurs when the constituents of concrete provide an initial source of sulphates when the concrete has experienced temperature above 65-70°C (Collepardi, 2003). DEF in concrete has been responsible for the premature deterioration of several structures in France (Pavoine et al., 2012).

Various cases of damage caused by DEF mostly occurred not only in precast members which made by high temperature curing, but also in mass concrete production in which the temperature is risen excessively from the heat of hydration (Pavoine et al., 2012).

As discussed by Escadeillas et al. (2007), there are the conditions necessary for the occurrence of DEF including:

• An excessive rise of temperature during the casting of the concrete when high heat of hydration of large masses of concrete is produced;

• High temperature curing above 65-70°C in the process of steam curing of concrete, especially in precast products. This high temperature (60–70 °C) prevents the formation of non-expansive preliminary ettringite;

• Presence of sulfates, essentially originating from the cement and, to a lesser extent, from the aggregate or the mixing water. These sulfates can react with the aluminates existing in cement in presence of water to form delayed expansive ettringite;

• When the cement is exposed to a moist environment or water (bridges, dams, rail ties,…).

They also reported that supplementary treatments, such as preliminary microcracking or wetting/drying cycles, are not necessary for the occurrence of DEF. However, they contribute to a slight acceleration of the reaction.

Expansion caused by the occurrence of DEF is affected by the nature and size grading of the aggregate; expansion is very slow in mortars made with limestone sand while it is faster in the mortars containing quartz aggregates (Heinz et al., 1989; Yang et al., 1999). The aggregate size seems to be an important parameter as well. Fu, Ding and Beaudoin (1997)

reported that the smaller the aggregate size, the larger the concrete swelling. Grattan-Bellew et al. (1998) observed the same behaviour in siliceous aggregates (quartz) sand.

There are some studies shown that some pozzolanic additions were effective in preventing the delayed ettringite formation. Ramlochan et al. (2003) reported that a small proportion of metakaolin (>8%) is able to reduce or eliminate the long-term expansion caused by DEF. They concluded that this is due to the high content of Al_2O_3 in the metakaolin and the leaching effect of reducing the alkali hydroxide of the pore solution. They also reported that cement substitution rate by 25% of blast furnace slag is required to remove the long-term expansion. However, higher rates of blast furnace slag may be needed if cements with very high levels of sulfate or alkaline are used. Fly ash required to restrain expansion depends on their lime concentration. Fly ash with low concentrations of lime can be more effective when used with low substitution rate (15-25%), while the fly ash with a high concentration of lime seems to be effective to more degree of substitution high (25-35%). They also showed that the partial substitution of cement by silica fume up to 8% did not control the long-term expansion caused by DEF. However, the beginning of the expansion was delayed due to the low permeability of mortars containing silica fume.

The effect of natural pozzolan on the DEF was studied by Nguyen et al. (2013). Their experimental results indicated that the fineness of the natural pozzolan significantly affects the kinetics of expansion caused by DEF. Expansion can be reduced or eliminated by addition of a finely blended natural pozzolan as partial replacement of cement. However, the substitution of the cement by the coarse natural pozzolan is not only ineffective, but also accelerates the expansion phenomenon.

2.5 EFFECT OF FIBRE ON MECHANICAL PROPERTIES OF CONCRETE

Concrete as a cementitious material exhibits brittle tensile behaviour. However, this behaviour can be significantly improved by adding discontinuous fibres. Romualdi and Batson (1963) proposed using short randomly oriented fibres in order to improve the matrix brittle behaviour under tensile loading. Johnston (1985) reported that the addition of steel fibres to concrete significantly increases the total energy absorbed prior to complete separation of the specimen. Johnston and Zemp (1991) found that the presence of steel fibres improves fatigue properties. Today, several types of reinforcing fibres, in different materials

(such as steel, polymer, glass, carbon) and shapes (such as straight, twisted and hook-ended) are widely produced and used.

The main advantage of using discontinuous fibres in concrete is usually only realized after the concrete cracks. In other words, fibres start playing an active role when the concrete has cracked. The fibres are able to prevent a sudden loss in load-carrying capacity of the cracked composite by providing a load transfer mechanism across the crack, which results in a pseudo-ductile behaviour. When a load is applied to fibre reinforced concrete, it is distributed to both the matrix and the fibres. The transmission of forces between the fibres and the matrix occurs through interfacial bond, defined as the bond shear stress at the interface between the fibre and the surrounding matrix. The fibres contribute primarily to the post cracking response of the composite by bridging the cracks and providing resistance to crack opening (Naaman and Najm, 1991; Barros et al., 2005; Zhou and Uchida, 2017; Qi et al., 2018).

2.5.1 Compressive Strength

Ramakrishnan et al. (1980), Soroushian and Bayasi (1991), Khaloo and Kim (1996), and Thomas and Ramaswamy (2007) found that steel fibres do not significantly increase the peak compressive strength. No increase was observed by Williamson (1974) while Fanella and Naaman (1985) found only a slight increase in the compressive strength. Thomas and Ramaswamy (2007) reported that the increase in peak strength was less than 10% when fibres were added in volume fractions of up to 1.5%. Khaloo and Kim (1996) reported a higher strain at peak stress (less than 30%) in the presence of steel fibres.

On the other hand, Khaloo and Kim (1996) observed a maximum increase in compressive strength of up to 37% for SFRC with a fibre volume fraction of 1.5%.

In the compressive strength tests conducted by Soroushian and Bayasi (1991), the results showed that hooked and crimped steel fibres are more effective in enhancing the compressive strength and post-peak behaviour in comparison to straight steel fibre (**Figure 2.8**). No significant difference in the post-peak behaviour of concrete with hooked and crimped steel fibres was observed. There was also not much increase in compressive strength, in the case of mortar mixtures.

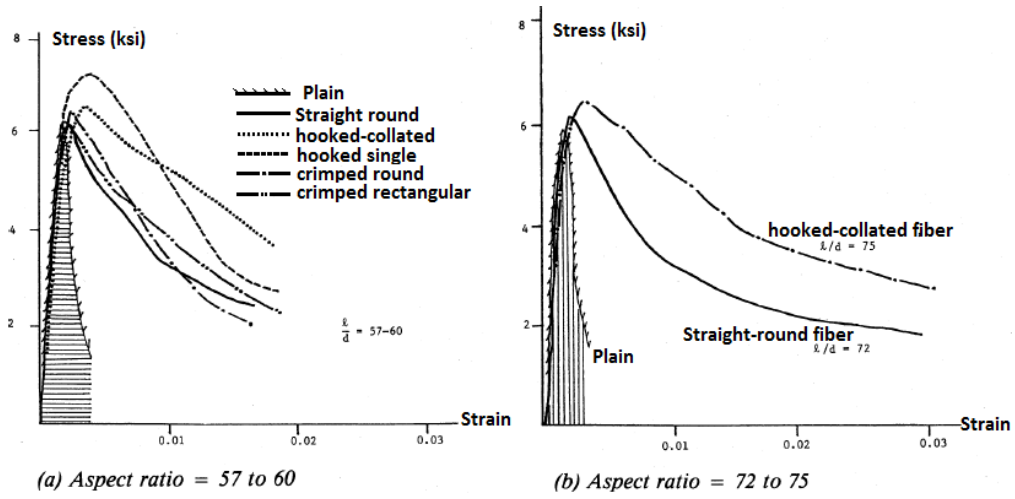

Figure 2.8 Compressive stress-strain behaviour in different fibre types and fibre aspect ratios (Soroushian and Bayasi, 1991)

Wu et al. (2016) observed that the UHPC with hooked-end fibres had the highest compressive strength in comparison with UHPC with straight fibres. **Figure 2.9** illustrates the effects of fibre shape on the compressive strength of UHPCs. The results also revealed that the compressive strength increased with the increase of fibre content.

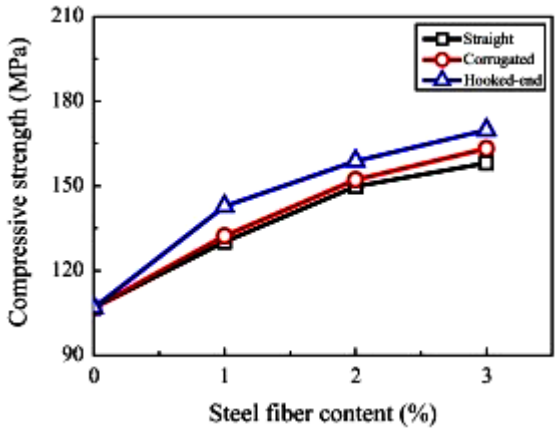

Figure 2.9 Effects of steel fibre content on compressive strengths of UHPC at 28 days (Wu et al., 2016).

A High Strength Concrete (HSC) always exhibits a steeper descending stress–strain curve in compression than a Normal Strength Concrete (NSC) (Löfgren, 2005). The rapid decrease in compressive strength in the post-peak load region results in a brittle mode of failure (Palmquist and Jansen, 2001). The schematic description of HSC and NSC behaviour in compression is presented in **Figure 2.10**. In order to increase the compressive strength without sacrificing the ductility, discrete steel fibres as reinforcement should be added to HSC (Hsu and Hsu, 1994). Under service loads in a High-Strength Steel Fibre Reinforced

Concrete (HSFRC), cracks can develop and propagate. Marar, Eren and Çelik (2001) observed that the compressive strength of HSFRC improved with the increase in fibre volume at each fibre aspect ratio. Daniel and Loukili (2002) reported that the compressive strength of HSFRC was enhanced by 15%, in comparison to HSC. The effect of fibres on the compressive strength enhancement is highly dependent on the fibre aspect ratio and the fibre content in HSFRC (Eren and Çelik, 1997). Moreover, Chunxiang and Patnaikuni (1999) reported that in HSC containing 3% steel fibre the 28-day and 76-day compressive strength exhibited 22% and 24% strength enhancement respectively, in comparison with HSC without fibre.

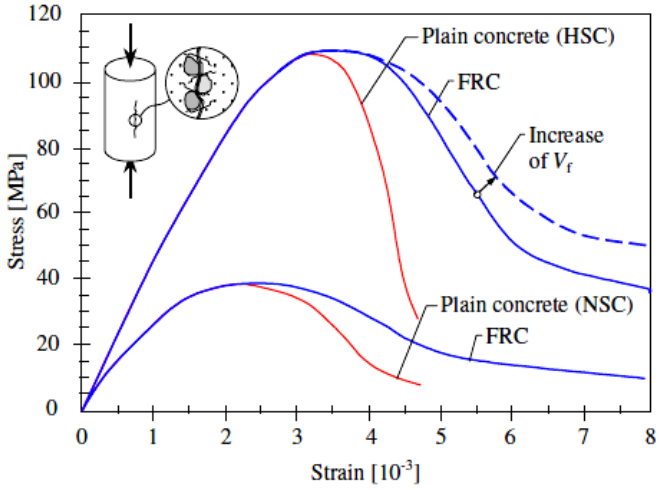

Figure 2.10 Schematic description of the behaviour of FRC in compression (Löfgren, 2005)

Abbas, Soliman and Nehdi (2015) reported that higher compressive strength was achieved by addition of fibres due to less entrapped air, leading to improved density and hence higher compressive strength.

Yoo, Lee and Yoon (2013) investigated the effect of fibre content on the mechanical properties of UHPC. Four different micro fibre contents of 1%, 2% and 4% (per volume) was used. The highest compressive strength of 207.2 MPa was achieved for UHPC containing 3% fibre (volume fraction). This strength was 5.3%, 2.7% and 12.1% higher than the compressive strength of UHPC containing 1%, 2% and 4% fibre (by volume), respectively. Due to the non-homogenous dispersion of fibres in the mixture the lowest compressive strength was achieved in UHPC containing 4% fibre (by volume). **Figure 2.11** presents the effect of fibre volume fraction on the compressive strength.

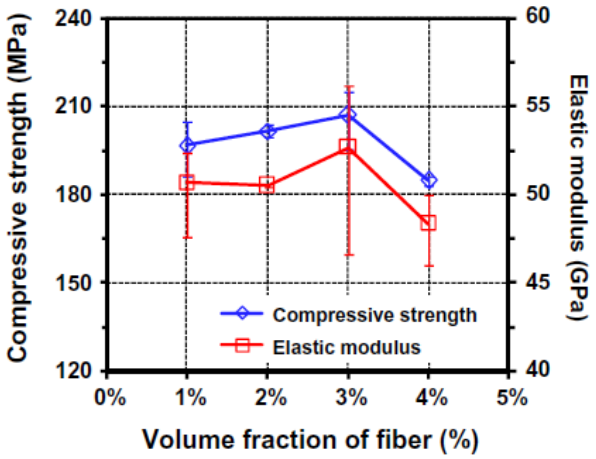

Figure 2.11 Effect of fibre volume fraction on compressive strength (Yoo et al., 2013)

Yoo et al. (2014) studied the effect of fibre length on the compressive strength. Four different fibre lengths (13, 16.3, 19.5 and 30 mm) were used. No significant difference in the compressive strength was observed. The highest compressive strength was only 0.9% to 3.6% greater than the rest.

2.5.2 Tensile Behaviour

The tensile behaviour of FRC as cement based material, can be classified as either strain softening (a quasi-brittle material), or pseudo strain-hardening as illustrated in **Figure 2.12**. This behaviour can to be captured in a direct tensile test. Strain softening occurs when a localised single crack determines the post-peak behaviour. No strength improvement can be observed after the matrix cracks. However, in the pseudo strain-hardening behaviour, post-cracking strength is higher than the cracking strength (Löfgren, 2005). In addition, it is accompanied by multiple cracking which results in high ductility. However, the tensile properties are difficult to capture experimentally. First of all, there is no standard test method to assess the direct tensile behaviour of SFRC. Secondly, in order to have a similar fibre distribution to the actual structural member, a large cross section is needed and gripping the end of such a cross section is difficult. Thirdly, direct tensile test results are usually significantly scattered. Since the location of cracks forming is not predictable, it is difficult to fix the gauge length, which leads to difficulty in interpreting the strain results. The last but not least problem is obtaining evenly distributed stresses throughout the cross section.

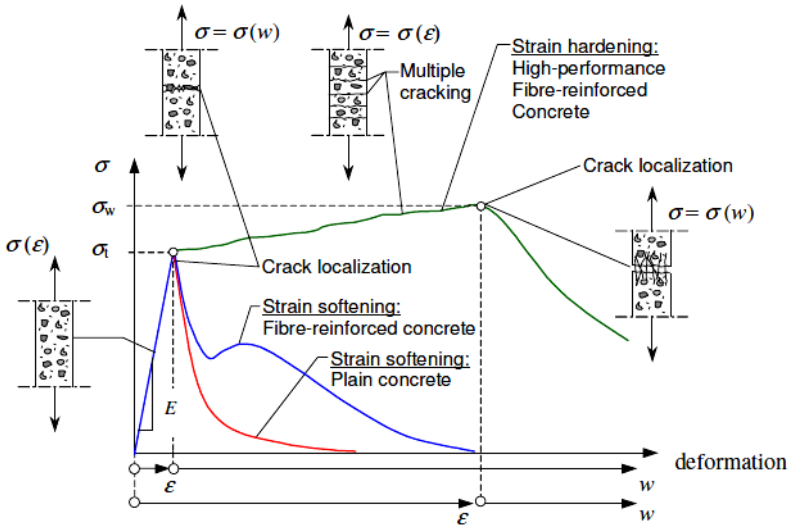

Figure 2.12 Classification of tensile behaviour of cement-based materials (Löfgren, 2005)

Wille, Kim and Naaman (2011) studied the effect of fibre content and fibre type on the tensile strength of UHPFRC. The volume fraction of fibres varied from 1% to 2.5%. The properties of the fibres are shown in **Table 2.6**. Tensile behaviour of UHPFRC exhibited strain-hardening. As **Figure 2.13** shows, tensile strength is improved by increasing the fibre volume fractions. The highest ultimate tensile strengths (up to 15 MPa) were obtained at the highest fibre content, regardless of fibre type. In other words, the type of fibre did not affect the ultimate tensile strength. However, this observation did not hold true for the strain at peak stresses. The highest strain at peak stresses of 2.4%, 4.7%, 6.0% and 6.1% were obtained from the UHPC containing 2.5% smooth fibre, 1.5% hooked fibre, 2% high twisted fibre and 1.5% low twisted fibre, respectively. The results showed the effect of different fibres on the post-cracking behaviour of UHPFRC.

Table 2.6 Properties of the fibres (Wille et al., 2011)

Form	Number of twists	d_f (mm)	ℓ_f (mm)	ℓ_f/d_f	Tensile strength (MPa (ksi))
Straight (S)	0	0.20	13	65	≈2600 (377)
Hooked (H)	0	0.38	30	79	≈2900 (420)
High twisted (T_1)	16	0.30	30	100	≈2100 (304)
Low twisted (T_2)	6–8	0.30	30	100	≈3100 (449)

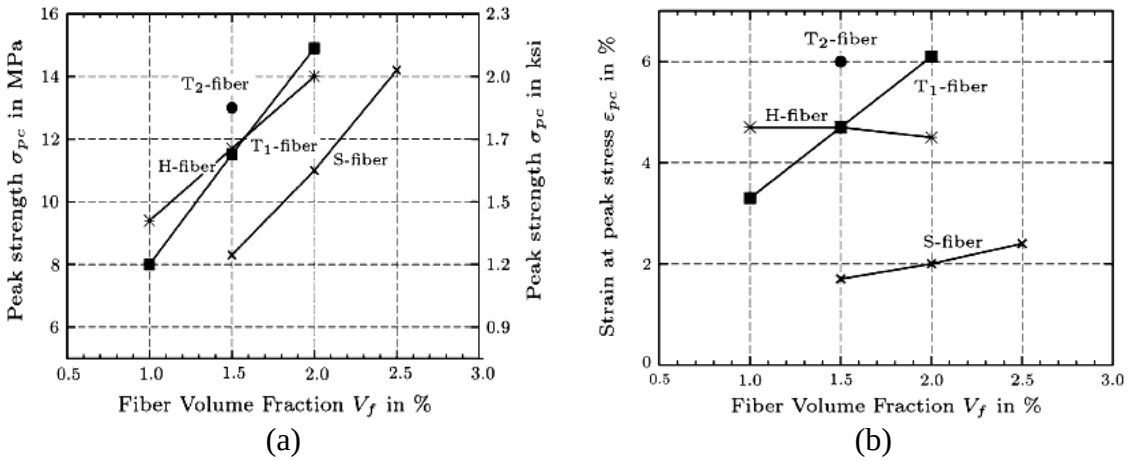

Figure 2.13 Effect of fibre type and content on a) maximum tensile stress, b) strain at peak stress of different UHPFRC (Wille et al., 2011)

2.5.3 Flexural Behaviour

From a flexural test, the first-crack flexural strength and peak post-cracking flexural strength can be evaluated according to ACI Committee 544 (1988b). These strengths are calculated using the assumption of a linear strain distribution. The first-crack flexural strength is also known as modulus of rupture. Toughness is another important property determined from bending tests and defined as the area underneath the load versus deflection curve.

Steel fibres often have a much greater effect on the flexural strength of SFRC than on either the compressive or tensile strengths. Shah and Rangan (1971) found that by introducing 1% straight fibres (by volume), in a beam with a rectangular cross section the first-crack flexural strength increased by about 100%. An enhancement of 67% in first-crack flexural strength was observed by Wafa and Ashour (1992) when a 1.5% volume fraction of fibres with an aspect ratio of 80 was added to a high strength concrete (93 MPa). Elsaigh and Kearsley (2002) reported that increasing steel fibre content results in enhanced post-cracking strength (see **Figure 2.14**).

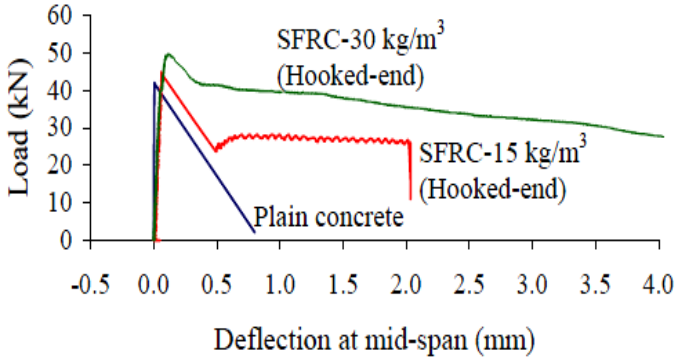

Figure 2.14 Effect of fibre content on the flexural behaviour of SFRC (Elsaigh and Kearsley, 2002)

Song and Hwang (2004) found that by adding 2% of hooked steel fibres (by volume) with an aspect ratio of 64 to a high strength concrete (85 MPa), up to 127% increase in the first-crack flexural strength was achieved. Thomas and Ramaswamy (2007) reported that by adding hooked steel fibres (0.5%-1.5%) with an aspect ratio of 60, up to 40% increase in the first-crack flexural strength of high strength concrete beams was observed.

Ramakrishnan et al. (1980) found that hooked steel fibres performed better than straight fibres in terms of providing a higher ultimate flexural strength and flexural toughness. The use of 0.6% hooked steel fibres (by volume) led to a post-cracking strength equal or greater than the first-crack strength. The superiority of hooked ended steel fibres in comparison to straight steel fibres was confirmed by Soroushian and Bayasi (1991) and Wu, Khayat and Shi (2018). **Figure 2.15** presents the effect of hooked and straight steel fibres on the flexural performance of concrete with a compressive strength of about 45 MPa.

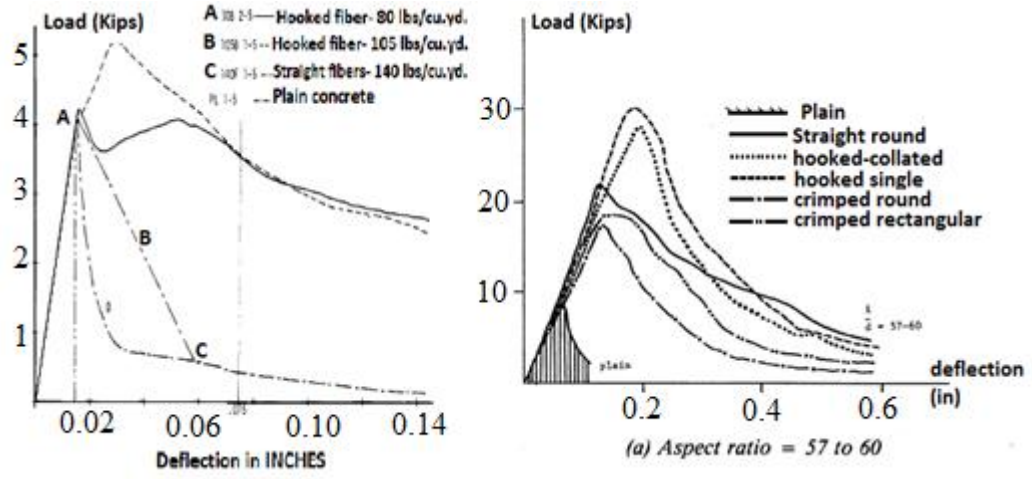

(a) Ramakrishnan et al. (1980) (b) Soroushian and Bayasi (1991)

Figure 2.15 Effect of hooked and straight steel fibres on flexural performance of concrete

Wu et al. (2016) reported that by increasing the fibre content from 1% to 3%, flexural strength improved. The flexural strength enhancement was higher when deformed steel fibres were used. This may be due to different bonding strength associated with fibre shape. As reported by Beglarigale and Yazıcı (2015), the bonding strength at fibre–matrix interface is mainly provided by chemical bond, anchorage mechanical force associated with fibre-end, and friction. Amongst different shape fibres, hooked-end fibres provide better mechanical interlock compared with other fibre shapes. **Figure 2.16** presents the effect of fibre content and type on the flexural strength of UHPC.

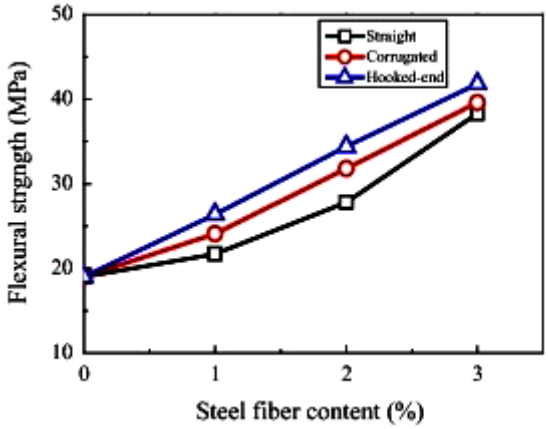

Figure 2.16 Effects of steel fibre content on flexural strengths of UHPC at 28 days (Wu et al., 2016).

Khaloo and Kim (1996) reported that adding the same type of fibres with the same fibre volume fraction resulted in higher improvement in modulus of rupture for normal strength concrete (31 MPa) than for mid-strength and high-strength concrete (50 and 83 MPa, respectively).

Yoo, Lee and Yoon (2013) reported that for the flexural behaviour of UHPFRC, the initial stiffnesses are nearly identical in beams containing different fibre contents (1% - 4%), while the load carrying capacity increased with increasing fibre volume fraction. The first cracking load showed independency of fibre content, i.e. increasing the fibre content made no difference in first cracking load. They concluded that increasing the fibre content improved the flexural strength, while reducing deflection and Crack Mouth Opening Displacement (CMOD) at peak load. Flexural behaviour of UHPFRC with various fibre volume fractions is illustrated in **Figure 2.17**. The highest compressive strength of 207.2 MPa for UHPC

containing 3% fibre content (by volume) and the lowest compressive strength of 182 MPa for UHPC containing 4% fibre content (by volume) were achieved.

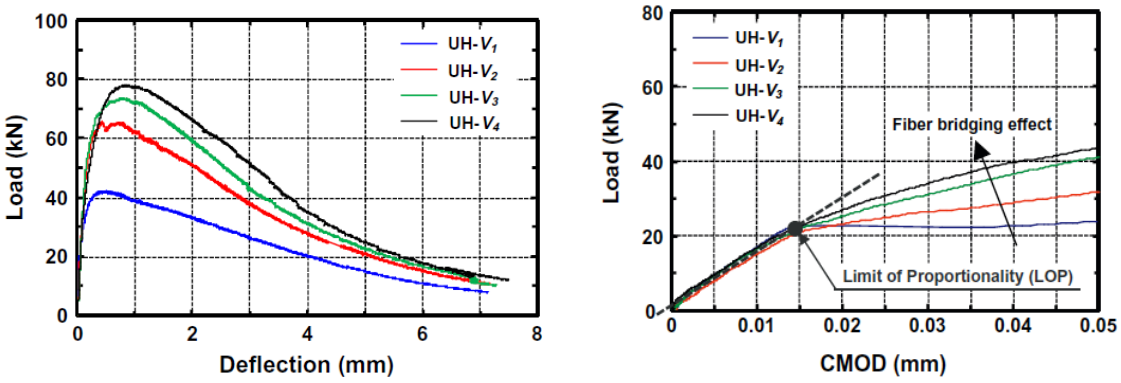

(a) (b)

Figure 2.17 Flexural behaviour of UHPFRCC with various fibre volume fractions a) load-deflection curve, b) initial flexural load and (CMOD) (Yoo et al., 2013)

The effect of different fibre lengths (13, 16.3, 19.5 and 30 mm) on the flexural behaviour of UHPC containing 2% fibre content (by volume) was studied by Yoo et al. (2014), revealing that the flexural strength of UHPFRC was enhanced by increasing the fibre length up to 19.5 mm. The flexural strength of UHPC containing 30 mm fibres exhibited a reduction because of non-uniform dispersion of fibres in the mixture. **Figure 2.18** illustrates the load-CMOD curves obtained from beams containing different fibre lengths. The compressive strengths of UHPFRC varied from 197 MPa to 204 MPa.

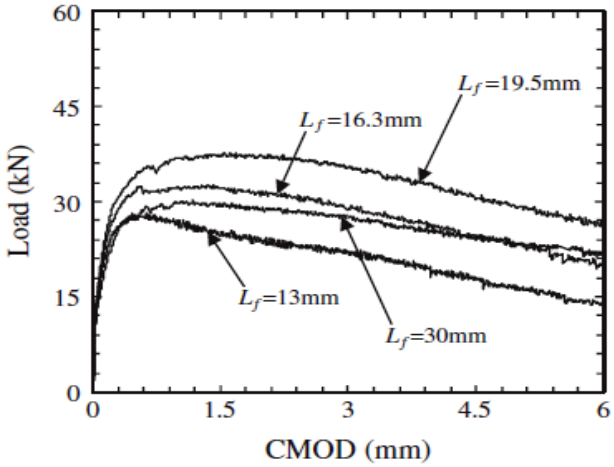

Figure 2.18 Effect of fibre length on the load–CMOD curves for UHPFRC beams (Yoo et al., 2014)

2.6 PRESTRESS LOSS

The magnitude of prestress force present in prestressed concrete beams continuously reduces during the lifetime of the structure (Páez and Sensale, 2018) . The reduction of prestress force is commonly referred to as the loss of prestress. Immediately after release of the strands, the initial prestress force decreases due to the elastic shortening of the concrete at the level of the steel. From then on, it decreases continuously due to the combined effects of shrinkage and creep strains of the concrete and relaxation of the steel.

2.6.1 Shrinkage

Shrinkage is a contracting volume change of concrete caused by evaporation of water or hydration of cement. Actually, there are several types of shrinkage in concrete called plastic shrinkage, drying shrinkage and autogenous shrinkage. Plastic shrinkage occurs usually during the first few hours after placing the fresh concrete in the moulds. This type of shrinkage occurs when at an unprotected concrete surface water evaporates at a higher rate than the rate of arrival of bleed water from the lower layers of the concrete to the concrete surface while the concrete is plastic (Nawy, 2009; Soutsos and Domone, 2018). When concrete is already in a hardened state, a loss of capillary water due to evaporation as well as water absorption by concrete will result in drying shrinkage. Due to the slow movement of water towards the surface of the concrete, evaporation makes other particles more compact (MacGregor and Wight, 2005). The drying shrinkage is initiated in cement paste while the volumetric contraction is constrained by aggregates in concrete. Therefore large cement to aggregate ratios would result in greater shrinkage in the concrete. More finely ground cement leads to more shrinkage, since larger cement surface areas result in more absorbed water to be lost. In high strength concrete with a low water to cement ratio, there is no sufficient mix water to hydrate all the cement, leading the cement paste to subject to self-desiccation. Self – desiccation results in the removal of water from the capillary pores, leading to autogenous shrinkage (Soutsos and Domone, 2018). **Figure 2.19** shows the shrinkage strain over time from initial t_0 to the final time t. As illustrated in the figure, the strain ε_{sh} increases with time but the rate of shrinkage will diminish with time.

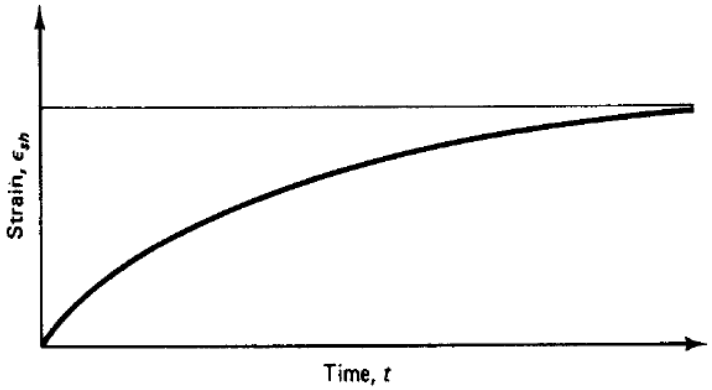

Figure 2.19 Shrinkage-time curve (Nawy, 2009)

Shrinkage is also affected by the shape and size of the concrete member. By keeping all factors identical, higher and quicker shrinkage would occur in a thick member than a thin one (ACI 209R-05).

The deformation of concrete with time is schematically shown in **Figure 2.20**. If the load is removed, after some period of time, an instantaneous recovery of the elastic strain occurs and then slower recovery of some of the creep takes place. As shown in **Figure 2.20**, the particular concrete was loaded at the age of 28 days that resulted in an instantaneous strain. The load was then sustained for 90 days. The creep is seen to increase the total deformation to almost 3 times as much as the instantaneous value. If the load was maintained, the deformation would have continued. When the load was removed the elastic– instantaneous strain recovered, and some creep recovery is seen to occur. If the concrete is reloaded at some later date, instantaneous and creep deformations develop again.

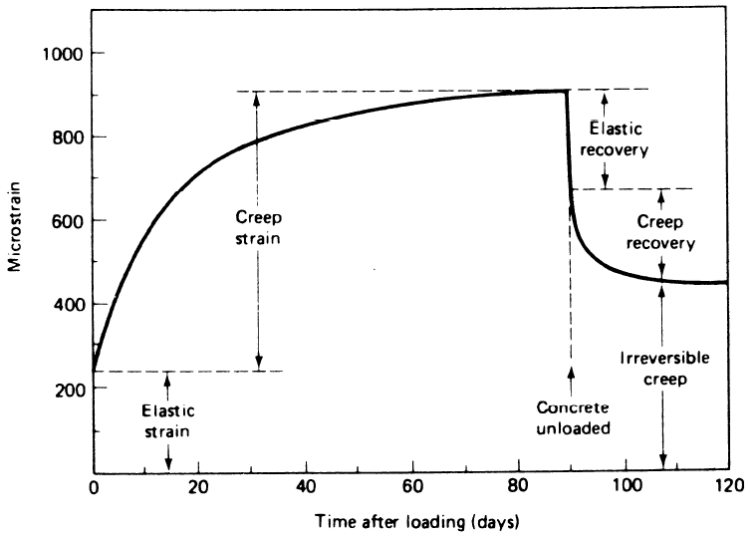

Figure 2.20 Time-Dependent strain in a concrete subjected to a sustained load for 90 days and then 30 days without a load (Neville et al., 1983)

2.6.2 Creep

Creep is defined as a tendency for concrete to slowly deform permanently under the influence of sustained stresses. When concrete is loaded in compression, it develops an instantaneous elastic strain (Wight and MacGergor, 2009). If the compression is sustained on the concrete over a duration of time, creep strains continue to develop due to the fact that absorbed water layers become thinner within the concrete under the load (Wight and MacGergor, 2009). Creep strain development occurs more rapidly initially after applying the load and the rate of creep tends to diminish with time. It is noteworthy that greater creep occurs in concretes with high cement contents, typical of UHPC. This higher creep is due to the lower aggregate content in the concrete because, like shrinkage, creep only occurs in the hydrated concrete paste (Wight and MacGregor, 2009).

There are two main types of creep called basic creep and drying creep. Basic creep refers to the change in strain as a result of a constant and sustained load when loss in moisture content is prevented, therefore basic creep is independent of the member size (ACI 209R-05). Basic creep always occurs when there is no moisture movement between concrete and ambient environment. On the other hand, drying creep can be defined as the additional creep that occurs when the specimen under load is also drying. This type of creep takes place when movement of the moisture is allowed. Drying creep is dependent on the size of the member.

The magnitude of shrinkage and creep is affected by concrete materials and mix design. The properties of aggregate have a considerable influence on the magnitude of shrinkage and creep losses in prestressed concrete over the lifetime of a structure including modulus of elasticity, aggregate content in concrete, absorption, cleanliness, and thermal expansion coefficient. However, modulus of elasticity is the most influential property (Mehta and Monteiro, 2006). In typical UHPC, high cement content is common. Mehta and Montiero (2006) observed that having a high cement content in concrete adversely affected shrinkage. Moreover, higher creep occurs due to the fact that, like shrinkage, only the hydrated concrete paste will creep (Wight and MacGregor, 2009). The term *creep coefficient* refers to the ratio of creep strain (after a long period of time) to elastic strain. The coefficient is affected by several factors including sustained load to the concrete compressive strength ratio, age at which the concrete was loaded, concrete element dimensions, the composition of the concrete and relative humidity (MacGregor and Wight, 2005; Nawy, 2009).

Loukili, Richard and Lamirault (1998) observed that thermal treatment of RPC reduced both shrinkage and creep. Curing the concrete at 90°C for 48 hours can reduce the creep of concrete specimens by complete drying of the concrete.

Garas, Kurtis and Kahn (2011) investigated the effect of thermal treatment on the creep in UHPC. They concluded that thermal treatment at 60 °C for 72 h and 90 °C for 48 h significantly decreased the compressive creep in comparison with the creep that UHPC with no thermal treatment experienced.

Creep and shrinkage values for UHPC have been recommended by AFGC (2002) and Japanese Society of Civil Engineers (JSCE) (2006). The AFGC (2002) recommends a total shrinkage strain of 550 microstrain and a creep coefficient of 0.8 when no steam treatment is applied. After standard steam curing (48-hours steam curing at 90°C) is applied, shrinkage strain is considered to be zero and a creep coefficient of 0.2 is recommended. Similar to AFGC (2002), JSCE (2006) recommended total shrinkage 550 microstrain and a creep coefficient of 1.2, in the absence of steam treatment. The JSCE recommends that a creep coefficient of 0.4 be used when UHPC is subjected to steam treatment. The JSCE provides recommended shrinkage strains for UHPC exposed to steam treatment, as seen in **Table 2.7**.

Table 2.7 Typical shrinkage strain values (10^{-6}) of UHPC (JSCE, 2006)

Standard heat curing (steam treatment)	**Age of UHPC**				
	< 3	4-7	28	90	365
	50	30	0		

2.6.3 Relaxation loss

Beside creep in concrete, prestressing steel undergoes creep because of constant strain with time, as well. The creep in the steel is called relaxation loss. It happens when the prestressing steel is initially stressed to more than half of its yielding stress. Higher initial prestressing results in increased relaxation loss. Besides that, temperature and type of steel also affect the relaxation loss (Marshall and Robberts, 1996).

2.7 BOND BEHAVIOUR IN PRESTRESSED BEAMS

Bond is necessary not only to allow composite action of steel and concrete, but also to control structural behaviour with sufficient ductility. Reinforcement for concrete members is based on the assumption that the reinforcement has minimum required anchored. If less than required anchorage is provided, the structure will be unable to resist the flexural, shear or torsional forces designed for, and if actual loads approach those assumed in design, a premature failure is likely to occur. Anchorage of reinforcement is generally provided by bond between the reinforcement and the concrete along a length of bar or tendon. In the case of precast, pretensioned construction, anchorage of prestressing bars is usually accomplished by means of bond along a straight length of each prestressing bar.

2.7.1 Bond definition

In prestressed concrete, the prestressing force is transferred to the concrete by bond at the end region of a member. The distance along the length of the member in which the effective prestressing force, f_{se}, is developed is called the transfer length. The stress and strain behaviour is assumed to be linear in the transfer zone for standard seven-wire prestressing strand (Cousins et al., 1990). Linear behaviour makes the bond stress uniform in the transfer zone.

The additional length required to develop an increase in prestressing bar tension from the effective prestressing stress, f_{se}, to ultimate strength of steel, f_{ps} is called the flexural bond length. The summation of these two lengths is called the development length. These lengths were best illustrated by Cousins et al. (1990) as seen in **Figure 2.21**.

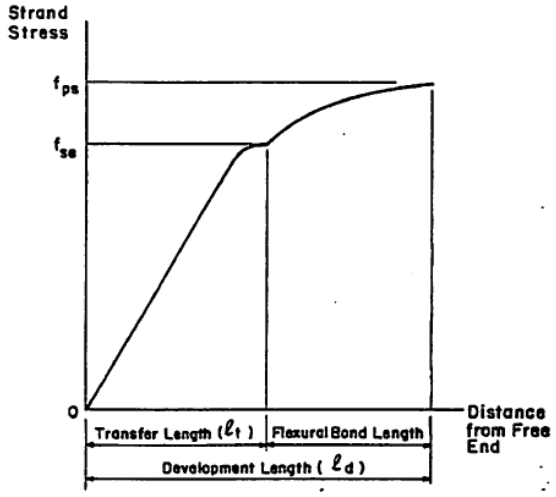

Figure 2.21 Variation of strand stress within the development length (Cousins et al., 1990)

2.7.2 Bond mechanisms

Combinations of several mechanism have been shown to contribute to bond between deformed bars and concrete, including adhesion, Hoyer effect and mechanical interlocking. These mechanisms can work singly or in combinations to resist slippage of reinforcing in concrete (Russell and Burns, 1993). Friction was found to play a large role in bond resistance (Janney, 1954), contributing to the Hoyer effect and mechanical interlocking.

Adhesion. Adhesion is a thin layer of glue that chemically forms an adhesive bond between the steel reinforcing and the concrete. However, once the reinforcing slips, adhesion is lost, and the bond stress that had been developed by adhesion drops to zero and the bond stress forms via other bond mechanisms. Adhesion does not contribute to the bond in the transfer zone (Russell and Burns, 1993), since the transfer zone is characterized by the bar moving relative to the surrounding concrete.

Hoyer effect. Hoyer effect contributes significantly to bond in the transfer zone. When a bar is stressed, the bar becomes longer and due to Poisson's effect the bar gets thinner. When a prestressing cable is cut, the release of the stress causes the prestressing bar to regain its original diameter towards the end of the transfer length, but this expansion is resisted by the concrete. The change of diameter from the original value (at the end) to the reduced value (after the transfer length), creates a wedge effect between the strand and concrete. As a result, the prestressing bar produces a normal force on the concrete, causing friction resistance surrounding the prestressing bar (see **Figure 2.22**). Once an external load is applied, the stress in the strand increases and the prestressing bar diameter reduces again. Thus, the frictional forces from the Hoyer effect reduce making the mechanical interlock the only force bonding steel and concrete.

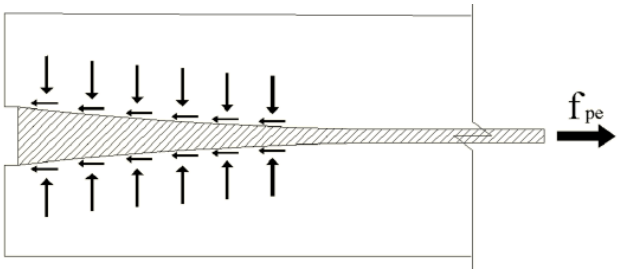

Figure 2.22 Hoyer Effect (Russell and Burns, 1993)

Mechanical Interlock. When the prestressing bar slips through the concrete due to prestressing or external loading, the concrete ridges formed around ribbed bars, resist the movement. This mechanism is known as mechanical interlock. This mechanism not only contributes to the bond around the strand in the transfer zone, but also, it is the main form of resistance in flexural bond (Russell and Burns, 1993).

2.7.3 Bond Failure in Beams

General bond failure occurs when high flexural bond stresses is extended to the transfer zone of a pretensioned member (Janney, 1954). An increase in the tensile stress of rebar in the transfer zone diminish the Hoyer's effect, making the bond stress due to mechanical interlock inadequate to resist steel rebar movement leading to sudden bond failure. Russell and Burns (1993) reported that bond failure also occurs when web-shear cracks propagate to the level of the strand in the transfer zone. The same type of failure was observed by Deatherage et al. (1994) and Mitchell et al. (1976).

In general, any significant increase in strand tensile stress in the bond zone will lead to a general bond failure by occurrence of slip between the steel rebar and concrete which takes place over a finite distance to release the high bond stresses (Janney, 1954; Hansen and Kaar, 1959). Since either flexural or shear cracking lead to high tension in strands, Russell and Burns (1993) concluded that if crack formation extends to the bond zone, especially the transfer zone, bond failure will occur.

Slip of deformed bars occurs due to either splitting of concrete by wedging action, or crushing of concrete in front of the ribs, leading to bar pull-out as a result of bond failure (Rehm, 1961; Lutz and Gergely, 1967).

Tepfers (1973) showed that when specimens are tested in pull-out tests, splitting failure can be predicted using Timoshenko's (1930) thick-walled cylinder formulas as an estimation for the concrete cover. He analysed the stress state in the concrete under bond forces and used a concrete ring model (see **Figure 2.23**) to evaluate the cracking resistance of the concrete cover as well as the peak bond stress in the specimens when the cover cracks.

Bar pull-out due to bond failure occurs if the volume of concrete surrounding the reinforcing bar is relatively large or the concrete is well confined against the splitting force (Eligehausen

et al., 1982; Filippou et al., 1983). On the other hand, splitting of concrete occurs if the reinforcing bars are closely spaced or the concrete cover is relatively small. When tensile splitting force generated by the bond action exceeds the capacity of the ring, bond failure occurs by splitting of the concrete cover due to formation of cracks parallel to the axis of the bars (Orangun et al., 1975; Cairns and Jones, 1995).

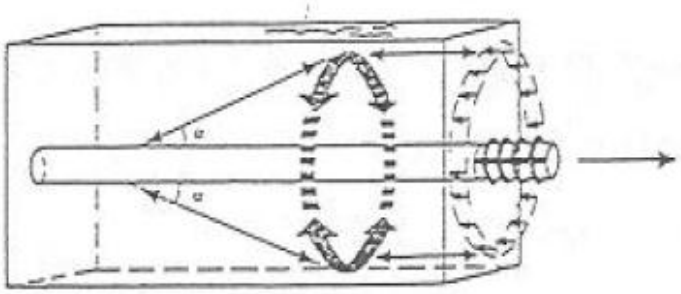

Figure 2.23: View of tensile ring (Tepfers, 1973)

Goto (1971) conducted tests to clarify the propagation of different types of cracks including internal cracks, secondary cracks and longitudinal cracks around the tensile reinforcing bars. He observed that the surface deformation of the reinforcing bars had a considerable effect on the formation of internal cracks. The results showed that internal cracks had a considerable influence on the bond mechanism between the steel and concrete. The angles of these cracks were normally within the range of 45 to 80° to the bar axis. The internal cracks formed around the reinforcing bars in concrete cylinders as shown in **Figure 2.24**.

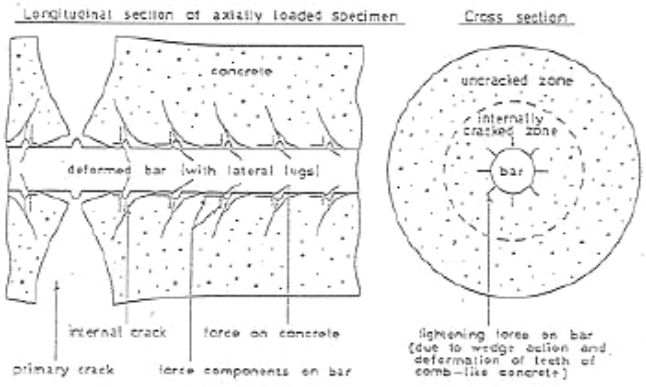

Figure 2.24 Internal cracks around the reinforcing bar embedded in concrete (Goto, 1971)

2.7.4 Factors Affecting Bond strength and transfer length

Over the years, many studies have been conducted to investigate the transfer length and the development length of prestressing strands. There are many factors that have been found to influence the development and transfer length and eventually bond behaviour. Some factors include: strand size (diameter), strand stress level, concrete strength, time dependent effects (losses), type of release (gradual or sudden), consolidation and consistency of concrete around strand, surface condition of strand (clean, rusted, epoxy-coated), confinement, cover and spacing, type of strand (stress relieved, low relaxation) as well as type of loading (static, repeated, impact) (Zia and Mostafa, 1977). Since only some parameters that affect bond strength were studied, the literature review covers only the relevant parameters.

2.7.4.1 Strand (bar) Size

An increase in strand diameter results in an increase in transfer and development lengths (Kaar et al., 1963). They also reported that the relationship between strand diameter and transfer length at release was approximately linear. Several studies by researchers such as Mathey and Watstein (1961), Eligehausen et al. (1982), Soroushian and Choi (1989) and Sozen and Moehle (1990) indicated a reduction in bond strength for increased bar size.

2.7.4.2 Strand (bar) geometry

Several research studies have reported the influence of deformation patterns and rib geometry on bond (Abram, 1913; Rehm, 1961; Goto, 1971; Savic et al., 2018). Abrams (1913) investigated the bond resistance of plain and deformed reinforcing bars by conducting pull-out and beam test. The test results revealed that higher bond resistance was achieved by using deformed bars than plain (smooth) bars.

Rehm (1961) reported that when a reinforcing bar slips, either splitting or pull-out can occur. The type of failure depends on the ratio of rib spacing to the rib height. If this ratio is greater than 10 and the rib face angle (the angle between the face of the rib and the longitudinal axis of the bar, *a* in **Figure 2.25**.a) is greater than 40°, the concrete in front of the rib crushes, leading to the formation of wedges and the development of tensile stress perpendicular to the bar axis (**Figure 2.25**.b). This phenomenon leads to splitting of surrounding concrete by the formation of transverse cracking caused by tensile stress. He observed that if the ribs had a spacing to height ratio of less than 7, with a rib face angle greater than 40°, the concrete in front of ribs gradually crushes, leading to a pull-out failure. Lutz, Gergely, and Winter (1966)

also observed that if the rib face angle is less than 30°, no crushing of concrete occurs. Skorobogatov and Edwards (1979) concluded the same, based on tests using bars with face angles of 48.5° and 57.8°. They reported that these different face angles are not affecting bond strength, because the high face angle is flattened by the crushed concrete in front of the ribs.

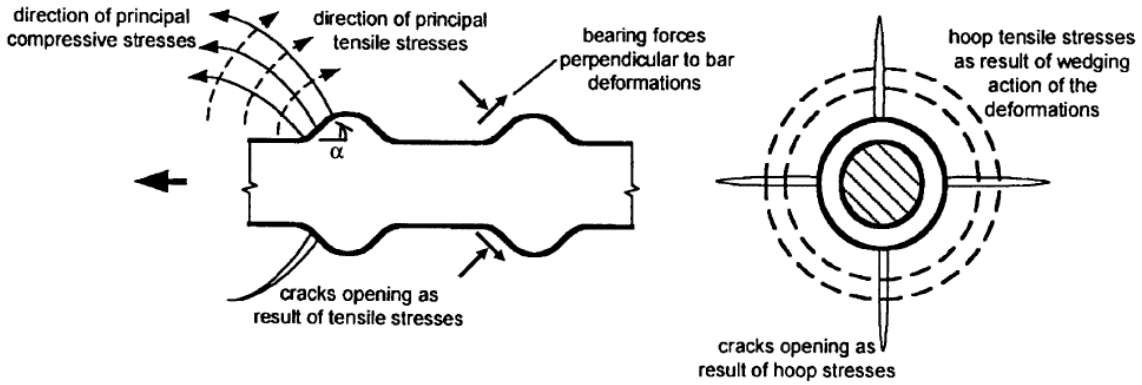

Figure 2.25 a) Rib face angel, b) tensile stress due to wedging (ACI 408 Committee, 2003)

2.7.4.3 Concrete Strength

There are numerous studies investigating the effect of compressive strength on transfer and development length (Momeni et al., 2018; Yang et al., 2018). The effect of compressive strength originates from bond mechanisms over the transfer length which is primarily due to friction between the strand and the concrete. The friction is caused by radial expansion of the strand at release that takes places due to Poisson's effect. Barnes, Grove and Burns (2003) concluded that this friction depends on how well the concrete surrounding the strand behaves under the pressure caused by the increasing circumference. Radial cracking in the concrete surrounding the strand occurs due to the release, leading to the concrete softness. Therefore, the concrete behaviour against radial expansion improves for higher tensile strength and stiffness. Higher compressive strength can enhance both tensile strength and stiffness (Barnes et al. 2003). So, by compressive strength enhancement, better friction and shorter transfer lengths can be achieved (Mitchell et al., 1993; Lane, 1998; Ramirez and Russell, 2008).

Numerous studies have been conducted to develop equations to estimate the transfer and development length. In almost all equations, the effect of concrete properties is represented as

the square root of the compressive strength (Zia and Mostafa, 1977; Mitchell et al., 1993; Lane, 1998; Ramirez and Russell, 2008).

A recent study on the effect of compressive strength on bond strength was conducted by Khandaker and Hossain (2008), who performed pull-out tests on normal and lightweight concrete. They found that bond strength increases with the enhancement of compressive strength. Holschemacher et al. (2005) observed that ultra high-strength concrete has very high bond strength and stiffness as a result of high compressive strength and modulus of elasticity.

Yuan and Graybeal (2015) observed that an increase in the compressive strength of the UHPC results in bond strength enhancement. They reported that compressive strength, or the square root of compressive strength, cannot represent UHPC bond strength. In order to evaluate the bond strength of steel bars in UHPC, other UHPC mechanical properties, especially those relevant to the post-cracking tensile behaviour of UHPC may be more appropriate to consider. For high-strength concrete, crushing of the concrete in front of the bar ribs is prevented by the higher bearing capacity which results in local slip reduction. Due to the reduced slip, fewer ribs transfer load between the steel and the concrete, which leads to the local tensile stresses increasing, causing splitting failure in the concrete, before achieving a uniform distribution of the bond force (Azizinamini et al., 1993; Azizinamini et al., 1995).

Dancygier, Katz and Wexler (2010) observed that the bond strength in HSC specimens was higher than that of NSC specimens. The strength difference was more pronounced in the presence of fibre. High-compressive strength concrete is mostly achieved by the addition of silica fume. Studies show that the presence of silica fume reduce bond strength by providing a smooth failure surface (Hamad and Itani, 1998). However, this effect is counteracted by other factors like fibres and high compressive strength, and their combination would result in a net increase in the bond strength.

2.7.4.4 Concrete cover

One of the factors that affects the bond strength is concrete cover (Saleem et al., 2012; Savic et al., 2018). Yerlici and Ozturan (2000) also reported that the thickness of cover concrete can be referred to as an important factor affecting the bond strength in reinforced high-performance concrete. Marchand et al. (2016) described the effect of concrete cover on the embedment length in a graph expressing the bond stress as a function of the compressive

strength and the ratio of the bar diameter with respect to the concrete cover. Limited concrete cover has been listed by Saleem et al. (2012) as one of the factors which reduces the bond strength. They believed that limited cover could not only lead to premature failure, but also make it more difficult to provide shear stirrups to avoid shear and splitting failure.

Yuan and Graybeal (2014) recently listed concrete cover as one of the factors affecting the bond strengths of UHPC. Sozen and Moehle (1990) and Yuan and Graybeal (2015) indicated that bond strength increases with side cover. Tastani and Pantazopoulou (2010) concluded that splitting failure can be avoided by both transverse reinforcement and increased cover.

Fehling and Lorenz (2013) reported that increasing cover widths and embedment lengths enhanced the bond strength, provided that these factors are sufficient for bar yielding. E.g. with a concrete cover of 1.5*ds* (*ds* is diameter of reinforcing steel) and an embedment length of 8*ds* yielding of the bar occurred; for specimens with a concrete cover of 2.5*ds* and an embedment length of 5*ds* the bars experienced yielding.

2.7.5 Effect of Fibre on Bond performance

Harajli and Salloukh (1997) reported that the inclusion of up to 2% hooked fibres (by volume fraction), causes bond strength to increase by up to 55%. Horiguchi, Saeki and Fujita (1988) found that increasing the fibre content to 2.5% (by volume), improved the bond strength by 60%. Harajli, Hamad and Karam (2002) investigated the effect of fibres on bond behaviour in normal-strength concrete (28 MPa). They found that increasing fibre content from 1 to 2% (volume fraction of fibres), caused bond strength to improve by 26 and 33% when compared to plain NSC.

Hamad, Harajli and Jumaa (2001) studied the effect of steel fibres on bond strength of high-strength concrete (78 MPa compressive strength). High-strength concrete beams were tested with spliced bars. It was observed that the presence of steel fibres in the splice region increased the bond strength as well as the ductility (see **Figure 2.26**). They concluded that steel fibres help to confine the splices, thus changing the brittle failure mode to a ductile one.

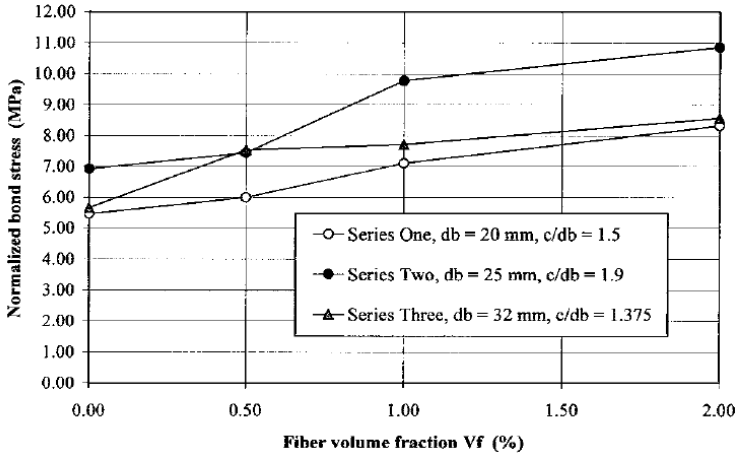

Figure 2.26 Variation of normalized bond stress with fibre content (Hamad et al., 2001)

Plizzari (1999) observed that higher displacement ductility occurred for specimens containing 0.38% (volume fraction) of steel fibres in pull-out tests. Fibres were more efficient in HSC. He reported that fibres limit radial cracking near the reinforcement bar, leading to the confinement action around the bar. This phenomena results in bond strength improvement caused by the inclusion of fibres. Chao, Naaman and Parra-Montesinos (2009) concluded that limiting the crack width through bridging and confinement through the use of fibres, led to a higher bond resistance. This also results in more ductile bond failure.

Azizinamini et al. (1993) carried out bending experiments to study the bond between deformed steel bars and HSC. They concluded that bond stresses that developed in deformed bars in HSC are highly non-uniform along the bar length. These non-uniform bond stresses developed such that higher bond stress developed near the loaded end of the bar, reducing away from this point. The bond stresses in HSC actually only developed along a few ribs of the deformed bar, near the applied load. They hypothesized that, although uniform stress distribution along the bar length is a common design assumption for smooth bars, bond failure may occur in high-strength concrete prior to uniform stresses developing.

Yerex, Wenzel and Davies (1985) studied the effect of polypropylene fibre reinforcement on the bond between concrete and conventional mild steel reinforcement. They conducted ASTM Standard Pull-out Tests. The results showed that the addition of polypropylene fibres to the concrete did not adversely affect the bond strength. Furthermore, increasing the fibre content did not affect the bond strength or transfer length.

Ezeldin and Balaguru (1989) investigated the effect of steel fibre on the bond behaviour of normal strength concrete (34.5 MPa) and high-strength concrete (75.9 MPa). They observed that the presence of fibres modified the explosive concrete splitting (failure type) to a ductile failure. Fibres also improved the bond strength of those specimens having large bar diameters (16 mm or more), when compared to those having 9 mm diameter bars, as seen in **Figure 2.27** (a). Fibres contribute to confining the concrete, resulting in bond strength enhancement when larger bars are used. The increase in compressive strength was attained due to the reduction of water content, as well as inclusion of silica fume in the mix. Although the presence of silica fume enhanced the bond strength (see **Figure 2.27** (b)), it caused more brittle bond failure.

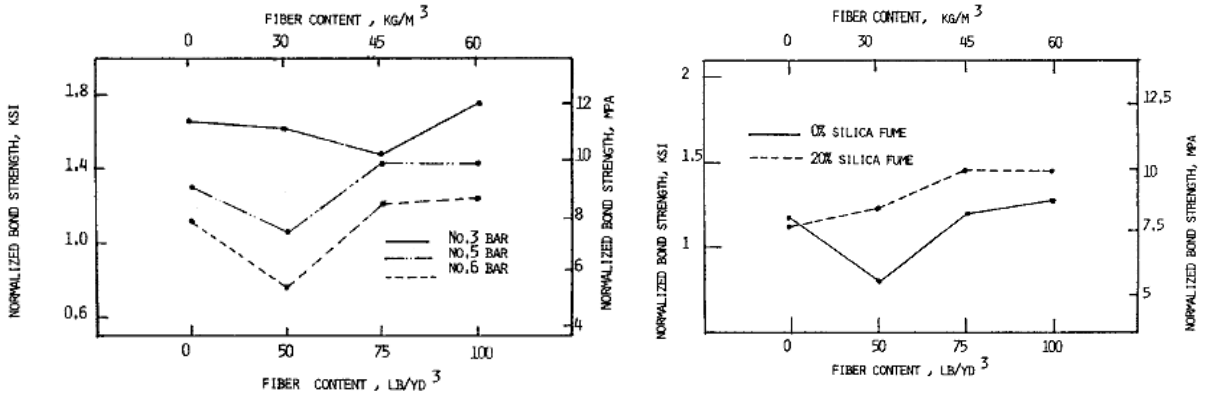

(a) (b)

Figure 2.27 Bond strength versus fibre content a) different bar sizes, b) different silica fume content (Ezeldin and Balaguru, 1989)

Harajli (1994) observed the improvement in the ductility of splitting bond failure, when compared to conventional concrete, unconfined by ordinary transverse reinforcement, in the presence of steel fibres. The improvement in ductility is particularly significant if bond failure occurs prior to yielding of the reinforcing bars.

Dancygier, Katz and Wexler (2010) reported that the addition of fibres can reduce the bond strength by causing local disturbance of the concrete matrix near the embedded rebar. Chan, Chen and Liu (2003) also observed a reduction in bond strength caused by the addition of fibre.

2.7.6 Anchorage zone

The anchorage is used to maintain the tendons in tension until the concrete has hardened sufficiently. Once the concrete in the member has reached sufficient strength, tendons are

released to transfer prestressing force to the member. The mechanism by which the prestressing force is transferred to the concrete at the end of a prestressed concrete member can cause the formation of longitudinal cracks in these regions. These cracks can cause the member to become unserviceable and, in extreme cases, can cause failure of the member if no suitable reinforcement is provided to control the crack formation. These longitudinal cracks are called spalling cracks in the case of prestressed and post-tensioned members and bursting cracks in the case of post-tensioned members (Marshall and Robberts, 1996).

In a prestressed member, the large concentrated forces (prestressing forces) act on the anchorage zones and gradually transfer to the surrounding concrete by the action of bond over the transfer length. This action causes development of large tensile stresses in the concrete in the anchorage zones, leading to the formation of spalling cracks in these zones. To limit the width and length of the crack providing stirrups is necessary. In a post-tensioned member, the prestressing force is transferred from the tendon to the concrete by direct bearing through the anchorage. As a result, a cone of highly compressed concrete develops leading to split the concrete behind the anchorage. This splitting action causes transverse bursting tensile stresses leading to the formation of longitudinal bursting cracks. To control bursting cracks spirals or stirrups can be used behind the anchorages (Marshall and Robberts, 1996).

2.8 FAILURE OF REINFORCED CONCRETE BEAMS

In general, a RC beam can fail due to either moment or shear action. The type of failure is dependent on several parameters including the shear span to effective depth ratio (a/d), longitudinal reinforcement ratio, presence or absence of shear reinforcement. Failure in flexure most probably occurs in slender beams (a/d>4) due to crushing of the compression region near the point of loading. Prior to crushing, the longitudinal reinforcement may or may not yield, depending on the amount of reinforcement. If the reinforcement experiences extensive yielding, the beam will exhibit a ductile behaviour prior to failing. If the amount of reinforcement is too small, the reinforcement may rupture before the crushing of concrete (Dinh, 2009).

For short (a/d <3) or slender beams with a high tensile reinforcement ratio, failure may occur due to the formation of diagonal cracks. These cracks may form at the beam mid-height or from the top of flexural cracks. Shear failure in beams without shear reinforcement occurs in

one of these forms: Splitting of concrete under diagonal tension crack, Web crushing under compression, Splitting or crushing of concrete in the compressive zone, Splitting of concrete along the longitudinal reinforcement. For more information, see **Appendix A.**

2.8.1 Parameters affecting shear resistance

Prestressed/non-prestressed concrete beams under the combination of shear forces and bending moments may fail in shear before reaching ultimate flexural strength, if it is not properly designed for shear. Shear failure can occur very abruptly and without any warning due to a lack of ductility. The parameters which affect the shear strength of prestressed/non-prestressed concrete beams without shear reinforcement are: the geometric configuration of the cross-section, the concrete strength, the level of prestressing, the position of the prestressing tendons and the shear span.

2.8.1.1 Geometric configuration

The effect of the geometric configuration of cross-section has been studied in several investigations (Swamy and Bahia, 1985; Rosenbusch and Teutsch, 2002; Chen et al., 2018c). Ferguson and Thompson (1953) as well as Leonhardt and Walther (1961) showed that by increasing the web width, the failure loads increased.

The effect of flange dimensions on the shear strength was investigated by Taub and Neville (1960) to compare the shear strength of rectangular and T beams with similar web width. The effect of flange width on shear strength was reported by Placas and Regan (1971) for T beams with a 150 mm web width. In beams with 300 mm or wider flanges, greater ultimate shear strength (about 20%) was observed in comparison to rectangular beams. It was concluded that only the portion of the flange immediately adjacent to the web could transfer a component of the shear in the compression zone. Rosenbusch and Teutsch (2002) showed that by changing the flange width (from 20 to 30, and to 40 inches) no significant changes occur in load versus deflection response. According to their study, beams with a flange thickness of either 4 inches or 6 inches, responded comparably to rectangular beams with the same height.

2.8.1.2 Beam size

The effect of beam size was investigated by Leonhardt and Walther (1961), Kani (1967) and Taylor (1972). Leonhardt and Walther (1961) concluded that shear strength was fairly

independent of the beam size in beams with external similarity and constant bond quality. Kani (1967) studied the effect of different beam depths on the shear capacity. It was found that shear stress at failure decreased with increasing beam depth. Kani concluded that by increasing the depth, due to the increase of 'wedging bond action' of the reinforcement, splitting forces increased, leading to the failure of deeper beams by splitting along the reinforcement. This behaviour was not observed in smaller beams.

Taylor (1972) showed that by changing the coarse aggregate size in proportion to the beam size, the size effect could be reduced. For concrete beams with depth to width ratios larger than 4 (d/b>4), a reduction factor of 0.6 was suggested by Taylor (1972).

2.8.1.3 Concrete compressive strength

The cause of the failure of the beam under shear can be attributed to the diagonal tension crack formation. The diagonal cracking load can be related to the tensile strength of concrete. In several studies it was found that the tensile strength has a proportional relation to the compressive strength (Sozen et al., 1959; Evans and Hosny, 1958; Evans and Schumacher, 1963; Hsu, 2017).

Narayanan and Darwish (1987) tested steel fibre reinforced concrete and reported that for the same fibre factor ($F= (L_f/D).\ \rho_f.\ d_f$), the shear strength increases with increasing compressive strength (from 42 MPa to 62 MPa). Moreover, the rate of increase in shear strength also improved when the fibre factor was increased from 0.19 to 0.50. **Figure 2.28** displays the effect of compressive strength on the shear strength of fibre reinforced beams with different ranges of longitudinal reinforcement and shear span to depth ratios.

Generally, an increase in SFRC compressive strength leads to beam shear strength improvement. Kwak et al. (2002) found that when the concrete strength was doubled while keeping everything else the same, the shear strength was enhanced by about 20% for slender beams (a/d=4) and 26% for shorter beams (a/d=2). Moreover, compressive strength appeared to affect shear cracking strength more than failure load.

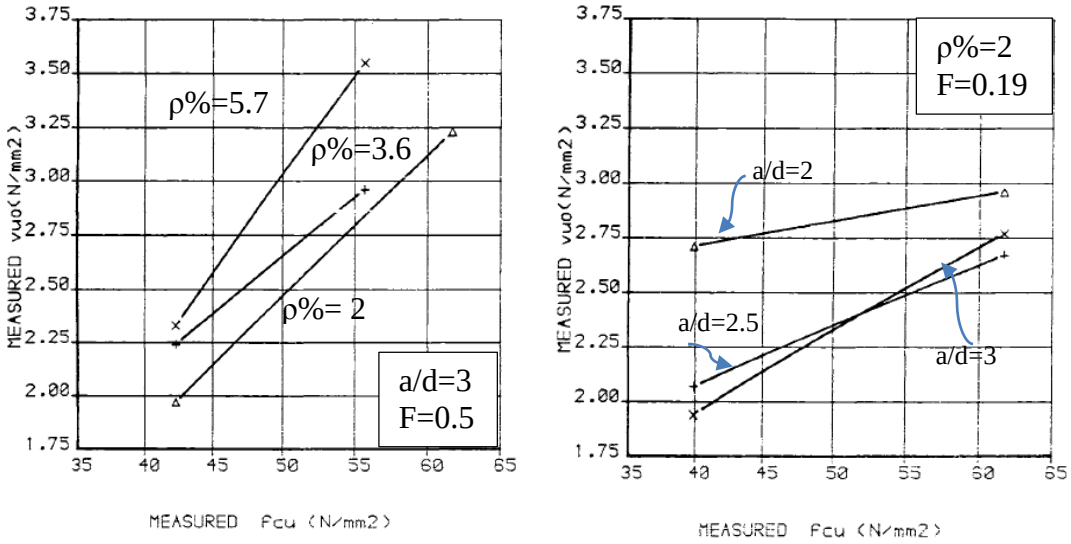

(a) (b)

Figure 2.28 Effect of compressive strength on the shear strength of RC beams with varying a) longitudinal reinforcement, b) shear span-depth ratio (Narayanan and Darwish, 1987)

2.8.1.4 Longitudinal reinforcement ratio.

The effect of longitudinal tensile reinforcement ratio on beam shear strength has been extensively investigated by several researchers (Ashour et al., 1992; Swamy et al., 1993; Tompos and Frosch, 2002; Johnson, 2018). It was concluded that a higher ratio of tensile longitudinal reinforcement resulted in a higher shear stress at failure due to increased dowel action and a deeper compression zone.

In UHPC beams without shear reinforcement, the contribution of dowel action to the shear strength becomes considerable and also is an important factor in assuring a non-brittle type of shear failure.

The effect of different reinforcing steel ratios (0.2, 0.35, 0.41 and 0.5) on the ultimate shear load of UHPC reinforced girders was studied by Wu and Han (2009). **Figure 2.29** displays the effect of reinforcing steel ratio on the behaviour of the girders with shear span to effective depth ratio of 4 and 2% steel fibres (volume fraction). Although shear resistance capacity was expected to be very low, the girder with the lowest reinforcing ratio of 0.2 failed in flexure because of the low reinforcing ratio. The other girders with higher reinforcing ratios experienced shear failure.

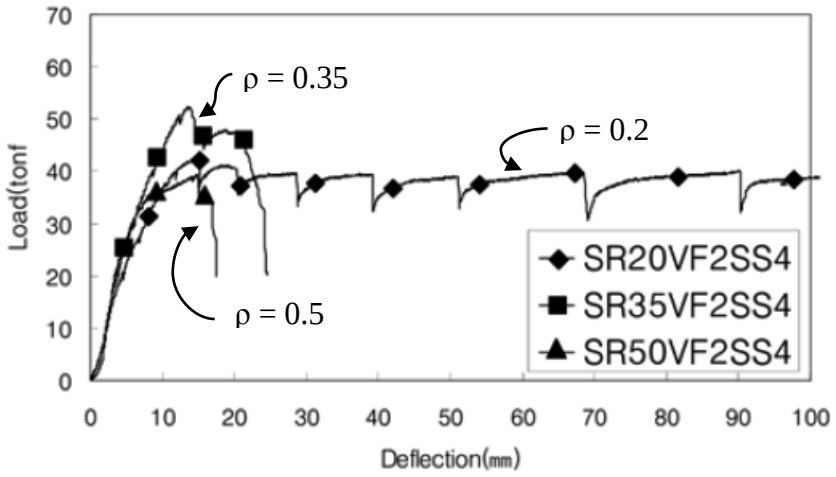

Figure 2.29 Effect of reinforcing steel ratio on the behaviour of the girders with a/d =4 and 2% steel fibre (Wu and Han, 2009)

2.8.1.5 Prestressing

The extra compressive stresses which are induced by the prestressing force, reduce the final tensile stress caused by shear (Dolan and Hamilton, 2019). Narayanan and Darwish (1987) studied the shear strength of non-prestressed and prestressed beams with different levels of prestressing. Their results showed that shear strength improved when increasing the prestressing force. However, the pattern of failure in shear for non-prestressed beams was similar to that of prestressed beams. In other words, the failure modes for beams were not affected by prestressing.

Voo, Foster and Gilbert (2006) investigated the effect of different levels of prestressing on UHPC girders. They reported, that by comparing the crack patterns in the shear beams with 0%, 15% and 30% prestressing (of ultimate tensile strength of strands), the shear cracking load was affected marginally by the prestressing level. However, level of prestressing had a significant influence on the rate of crack growth. Moreover, by increasing the level of prestressing from 0% to 15% that ultimate shear strength was enhanced by 16%. **Figure 2.30** displays the crack patterns of non-prestressed and prestressed beams, with two different prestressing levels (15% and 30% of ultimate tensile strength). All the girders failed in shear by formation of diagonal cracks in the web, regardless of levels and presence of prestressing.

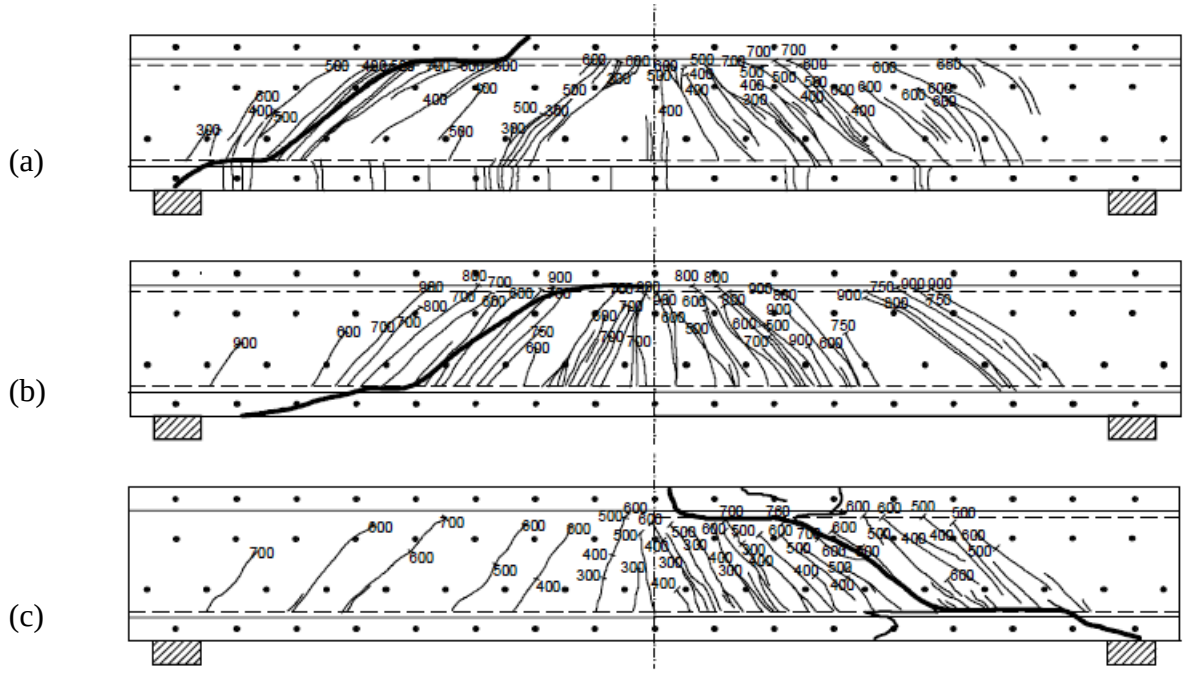

Figure 2.30 Crack patterns of beams a) non-prestressed; different level of prestressing of, b) 30% of ultimate tensile strength, c) 15% of ultimate tensile strength (Voo et al., 2006)

2.8.1.6 Shear span ratio

Shear span-depth ratio played a major role on shear strength of beams (Li and Leung, 2017). Ultimate shear strength decreases with increasing a/d (Batson et al., 1972; Mansur et al., 1986; Lim et al., 1987; Murty and Venkatacharyulu, 1987; Ashour et al., 1992; Li, Ward and Hamza, 1992).

Kwak et al. (2002) observed that by increasing a/d, the average shear stress at failure consistently decreased. Similar results were obtained for the average shear stress at the onset of shear cracking. The reason can be attributed to the reduced effectiveness of the arching action and dowel action as a/d increases. Besides, the beams with small a/d ratios showed higher loading capacity after shear cracking than the beams with large a/d ratios. As an example, at an a/d=2.0, the fibre reinforced beams sustained up to 311% of the cracking shear, while in the beams with a/d=3.0 and 4.0, an ultimate shear up to 230% of the cracking shear was sustained. This difference can be due to not only the instability of the arch mechanism at large a/d ratios, but also the interaction between flexural and shear modes of failure. Since, failure mode changed from shear to flexural by increasing a/d from 3 to 4 in the fibre reinforced concrete beams.

2.8.1.7 Presence of fibre

Dhonde (2006) reported that beams containing fibre exhibited better performance in controlling shear crack widths than beams with mild steel shear reinforcement. It was indicated that the replacement of stirrups by steel fibres plays an important role in the control of crack width and propagations.

Padmarajaiah and Ramaswamy (2001) found that in fully prestressed beams with a fibre content of 1.5 %, a shear strength enhancement up to 20 % was observed at the first crack as well as the peak load. They also found that the inclusion of fibre alters the a/d ratio that divides the flexure and shear critical failure mode. Thomas and Ramaswamy (2006) observed shear strength enhancement by inclusion of fibres. Moreover, they concluded that high strength concrete benefits more from fibres due to stronger bond between fibres and high strength concrete.

Meda et al. (2005) concluded that prestressed beams containing steel fibres exhibited a similar, or even better, post cracking behaviour than the beams with a minimum amount of shear reinforcement. They also observed the effect of steel fibres on the reduction of the shear crack widths, which led to improvement of concrete durability.

Tan, Paramasivam and Murugappan (1995) reported that the addition of steel fibres enhanced the ultimate shear strength of partially prestressed concrete (PC) beams. The shear cracking load was enhanced by increasing the fibre content. They mentioned the possibility of shear reinforcement replacement by an equivalent amount of steel fibres, without significantly affecting the behavior and shear strength of partially prestressed concrete beams.

Langsford, Lloyd and Sarker (2007) conducted experiments on fully prestressed steel fibre reinforced concrete beams without stirrups. The shear span to depth ratio was ranging from 1.5 to 2 and steel fibre contents from 0.5 to 1.2 % volume fraction. They found that adding 0.5 % fibre (volume fraction) caused the shear carrying capacity to improve by 30% and 25 % at a/d ratios of 2.0 and 1.5, respectively. The improvement in shear capacity was 50% and 33 % with the addition of 1.2 % volume fraction of steel fibres for a/d ratios of 2.0 and 1.5, respectively.

Narayanan and Darwish (1987) studied the shear strength of simply supported rectangular prestressed concrete beams, containing steel fibres as web reinforcement. It was found that the ultimate shear strength was enhanced by up to 95 % through the addition of steel fibres. Moreover, the failure mode for beams was not affected by prestressing.

Voo, Foster and Gilbert (2006) studied the ability of fibres to resist shear in UHPC prestressed beam. The beams with a depth of 650 mm were designed to fail in shear. Two different types of fibre (13 mm straight fibres with 1800 MPa tensile strength and 30 mm hooked fibres with 1200 MPa tensile strength) were used separately or blended to reinforce the UHPC. They concluded that neither the quantity nor the types of fibre significantly affected the cracking load. However, fibre type influenced the rate of crack propagation as well as failure loads. They reported that by increasing the hooked fibre content and reducing the straight steel fibres volume fractions, a reduction in failure loads was observed. This showed that the hooked fibres were more affected by fibre fracture than the short straight fibres. There is a lack of information explaining if this behaviour was due to the lower tensile strength of hooked fibre or not.

Baby, Marchand and Toutlemonde (2013) investigated the combination of fibres and stirrups as shear reinforcements in UHPFRC I-beams. Two types of beams with I-shaped cross sections were chosen, including prestressed and non-prestressed beams. The beams were 3 metre long with a total depth of 380 mm. In the mixes, 13 mm and 20 mm straight steel fibres were used, with volume fractions of 2% and 2.5%, respectively. Shear failure with diagonal tension cracks, was observed in all beams, except the non-prestressed beams with stirrups. They exhibited large open diagonal cracks, although they failed in bending. The authors reported that shear strength was enhanced by the presence of stirrups in prestressed and non-prestressed beams. However, crack opening was controlled by stirrups before their yielding.

Wu and Han (2009) investigated the effect of different fibre volume fractions (1%, 2% and 3%) on the ultimate shear load of UHPC reinforced girders. They reported that by increasing the steel fibre volume fraction, greater force resisting capacity of the girder was achieved. Since higher tensile strength is achieved by higher steel fibre content, the softening is larger for the material with higher fibre volume fractions. **Figure 2.31** shows the effect of fibre content on the behaviour of girders with similar a/d ratio (4) and a longitudinal reinforcement ratio of 0.5%.

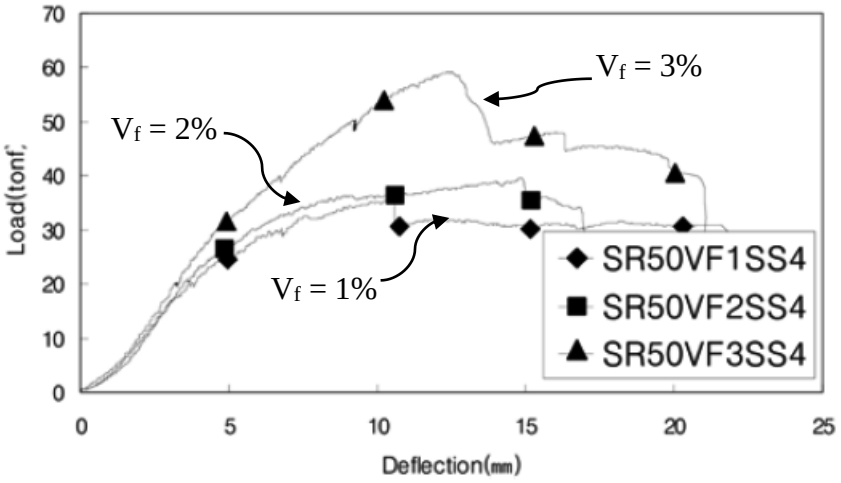

Figure 2.31 Effect of fibre on the behaviour of girders with similar a/d = 4 and ρ=0.5 (Wu and Han, 2009)

Kwak et al. (2002) reported that the addition of steel fibres in the concrete substantially affected the cracking patterns in the beams. The beams containing no fibres with a/d=2 experienced shear failure. By increasing the fibre volume to 0.50 and 0.75%, the failure mode changed to a combination of shear and flexure. Moreover, in the beams with a/d= 3 or 4, the failure mode changed from shear to flexure. They also reported the effect of fibre on enhancing the average shear stress at shear cracking. However, the ultimate shear strength benefits more than the cracking shear stress. The enhancement in ultimate shear strength was more pronounced than the cracking shear stress. **Figure 2.32** illustrates the effect of fibre volume on the ultimate shear stress.

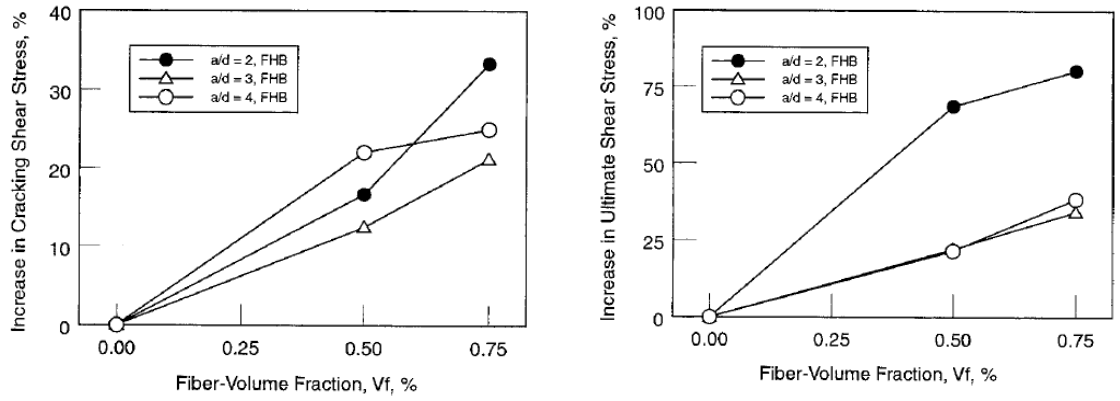

(a) (b)

Figure 2.32 Effect of fibre on a) cracking shear stress, b) ultimate shear stress (Kwak et al., 2002)

2.9 CONCLUSION AND STUDY MOTIVATION

From the review of existing literature it can be seen that there is interest in the modification of typical UHPC mix designs to make this type of concrete with superior mechanical properties more practical to use in large-scale projects. The modifications include the types of cementitious materials as well as aggregate type and size. It was concluded that other than silica flour or quartz powder, GGBS, fly ash as well as limestone powder can be considered as cementitious materials in UHPC. Besides, the typical fine aggregate size of 600 µm can be changed to include aggregate with bigger sizes (up to 5 mm). Moreover, by considering different curing regimes, UHPC can be made more appealing to industry.

Studies on bond performance concluded that different factors including bar size and geometry, concrete strength and cover influence bond strength and transfer length. Higher compressive strength leads to shorter development lengths. Fibres show a significant effect on the bond strength and bond failure behaviour.

There are different parameters that affect beam behaviour and types of failure under flexure. Effects such as cross-section shape, longitudinal reinforcement ratio and shear span ratio determine whether beams undergo flexural failure or shear failure. In some studies fibres were used to change the type of failure from shear failure to flexure by enhancing shear resistance.

Based on the literature review, UHPC is mostly limited to laboratory work and not widely applied in industry due to high manufacturing expenses. To make the applications of UHPC members more appealing to industry, more considerations and measurements in the manufacturing process are required to make UHPC more practical and economical. The evaluation of mechanical properties of UHPC will give an idea of the possibility for manufacturing UHPC using local materials while maintaining superior mechanical properties. Manufacturing practical and economical UHPC will make a valuable contribution to promoting the use of UHPC in South Africa.

CHAPTER 3 PRELIMINARY INVESTIGATION ON THE DEVELOPMENT OF A LOCAL MIX DESIGN AND CURING REGIME

3.1 INTRODUCTION

As the main aim of the thesis to promote UHPC utilization, comprehensive study is required to develop a local mix design. As a part of achieving the mix design, the materials used in the procedure are introduced. The step by step procedure which led to the final mix design is described. Economical aspect of the proposed mix design is evaluated. As part of the mix design study, the effect of different types of fibre on the mechanical properties of the achieved UHPC is discussed. The mechanical properties considered are compressive strength, elastic modulus, splitting tensile strength as well as direct tensile and flexural strength due to their importance for early-age and long-term properties required for UHPC and UHPFRC prestressed beams.

In prestressed beams (as an example of UHPC application), curing regime plays an important role not only due to the importance of achieving minimum early-age compressive strength at the time of wire releasing, but also to gain the high compressive strength (over 150 MPa) required for UHPC. Besides, considering a practical curing method is essential to promote UHPC application. So, a comprehensive study on a practical curing regime has been conducted. Different curing regimes were considered for each series of UHPC containing different types of fibre, including heat treatment in 85°C water for different curing durations (1, 3, 6 and 28 days) as well as standard curing regimes. To conduct further investigation on curing regime and its effect on the compressive strength of UHPC, heat treatment with different water temperatures (65°, 85° and 92°) was considered based on the literature review. Eventually the final mix design, incorporating only local materials as well as a practical curing regime is introduced.

3.2 MATERIALS

Although literature analysis played a significant role in the selection of materials of this study, the materials availabilities in the local markets of South Africa were the most

influential parameter in eventual decision-making. Thus this study focuses on local materials available in South Africa markets and the only imported materials used in this study are the fibres introduced below. The materials considered in the process of this thesis are listed as follows:

- Cementitious materials:
  - Portland cement (PC): CEM I 52.5N, CEM II/A 42.5R and CEM II/A 52.5N with relative densities of 3.14, 2.95 and 3.02 respectively;
  - Silica fume: condensed silica fume (CSF) and undensified silica fume (USF) with the relative densities of 2.2 for both;
  - Ground Granulated Blast Furnace Slag (GGBS) with the relative density of 2.93;
  - Fly ash (FA) with the relative density of 2.2.
- Aggregate:
  - Silica (<600µm) with relative density of 2.65;
  - Dolomite (600µm-1.18 mm) with relative density of 2.86;
  - Andesite (0.15-3.35 mm; 4.75-6.7 mm) with relative density of 2.96.
- Fibre:
  - Hook-ended fibre (ultimate tensile strength of 1000 MPa);
  - Micro fibre (ultimate tensile strength of 2500 MPa);
  - Locally available fibre (ultimate tensile strength of 1000 MPa).
- Chemical admixtures:
  - Polycarboxylate-based superplastisizer with a relative density of 1.06;
  - Finally, a retarder was used to keep the mix workable for longer.

The chemical compositions of the cementitious materials are given in **Table 3.1** and the particle size distributions of the materials are given in **Figure 3.1**.

Table 3.1 Chemical compositions of cement, USF and GGBS

CHEMICAL COMPOSITIONS OF CEMENT, USF AND GGBS										
	SiO_2	**MgO**	**Al_2O_3**	**SO_3**	**K_2O**	**CaO**	**Fe_2O_3**	**TiO_2**	**Na_2O**	**LOI**
CEM I 52.5N (%)	11.67	---	1.72	1.85	<LOD	82.41	7.27	0.42	---	1.77
CEM II/A 42.5R (%)	14.15	---	3.50	1.82	<LOD	76.87	5.32	0.72	---	---
CEM II/A 52.5N (%)	13.34	---	2.63	2.28	<LOD	78.46	5.74	0.64	---	---
USF, CSF(%)	95.00	0.25	<0.10	0.30	0.63	0.70	<0.10	---	0.18	2.00
GGBS (%)	34.87	8.03	14.38	1.96	0.72	37.05	0.89	0.72	<0.01	0.16
Fly ash (%)	55.14	0.81	32.17	0.13	0.76	4.50	3.61	1.50	<0.01	0.67

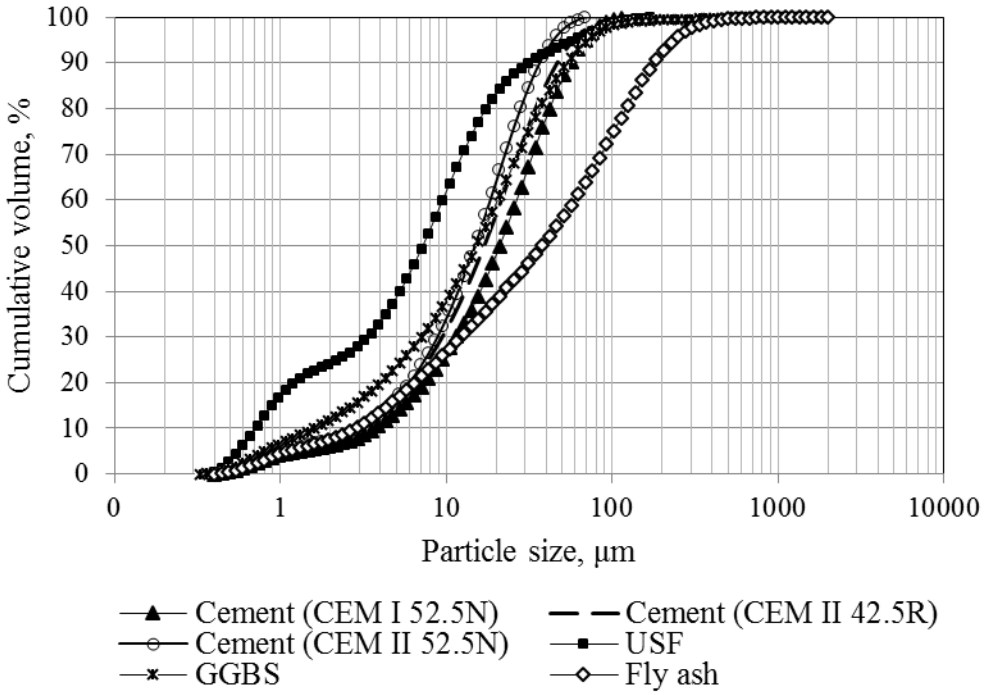

Figure 3.1 Particle size distribution of cements, USF and GGBS

In this study two types of hook-ended fibre with different tensile strength as well as micro fibre and slit sheet fibre were used. Their shape and properties are provided in **Figure 3.2** and **Table 3.2**, respectively.

Figure 3.2 The shape of fibres.
a) Hook-ended (Type I), b) Hook-ended (Type II), c) Micro fibre, d) Slit sheet and e) locally available fibre

Table 3.2 Properties of the steel fibres

Type of fibres	Shape	Cross section	Diameter (mm)	Length (mm)	Tensile strength (MPa)
Hook-ended (Type I)	Hooked	Round	0.45	30	1000
Hook-ended (Type II)	Hooked	Round	0.35	30	3000
Micro fibre	Straight	Round	0.2	13	2500
Slit sheet	Straight	Rectangular	NA	25	1000
Locally available fibre	Straight	Round	0.26	13	1000

3.3 MECHANICAL PROPERTIES TESTING METHOD

3.3.1 Compressive strength

The compressive strength of UHPC and UHPFRC was determined using 100 mm cubes. The cubes were tested according to the procedure prescribed in SANS 5863 (2006). At least three cubes were tested for strength determination and values reported are average of the three strength values.

3.3.2 Modulus of Elasticity

The Modulus of Elasticity was obtained from cylinder specimens (100 mm diameter, 200 mm length). The testing procedure was based on ASTM C469 / C469M-14 (2014) and performed in compression with a strain-measuring device attached to the specimen, to record the vertical strains. The linear slope of the elastic portion of the stress-strain curve was taken as the modulus of elasticity. The elastic portion of the stress-strain curve is assumed to be up to 40% of the ultimate compressive strength ($0.4f`_c$).

3.3.3 Splitting tensile strength

The splitting tensile test was used to determine the indirect tensile strength of concrete. The test was conducted on 100x200 mm cylinders. The load was applied over the entire length of the specimens which led to the splitting of cylinders across the diameter (ASTM C496 / C496M-17, 2017).

3.3.4 Flexural strength

Three beam specimens measuring 100 x 100 x 500 mm were cast to determine the flexural behaviour of the UHPFRC beams using a four-point bending test. The beam tests were conducted using a closed-loop Material Testing System (MTS) applying displacement at a

rate of 0.2 mm/minute. Mid-span deflections were measured by using two LVDTs. The load was applied by using two bearing rollers (one of them a swivelling roller) 100 mm apart while the beam supports were 300 mm apart. The beams were cast and tested in accordance to the procedure prescribed by the Japanese Concrete Institute (1983). The test set-up is presented in **Figure 3.3**. It's noteworthy that the described four-point test method was designed to investigate only the flexural strength for this chapter; wherever the bending test is carried out, the testing procedure and method will be explained.

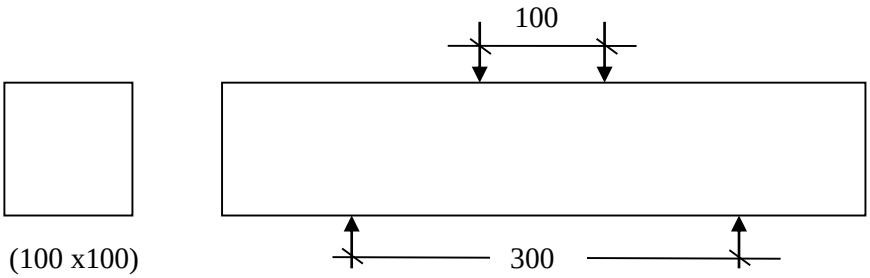

Figure 3.3 Test set-up for flexural strength measurement according to the Japanese Concrete Institute (1983) (Dimensions in mm)

3.3.5 Direct tensile strength

Dog-bone specimens were used in order to measure the direct tensile strength. The dimensions of the specimen can be seen in **Figure 3.4**. A clip gauge was used to measure the elongations which occurred during the direct tensile test. Reinforcing bars were placed on the both end of the specimens to assure that failure occurred within the central part of the specimens.

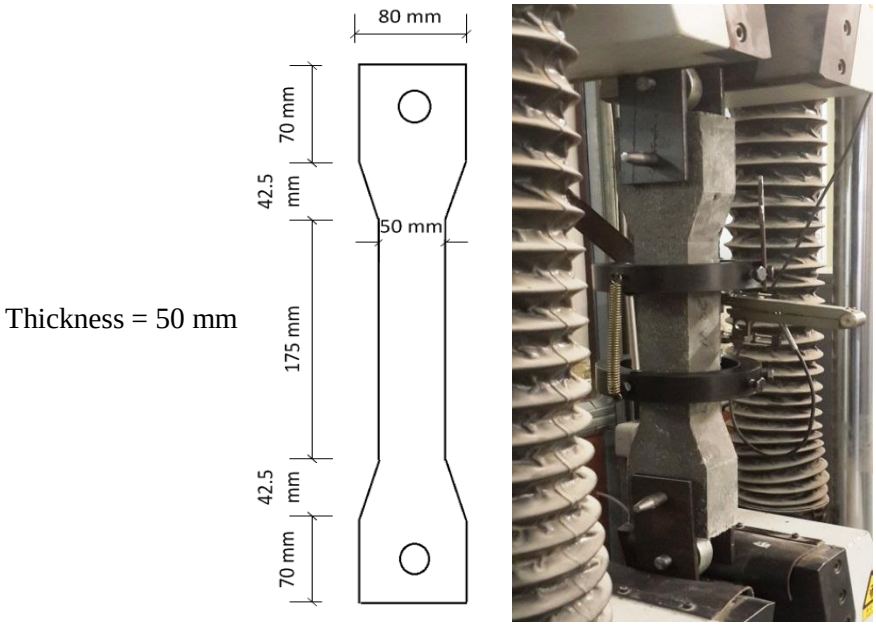

Figure 3.4 Dog-bone specimen and the direct tensile test set-up

3.4 THE PROCEDURE TO DETERMINE THE MIX COMPOSITION

The main aim of the mix designs conducted in this study was reducing the cost as well as making the concrete practical to use while providing optimal properties at the same time.

In the first set of tests, the effect of silica sand and dolomite sand on the compressive strength was investigated. The mix designs were chosen according to the literature reviewed. The first mix designs are presented in **Table 3.3**. The water to cement ratio was kept constant at 0.25 (Kang and Kim, 2011; Yoo, et al., 2014a; Yoo et al., 2014b;). The retarder content was 2.5% of the cementitious materials weight. The ratio of aggregate to cement (by weight) was taken as 0.5. Hooked steel fibres with a length of 45 mm and a diameter of 0.45 mm were used in the mixes. It is worth mentioning that in the developed mix designs, the admixture consisted of one third superplasticizer and two thirds retarder, respectively.

Table 3.3 Initial mix designs

Material	**Mix 1 (Silica sand)**		**Mix 2 (Dolomite sand)**	
	kg/m^3	**litre/m^3**	**kg/m^3**	**litre/m^3**
Cement (CEM I 52.5N)	900	286.6	910	290.8
CSF	300	136.4	305	138.3
Fly ash	300	136.4	305	138.3
Silica sand (< 600µm)	450	169.8	-----	----
Dolomite sand (600µm,1.18µm)	-----	----	455	159.1
Water	226	226.0	230	230.0
Hook-ended fibre (Type I)	152	19.6	152	19.6
Admixture	27	25.5	27	25.5
Σ	2355	1000	2385	1000

During the first stages of experimental work the compressive strength was chosen as a main indicator of material properties. No additional testing to evaluate other mechanical or durability properties was performed for these mixes. In order to get results as soon as possible, 3-day and 7-day compressive strengths were determined using sets of three 100 mm-cubes and the results reported are average strengths. After storing the cubes in a laboratory room at 24°C and 98% relative humidity for 24 hours, the cubes were stored in two different curing regimes including 24°C water according to the South African standard (SANS 5861-3:2006) and 80°C steam by storing the cubes in a closed bath exposing to 80°C steam.

The results are shown in Figure 3.5. For samples kept in 24°C water, the compressive strength of the mixes containing silica sand is just slightly higher than those containing dolomite sand. The compressive strength differences for samples that experienced steam curing are more pronounce. Despite the results showing that mixes containing silica sand showed marginally higher compressive strength, dolomite sand was considered in further trial mix designs. The reason was that the use of dolomite aggregate is known to result in concrete with a higher stiffness or E-value (Alexander and Mindess, 2005) and E-value is an important early-age property for a prestressed beam.

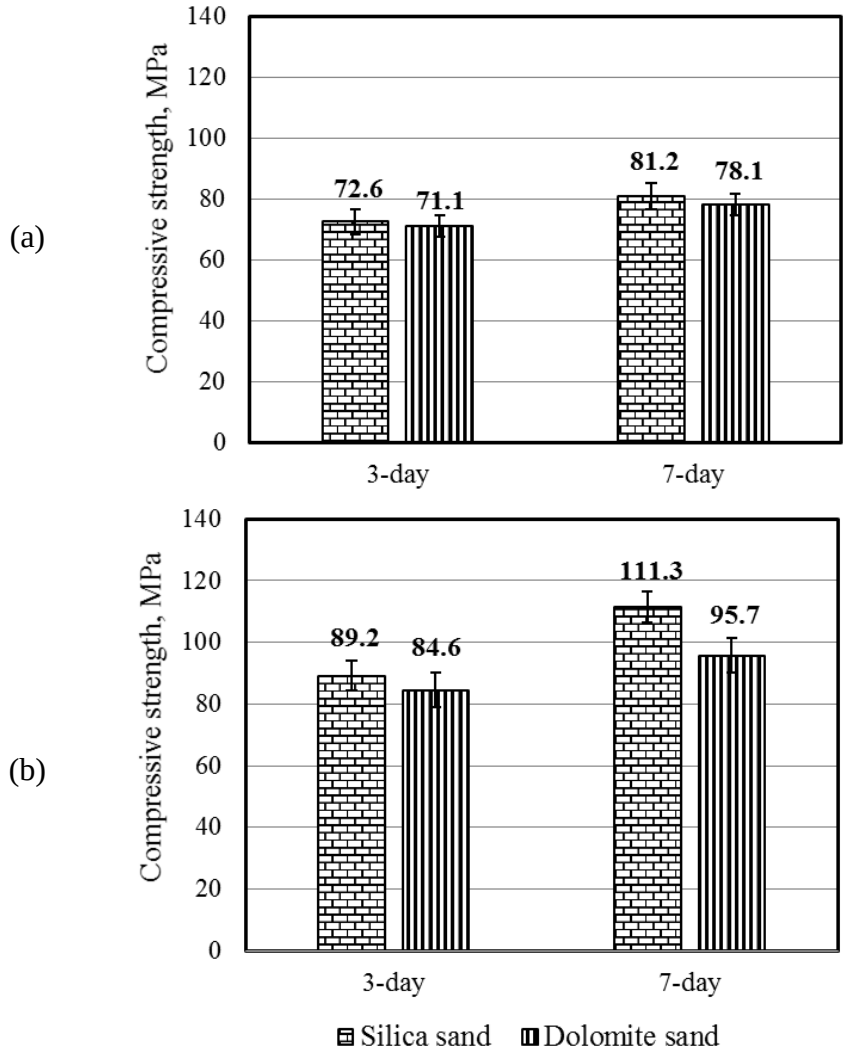

Figure 3.5 Effect of silica and dolomite sand on compressive strength a) Cured in 24°C water, (b) Cured in 80°C steam

The effect of different cementitious materials (besides CSF) on the compressive strength was established by using Fly ash and GGBS as additional cementitious materials. Either the Fly ash or GGBS to cement ratio was kept constant at 0.17. The combination of 2% hooked fibre (by volume) and 0.5% micro fibre (by volume) was added. Addition of micro fibre led to the

use of higher content of admixture to keep the mix workable. The mix designs are shown in **Table 3.4**.

The results, as given in **Figure 3.6**, indicate that the concrete containing GGBS has higher early-age compressive strengths in comparison with concrete containing fly ash, when they experience 80°C steam, unlike when the concrete was stored in 24°C water. These results indicate that GGBS is more reactive within the first days of heat curing which is favourable for achieving high early strength for prestressed beams, therefore GGBS was chosen as a cementitious material besides silica fume.

One of the purposes of this study is making UHPC more economical. Increasing the aggregate content is one of the ways to make UHPC cheaper. The effect of aggregate content on the compressive strength was thus established by using ratios of aggregate to cement (by weight) of 0.9 and 1.1. The latter ratio was taken from the studies carried out on UHPC (Kang and Kim, 2011; Yang, et al., 2012; Yoo, et al., 2013; Yoo, et al., 2014a).

Table 3.4 Mix designs with different cementitious materials

Material	**Mix 3 (Fly ash)**		**Mix 4 (GGBS)**	
	kg/m^3	**litre/m^3**	**kg/m^3**	**litre/m^3**
Cement (CEM I 52.5N)	875	278.7	870	277.1
CSF	290	131.8	290	131.8
Fly ash	145	65.9	----	----
GGBS	----	----	145	49.5
Dolomite sand (< 1 mm)	685	239.5	735	257.0
Water	220	220.0	220	220
Hook-ended fibre (Type I)	152	19.6	152	19.6
Micro fibre	39	5.0	39	5.0
Admixture	44	41.5	44	41.5
Σ	2450	1000	2495	1000

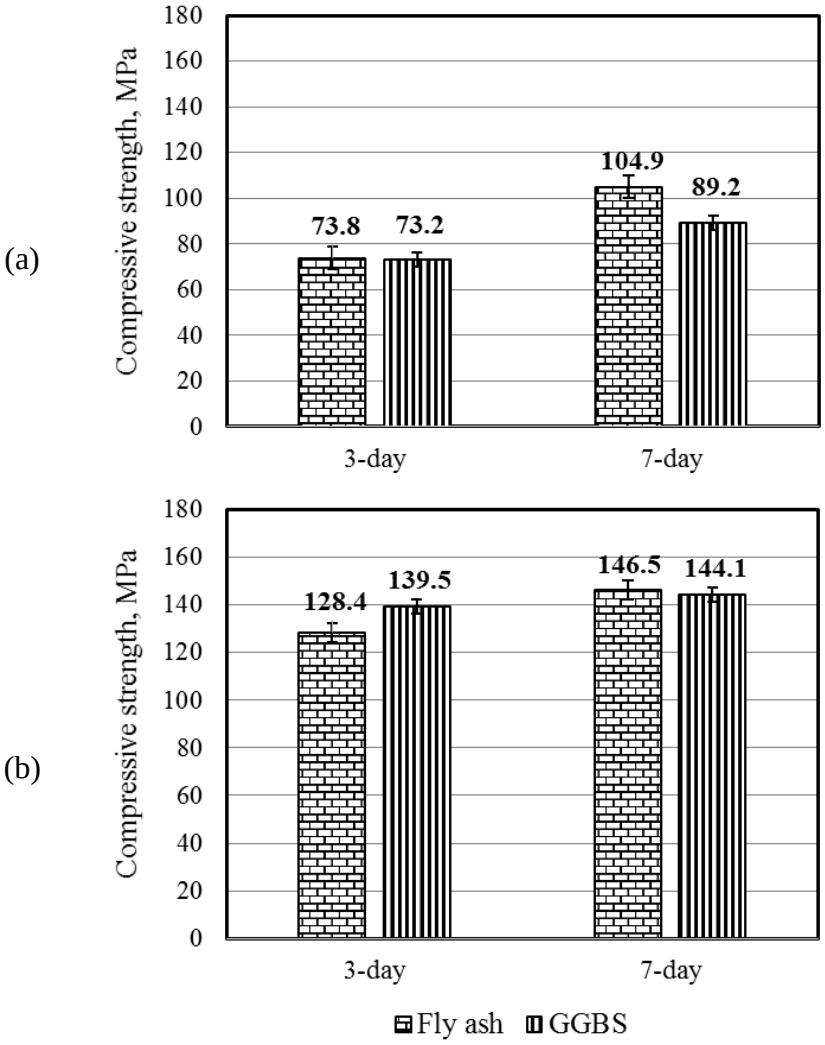

Figure 3.6 Effect of cementitious material on the compressive strength a) Cured in 24°C water, (b) Cured in 80°C steam

In these mix designs Condensed Silica Fume (CSF) was replaced with Undensified Silica Fume (USF) as can be seen in **Table 3.5**. After crushing the cubes for the previous mix designs, balls of silica fume was observed showing that the condensed silica fume did not disperse during the mixing procedures in the trail mix designs shown in **Table 3.4**. The possibility of applying coarser aggregate in the mix design was evaluated by using andesite sand with a maximum size of 3.35 mm. The aggregates were sieved to eliminate aggregate sizes smaller than 0.15 mm. Since concrete containing andesite as an aggregate, provide of higher compressive strength (Alexander and Mindess, 2005), dolomite sand was replaced by andesite. The ratio of USF to cement was taken as 0.2. Both mixes contained 4% fibre content (by volume) to check to what extent the higher fibre content affects the workability.

Table 3.5 Mix designs with different aggregate contents

Material	Mix 5 (Agg/C=0.9)		Mix 6 (Agg/C=1.1)	
	kg/m^3	litre/m^3	kg/m^3	litre/m^3
Cement (CEM I 52.5N)	875	278.7	810	258
USF	175	79.5	165	74.8
GGBS	265	90.4	245	84.0
Andesite sand (Min:0.15mm, Max: 3.35 mm)	790	266.9	900	304.1
Water	210	210.0	205	205.0
Hook-ended fibre (Type I)	155	20.0	155	20.0
Micro fibre	155	20.0	155	20.0
Admixture	40	37.7	37	34.9
Σ	2665	1000	2672	1000

The results for 7-day and 28-day compressive strength with different aggregate contents are presented in Figure **3.7**. Higher compressive strengths were achieved with higher aggregate contents and therefore, the ratio of aggregate to cement was taken as 1.1 for the next trial mix design. It was noticed even by keeping the admixture content (3% of cementitious materials) similar to the last mixes, more flowable mixes were achieved before addition of fibres to the fresh mixes. Since, it was a significant workability reduction after addition of the fibres, it was decided to keep the fibre content to 2% of volume fraction to keep the mixes more workable.

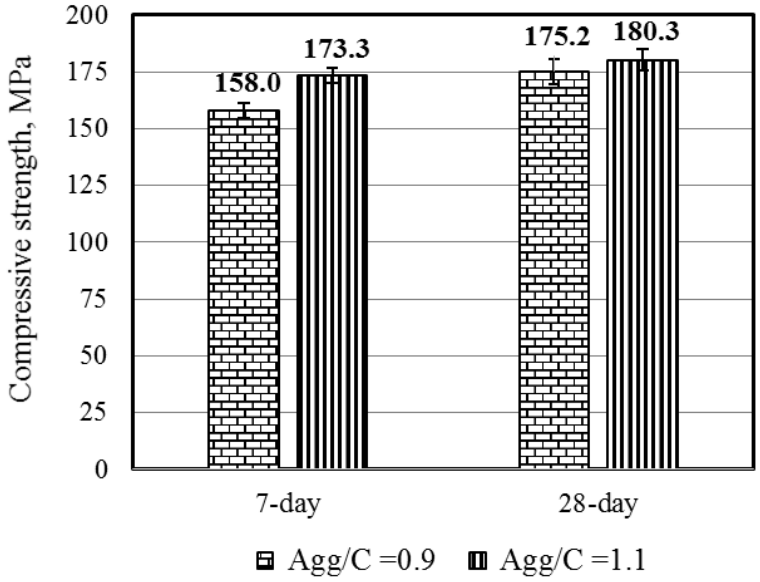

Figure 3.7 Effect of aggregate content on compressive strength (cured in 80°C steam)

The effect of higher USF content on the compressive strength was determined while the aggregate to cement ratio was kept constant at 1.1. The ratio of USF to the cement was increased to 0.3. The mix design is shown in **Table 3.6**. In these trial mix designs, aggregates were sieved to eliminate the aggregate sizes smaller than 0.15 mm.

Table 3.6 Mix designs with higher USF content

Material	**Mix 7 (USF/C=0.3)**	
	kg/m^3	**litre/m^3**
Cement (CEM I 52.5N)	825	264.3
USF	250	113.6
GGBS	165	56.3
Andesite sand (Min:0.15mm, Max: 3.35 mm)	915	309.1
Water	205	205.0
Hook-ended fibre (Type I)	155	20.0
Admixture	37	34.9
Σ	2552	1000

These results were compared to those obtained for Mix 6 (Agg/C=1.1) in which the ratio of USF to cement was 0.2. The comparison as presented in **Figure 3.8** shows that by increasing the ratio of USF to cement, the compressive strength increased. This can be attributed to the fact that a higher USF content results in a higher SiO_2 (silicon dioxide) content and also a higher packing density. A ratio of USF to cement of 0.3 was thus used for the next trial mix design.

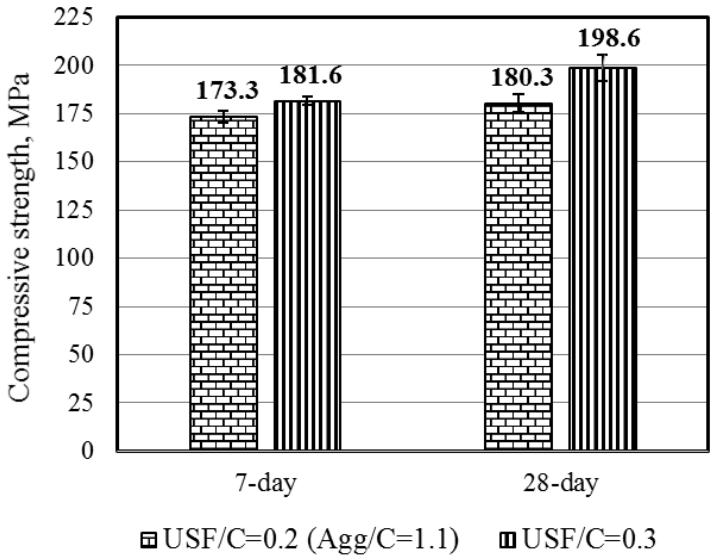

Figure 3.8 Compressive strength with different USF contents (cured in 80°C steam).

In the next mix design the effect of higher GGBS content on the compressive strength was studied while the aggregate to cement ratio was kept constant at 1.1. The ratio of USF to the cement was taken as 0.3. The mix design is shown in **Table 3.7**. For the trial mix design, aggregates were sieved to eliminate the aggregate smaller than 0.15 mm.

Table 3.7 Mix design with higher content of GGBS

Material	**Mix 8 (GGBS/C=0.3)**	
	kg/m^3	**litre/m^3**
Cement (CEM I 52.5N)	795	253.2
USF	240	109.1
GGBS	250	85.3
Andesite sand (Min:0.15mm, Max: 3.35 mm)	875	295.6
Water	205	205.0
Hook-ended fibre (Type I)	152	19.6
Admixture	35	33.0
Σ	2552	1000

From **Figure 3.9** it can be seen that increasing the GGBS content results in a marginal decrease in the compressive strength. Higher compressive strengths were achieved when the ratio of GGBS to cement was 0.2 and this can be attributed to the packing density. It seems that increasing the GGBS content results in a lower packing density thus causing a strength reduction. For the further mix designs 0.2 was used as the ratio of GGBS to cement.

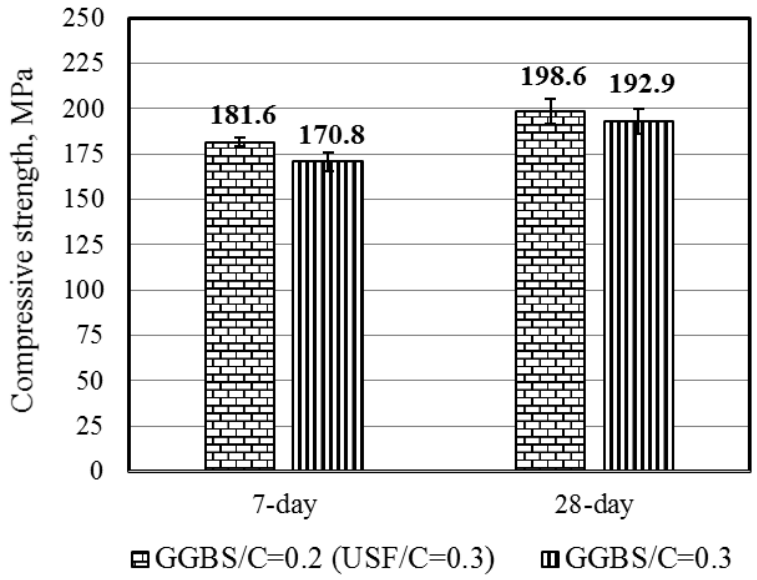

Figure 3.9 Effect of GGBS content on compressive strength (cured in 80°C steam)

The effect of aggregate content and size were considered next. In Mix 9, the ratio of aggregate to cement was 2 with a maximum aggregate size of 4.75 mm, while in Mix 10, the ratio of aggregate to cement was 2.5 and the maximum aggregate size was 6.7 mm. The particle size distribution of the aggregate is provided in **Figure 3.10**. It is worth mentioning that the aggregates were not sieved and were used as it was provided by the supplier. The mix designs are shown in **Table 3.8**. The ratio of sand to stone in Mix 10 was established using a dry packing density method as suggested by Mostert (2016) where different sand and stone combination are dropped from an elevated cone into a container. The dry packing density of the combinations is measured. The sand to stone ratio which resulted in the highest dry packing density is considered to be the optimum ratio.

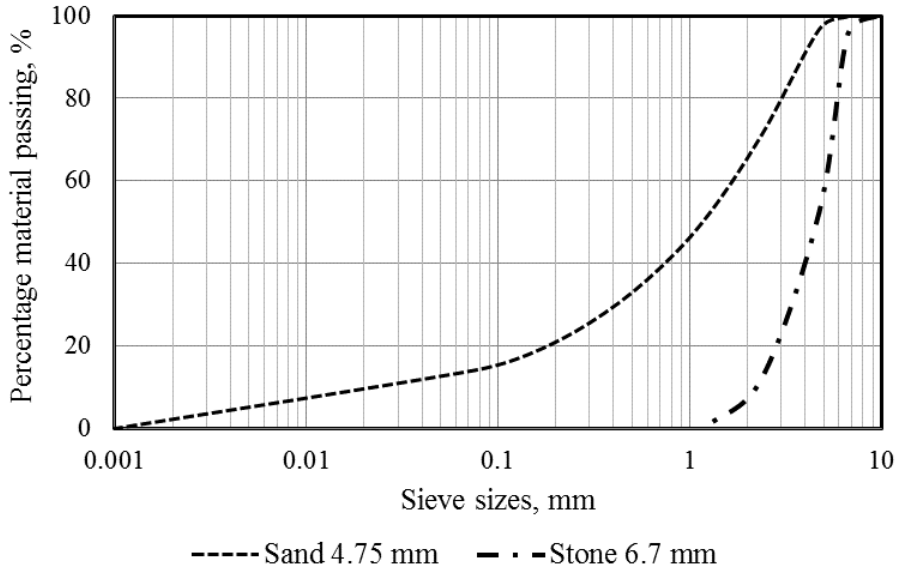

Figure 3.10 The particle size distributions of andesite aggregate

Table 3.8 Mix designs with different aggregate content and size

Material	**Mix 9 (Agg/C= 2)**		**Mix 10 (Agg/C= 2.5)**	
	kg/m^3	**litre/m^3**	**kg/m^3**	**litre/m^3**
Cement (CEM I 52.5N)	665	211.8	590	187.9
USF	200	90.9	180	81.8
GGBS	135	46.0	120	40.9
Andesite sand (Max:4.75 mm)	1330	449.3	1040	150.3
Andesite stone (Max: 6.7 mm)	----	----	445	351.3
Water	165	165	150	150.0
Hook-ended fibre (Type I)	152	19.6	152	19.6
Admixture	20	18.9	20	18.9
Σ	2667	1001	2697	1001

The effect of aggregate content and size are presented in **Figure 3.11**. There is no significant differences between the compressive strengths obtained using aggregate to cement contents of 2 and 2.5. The main difference would however be cost. By introducing higher aggregate contents, the final cost for the mix as well as the production of CO_2 are reduced. Reduction in the cement consumption is one of the global concerns which relates to global warming and thus a higher aggregate content will be used. The curing regime was changed to submerging the specimens in 85°C water.

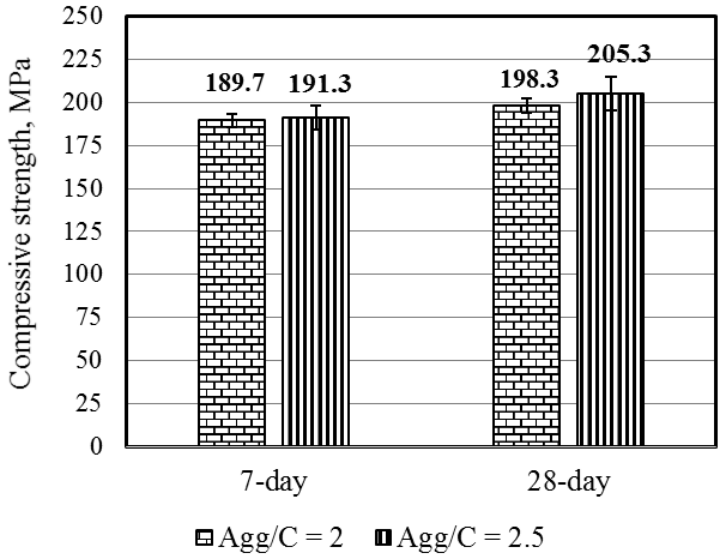

Figure 3.11 Effect of aggregate content and size on compressive strength (cured in 85°C water)

The purpose of the next trial mix design was to increase the packing density by introducing fly ash as filler. Fly ash was used to replace a portion of fine aggregate and cement. The proposed mix design is presented in **Table 3.9**.

Table 3.9 Trial mix design with fly ash as a filler

Material	**Mix 11 (Fly ash as filler)**	
	kg/m^3	**litre/m^3**
Cement (CEM I 52.5N)	540	172.0
USF	175	79.5
GGBS	120	40.9
Fly Ash	100	45.4
Andesite sand (Max:4.75 mm)	445	150.3
Andesite stone (Max: 6.7 mm)	950	320.9
Water	150	150.0
Hook-ended fibre (Type I)	152	19.6
Admixture	22	20.7
Σ	2654	1000

Figure 3.12 presents the comparison between the compressive strength of UHPFRC with and without fly ash as filler. Two different curing regimes were considered: 1) submerging the specimens for 3 days in 85°C water, then stored in 24°C water till the testing time, 2) storing the specimens in 24°C water till the testing time. The results indicated that by including fly ash in the mix, compressive strength at 7 days and 28 days reduced. It means that the packing density did not increase by including Fly ash.

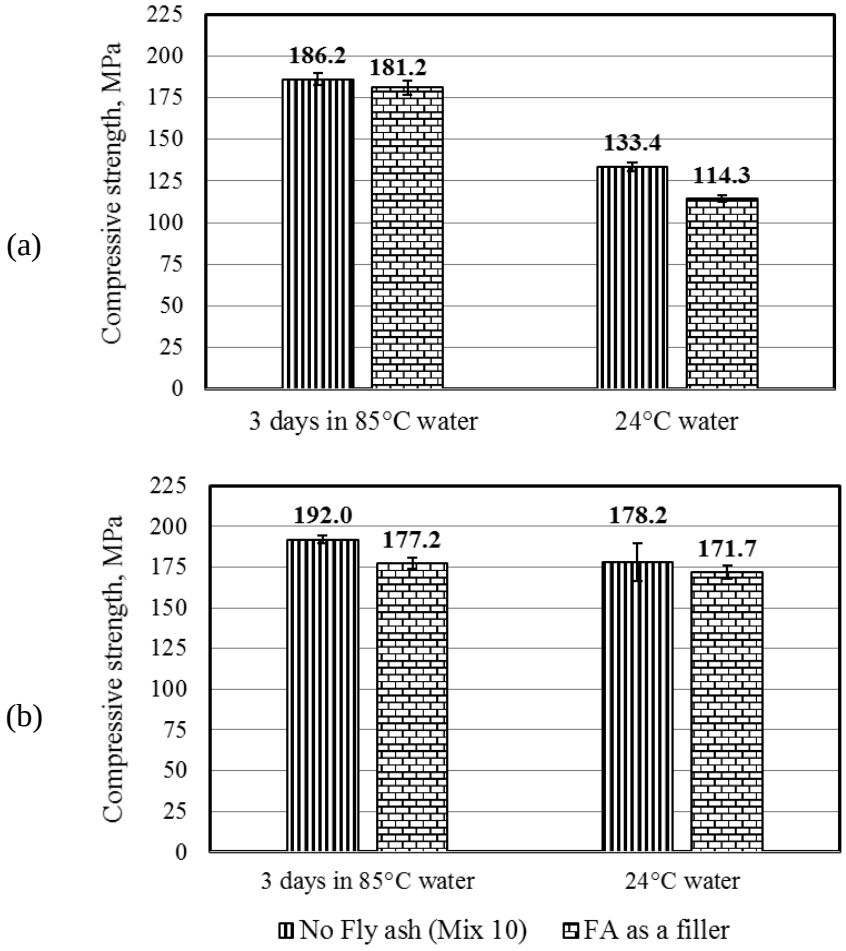

Figure 3.12 Compressive strength of UHPFRC with and without fly ash a) 7-day strength, b) 28-day strength

The effect of higher aggregate content was investigated more in Mix 12 as indicated in **Table 3.10**. The ratio of aggregate to cement was increased to 3. The aggregate type and grading were the same as Mix 10 (Agg/C= 2.5).

Table 3.10 Trial mix design with higher aggregate content

Material	Mix 12 (Agg/C = 3)	
	kg/m^3	litre/m^3
Cement (CEM I 52.5N)	540	172.0
USF	160	72.7
GGBS	105	35.8
Andesite sand (Max:4.75 mm)	485	163.8
Andesite stone (Max: 6.7 mm)	1130	381.7
Water	135	135.0
Hook-ended fibre (Type I)	152	19.4
Admixture	21	19.8
Σ	2728	1000

In **Figure 3.13** the compressive strengths achieved from Mix 12 (Agg/C = 3) is compared to the strengths obtained from Mix 10 (Agg/C = 2.5). There is no significant differences between the compressive strengths obtained using aggregate to cement contents of 2.5 and 3 at both 7 and 28 days. The main difference would however be cost when higher aggregate content is introduced. However, the workability of the mixture 12 was an issue resulting in a higher labour effort for casting. Low workability led to higher air contents in the samples of mix 12 comparing to mix 10 (more than twice- see **Table 3.11**) as well. These issues resulted in disregarding this mix design and considering Mix 10 (Agg/C = 2.5) as the final mix design.

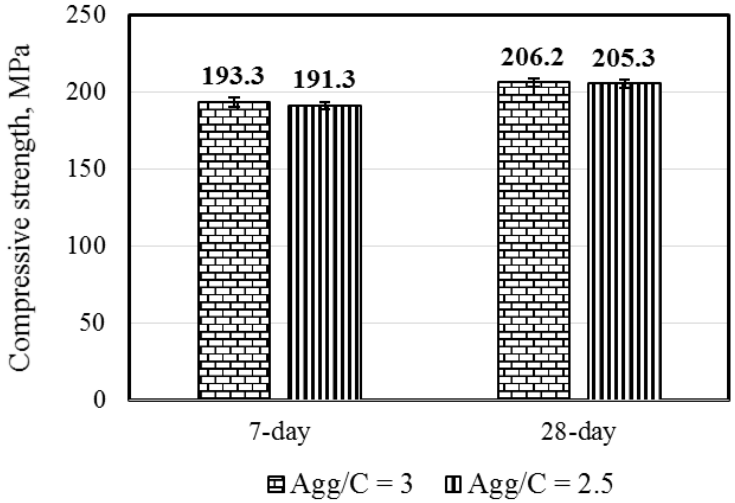

Figure 3.13 Effect of higher aggregate content on compressive strength (cured in 85°C water)

For comparative purposes **Table 3.11** contains an indication of workability for all the mixes as compared through visual observation. In addition, this table reports air content of all those mixes. The air content of mixes were evaluated by measuring the densities of cast samples and comparing the actual densities with the theoretical densities based on exact mix compositions and relative densities of mix components. It's noteworthy that by reducing the cement content from 900 kg/m^3 in Mix 1 to 590 kg/m^3 in Mix 10, the corresponding densities increased from 2355 kg/m^3 to 2697 kg/m^3, respectively.

Table 3.11 Workability and air content of Mixes

Mix No.	**1**	**2**	**3**	**4**	**5**	**6**	**7**	**8**	**9**	**10**	**11**	**12**
Workability	Good	Good	Good	Fair	Good	Good	Good	Poor	Good	Good	Fair	poor
Air content (%)	9.14	9.28	3.04	2.93	0.90	0.89	1.21	1.64	2.52	0.77	1.59	1.69

The workability of Mix 10 as the final mix design was evaluated by not only using the flow table test for the mix containing no fiber and obtaining a flow of 435 mm, but also conducting slump tests with different fibers and measuring slumps between 85 mm and 120 mm (Vatannia et al., 2016a).

For all the initial trial mixes only small batches were cast. It was realized during the casting of bigger batches (60 litres) that the setting time was so short that setting of the concrete occurred during the casting process. Since casting full-size beams is one of the objectives in this study, enough time is required to cast the beams before setting occurs. The early setting despite adding retarder can be attributed to the fact that the available retarder could not retard the hydration of this specific cement. Further experiments revealed that combining two different cements (CEM II/A 42.5R and CEM II/A 52.5N) solved the early setting issue. The cement combinations were used for the investigations on pull out performance behaviour (see CHAPTER 5) and onward.

3.5 MATERIAL COST OF THE MIX DESIGNS

The main concerns in the mix design are economics and practicality in a way that all the materials are available in South Africa and no milling of materials is required. The environmental impact was taken into account during the development of the final mix design

and the cement consumption has been reduced from 900 kg/m^3 to 590 kg/m^3 without a significant decrease in strength as indicated in **Figure 3.14**.

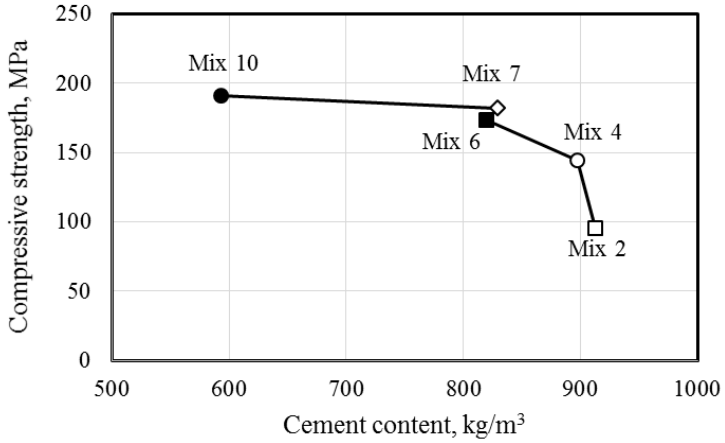

Figure 3.14 Effect of cement content on compressive strength

As stated before, high manufacturing cost including material cost leads to a limited use of UHPC in industry. This concern was addressed in this study by increasing the aggregate content and sizes, using supplementary cementitious materials beside cement.

Figure 3.15 compares the unit cost (ZAR/m^3) normalized by the 7-day compressive strength (ZAR/m^3/MPa) of the UHPC mixtures subjected to heat treatment curing. The results are compared to the unit cost per compressive strength of the typical UHPFRC (see **Table 1.1**). The unit cost included the costs of all ingredients for producing the UHPFRC mixtures, except for transportation costs. The unit cost of cement (CEM I 52.5N), SF, USF, GGBS, dolomite sand, andesite sand, admixtures and steel fibre are 1700, 2200, 2500, 739.39, 244.46, 297.62, 2120 and 21900 ZAR/ton, respectively. The unit costs per compressive strength for Mix 2, Mix 4, Mix 6, Mix 7 and Mix 10 are 60.8, 46.3, 52.5, 32.4 and 28.0 ZAR/m^3/MPa, respectively. It is noteworthy that the unit cost per compressive strength in the typical mix design was reported 7.6 USD/m^3/MPa (~109 ZAR/m^3/MPa) by Meng (2017). This significant cost reduction can be attributed to the fact that in the proposed mix designs supplementary cementitious materials were used, fine sand and quartz ground were replaced by conventional concrete sand (andesite and dolomite).

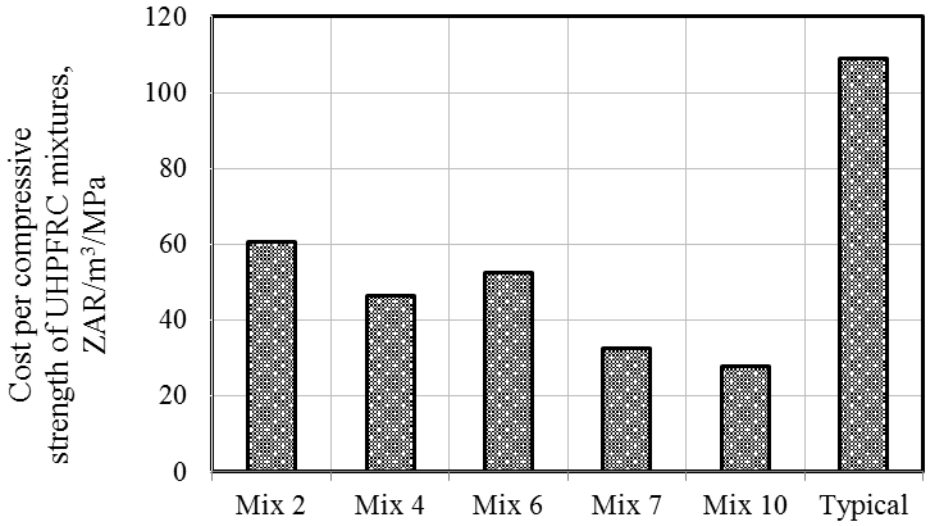

Figure 3.15 Unit cost per unit compressive strength of UHPFRC mixtures

3.6 COMPREHENSIVE STUDY ON THE EFFECT OF DIFFERENT TYPES OF FIBRE AND CURING REGIME ON THE MECHANICAL PROPERTIES OF UHPC

Mechanical properties of the UHPC after the addition of different types of fibre (2% by volume) were investigated further. The fibres include two types of hooked steel fibre, micro steel fibre and slit sheet fibres.

In the procedure of the fibre addition to the mixtures, there was no difference in the fibre uniformity and the distribution through the procedure except for micro fibres which two interesting phenomena occurred. During mixing process, fibre balls were formed in spite of adequate mixing or in other words lack of adequate fibre dispersion in the mixture occurred and during the casting process the authors observed fast setting and drying of the mix before filling the moulds. The reasons of these phenomena could be due to the high aggregate content and the low water to cement ratio as well as high surface area of micro fibre.

As a result, four series of UHPFRC and one series of UHPC without fibre were studied. The mechanical properties considered are compressive strength, elastic modulus, splitting tensile strength as well as direct tensile and flexural strength.

Different curing regimes were also considered for each series of UHPFRC. After storing the specimens in the laboratory at 24°C with 98% relative humidity for 24 hours, two different

types of curing regimes were taken into account: 1) heat treatment at 85°C water, 2) standard curing regime (24°C water). For the heat treatment, four different curing durations were considered where the samples were kept in 85°C water for 1, 3, 6 or 28 days. After the heat curing, the specimens were kept in 24°C water up to the testing time.

The standard curing regime was performed by submerging the specimens in 24°C water for different durations of 6 days, 13 days and 27 days.

In total, 141 cubes, 57 cylinders, 30 dog-bones and 30 prisms were tested to determine compressive strength, E-value, tensile strength and flexural strength respectively. The experiments performed for different curing regimes are listed in **Table 3.12**. Compression tests were performed at 7 days and 28 days for those cubes which experienced 1, 3 and 6 days of heat treatment.

The results indicating the effect of different types of fibre on the mechanical properties of UHPC, is only presented for the curing regime of 3 days of heat treatment, for the sake of brevity. The results for the other curing regimes can be seen in Appendix B.

The results indicating the effect of curing regime on the mechanical properties of UHPFRC is presented for those containing hook-ended (Type II), for the sake of brevity. Also, the results have been compared to that obtained from UHPC without fibres. Besides, the compressive strength results for the other fibre types are compared.

Table 3.12 Studies regarding with effect of different types of fibre and curing regimes on the mechanical properties

Fibre type	**Curing regime**	**Experiments***	**No. of specimens**	**Ages (days)**
Hook-ended (Type I)	Heat treatment (1 day)	f_c'	3 cubes	28
	Heat treatment (3 days)	f_c'	6 cubes	7, 28
	Heat treatment (6 days)	f_c', f_{ct}, f_{cdt}, E-value, MOR	6 cubes, 6 cylinders, 3 dog-bones and 3 prisms	7, 28
	Heat treatment (28 days)	f_c'	3 cubes	28
	Standard curing (7 days)	f_c'	3 cubes	7
	Standard curing (14 days)	f_c'	3 cubes	14

	Standard curing (28 days)	f_c', f_{cst}, f_{cdt}, E-value, MOR	3 cubes, 6 cylinders, 3 dog-bones and 3 prisms	28
Hook-ended (Type II)	Heat treatment (1 day)	f_c'	6 cubes	7, 28
	Heat treatment (3 days)	f_c'	6 cubes	7, 28
	Heat treatment (6 days)	f_c', f_{cst}, f_{cdt}, E-value, MOR	6 cubes, 6 cylinders, 3 dog-bones and 3 prisms	7, 28
	Heat treatment (28 days)	f_c'	3 cubes	28
	Standard curing (7 days)	f_c'	3 cubes	7
	Standard curing (14 days)	f_c'	3 cubes	14
	Standard curing (28 days)	f_c', f_{cst}, f_{cdt}, E-value, MOR,	3 cubes, 6 cylinders, 3 dog-bones and 3 prisms	28
Micro fibre	Heat treatment (1 day)	f_c'	6 cubes	7, 28
	Heat treatment (3 days)	f_c'	6 cubes	7, 28
	Heat treatment (6 days)	f_c', f_{cst}, f_{cdt}, E-value, MOR,	6 cubes, 6 cylinders, 3 dog-bones and 3 prisms	7, 28
	Heat treatment (28 days)	f_c'	3 cubes	28
	Standard curing (28 days)	f_c', f_{cdt}, E-value, MOR,	3 cubes, 3 cylinders, 3 dog-bones and 3 prisms	28
Slit sheets	Heat treatment (1 day)	f_c'	6 cubes	7, 28
	Heat treatment (3 days)	f_c'	6 cubes	7, 28
	Heat treatment (6 days)	f_c', f_{cst}, f_{cdt}, E-value, MOR,	6 cubes, 6 cylinders, 3 dog-bones and 3 prisms	7, 28
	Heat treatment (28 days)	f_c'	3 cubes	28
	Standard curing (7 days)	f_c'	3 cubes	7
	Standard curing (14 days)	f_c'	3 cubes	14
	Standard curing (28 days)	f_c', f_{cst}, f_{cdt}, E-value, MOR,	3 cubes, 6 cylinders, 3 dog-bones and 3 prisms	28
No fibre	Heat treatment (1 day)	f_c'	6 cubes	7, 28
	Heat treatment (3 days)	f_c'	6 cubes	7, 28
	Heat treatment (6 days)	f_c', f_{cst}, f_{cdt}, E-value, MOR,	6 cubes, 6 cylinders, 3 dog-bones	7, 28

			and 3 prisms	
	Heat treatment (28 days)	f_c'	3 cubes	28
	Standard curing (7 days)	f_c'	3 cubes	7
	Standard curing (14 days)	f_c'	3 cubes	14
	Standard curing (28 days)	f_c', f_{cst}, f_{cdt}, E-value, MOR,	3 cubes, 6 cylinders, 3 dog-bones and 3 prisms	28

* f_c', f_{cst}, f_{cdt} stand for compressive strength of cubes, splitting tensile strength and direct tensile strength, respectively.

3.6.1 Mechanical properties of UHPC reinforced with different types of fibre

The curing regimes considered for determining the effect of fibre type on the mechanical properties of UHPC include:

- Heat treatment for 3 days, followed by water curing in 24°C water up to the day of testing: 114 cubes to measure the compressive strength at 7 days and 28 days.

- Heat treatment for 6 days following by water curing at 24°C water up to the day of testing: 30 cylinders, 15 dog-bones and 15 prisms for measuring E-value, splitting tensile strength, direct tensile strength and flexural strength at 28 days.

- Standard curing regime: 30 cylinders, 15 dog-bones and 15 prisms for measuring E-value, splitting tensile strength, direct tensile strength and flexural strength at 28 days.

Hook-ended (Type I) and Hook-ended (Type II) are called Low strength and High strength hooked fibre, respectively. The results have been compared to each other as well as with the results obtained from UHPC without fibres.

3.6.1.1 Compressive strength

Figure 3.16 reports the 28-day compressive stress-strain curves of UHPC reinforced with 2% (by volume fraction) of different fibres. UHPFRCs show linear behaviour of samples up to 80% of the ultimate compressive strength (the slope is constant before first crack). At this stage the first crack occurs and the fibres begin to play their role which leads to nonlinear behaviour of the concrete. Actually, the nonlinear behaviour is dependent on the number and orientation of fibres, which determine whether an increase in compressive strength occurs. At

the post-cracking stage, the fibres enhanced the compressive strength of the concrete after reaching the nonlinear stage. The increase in strength for UHPC reinforced with low strength hooked fibres, high strength hooked fibres, micro fibres and slit sheet fibres are 18.4%, 20.2%, 27.8% and 12.48% respectively with the following average strains at maximum load: 0.0075, 0.0111, 0.0082 and 0.007. Fibres also caused ductile behaviour leading to a decrease in explosive and brittle behaviour. UHPC reinforced with high strength hooked fibres shows the most ductile behaviour. This behaviour can be attributed to the high tensile strength of the fibres as well as their shape which leads to a stronger bond between the fibre and the matrix.

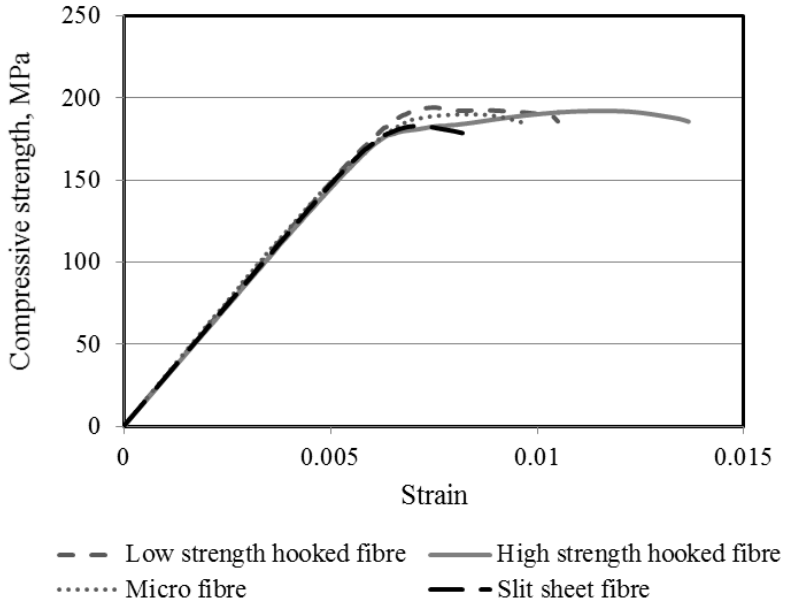

Figure 3.16 Compressive behaviour of UHPC reinforced with different types of fibre at 28 days

In **Figure 3.17** the ultimate compressive strengths for four type of UHPFRC are compared to UHPC. Fibres increased the compressive strength of UHPC. The lowest compressive strength enhancement in UHPFRC was achieved for the mixes containing slit sheets. This can be attributed to the high bulk density of that fibre which leads to a low number of fibres provided in a 2% volume fraction in comparison with other fibres. Moreover, due to the higher tensile strength of hook-ended fibre (Type II) in comparison with hook-ended fibre (Type I), one may expect to see higher strength from UHPC reinforced by high strength hooked fibres, however in reality the strength decreased. This can be caused by the higher air content of that mixture as well as the glue used to bind the fibres for easing the mixing process.

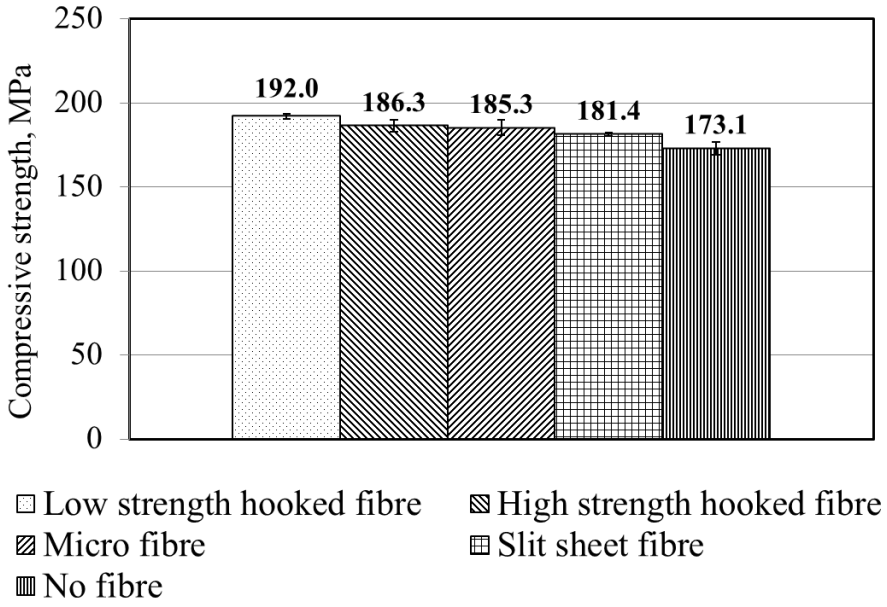

Figure 3.17 Compressive strength of UHPC reinforced by different types of fibres at 28 days

3.6.1.2 Direct tensile strength

The direct tensile behaviour of UHPFRC is shown in **Figure 3.18**. Except for UHPC containing micro fibres cured in the standard curing regime, no strain-hardening behaviour is observed for the other dog-bone specimens after cracking. However, the lack of brittle failure in post cracking behaviour of UHPFRC is clear. Heat treatment results in slightly lower post-cracking strength for all fibre types.

According to **Figure 3.19**, the highest direct tensile strengths in both curing regimes were achieved for UHPC containing high strength hooked fibre and micro fibres. The slit sheets do not have a major effect on the tensile strength and behaviour (see **Figure 3.18**). It could be related to their lower tensile strength as well as their low available number in the cross section. In addition, due to their smooth surface condition less resistance develops against their pulling out from the matrix. It is noteworthy that the direct tensile strength results can vary due to the dependency on the numbers of fibres as well as their orientation in the section. UHPC containing low strength hooked fibre exhibited higher tensile strength than UHPC containing slit sheet fibre, despite the similarity in ultimate tensile strength of fibres (1000 MPa). This is due to the mechanical contribution of the hooks in hooked fibres which provides higher resistance to pullout than smooth fibres (Naaman and Najm, 1991; Abu-Lebdeh et al., 2011).

As seen in **Figure 3.19**, heat treatment led to a strength reductions when comparing to strengths obtained from the standard curing regime. This may attribute to the higher compressive strengths obtained for the UHPC matrix cured in the standard curing regime (Naaman and Najm, 1991; Abu-Lebdeh et al., 2011; Tuyan and Yazici, 2012). The strength reduction is probably due to the weaker bond between the fibres and the matrix that developed in the heat treatment curing regimes (Yazici et al., 2009).

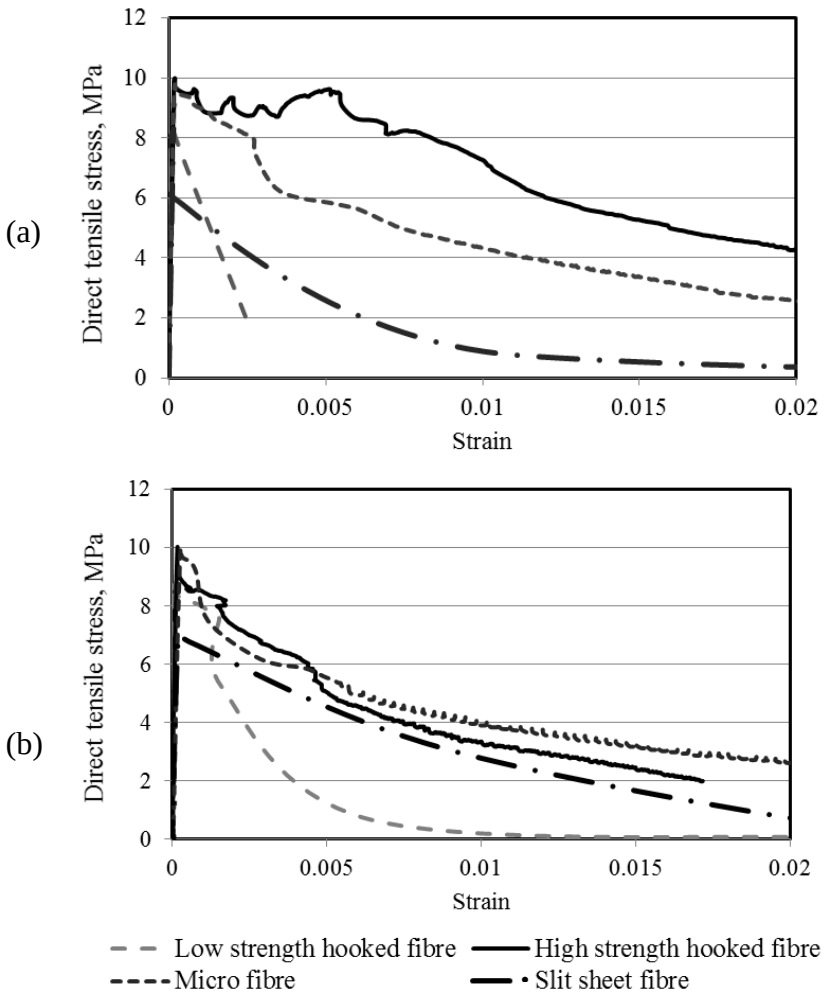

Figure 3.18 Direct tensile behaviour of UHPC reinforced with different fibres a) Standard curing regime, b) Heat treatment

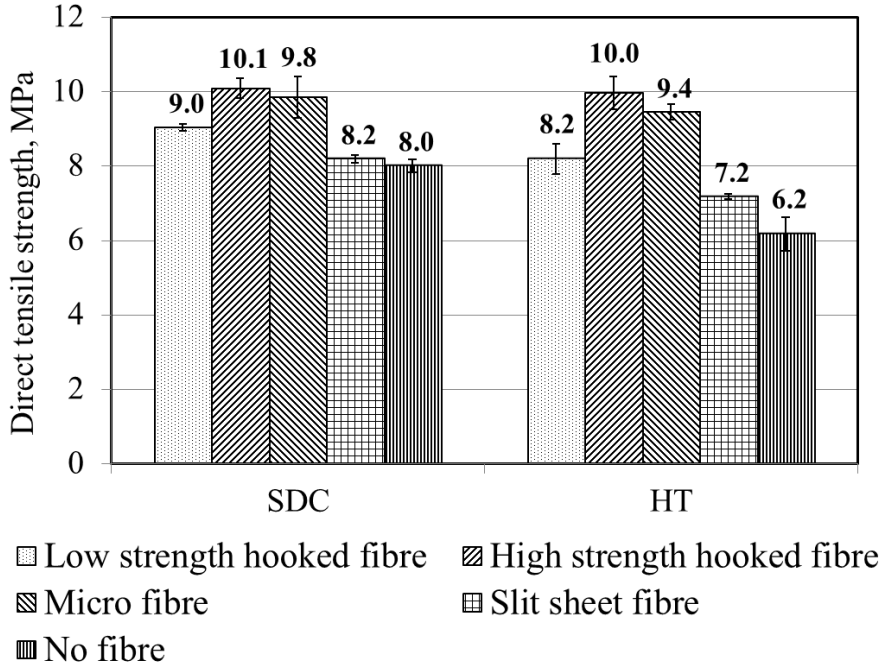

Figure 3.19 Direct tensile strength of UHPC reinforced with different fibres (SDC: Standard curing, HT: Heat treatment)

3.6.1.3 Flexural strength

All the beams tested in flexure cracked in the maximum moment region within the middle third of the beams. One main crack propagated upward which led to beam failure. For the beams containing low strength hooked fibres and slit sheet, the fibres along the crack plane failed as a result of their weak tensile strength, while in the beams reinforced by high strength hooked fibres and micro fibres no fibre failure was observed and the fibres pulled out.

Figure 3.20 presents the flexural behaviour of UHPFRC. The beams containing high strength hooked fibres and micro fibres show significant ductility and energy absorption in comparison with the other beams. For the beams reinforced by high strength hooked fibres and micro fibres post cracking strength improved and this behaviour was displayed numerically in **Table 3.13**. As seen in **Figure 3.20**, the beams containing micro fibres have higher flexural strengths than the other beams. This can be explained by the even distribution of fibre throughout the matrix, and the higher available number of fibres along the crack plane in comparison with the other mixtures.

Table 3.13 shows the results of the flexural behaviour obtained from four-point bending tests on UHPFRC beams cured in both curing regimes. The reported flexural behaviour contains

the flexural strength, the percentage increase in strength after cracking, and the total energy absorption. In general, the beams cured in 24°C water had higher strength than those that experienced the heat treatment. The reason may be due to the weaker bond between the fibres and matrix caused by heat treatment curing regimes (Yazici et al., 2009).

In beams containing high strength hooked fibres and micro fibres, the strength enhancement after cracking is not only more significant, but the total energy absorption is also higher. In other words, micro fibres and hook-ended fibres (Type II) provide high ductility in beams. In beams containing slit sheet fibres, no strength enhancement was observed after the formation of cracks. The reason can be due to the low number of slit sheet fibres along the crack plane as well as the smoothness of the fibre surface.

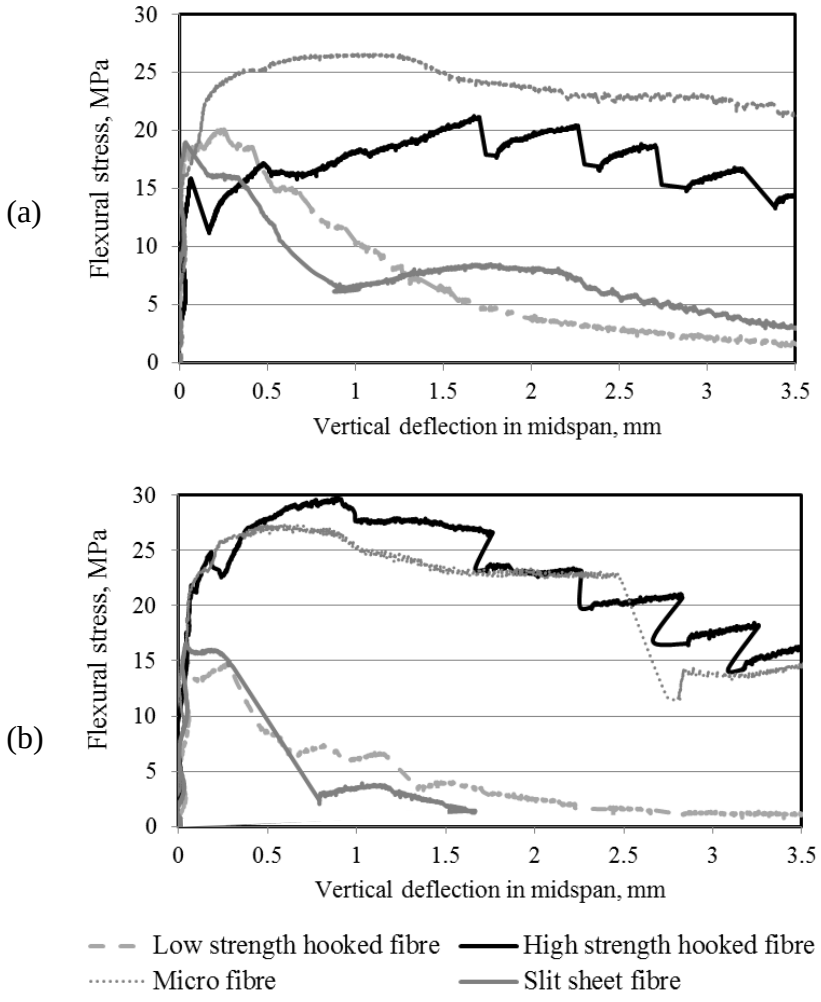

Figure 3.20 Flexural behaviour of UHPC containing different types of fibres a) Standard curing regime, b) Heat treatment

Table 3.13 Flexural behaviour in UHPC containing different types of fibres

Beams	Curing regime	Flexural strength (MPa)	Strength increase after cracking%	Energy absorption (KN.mm)
Low strength hooked fibres	SDC	20.37	6.02	27.42
	HT	16.77	0.72	19.04
High strength hooked fibres	SCD	21.04	36.17	80.72
	HT	25.82	33.71	84.91
Micro fibres	SDC	27.82	57.84	102.32
	HT	26.44	45.31	93.97
Slit sheet fibres	SDC	18.19	2.34	19.62
	HT	16.52	0	14.51

3.6.1.4 Splitting tensile strength

Figure 3.21 presents the splitting tensile behaviour of UHPC containing different types of fibres. Under standard curing condition, UHPFRC containing high strength hooked fibres exhibits significant ductile behaviour. Comparing the splitting tensile behaviour of the UHPFRC in both curing regimes, shows the post-cracking behaviour is dependent on the number of fibres as well as their orientations on the failure plane. A splitting tensile strength of 8.3 MPa was obtained for UHPC without fibre. By adding fibres a significant effect on the post-cracking behaviour of UHPFRC was observed. For instance, the increase in the strength of UHPFRC after the first cracking can be noted as 35%, 42%, 38% and 17% for low strength hooked fibres, high strength hooked fibres, micro fibres and slit sheet fibres respectively.

The splitting tensile strengths of UHPC containing different types of fibre were compared in **Figure 3.22**. The addition of fibres enhanced the ultimate strengths significantly. Splitting tensile strengths of UHPC were enhanced by up to 71%, 84%, 87% and 20% through the addition of low strength hooked fibres, high strength hooked fibres, micro fibres and slit sheet fibres, respectively. The high strength obtained in UHPC reinforced with micro fibres can be attributed to the even dispersion of micro fibres throughout of the mixture as well as the relatively high number of fibres provided in 2% volume fraction. However, the lowest strength was obtained for UHPC containing slit sheet fibres. UHPC containing hook-ended (Type I) (low strength hooked fibre) showed a much more significant improvement (up to

71%) in splitting tensile strength when comparing to the strength obtained from including slit sheets fibres. The splitting tensile strength of UHPC containing micro fibres that was exposed to a standard curing regime was not determined due to lack of specimens.

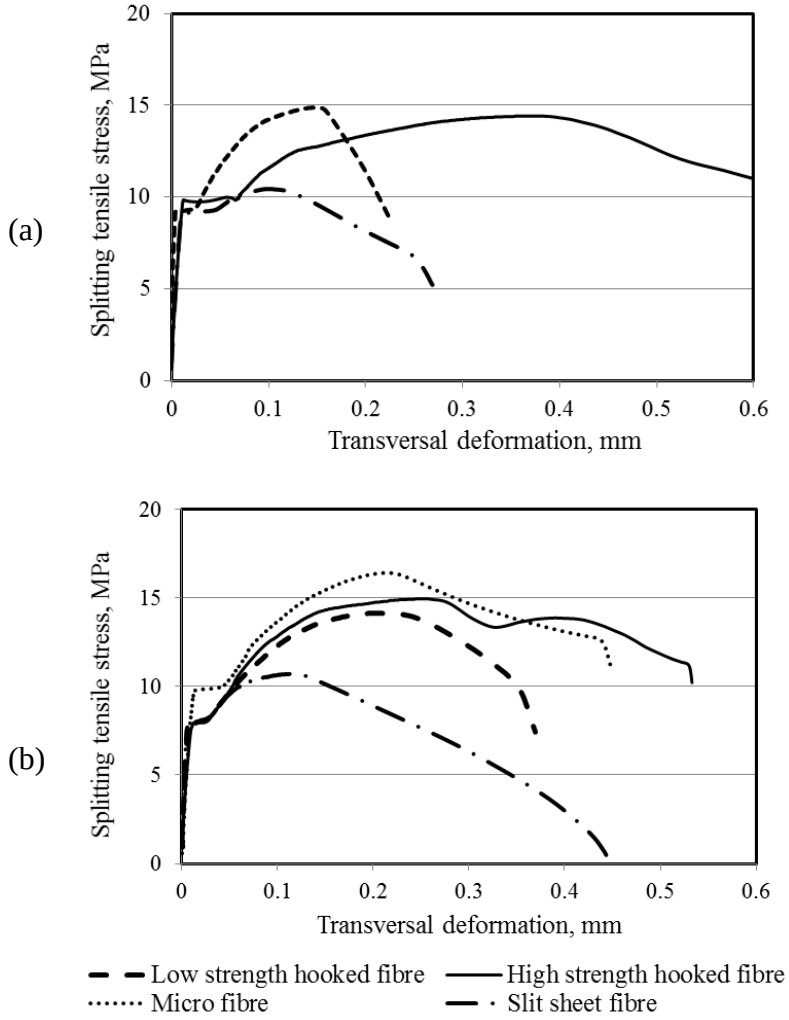

Figure 3.21 Splitting tensile behaviour of UHPC containing different types of fibres a) Standard curing regime, b) Heat treatment

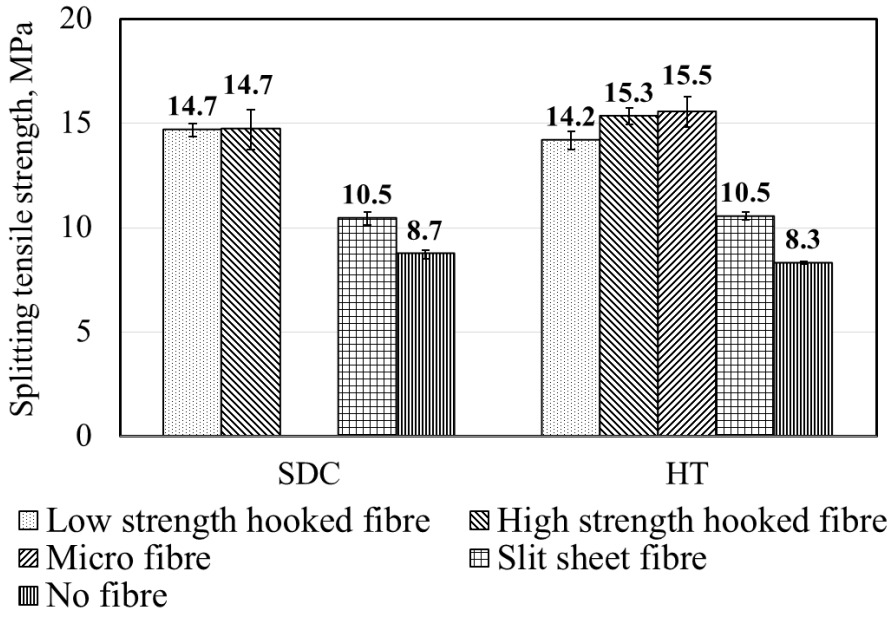

Figure 3.22 Splitting tensile strength of UHPC containing different types of fibres

3.6.1.5 Elastic modulus

In **Figure 3.23** the modulus of elasticity obtained for UHPFRCs can be seen for UHPC containing hooked fibres exposed to a standard curing regime. No difference in elastic modulus was observed and it seems that types of fibres did not affect the elastic modulus significantly.

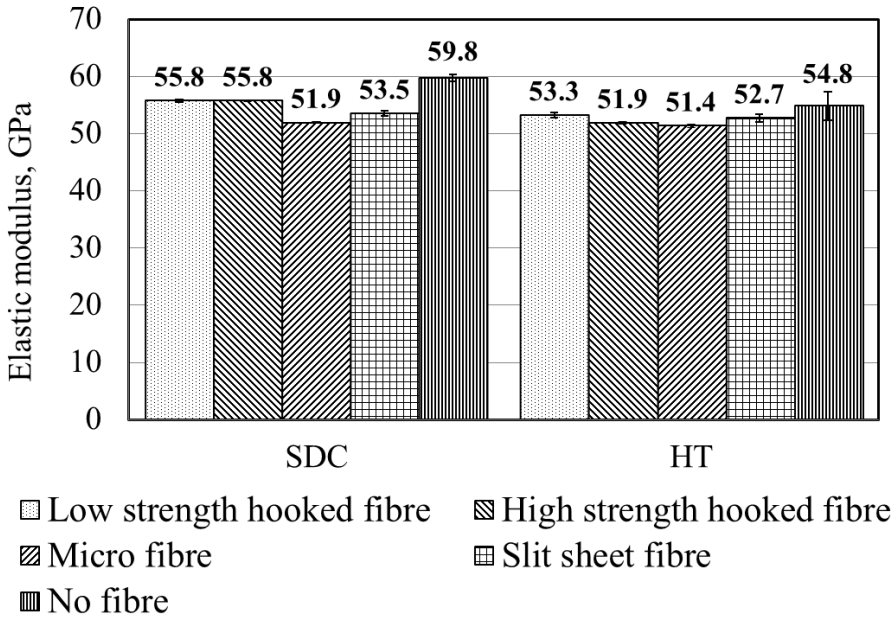

Figure 3.23 Elastic modulus of UHPC reinforced with different types of fibre

3.6.2 Effect of different curing regime on UHPC reinforcing with different types of fibre

The curing regimes considered for evaluating UHPFRC included:

- Heat treatment for 1, 3 and 6 days, followed by water curing in 24°C water up to the day of testing: 78 cubes to measure the compressive strength at 7 days and 28 days.
- Heat treatment for 27 days: 12 cubes to measure the compressive strength at 28 days.
- Heat treatment for 6 days, followed by water curing in 24°C water up to the day of testing: 12 cylinders, 6 dog-bones and 6 prisms for measuring E-value, splitting tensile strength, direct tensile strength and flexural strength.
- Standard curing regime: 24 cubes, 12 cylinders, 6 dog-bones and 6 prisms for measuring compressive strength, E-value, splitting tensile strength, direct tensile strength and flexural strength after 7 days and 28 days.

Hook-ended fibres (Type I) and Hook-ended fibres (Type II) are called High strength hooked fibre and Low strength hooked fibre, respectively. As seen in the figures, 1-HT, 3-HT, 6-HT and 27-HT indicate 1, 3, 6 and 27 days in heat treatment, respectively and 6-SDC and 27-SDC stand for 6 and 27 days in the standard curing regime.

3.6.2.1 Compressive strength

Figure 3.24 indicates the effect of different durations of heat treatment and standard curing regime on the 7-day compressive strength of UHPC and UHPC reinforced with high strength hooked fibre. By increasing the duration of heat treatment for UHPC reinforced with high strength hooked fibre from 1 day to 3 days and 6 days, the compressive strengths were enhanced by 5.5% and 11.2%, respectively. For UHPC, the enhancement in compressive strength from 1 day to 3 days of heat treatment was found to be up to 7.7%. However, by increasing the duration of heat treatment from 1 day to 6 days, the compressive strengths reduced by 4%. This strength reduction can be caused by the process of the cubes cooling down after heat curing. This process may cause the formation of micro cracks in the specimens. In the specimens containing fibre, this phenomena may be controlled by the presence of fibre to bridge the cracks and prevent the strength reduction.

By comparing the compressive strengths of UHPC and UHPFRC exposed to the standard curing regime to those that experienced heat treatment, the results show the significant effect of heat treatment (even for 1 day) on the early-age compressive strength of this type of concrete. In order to obtain a compressive strength exceeding 180 MPa heat treatment for 3 days would be a suitable curing regime.

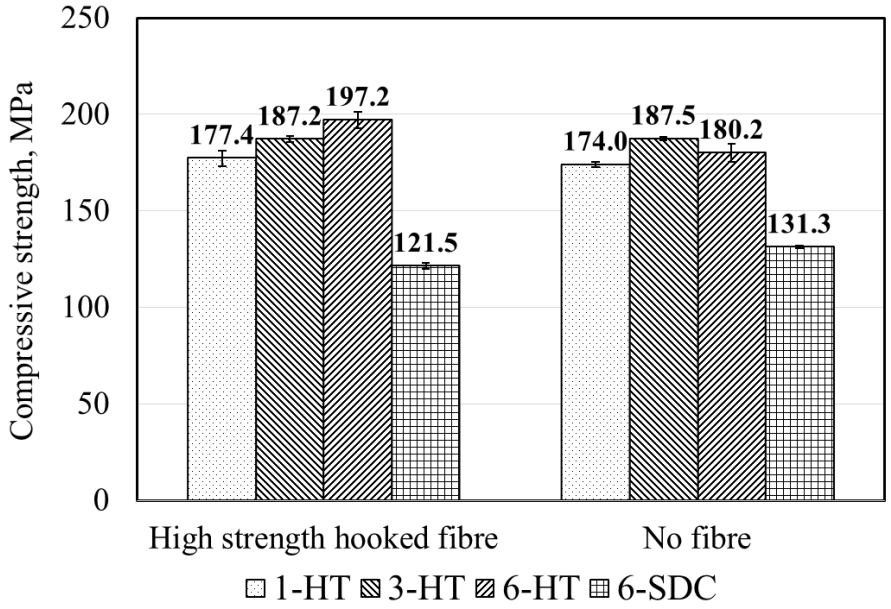

Figure 3.24 Compressive strengths at different curing regimes at 7 days

Figure 3.25 shows the effect of different durations of heat treatment and standard curing on the 28-day compressive strength of UHPC and UHPC reinforced with high strength hooked fibre. UHPC containing high strength hooked fibre showed a similar trend to the 7 days compressive strength results (shown in **Figure 3.24**), where strength increased with increasing the heat treatment durations from 1 day to 6 days. A compressive strength of 210.6 MPa was achieved when the specimens experienced 27 days of heat treatment. This long heat treatment duration is not considered to be practical or economical. The samples were cured such to find the highest possible compressive strength that can be expected from the UHPFRC. Even after 28 days, the compressive strength of UHPC reinforced with high strength hooked fibre cured in a standard curing regime showed almost the same strength as those experienced after 1 day of heat treatment.

For UHPC, the enhancement in compressive strength from 1 day to 3 days of heat treatment was up to 7.7%, while strength reduction was observed when the heat treatment duration was

increased from 1 to 6 days. The reason for the strength reduction can be due to the process of moving the specimen after 6 days from 85°C water (heat treatment) to 24°C water (standard curing regime). This may affected these specimens more than the ones that stayed in 85°C water for the shorter times. This process may cause the formation of micro cracks in the specimens. In the specimens containing fibre this phenomena may be controlled by the presence of fibre bridging the cracks thus preventing strength reduction.

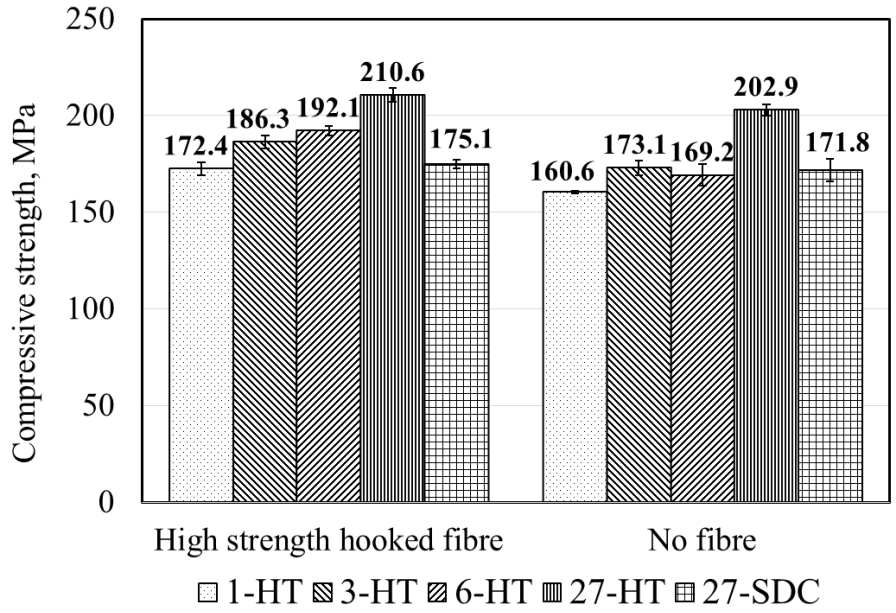

Figure 3.25 Compressive strengths at different curing regimes at 28 days

Figure 3.26 shows the effect of duration of heat treatment on the 7-day and 28-day compressive strengths of UHPC containing high strength hooked fibre. No significant difference in the 7-day and 28-day compressive strengths was noticeable for different durations of heat treatment. In other words, no strength gain was observed between 7 days and 28 days. For the practical purposes the compressive strengths obtained after 7 days is equivalent to the 28-day compressive strength.

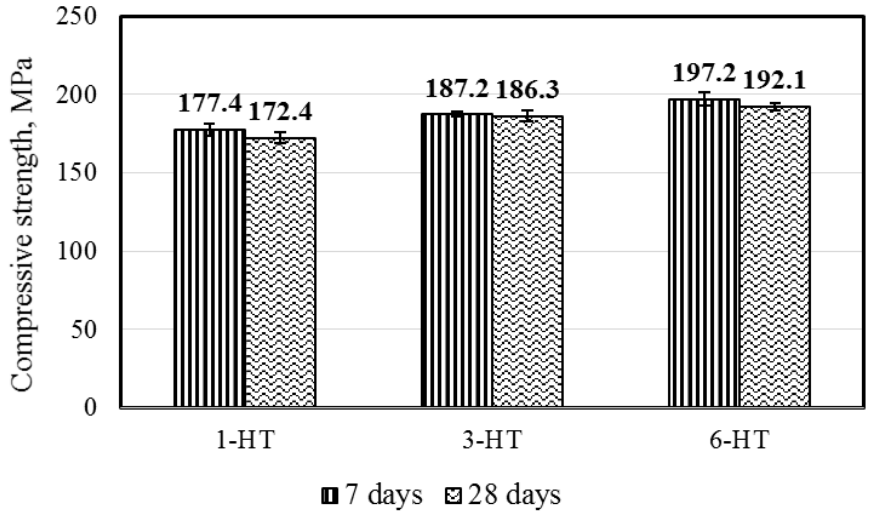

Figure 3.26 Effect of duration of heat treatment on 7-day and 28-day compressive strength of UHPC containing hook-ended fibre (Type II)

The effect of duration of heat treatment on the 7-day and 28-day compressive strength of UHPC can be seen in **Figure 3.27**. Strength reductions of up to 7.7 % are noticed between 7 days and 28 days. This can be due to thermal shock occurring in the specimens during the moving of the specimens from hot baths to standard curing baths. The heat gradient may cause micro cracks and this effect can be more pronounced in UHPC without fibre. This behaviour was a concern which led to more focused studies presented in section 3.7.

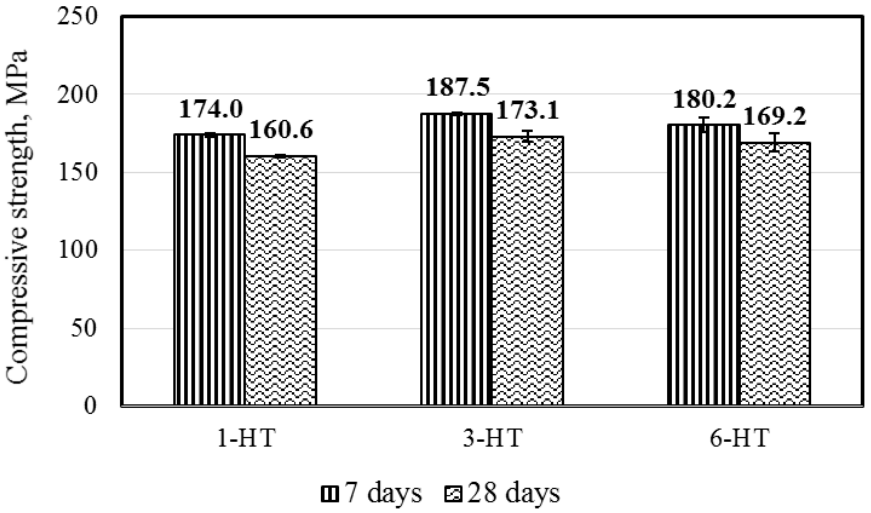

Figure 3.27 Effect of duration of heat treatment on 7-day and 28-day compressive strengths of UHPC

In the following, the compressive strength of UHPC in the presence of other fibres can be found in **Figure 3.28**. The discussion presented for UHPC reinforced with High strength hooked fibre, is also valid here.

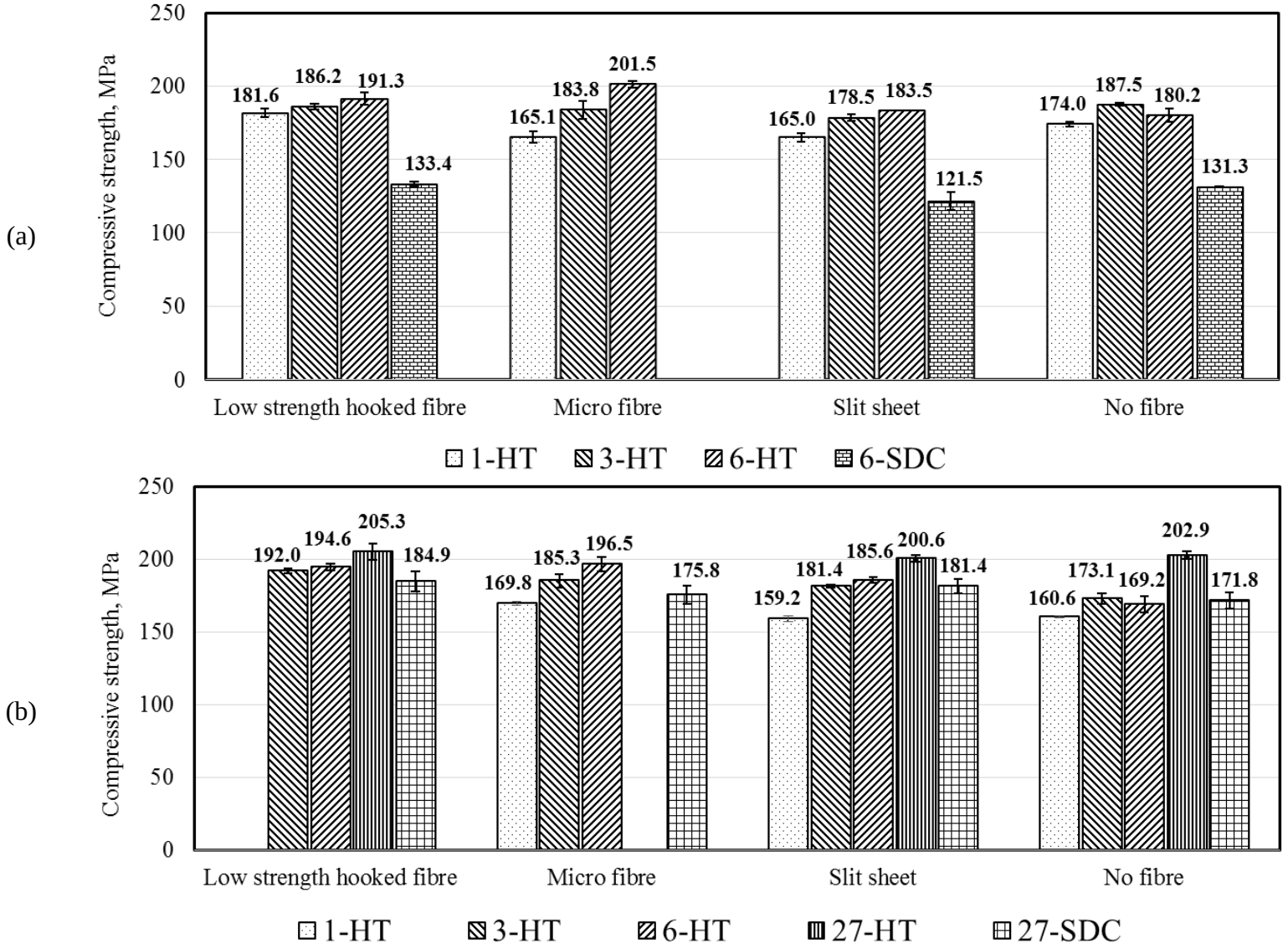

Figure 3.28 Compressive strengths of UHPC and UHPFRC at different curing regimes at, a) 7 days, b) 28 days

3.6.2.2 Direct tensile strength

In **Figure 3.29** the direct tensile strengths of UHPC and UHPC containing high strength hooked fibre are compared for different curing regimes. In UHPC containing high strength hooked fibre, no difference was observed between the strength for both curing regimes. However, the direct tensile strengths for UHPC without fibre seem to be affected by different curing regimes. Higher tensile strengths were achieved when a standard curing regime was applied.

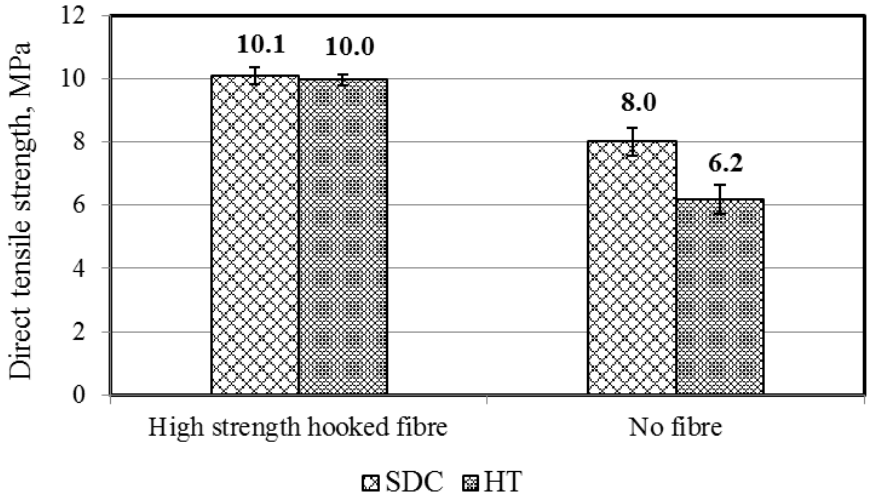

Figure 3.29 Effect of different curing regime on direct tensile strength of UHPC and UHPC containing hook-ended fibre (Type II)

3.6.2.3 Flexural strength

The flexural strengths of UHPC and UHPC containing high strength hooked fibre for different curing regimes are presented in **Figure 3.30**. For UHPC without fibre, the flexural strengths were identical regardless of curing regime type. However, in UHPFRC, the flexural strength obtained for the specimens that experienced heat treatment showed 36% higher strength than the ones experienced standard curing regime. The comparison between the flexural strength for UHPC and UHPFRC such as the energy absorption and strength enhancement is presented in more details in section 3.6.1.3.

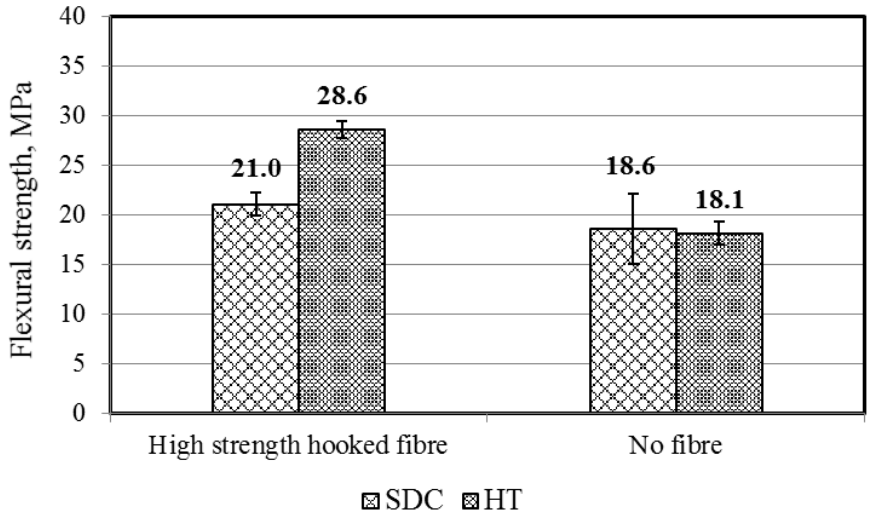

Figure 3.30 Effect of different curing regime on flexural strength of UHPC and UHPC containing hook-ended fibre (Type II)

3.6.2.4 Splitting tensile strength

The results for the splitting tensile strength of UHPC and UHPC containing high strength hooked fibre for different curing regimes are presented in **Figure 3.31**. For UHPC without fibre, the splitting tensile strengths were almost the same regardless of curing regime. The same behaviour was observed for UHPFRC.

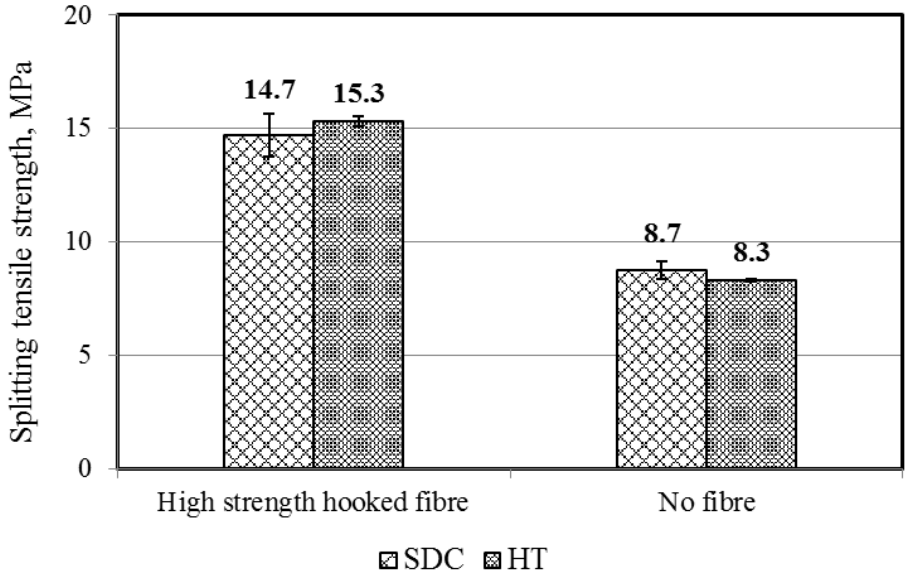

Figure 3.31 Effect of different curing regime on splitting tensile strength of UHPC and UHPC containing hook-ended fibre (Type II)

3.6.2.5 Elastic modulus

Figure 3.32 shows the elastic modulus of UHPC and UHPC containing high strength hooked fibre for different curing regimes. Since the modulus of elasticity describes the stiffness of

material, specimens which were under standard curing conditions shows higher stiffness than those that experienced heat treatment. This behaviour can be attributed to the heat treatment. It seems heat treatment causes micro crack formation in the specimens which leads to lower stiffness. This difference between the modulus of elasticity is more pronounced for the samples with no fibre. It seems that fibres in UHPC containing hook-ended fibres (Type II) can successfully bridge the cracks in such a way that the heat treatment damage effect is not considerable. The same behaviour was observed for other UHPFRC studies.

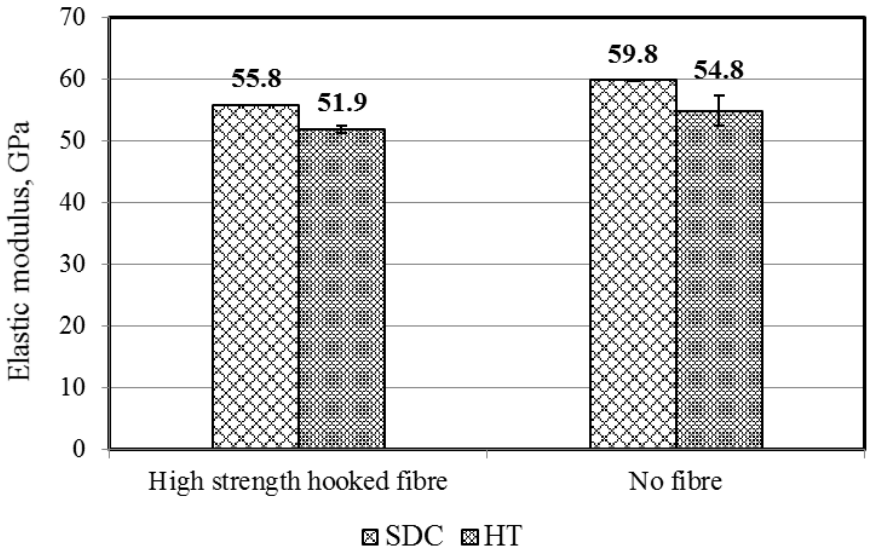

Figure 3.32 Elastic modulus of UHPC and UHPC containing hook-ended fibre (Type II) for different curing regimes

3.7 CURING REGIME: THE EFFECT OF HEAT GRADIENT ON THE COMPRESSIVE STRENGTH OF UHPC

The studies showed that curing regime plays an important role on the compressive strength of UHPC (see section 3.6.2.1). The compressive strengths of UHPC containing different types of fibre at different ages (see section of 3.6) were plotted in **Figure 3.33**. The results showed that the 28-day compressive strengths are lower than the 7-day strength for the UHPC containing no fibre and UHPC reinforced by hook-ended fibre (Type II). However, the strength reduction in other UHPFRCs was negligible. These results indicate the possibility of thermal shocking as a result of high heat gradient during the curing procedure. This phenomenon can happen either when cubes are placed in 85°C water after 24 hours curing at room temperature or at the time of moving cubes from 85°C to 24°C water. Besides, the strength loss can be the result of the glue used to make it easier to mix in this type of fibres.

There is thus a concern that the glue might affect the compressive strength, especially when high fibre contents are used.

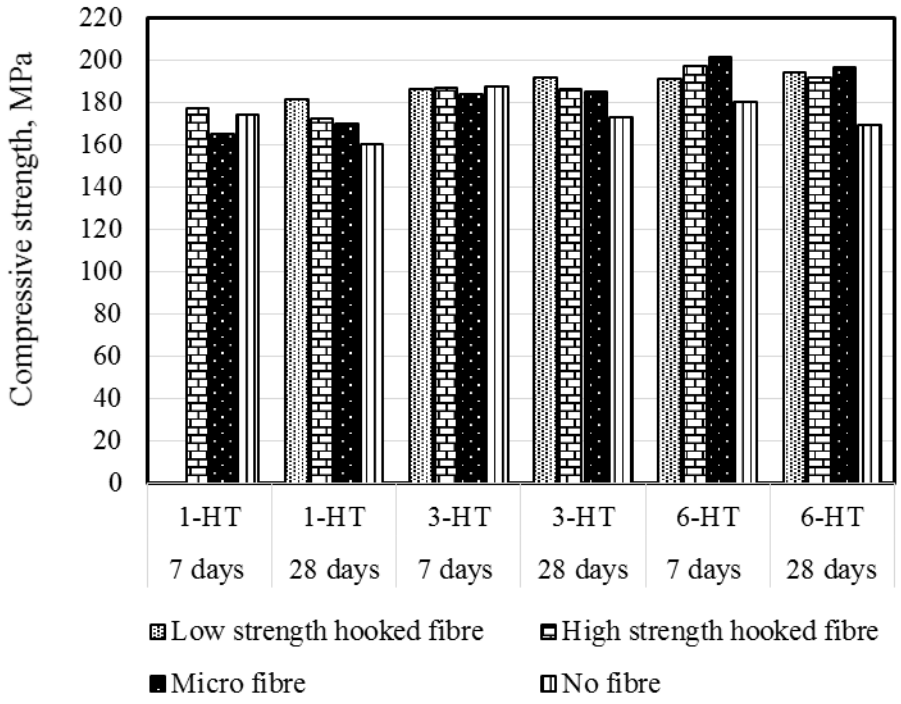

Figure 3.33 Compressive strength of UHPFRC for the different curing regimes (Vatannia, et al., 2016a)

These results inspired an investigations into the possibility of thermal shocking as a result of high heat gradient during the curing procedure. So, two different curing regimes with different procedures were investigated.

Firstly, the effect of different heat gradients on the compressive strength of UHPC was studied where after cubes were cured in a way that thermal shocking occurred during the curing time. It is noteworthy that these studies were first carried out on UHPC containing no fibre as the effect of thermal shocking is more pronounced for UHPC containing no fibres.

Secondly, UHPC was reinforced with hook-ended fibre (Type II) due to the strength reduction observed from 7 days to 28 days in UHPC reinforced with hook-ended fibre (Type II). The compressive strength of UHPFRC which experienced no thermal shocking during the curing process was used as reference.

The curing regimes for the first part of the study were as follows:

- Heat treatment at 65°C for 5 days followed by immediate water curing at 24°C up to the day of testing (7, 28 and 90 days).
- Heat treatment at 65°C for 5 days followed by storing under plastic sheets in a laboratory room at 24°C and 98% relative humidity up to the day of testing (7, 28 and 90 days).
- Heat treatment at 85°C for 5 days followed by immediate water curing at 24°C water up to the day of testing (7, 28 and 90 days).
- Heat treatment at 85°C for 5 days followed by storing under plastic sheets in a laboratory room at 24°C and 98% relative humidity up to the day of testing (7, 28 and 90 days).
- Heat treatment at 92°C for 5 days followed by immediate water curing at 24°C up to the day of testing (7, 28 and 90 days).
- Heat treatment at 92°C for 5 days followed by storing under plastic sheets in a laboratory room at 24°C and 98% relative humidity up to the day of testing (7, 28 and 90 days).
- Standard curing regime.

The curing regimes for the second part of the study were as follows:

- Heat treatment at 85°C for 3 days followed by water curing at 24°C up to the day of testing (7 and 28 days). The rising and falling of the water temperature was controlled to avoid thermal shocking. The temperature of the water bath was gradually increased from room temperature to 85°C. At the end of heat treatment, the temperature of the water was allowed to fall gradually to room temperature. The cubes were then stored in 24°C water up to the day of testing.

Moreover, hook-ended (Type II) steel fibres were added to the mix design in two different conditions. In one batch the fibres were added to the mix while they were glued as they were provided from the supplier and in the other batch the fibres were added after washing all the glue from the fibres.

It is noteworthy that the compressive strength of UHPC cured in 24°C water after heat treatment was measured by the cubes that been saturated in water before testing while the compressive strength of UHPC cured in room at 24°C after heat treatment were measured by the cubes in a dry condition.

3.7.1 Compressive strength of UHPC cured in the 24°C water after heat treatment

The compressive strength of UHPC where heat treatment was followed by 24°C water curing can be seen in **Figure 3.34**. A drop in strength can be observed from the 7-day strength to the 28-day strength at curing temperatures of 65°C and 92°C. It is worth noting that the reductions in the compressive strength from 7-day to 28-day strength were not significantly affected by the different heat gradients. At the highest heat gradient one may expect the higher reductions in the compressive strength, but this reduction is the same as the one observed for the lowest heat gradient. Interestingly, the 90-day compressive strengths increase in a way that exceeds the 7-day strengths. It seems that the pozzolanic reaction has continued, resulting in the strength enhancement.

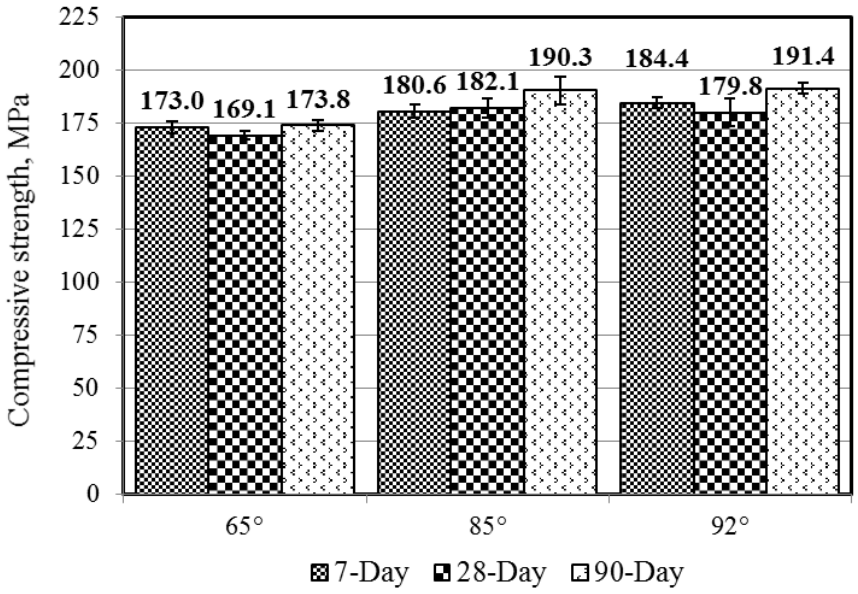

Figure 3.34 Compressive strength of UHPC cured at different temperatures (Vatannia et al., 2016b)

In **Figure 3.35** the effect of different curing temperatures on 7, 28 and 90-day strengths of UHPC placed in 24°C water after the heat treatment are compared. It shows that increasing the temperature of heat treatment from 65° to 92°C leads to an increase in 7-day strength from 173 to 184.4 MPa while this trend is not observed for 28-day strengths. The 28-day compressive strength of UHPC exposed to 92°C was lower than the strength of cubes

exposed to 85°C heat treatment. An enhancement in 90-day compressive strength is observed for increased temperature of heat treatment.

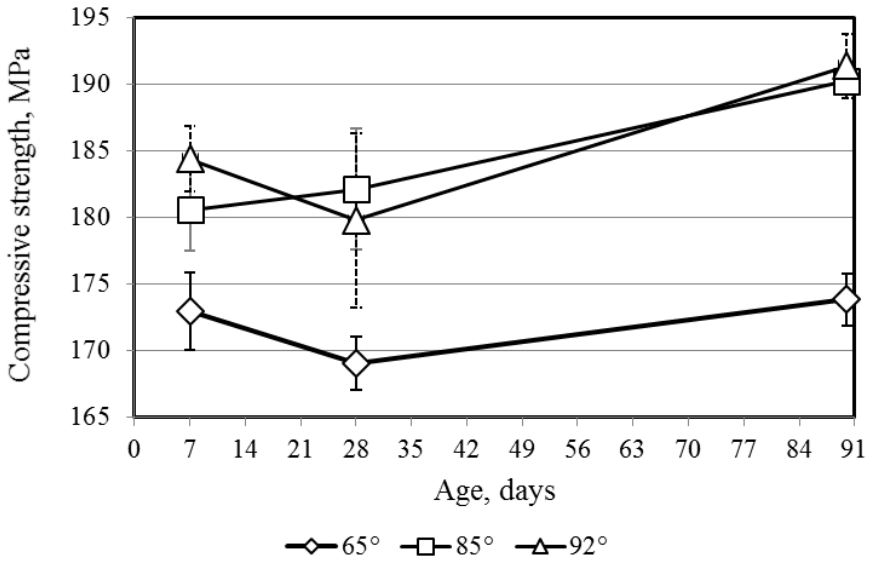

Figure 3.35 The effect of heat curing temperature on compressive strength

The compressive strength of non-heat treated UHPCs (cured only in 24°C water) is shown in **Figure 3.36**. These results indicate that UHPC cured at 24°C has the same 28-day compressive strength, as well as higher 90-day compressive strength than the concrete that experienced heat treatment at 65°C. While, heat treatment at 65°C may limit DEF, but it is not an economical curing regime, since, the same 28-day strength, and higher 90-day compressive strength is achievable by applying the standard water curing regime.

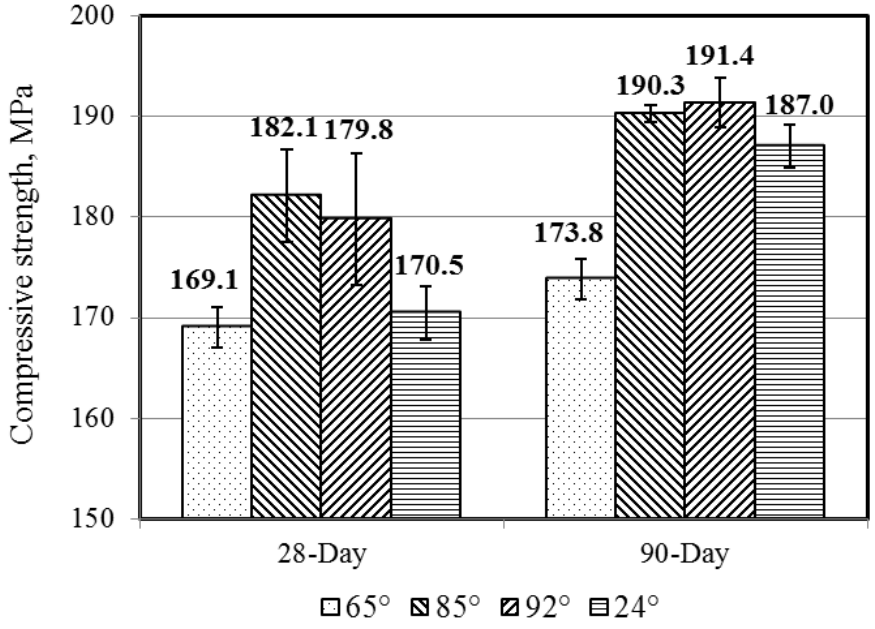

Figure 3.36 Comparison between normal curing and heat curing

3.7.2 Compressive strength of UHPC cured in room at 24°C after heat treatment

UHPC cured in a laboratory room at 24°C after the heat treatment, showed no reduction in strength between 7-day and 28-day strengths, as can be seen in **Figure 3.37**. This can be attributed to the fact that the samples did not experience thermal shocking during the curing process. However, it seems that curing the samples in the laboratory room at 24°C adversely affected the 90-day compressive strength. A 2.4% and 5.5% reduction were observed in the compressive strength of cubes which experienced 85°C and 92°C heat treatment, respectively. No reduction in 90-day compressive strength occurred in samples that experienced 65°C heat treatment. This can be attributed to the limited DEF in UHPC.

Strength loss at 90 days for the samples exposed to 85°C and 92°C can be attributed to either "self-desiccation" or the "crossover effect" or a combination of both effects (Jensen and Hansen, 1999). Self-desiccation causes autogeneous shrinkage and a RH-drop without any moisture leaving the concrete. The rate and final relative humidity (RH) level depends only on the water cement ratio, type of cement and temperature conditions during curing. The autogeneous shrinkage might be high enough to cause internal cracking and therefore decreased the strength. The crossover phenomena occur in samples exposed to high temperature at early ages. This phenomena cause strength loss at later ages as a result of non-uniform distribution and rapid formation of the Calcium Silicate Hydrate crystals within the pores and the hardening paste. Since the crossover effect can only occur in samples that experienced a temperature exceeding 65-70°C at early ages (Türkel and Alabas, 2005), the strength loss did not occur in the samples exposed to 65°C while it happened in samples that experienced higher temperatures. It seems that self-desiccation can also amplify the strength loss. Since the samples cured in the laboratory room after heat treatment did not have access to water, the self-desiccation affected the 90-day strength and led to the strength loss. The reason that no strength loss was observed at 90 days in the samples cured in water after the heat treatment is the access of samples to water, despite the crossover effect. Curing the samples in water after heat treatment helps them to suck up water, thus compensating the low water to cement ratio, resulting in more hydration taking place.

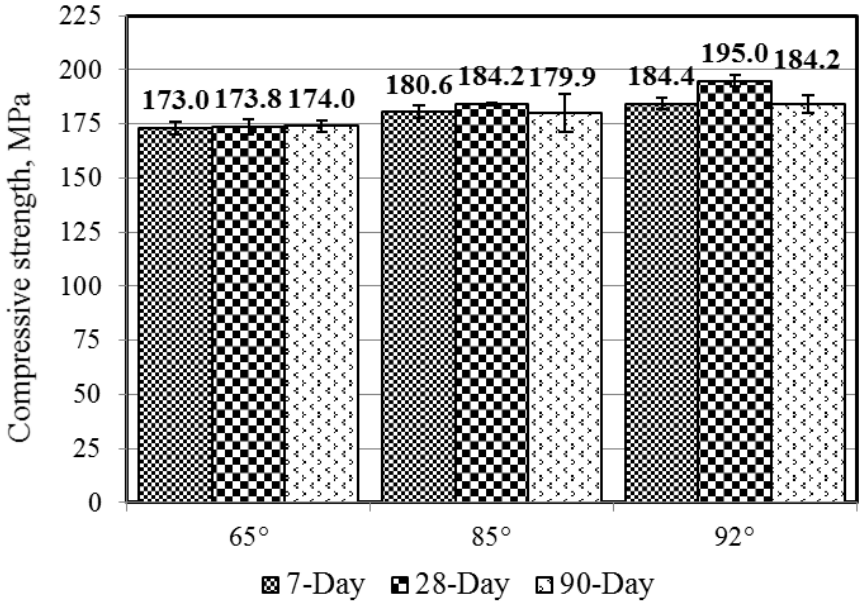

Figure 3.37 Compressive strength of UHPC cured at different water temperatures followed by 24°C laboratory room

The effect of different curing temperatures on 7, 28 and 90-day strengths of UHPC placed in the 24°C laboratory room after the heat treatment can be seen in **Figure 3.38**. Increasing the temperature from 65°to 92°C leads to compressive strength enhancement at 7, 28 and 90 days. The strength loss for the samples exposed to 92°C heat treatment from 28-day to 90-day strength indicates that self-desiccation still remains a problem. In order to avoid that, it is recommended that the samples that experienced 92°C heat treatment should be stored in water after heat treatment.

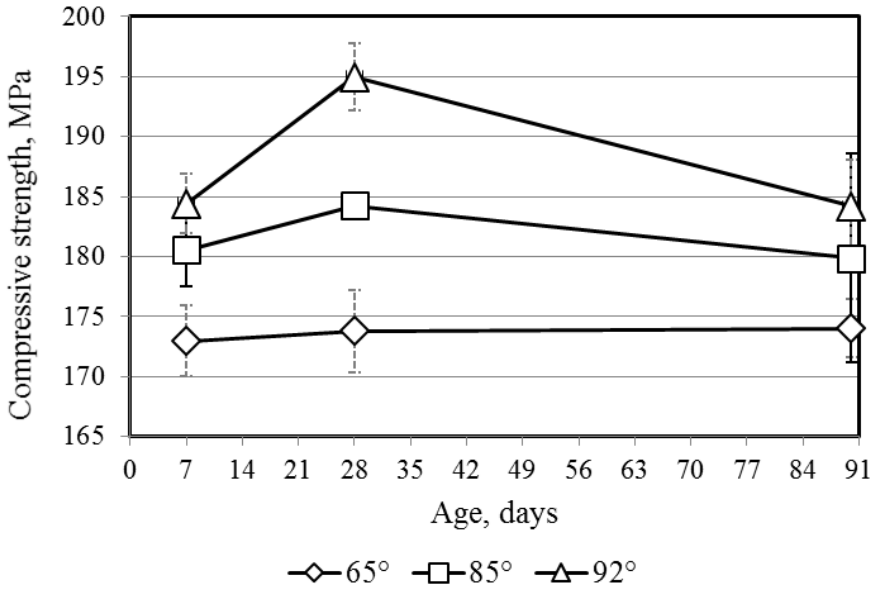

Figure 3.38 The effect of temperatures on the compressive strengths of UHPC placed in 24°C laboratory room

The results showed that thermal shocking has a negative effect on the compressive strength. Care should be taken to avoid thermal shocking in heat curing regimes.

3.7.3 Compressive strength of UHPFRC experienced no thermal shocking

Figure 3.39 shows the compressive strength of UHPC containing hook-ended fibres (Type II) that experienced no thermal shocking during the curing regime. The compressive strengths of UHPC containing glued hook-ended fibre (Type II) (their original format), showed a slight strength reduction (2.6%) from 7 days to 28 days. However, no strength reduction is observed in the compressive strength of UHPC containing washed hook-ended fibre (Type II). In UHPC containing hook-ended fibre (Type II) (original format), the compressive strength reduction from 7 days to 28 days (up to 2.8%) takes place regardless of thermal shocking occurrence during the curing regime process (see section of 3.6.2.1). So, it seems that the glue is the reason of the strength reduction which has a minimal negative effect on the compressive strength of UHPC.

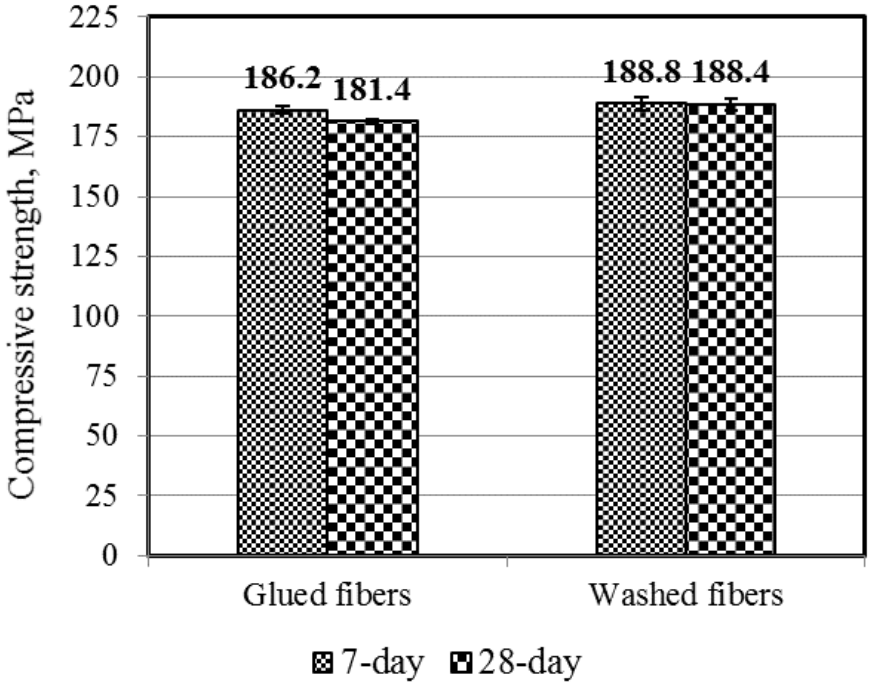

Figure 3.39 Compressive strength of UHPC containing hook-ended fibre (Type II) experienced no thermal shocking

3.8 UHPC REINFORCED WITH LOCALLY AVAILABLE FIBRE

Despite of significant mechanical properties achieved for UHPC reinforced with hook-ended fibre (Type II) and micro fibre, locally available fibre was chosen in order to produce

UHPFRC at the lowest possible cost. The shape and properties of locally available fibres were introduced in the section 3.2. The mechanical properties of UHPC reinforced with locally available fibres (using both andesite and dolomite as aggregate) were investigated, including compressive strength, modulus of elasticity and splitting tensile strength. The results for compressive strengths were evaluated at:

- 2 days after casting. The specimens were kept in a laboratory room covered in plastic sheets. No heat treatment was applied to the specimens;
- 3 days after casting. The specimens were kept in a laboratory room covered in plastic sheets. No heat treatment was applied to the specimens;
- 7 days after casting. After 3 days, the specimens were submerged in water. The temperature of the water bath was gradually increased from room temperature to 80°C. The specimens were exposed to 80°C water for 2 days. The rising and falling of the water temperature was controlled to avoid thermal shocking. At the end of heat treatment, the temperature of the water was controlled to fall gradually to room temperature;
- 28 days after casting. After heat treatment (2 days in 80°C water) the specimens were allowed to cool down to room temperature, covered in plastic sheets and kept in the laboratory room.

The specimens were kept up to 3 days in the laboratory room to evaluate the appropriate time at which UHPC can achieve a minimum compressive strength for the time of wire releasing in the future prestressed beams.

The compressive strengths of UHPC reinforced with locally available fibres containing different types of aggregate are presented in **Figure 3.40**. The compressive strengths at 7 and 28 days exceed 180 MPa for both UHPFRCs and are comparable to the previous studied UHPFRCs (see section 3.6.1.1). Regardless of aggregate type, no difference in compressive strengths was observed. However, UHPFRC containing dolomite showed higher workability due to the dolomite's round shape which might be taken into account during casting of large structural elements.

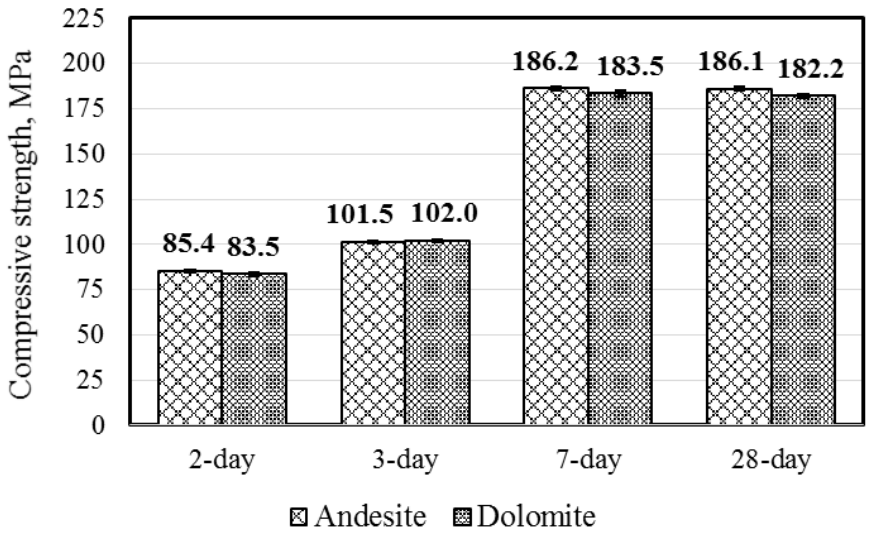

Figure 3.40 Compressive strength of UHPC reinforced with locally available fibres containing different types of aggregate

The modulus of elasticity and splitting tensile strength were measured at 28 days. 52.3 GPa and 19.0 MPa were achieved for modulus of elasticity and splitting tensile strength in UHPFRC containing andesite, respectively. No major difference was observed for the modulus of elasticity achieved in the previous UHPFRC mixes that experienced heat treatment. Higher splitting tensile strength was achieved with the locally available fibres. A modulus of elasticity and splitting tensile strength in UHPFRC containing dolomite of 56.9 GPa and 18.5 MPa respectively was achieved. These results motivated the utilization of locally available fibre in UHPC. Both dolomite and andesite are deemed suitable to produce UHPFRC.

3.9 FINAL MIX COMPOSITION AND CURING REGIME

After taking all the results obtained for UHPC mix designs tested during the research into account, a final mix design was chosen as presented in **Table 3.14**.

The curing procedure selected for this project was as follows:

The samples were kept covered by plastic sheets in a laboratory room with 98% relative humidity for 48 hours, then submerged in room temperature water. The water temperature was gradually increased to 80°C. The samples remained in the hot bath for 2 days, where after the temperature of the water decreased gradually to room temperature. After cooling down the samples were wrapped with plastic sheets and kept in a laboratory room up to the day of testing.

It is noteworthy that the unit costs of the final UHPFRC containing dolomite and andesite were 42.5 (ZAR/m^3/MPa) for both mix designs, while the unit cost for UHPC was 10.5 (ZAR/m^3/MPa). The significant difference is due to the locally available fibre cost (40500 ZAR/ton). Higher cost of locally available fibre leads to the significant cost difference between the final mix designs and the proposed mix designs presented in section 3.5.

Table 3.14 Final mix designs

Material	**UHPFRC with Dolomite (kg/m^3)**	**UHPFRC with Andesite (kg/m^3)**	**UHPC with Andesite (kg/m^3)**
Cement (CEM II/A 42.5R)	291	297	302
Cement (CEM II/A 52.5N)	291	297	302
USF	175	178	182
GGBS	115	120	120
Sand (Max:4.75 mm)	1020	1035	1055
Stone (Max: 6.7 mm)	440	445	455
Water	146	148	151
Locally available fibre	152	152	----
Admixture	21.8	22.2	22.7

Beside the material cost, the cost of high temperature extended curing time, extended mixing times in comparison with NSC mixing time was also considered.

For heat treatment, the time required for the water at room temperature (25°C) to reach 80°C was taken as 2 hours/m^3. It was assumed that 0.25 m^3 water would be enough to submerge 1 m^3 of concrete. A heat loss of 30% in the hot bath for the two days of heat treatment was assumed. Calculations were based on 0.25 m^3 water with specific heat capacity of 4.18 j/g°C. The electricity fee per kWh was taken as 2 ZAR/kWh. The cost of the energy required to increase and maintain the temperature of water at 80°C was calculated as 165 ZAR/m^3.

To estimate the cost of the extended mixing time, it was assumed that the mixing time in the production of UHPFRC was twice the mixing time in NSC production. A concrete mixer with 300 litre capacity and the productivity of 3 m^3/hour has an engine with 7.7 Hp (horse power) equal to 6 kW (Machineryenterprises, 2019). If the mixing time in UHPFRC is twice the mixing time in NSC, then an extra 6 kWh is needed which is 12 ZAR.

The extra labour costs for casting and consolidating 1 m^3 concrete were calculated using Eq. (3.1) and Eq. (3.2), respectively (Merta, et al., 2010):

$$C_{L,c} = c_L \cdot T_c \cdot V_c \quad \text{Eq. (3.1)}$$

$$C_{L,v} = c_L \cdot T_v \cdot A_{c,s} \quad \text{Eq. (3.2)}$$

where c_L (ZAR/h) denotes the labour costs per working hour (150 ZAR/h), T_c (h/m^3) represents extra concreting time (1 h/m^3) and V_c (m^3) denotes the volume of the concrete beam (1 m^3), T_v (h/m^2) is the extra vibration time required for the consolidation of concrete (1 h/m^2) and $A_{c,s}$ (m^2) is the concrete surface area (1 m^2).

Table 3.15 presents the extra costs in the process of UHPFRC fabrication when compared to initial cost for manufacturing NSC. These extra costs are only 6% of the material cost in UHPFRC.

Table 3.15 Summary of extra costs per cubic metre in UHPFRC fabrication

Extra cost	**Amount (ZAR)**
Energy required for the heat treatment	165
Energy required for extended mixing time	12
Labour costs for casting	150
Labour costs for consolidating	150
Σ	477

3.10 CONCLUSIONS

In this chapter, the preliminary experiments carried out to develop the mix design and curing regime were presented. Economical and practical UHPC can be manufactured to be suitable in large-scale applications. This accomplishment is possible as a results of several modifications to the typical UHPC mix design. These modifications include:

- The aggregate content has been increased to reduce the consumption of cementitious materials. An aggregate to cement ratio (by mass) of 2.5 was used, thus reducing the cement content to 593 kg/m^3.

- The aggregate size was increased. Andesite with a maximum particle size of 4.75mm and 6.7mm was chosen as a fine aggregate and coarse aggregate respectively. Dolomite with the same grading can be an alternative. No sieving was done for aggregates and they were used in the mix as they were supplied from the quarry.
- Portland cement (CEM II/A 42.5R and CEM II/A 52.5N), silica fume and Ground Granulated Blast Furnace Slag were considered as cementitious materials.
- Local straight steel fibre with 13mm length and 0.26 diameter was utilized to reinforce UHPC.

- Development of an economical UHPC is successfully achieved by increasing the aggregate content and sizes, using supplementary cementitious materials beside cement. The unit costs per compressive strength for the proposed mix design was significantly reduced from 109 ZAR/m^3/MPa for the typical mix design to 28.0 ZAR/m^3/MPa. All the materials used to manufacture UHPC were locally available. In the process of manufacturing, no milling or special mixer was used. Only equipment which are available in a standard concrete laboratory were used.

- An average compressive strength of 185 MPa was achieved for UHPC containing 2% by volume fraction of steel fibre.

- It was observed that fibre tensile strengths do not have a significant effect on the ultimate compressive strength of specimens. However, their effect can be observed on the post-cracking ductile behaviour of concrete. A compressive strength of 192 MPa is achievable with the proposed mix design after 72 hrs of heat treatment.

- Although no strain-hardening was observed in direct tensile behaviour, a considerable effect was seen on the post-cracking behaviour and energy absorption. With normal curing, direct tensile strengths of 10 MPa and 9.85 MPa were obtained for UHPC containing hook-ended fibre (Type II) (3000 MPa tensile strength) and micro fibres (2500 MPa tensile strength) respectively. The other UHPFRCs did not show desirable ductile behaviour due to the weak tensile strength of the fibres.

- The beams containing micro fibres and hook-ended fibre (Type II) gave a ductile respond under flexural loads and 28 MPa and 26 MPa were achieved as the flexural strength, respectively. Beams had a strength increase after first cracking of 50% and 35% respectively. This behaviour was not observed in the other UHPFRC.

- Fibres had a significant effect on the post-cracking behaviour and the ultimate splitting tensile strength of UHPFRC. The increase in the strength of UHPFRC after the first cracking can be noted as 42% and 38% for hook-ended fibre (type II) and micro fibres, respectively. UHPC containing hook-ended fibre (Type II) showed more ductility in the splitting tensile behaviour.

- It seems that heat treatment has a negative effect on the stiffness of UHPFRC and the elastic modulus obtained from cylinders that experienced standard curing is higher than those cured for 72 hrs in 85°C. This effect is more considerable in samples with no fibres.

- For UHPC cured in water after the heat treatment, a reduction in compressive strength from 7-day strength to 28-day strength was observed. It seems that thermal shocking has a negative effect on the compressive strength. It is worth mentioning that the reduction in strength was not significantly affected by the different heat gradients and did not continue at older ages as the 90-day compressive strengths exceeded the 7-day strengths.

- For UHPC cured in the laboratory at room temperature after the heat treatment, no reduction was observed from 7-day to 28-day strength. These samples did not experience thermal shocking. However, strength reductions occurred in the 90-day compressive strength in comparison to the 28-day strength of samples that experienced 85°C and 92°C heat treatment, respectively. The samples are not only exposed to the high temperatures (more than 65°C) at early ages, but the water to cement ratio is also low. The reason for strength loss at 90 day can be attributed to the either “self-desiccation” or “crossover effect” or the combination of both effects.

- Storing UHPC in water after the heat treatment eliminates the self-desiccation phenomena, thermal shocking of samples should be avoided.

- UHPC containing washed fibres showed no reduction in the compressive strength from 7-day to 28-days. However, a reduction was observed in UHPC reinforced with glued fibres. It seems that glue used to make it easier to mix fibres into concrete could have a negative effect on the compressive strength of UHPC. Additional research is needed to confirm this negative influence.

- UHPC reinforced with locally available fibres containing dolomite showed higher workability than the same UHPFRC containing andesite.

CHAPTER 4 EXPERIMENTAL SETUP TO DETERMINE LOSSES AND BOND BEHAVIOUR

4.1 INTRODUCTION

This chapter describes the study programme to evaluate not only shrinkage and creep but also the bond performance between the concrete and the prestressing wire. Drying shrinkage and creep were measured for UHPC and UHPFRC via calibrated LDVTs. The properties of the prestressing wire is presented and the test set-up to perform pull-out tests is illustrated. Pull-out test was performed on UHPC and UHPFRC containing andesite. Finally, the experimental programme including the specimens' specifications and ages is introduced.

4.2 DRYING SHRINKAGE

Drying shrinkage of UHPC and UHPFRC was measured using cylinder specimens (100 mm diameter, 300 mm length). The specimens were demoulded after 48 hours and stored in a room at 24°C and 95% humidity. Deformation was recorded using one LVDT for each specimen. The shrinkage set-up is illustrated in **Figure 4.1**.

Figure 4.1 Shrinkage set-up for UHPC and UHPFRC

4.3 CREEP

To measure the creep that could affect prestress losses in UHPC and UHPFRC two cylinder specimens (100 mm diameter, 300 mm length) were used for each mix. The creep specimens were loaded 2 days after casting (2-day age). Deformation was recorded using LVDTs taking readings every 60 seconds for the first 7 days, followed by a reading every 120 seconds for the rest of the duration of testing. The specimens and the set-up as indicated in **Figure 4.2** were kept in a room at 24°C and 95% humidity.

Figure 4.2 Creep set-up for UHPC and UHPFRC

4.4 PRESTRESSING STEEL WIRE PROPERTIES

Tensile testing was conducted on indented wires with a 7 mm diameter. The average ultimate strength and modulus of elasticity were measured. An MTS 250 Universal Testing Machine was used to apply tension to the wires until fracture. Each wire was centered and clamped into the grips. The tensile stress-strain behaviour of the prestressing wire is presented in **Figure 4.3**. The results confirmed the average ultimate tensile strength of 1750 MPa and a modulus of elasticity of 192 GPa.

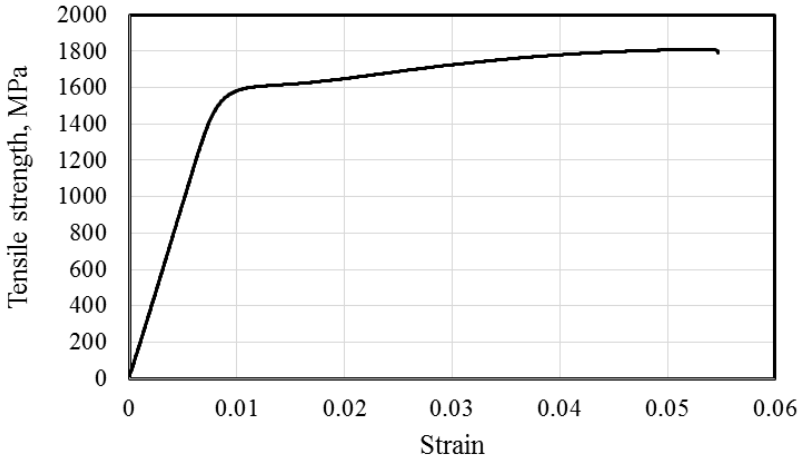

Figure 4.3 Tensile stress-strain curve of prestressing wire

4.5 PULL-OUT TESTING PLAN

Pull-out test was conducted to evaluate the bond performance between the concrete and the prestressing wire. Pull-out test was carried out on UHPC and UHPC containing 2% fibres (content by volume) and andesite as the aggregate. The tests were performed with three LVDTs measuring the slipping of the wire (as seen in **Figure 4.4**) while load is being applied to the wire. Each pull-out specimen consisted of a concrete cylinder with a wire embedded along its axis and protruding on both sides. Load was applied on the wire protruding on one side. Three LVDTs were mounted to touch the bottom face of the cylinder while attached to the wire, thus recording relative movement. The pull-out test set-up is shown in **Figure 4.5**. The cylindrical specimens were cast in different lengths and diameters of PVC tube. The tubes were left confining the concrete during testing not only for the sake of convenience, but also to hold the specimen together, once failure had occurred.

Figure 4.4 LVDT layout in pull-out test

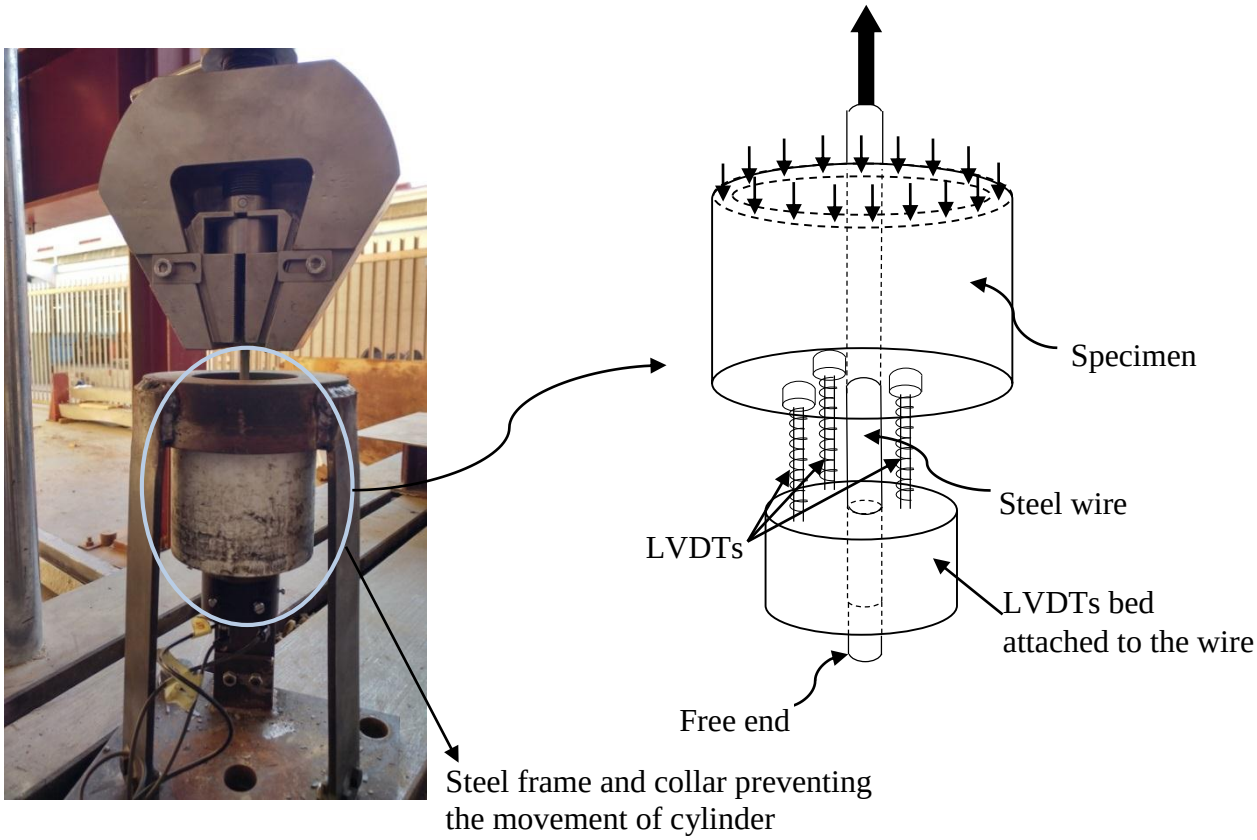

Figure 4.5 Pull-out testing set-up

This test program consisted of two parts. The first part of the test program involved the evaluation of the development length of the 7 mm diameter wire in UHPC containing fibre and no fibre. All the specimens had an identical diameter of 105 mm while their length were different including 75 mm, 100 mm, 125 mm and 150 mm. The pull-out test as well as concrete properties including compressive strength, modulus of elasticity and splitting tensile strength tests were performed 2 days, 7 days, 14 days, 28 days and 56 days after casting. More details about the specimens tested is provided in **Table 4.1**. The reason for testing the concrete properties as well as pull-out strength at 2 days is that the plan was to release prestressing wires in the beams 2 days after casting.

In the second part, the effect of concrete cover on bond strength was investigated. All the specimens had an identical length of 100 mm while the diameters were different including 45 mm, 70 mm and 105 mm. The pull-out test was performed 2 days and 28 days after casting. Compressive strength and modulus of elasticity were measured at 2 days and 28 days while splitting tensile strength was measured only at 28 days. More details about the specimens

tested is provided in **Table 4.2**. It is noteworthy that no identical batches were cast in both studies. The batches differed in that the cement aged, which would lead to different mechanical properties.

Table 4.1 Characteristics of the specimens tested for pull-out in the first part of study

Name	Length (mm)	Diameter (mm)	Fibre	Testing time
P-75L-105D	75	105	Yes & No	2 days
			Yes & No	14 days
			Yes & No	28 days
			Yes & No	56 days
P-100L-105D	100	105	Yes & No	2 days
			Yes & No	14 days
			Yes & No	28 days
			Yes & No	56 days
P-125L-105D	125	105	Yes & No	2 days
			Yes & No	14 days
			Yes & No	28 days
			Yes & No	56 days
P-150L-105D	150	105	Yes & No	2 days
			Yes & No	14 days
			Yes & No	28 days
			Yes & No	56 days

Table 4.2 Characteristics of the specimens tested for pull-out in the second part of study

Name	Length (mm)	Diameter (mm)	Fibre	Testing time
P-100L-45D	100	45	No	2 days
			Yes	28 days
P-100L-70D	100	70	Yes	2 days
			Yes & No	28 days
P-100L-105D	100	105	Yes & No	2 days
			Yes & No	28 days

4.6 BOND STRESS CALCULATION

According to Bandyopadhyay (2008) "bond stress (τ_{bd}) is defined as the shear force per unit nominal surface area of reinforcing bar. The stress is acting on the *interface between bars and surrounding concrete* and along the direction parallel to the bars." Bond stress is shown in **Figure 4.6** which presents the free-body diagram of a steel bar being pulled out of concrete.

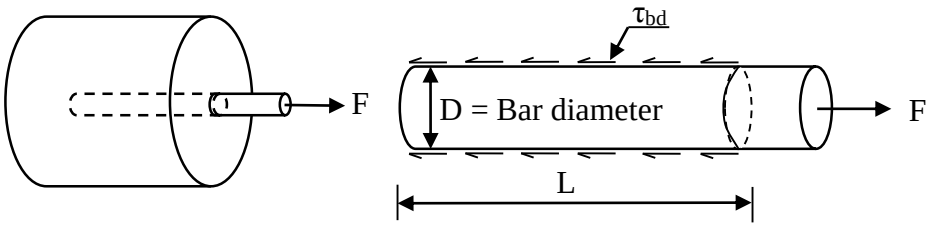

Figure 4.6 Free-body diagram of a steel bar being pulled out of concrete

One of the major assumptions considered in ACI 318-89 building code for the basic development length under tension is uniform bond stress distribution over the development length at ultimate. The bond stress (τ_{bd}) assumption in this study is based on ACI 318-89 and was calculated using Eq. (4.1), where D, L and σ_s represents bar diameter, embedment length and tensile stress in bar.

$$\tau_{bd} \times D\pi L = \sigma_s \times \pi D^2/4 \qquad \text{Eq. (4.1)}$$

Required embedment length is provided if the bond between the reinforcing bar and surrounding concrete is sufficient to transfer the force required to rupture the steel bar when the bar is under tension in a pull-out test.

CHAPTER 5 EXPERIMENTAL RESULTS OF DRYING SHRINKAGE, CREEP AND BOND PERFORMANCE

5.1 INTRODUCTION

This chapter covers the experimental results of not only drying shrinkage and creep tests but also of bond performance obtained from pull-out tests for UHPC and UHPFRC containing andesite.

In the first bond study, the results of development length was studied by comparing results for specimen with different lengths but identical diameter. The results of pull-out tests for UHPC and UHPFRC are compared for different ages of 3, 7, 14, 28 and 56 days. Finally, a summary of bond strength and tensile strength in prestressing wires are presented.

In the second study, the effect of concrete cover on bond strength is evaluated by considering specimen with different diameters but identical length. The results of pull-out tests for UHPC and UHPFRC are compared for ages of 2 and 28 days.

The mechanical properties for UHPC and UHPFRC, including the compressive strength, modulus of elasticity and splitting tensile strength, are reported for both studies. Different values for mechanical properties in the studies were achieved due to different batches of cement over a four year period.

5.2 DRYING SHRINKAGE RESULTS

The results of long-term drying shrinkage of UHPC and UHPFRC are presented in **Figure 5.1**. The results are presented in terms of micro strain calculations for each specimen. The results revealed that UHPFRC experiences higher drying shrinkage compared to UHPC. After 110 days, the drying shrinkage of 360 με and 250 με were respectively achieved for UHPFRC and UHPC which is much less than the value recommended by AFGC (2002) and JSCE (2006) (550 με). This phenomenon is generally accepted since the codes uses upper bound values for conservative designs and they are not predictive.

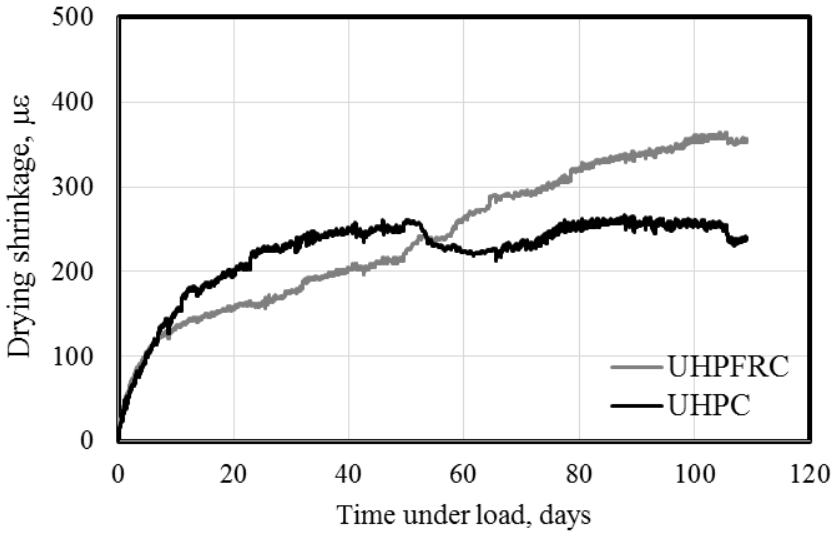

Figure 5.1 Drying shrinkage of UHPC and UHPFRC

5.3 CREEP RESULTS

The creep performance of UHPC and UHPFRC specimens is presented in **Figure 5.2**. Elastic strains have been deducted from the measured creep results. As seen in the figure, similar ultimate creep values were obtained for both UHPC and UHPFRC. Creep coefficients (ratio of the ultimate creep strain to the elastic strain) of 2.4 and 2.3 were achieved for UHPC and UHPFRC, respectively. These values are higher than those recommended by AFGC (2002) and JSCE (2006) (0.8). This phenomenon can be attributed to different material properties used in this research as well as the probable LDVT drifts where due to measurement of very small strains in this study, the results might be affected. However, as a recommendation to future works, further investigation with very accurate apparatus should be carried out in that regard.

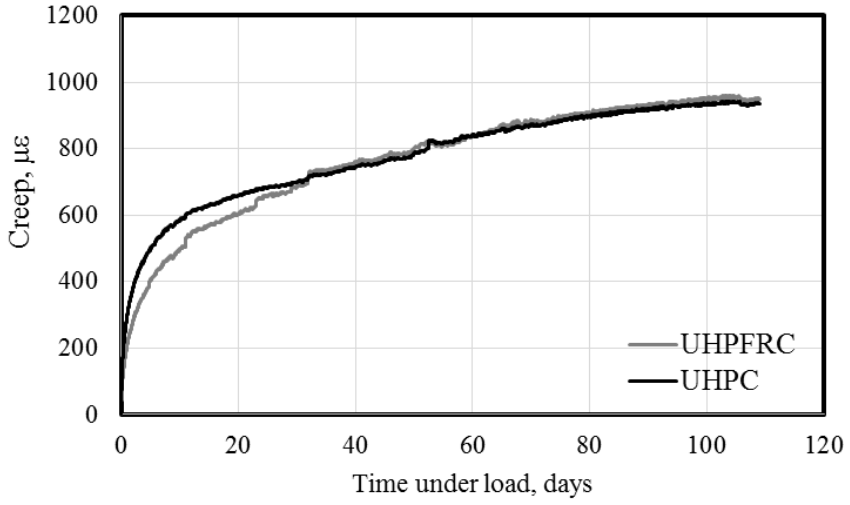

Figure 5.2 Creep in UHPC and UHPFRC

5.4 EVALUATION OF DEVELOPMENT LENGTH

5.4.1 Mechanical properties of UHPC and UHPFRC

Table 5.1 presents the properties of UHPC and UHPFRC including compressive strength, modulus of elasticity and splitting tensile strength at different ages. The compressive strength of 92.7, 158.2 and 166.0 MPa was achieved in the presence of fibres at the ages of 3 days, 7 days and 14 days, respectively. These results show the enhancement of the compressive strength over the time. Modulus of elasticity improved from 44.6 GPa to 53.7 GPa between the ages of 3 days and 7 days while no significant improvement was observed at later ages. The same trend was observed for the splitting tensile strength. No significant enhancement in splitting tensile strength occurred from 7 days to the later ages.

Table 5.1 Properties of UHPC and UHPFRC for steel bond length tests

		3 days	7 days	14 days	28 days	56 days
Compressive strength (MPa)	With fibre	80.8	158.2	166.0	168.5	160.4
	No fibre	85.7	152.1	158.3	160.0	162.3
Modulus of elasticity (GPa)	With fibre	42.8	53.7	54.3	54.9	54.2
	No fibre	43.7	56.1	55.2	56.1	56.4
Splitting tensile strength (MPa)	With fibre	12.0	16.1	16.5	19.0	17.9
	No fibre	7.4	9.9	9.9	9.9	8.3

5.4.2 Pull-out test results: Different lengths with identical diameter

In this part of study, three distinct failure modes for bond occurred: (1) concrete splitting, (2) bond failure and (3) wire rupture. Concrete splitting takes place due to the formation of longitudinal cracks spreading radially as a result of wedging action. Bond failure occurs if the bond length is too short to transfer the full load required to fracture the wire. Wire fracture is an indication of sufficient bond length. **Table 5.2** presents the properties of specimens including length, age, fibre presence, maximum capacity of pull-out load and the type of failure. Under the "Specimen" column of this table, the following notations were used: P, L, f or nf and d which presents Pull-out, Length of specimen in mm, Specimens containing fibre or no fibre, and number of days of aging, respectively. In this section, this notation is used to identify the specimens. Each value indicated is the average of 3 specimens tested unless different failure mechanisms were observed where the number following the failure mode gives an indication of the number of specimens that failed in each mode.

The results indicate that in all the specimens with 75 mm length, bond failure occurred. It indicates that there is not sufficient embedment length in 75mm-length specimens. By providing more 125 mm embedment length (independent of fibre presence), wire rupture occurred in all specimens. This indicates that 125 mm is sufficient embedment length for 7 mm prestress wires in both UHPC and UHPFRC.

5.4.2.1 Pull-out results after 3 days

Figure 5.3 presents the pull-out behaviour of the specimen with 75 mm length 3 days after casting. No Slip occurred before 16 MPa. In the presence of fibre, after slip initiation, higher stresses were sustained in comparison to the specimens without fibre, which failed due to loss of bond. Another types of failure that occurred in the specimens without fibre, was loss of bond accompanying concrete cracking. This behaviour showed a sudden loss of bond stress due to the formation of cracks. However, complete bond loss did not occur. The failure was not sudden and failure of bond took place gradually. In the absence of the PVC cover, the specimen would have split into pieces after the formation of splitting cracks at the time of failure. The PVC cover kept the integrity of the specimens. i.e. The PVC cover does not provide any confinement on specimen, it helped to retain the integrity of the concrete after the formation of cracks.

Similar 3-day bond behaviour was observed for 100 mm bond length as can be seen in **Appendix C**.

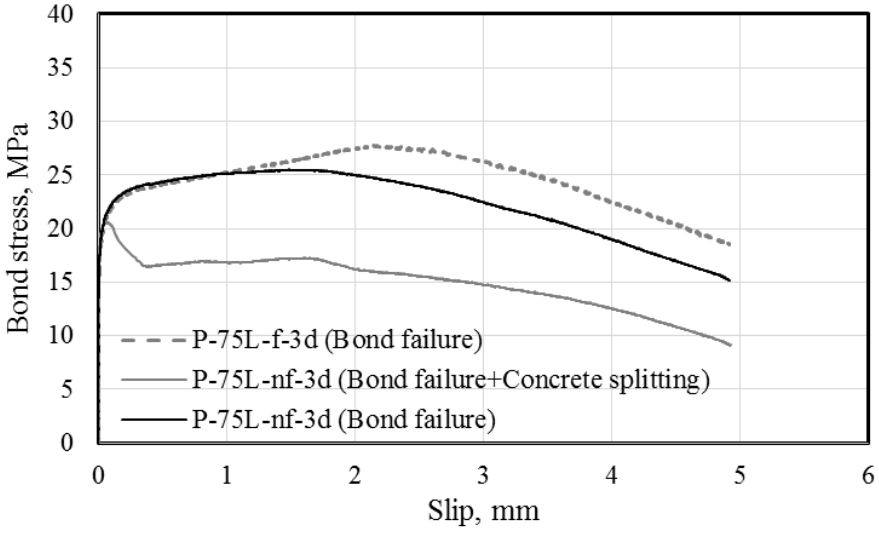

Figure 5.3 Pull-out behaviour of the specimens with 75 mm length after 3 days

Table 5.2 Pull-out results for specimens with different lengths but identical diameter

Specimen	Embedment Length (mm)	Diameter (mm)	Age (days)	Fibre	Load (kN)	Bond stress (MPa)	Stress in wire (MPa)	Failure mode
P-75L-f-3d	75	105	3	2%	44.26	26.83	1150	Bond
P-100L-f-3d	100	105	3	2%	55.48	25.23	1442	Bond
P-125L-f-3d	125	105	3	2%	50.03 67.18	18.20 24.44	1300 1746	Bond (2) Rupture (1)
P-150L-f-3d	150	105	3	2%	68.20 67.68	20.67 20.52	1771 1758	Bond (1) Rupture (2)
P-75L-nf-3d	75	105	3	No	36.26 42.04	21.98 25.49	942 1092	Bond+ Concrete splitting (2) Bond (1)
P-100L-nf-3d	100	105	3	No	59.43 51.00	27.02 23.19	1544 1325	Bond (1) Bond+ Concrete splitting (2)
P-125L-nf-3d	125	105	3	No	66.15	24.06	1719	Bond
P-150L-nf-3d	150	105	3	No	61.30 67.95	18.58 20.60	1593 1766	Bond (1) Rupture (2)
P-75L-f-7d	75	105	7	2%	64.43	39.06	1674	Bond
P-100L-f-7d	100	105	7	2%	67.79	30.83	1761	Rupture
P-125L-f-7d	125	105	7	2%	68.04	24.75	1768	Rupture
P-150L-f-7d	150	105	7	2%	68.40	20.73	1777	Rupture
P-75L-nf-7d	75	105	7	No	44.25	26.83	1150	Concrete splitting
P-100L-nf-7d	100	105	7	No	67.60 58.00	30.74 26.37	1756 1507	Rupture (2) Concrete splitting (1)
P-125L-nf-7d	125	105	7	No	68.76 67.74	25.01 24.64	1786 1759	Rupture (2) Concrete splitting (1)
P-150L-nf-7d	150	105	7	No	67.89	20.58	1764	Rupture
P-75L-f-14d	75	105	14	2%	63.31	38.38	1645	Bond
P-100L-f-14d	100	105	14	2%	67.70	30.78	1759	Rupture
P-125L-f-14d	125	105	14	2%	68.61	24.96	1783	Rupture
P-150L-f-14d	150	105	14	2%	68.87	20.88	1789	Rupture

P-75L-nf-14d	75	105	14	No	45.88	27.82	1192	Concrete splitting
P-100L-nf-14d	100	105	14	No	67.09 67.21 43.50	30.50 30.53 19.78	1742 1746 1130	Rupture (1) Bond (1) Concrete splitting (1)
P-125L-nf-14d	125	105	14	No	67.45	24.54	1753	Rupture
P-150L-nf-14d	150	105	14	No	67.82	20.56	1762	Rupture
P-75L-f-28d	75	105	28	2%	65.62	39.78	1705	Bond
P-100L-f-28d	100	105	28	2%	67.68	30.78	1759	Rupture
P-125L-f-28d	125	105	28	2%	68.79	25.02	1787	Rupture
P-150L-f-28d	150	105	28	2%	67.41	20.43	1752	Rupture
P-75L-nf-28d	75	105	28	No	34.58	20.97	898	Concrete splitting
P-100L-nf-28d	100	105	28	No	40.12 68.36	18.24 31.08	1042 1776	Concrete splitting (2) Bond (1)
P-125L-nf-28d	125	105	28	No	68.81	25.03	1788	Rupture
P-150L-nf-28d	150	105	28	No	67.08	20.33	1743	Rupture
P-75L-f-56d	75	105	56	2%	63.26	38.35	1644	Bond
P-100L-f-56d	100	105	56	2%	67.59	30.73	1756	Rupture
P-125L-f-56d	125	105	56	2%	67.75	24.65	1760	Rupture
P-150L-f-56d	150	105	56	2%	67.36	20.42	1750	Rupture
P-75L-nf-56d	75	105	56	No	40.17	24.36	1044	Concrete splitting
P-100L-nf-56d	100	105	56	No	61.41 68.00	27.92 30.92	1596 1767	Concrete splitting (2) Rupture (1)
P-125L-nf-56d	125	105	56	No	68.96	25.09	1792	Rupture
P-150L-nf-56d	150	105	56	No	67.46	20.45	1753	Rupture

Pull-out behaviour of the specimens with 150 mm embedment length after 3 days is shown in **Figure 5.4**. Both specimens with and without fibre experienced wire rupture and bond failure. In the specimens without fibre, which experienced bond failure, slipping took place at a lower pull-out load and the steel wire was pulled out with less bond resistance.

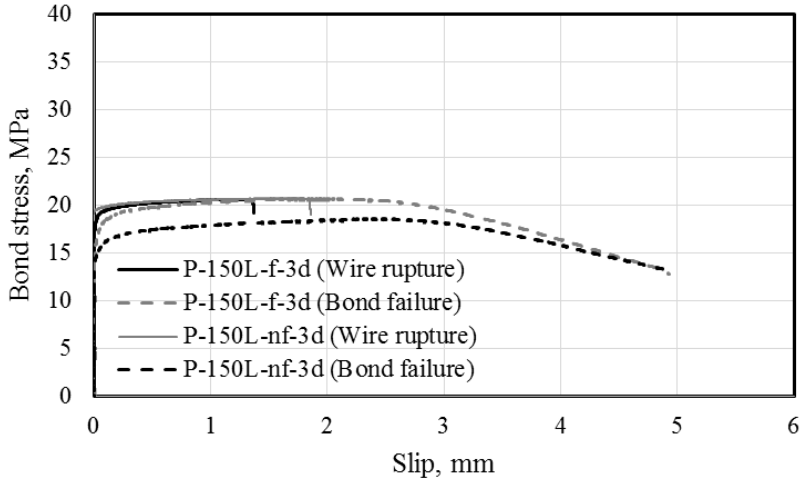

Figure 5.4 Pull-out behaviour of the specimens with 150 mm length after 3 days

5.4.2.2 Pull-out results after 7 days

Pull-out behaviour of the 75mm-length specimens after 7 days is presented in **Figure 5.5**. In the presence of fibre, no slipping occurred before 19.4 MPa. After slip initiation, the fibres significantly improved the bond resistance against pull-out load, which led to enhancement of capacity of pull-out resistance to 37.6 MPa. In contrast, in the specimens with no fibre, sudden bond loss took place, due to concrete splitting with limited slipping. Due to insufficient embedment length, bond failure was observed in samples containing fibre. Results for additional tests can be seen in Appendix C.

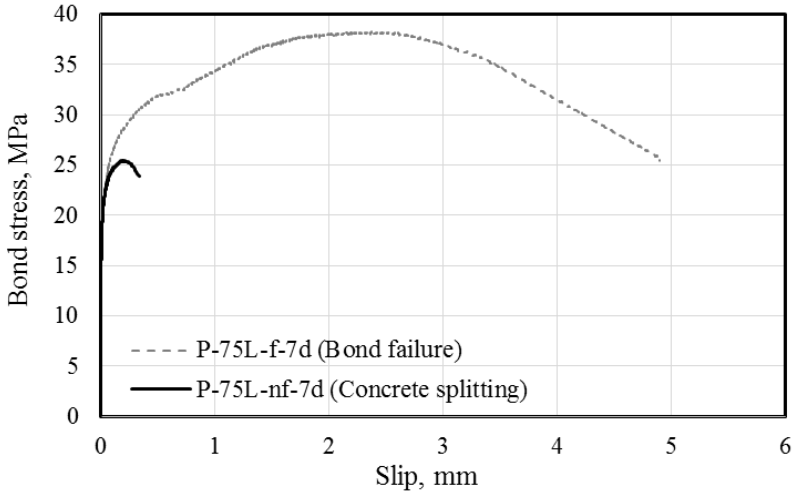

Figure 5.5 Pull-out behaviour of the specimens with 75 mm length after 7 days

Figure 5.6 displays the results of pull-out tests for 150mm-length after 7 days. As seen in this figure, in both samples with fibre and without fibre samples, the slipping started at about 18.2 MPa. However, the presence of fibres helped the steel wire reach yielding load earlier, due to the improved interaction at the steel wire-concrete interface. The same behaviour was observed for the shorter length (P-125L-f-7d and P-125L-nf-7d in **Figure C.3**). In the specimens without fibre, the wire ruptured after more slipping occurred in the specimens.

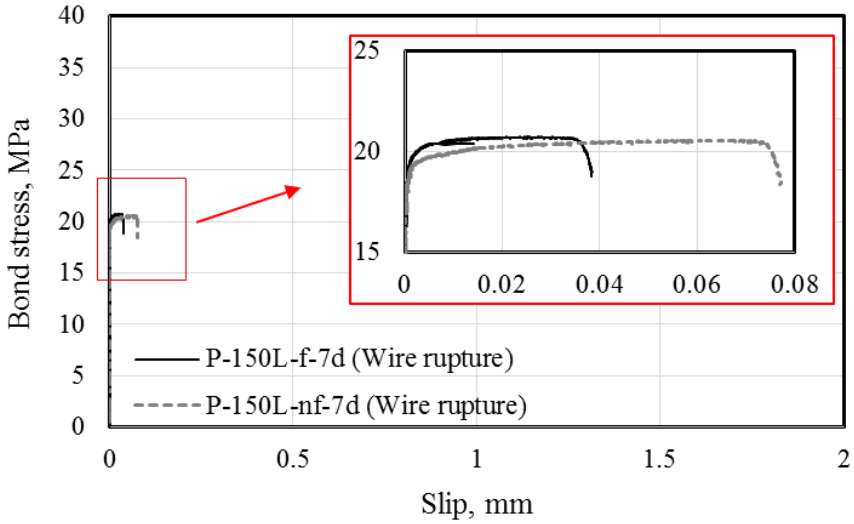

Figure 5.6 Pull-out behaviour of the specimens with 150 mm length after 7 days

Figure 5.7 presents the 7 day specimens after failure. In P-75L-nf-7d, the crack formation at the time of the failure can be observed in **Figure 5.7.a** representing the concrete splitting as a type of failure. No cracking was observed in P-75L-f-7d (**Figure 5.7.b**). In P-100L-f-7d and P-100L-nf-7d, almost all the specimens failed by the wire rupture (as seen in **Figure 5.7.c** and **d**) except one of the no-fibre specimen, which failed by concrete splitting. This failure occurred due to the formation of longitudinal cracks spreading radially as a result of wedging action. The cracks displayed in the figure indicate that the specimens failed due to concrete splitting. In the 125mm-length specimens with no fibre, two types of failure (wire rupture and concrete splitting) took place, while in the 125mm-length specimens containing fibre only one type of failure (wire rupture) occurred (**Figure 5.7.f**). As seen in **Figure 5.7.e,** in the specimen on the left, the wire ruptured accompanying by a cone of concrete. The formation of a cone of concrete did not happen in the other specimens which experienced wire rupture. Independent of fibre presence, the 150mm-length specimens failed due to wire rupture (**Figure 5.7.g** & **Figure 5.7.h**). The least damages occurred in the 150mm-length specimens with no fibre in comparison with the other no fibre-specimens with lengths of 75 mm, 100 mm and 125 mm.

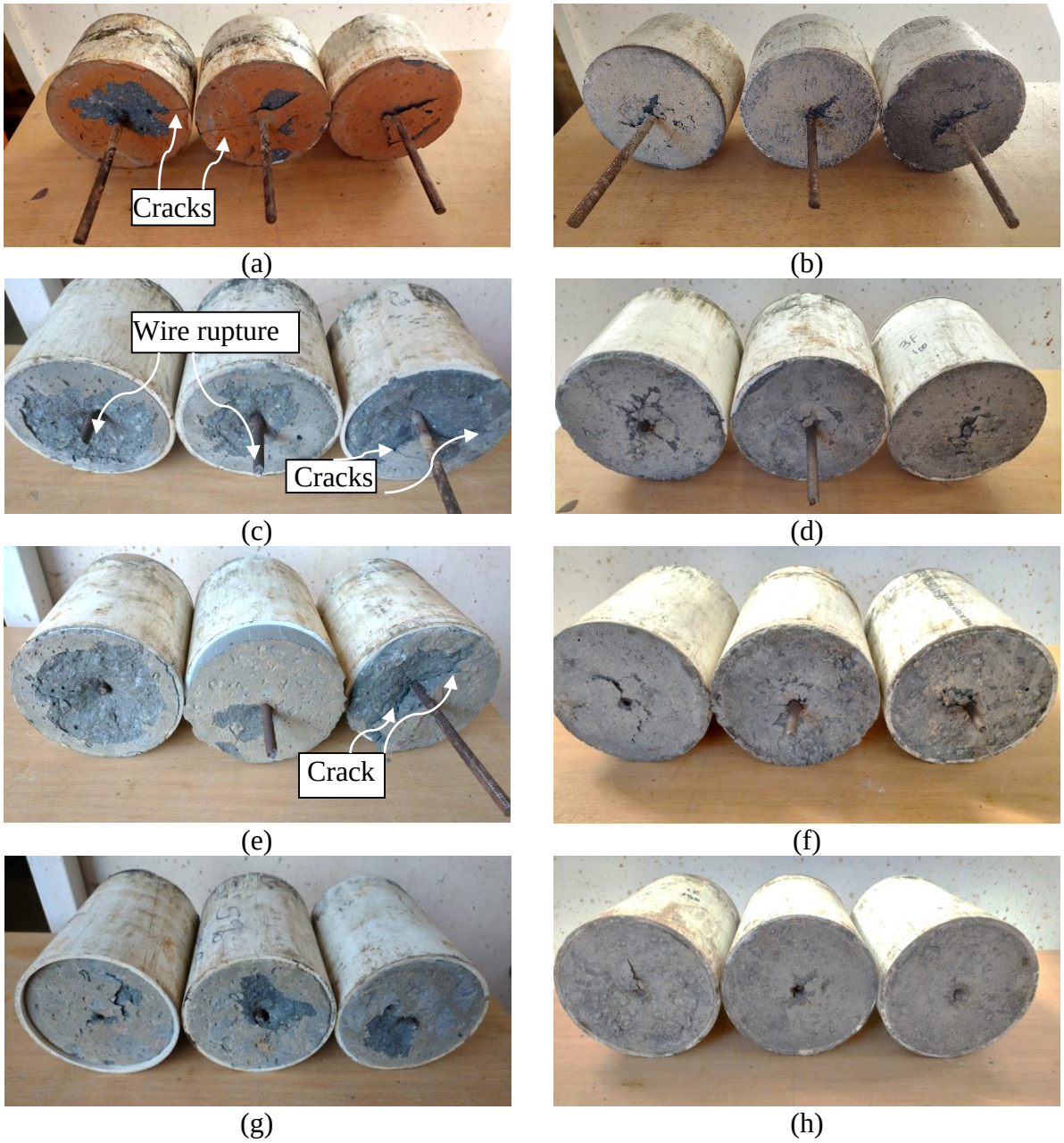

Figure 5.7 Specimens after pull-out test after 7-day a) P-75L-nf-7d, b) P-75L-f-7d, c) P-100L-nf-7d, d) P-100L-f-7d, e) P-125L-nf-7d, f) P-125L-f-7d, g) P-150L-nf-7d, h) P-150L-f-7d

Results for tests conducted 14 days after casting can be seen in Appendix C.

5.4.2.3 Pull-out results after 28 days

Pull-out behaviour of the specimens with 75 mm length after 28 days can be seen in **Figure 5.8**. In the specimens with no fibre the sudden formations of cracks led to the complete loss of steel wire-concrete bond. The specimens failed due to the concrete splitting. This type of behaviour was not observed in the specimens containing fibre. In these specimens, after the initiation of slipping at about 24.2 MPa, the bond was maintained which

led to the pull-out load enhancement up to 40 MPa. This can be attributed to the presence of fibres at the interface of concrete and the steel wire. After reaching to the maximum capacity of the specimens, they failed due to bond failure.

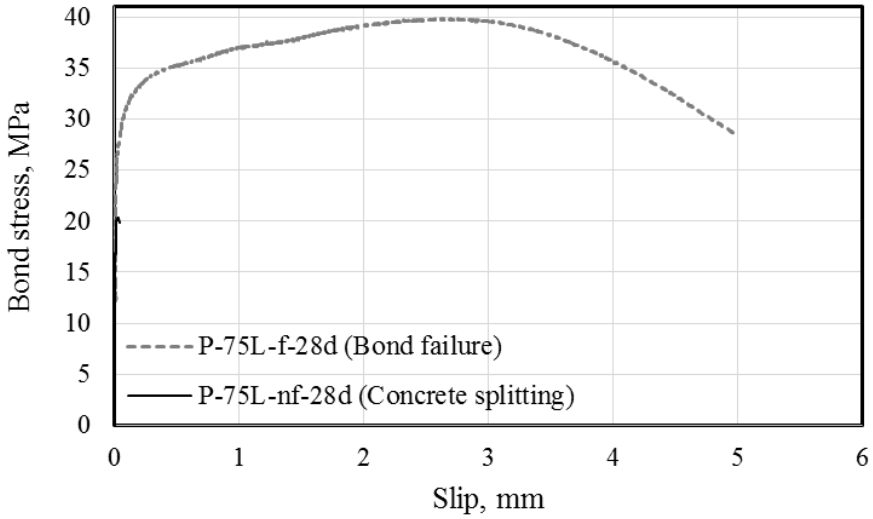

Figure 5.8 Pull-out behaviour of the specimens with 75 mm length after 28 days

The pull-out behaviour of specimens with 100 mm length after 28 days is shown in **Figure 5.9**. The specimens with fibre reached a higher pull-out load at slipping initiation in comparison with the specimens with no fibre. The specimens containing no fibre showed two types of failure: concrete splitting & bond failure. The specimen that experienced concrete splitting failure exhibited the least pull-out load capacity in comparison with the specimens that experienced bond failure. The no-fibre specimens which experienced bond failure, reached a maximum capacity of 30.9 MPa at 1.8 mm slip. The pull-out load dropped after further slipping which led to bond failure.

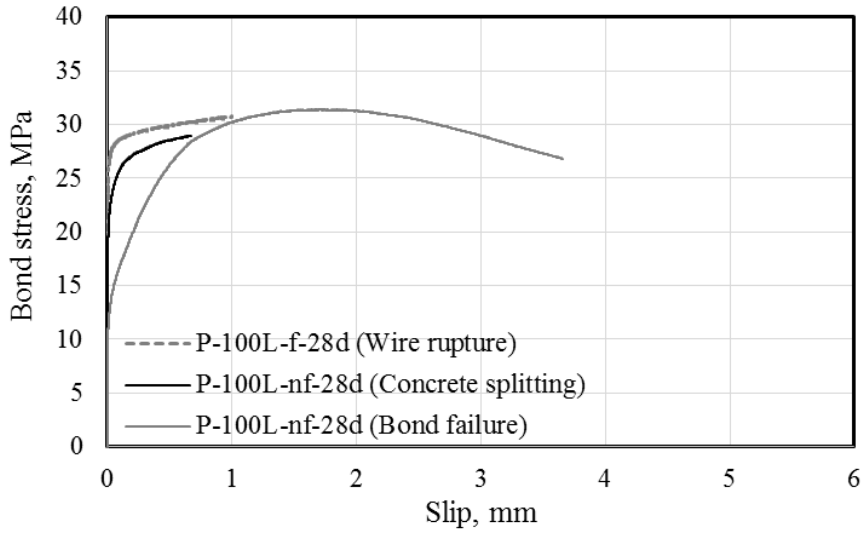

Figure 5.9 Pull-out behaviour of the specimens with 100 mm length at 28 days

The behaviours of 125mm-length specimens are presented in **Figure 5.10**. Interestingly, the sets of fibre and no-fibre specimens showed similar behaviours under pull-out load. Each set of these specimens had two different responses to the pull-out test. In the presence of fibre, specimens started slipping at different loads (11.6 MPa and 20 MPa), and eventually they failed due to wire rupture. A similar trend was observed for specimen without fibre. According to this figure, after 28 days, 125mm embedment length is a sufficient bond length to have less damage to the steel wire-concrete bond.

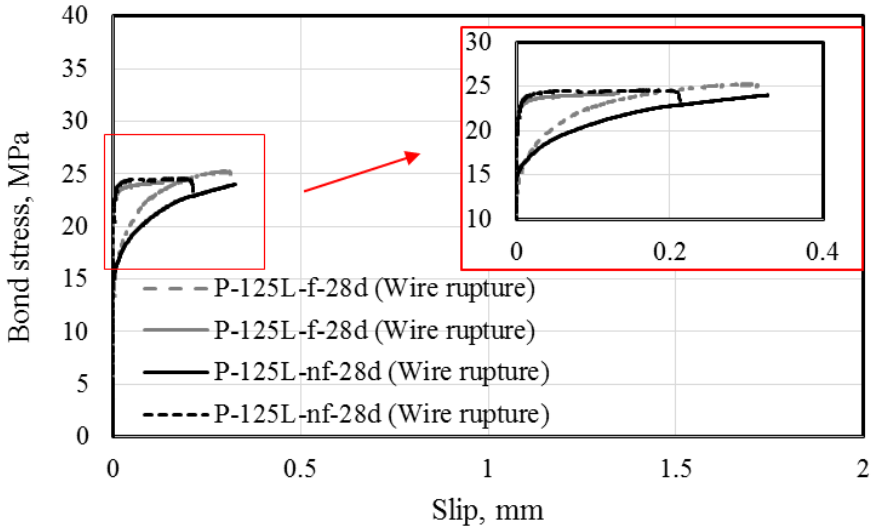

Figure 5.10 Pull-out behaviour of the specimens with 125 mm length after 28 days

Results for additional pull-out tests after 28 days as well as the results for pull-out tests conducted after 56 days can be seen in Appendix C.

5.4.3 Comparison of the pull-out test at different ages

Pull-out test results including bond stress and tensile stress in wires are presented in **Figure 5.12**, where **Figure 5.12.a** presents the results for no fibre-specimens. As seen in **Figure 5.12.a**, the specimens with 75 mm embedment length experienced bond stresses ranging between 21 and 28 MPa. In this Figure, the lowest stress occurred in 3 days and 28 days specimens while the highest was observed at 14 days. According to this figure, no trend was observed in either 75 mm-specimens or 100 mm-specimens due to the unpredictability of bond strength causing scattered results. Interestingly, at 125 mm embedment length, no difference in the bond stresses were observed (regardless of age) in specimens with no fibre. In other words, similar bond stresses were achieved in all ages. The same phenomena was noticed for the specimens with 150 mm embedment length. In contrast with **Figure 5.12.a**, **Figure 5.12.b** presents the results of specimens in the presence of fibre. As presented in

Figure 5.12.b, for different ages from 7 days to 56 days, similar bond stresses were obtained for different embedment lengths. E.g. for 100 mm embedment length, no significant change in bond stress was noticed for ages of 7 days to 56 days. This shows, in the presence of fibre, no improvement of bond stress takes place after 7 days. In other words, at the age of 7 days sufficient bond resistance at the concrete-steel wire interface was developed. According to this figure, at the age of 3 days, for the embedment lengths of 75 mm and 100 mm, lower stresses (up to 30%) were achieved in comparison with 7 days or older specimens. For longer embedment lengths, the effect of age on bond stress could not be determined as the bond strength exceeded the wire strength within 7 days.

The comparison between the bond stresses of 75 mm and 100 mm-specimen of UHPFRC with UHPC shows that not only scattered results were obtained in the specimens without fibre, but also lower bond stresses were achieved. These results confirm that fibres significantly affect the bond strength. According to **Figure 5.12.a** & **b**, fibres however did not influence the bond stress values for longer embedment lengths. The effect of embedment lengths as well as age on the tensile stress in the steel wires in the absence and presence of fibre are shown in **Figure 5.12**. The tensile stresses were scattered in the specimens with embedment lengths of 75 mm and 100 mm for the samples containing no fibre. None of the steel wires reached yielding stress before being pulled from the concrete. The steel wires embedded for 125 mm in specimens without fibre exceed the yielding stress at all ages and also reached ultimate tensile stress at all ages except at the age of 3 days and one specimen at the age of 7 days. These results prove that 125 mm embedment length should be enough to provide sufficient steel wire-concrete bond strength at ages exceeding 7 days for UHPC. The wires embedded for 150 mm reached the ultimate tensile wire strength regardless of age. However, one out of three 150 mm-specimens at the age of 3 days failed due to bond loss with the wire being pulled from the specimen before the steel wire ruptured. This confirms that insufficient bond has been developed after 3 days. After 7 days or more, 150 mm can thus be considered as sufficient embedment length (development length) for UHPC.

In the presence of fibres, the maximum pull-out load recorded in all the samples tested at ages older than 3 days resulted in tensile stress in the wires exceeding the yielding strength. These results confirms that UHPFRC needs 100 mm embedment length to achieve sufficient steel wire-concrete bond strength. The results indicate that the fibres significantly improve the bond resistance against pull-out load, enhancing the pull-out capacity, which lead to the

shorter development length required. More details on the pull-out load, slip at the peak load, bond stress and type of failure are tabulated in **Table 5.2**.

Figure 5.11 displays the slip that occurred at the peak load in the specimens containing fibre. The results show that by increasing the embedment length, the slip reduces significantly. This trend is observed at all ages. This result contradicts the results obtained in Saleem et al. (2012). However, they related the higher slippage in longer embedment to either local failure or lack of interlocking due to the absence of coarse aggregate. In this study, the presence of coarse aggregate may cause interlocking that controlled the slippage. The maximum slip took place in 75 mm-specimens at all ages. This can be attributed to bond failure, as the wire is being pulled out of the concrete it undergoes more slip. These results indicate that the inclusion of coarse aggregate in prestressed or non-prestressed beams could reduce the slippage of reinforcing wires in tension thus helping to maintain the bond between the pre-stressing steel wire and the concrete.

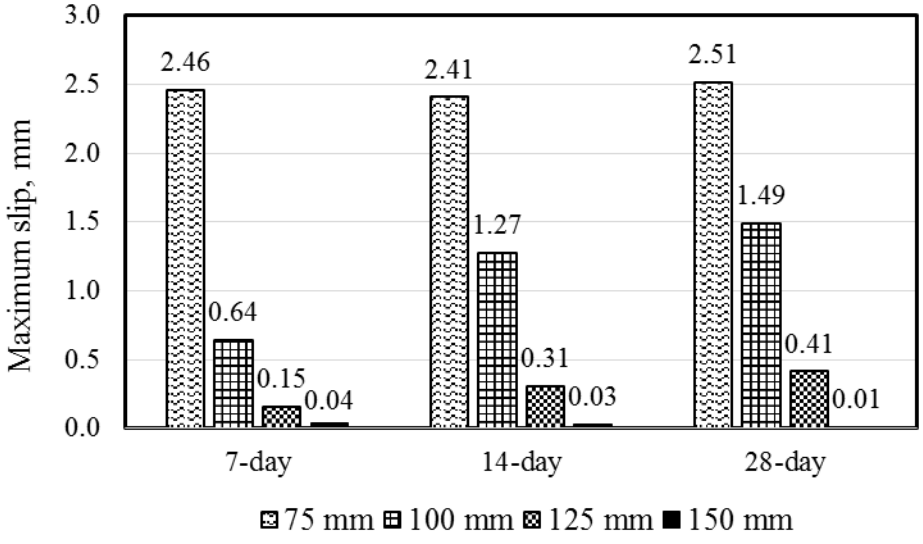

Figure 5.11 Slip at the peak load in the specimens containing fibre

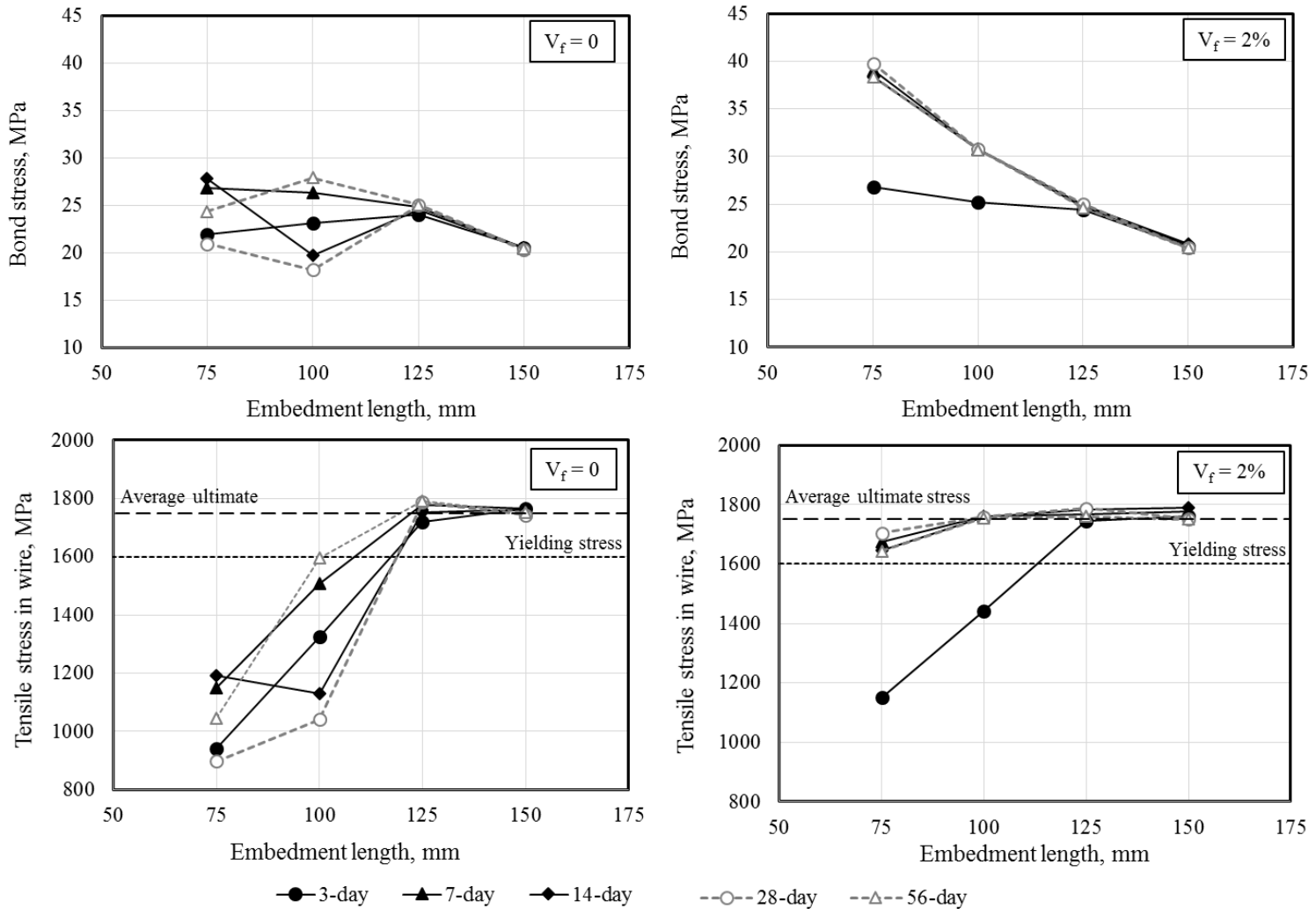

(a) (b)

Figure 5.12 Summary of the pull-out tests including bond and tensile stress in specimens with a) no fibre, b) 2% fibre (by volume fraction)

5.5 EFFECT OF CONCRETE COVER ON BOND STRENGTH

5.5.1 Mechanical properties of UHPC and UHPFRC

The properties of UHPC and UHPFRC including compressive strength, modulus of elasticity and splitting tensile strength at different ages are presented in **Table 5.3**. The inclusion of fibres enhances the compressive strength of UHPC by 5% and 6% for 2-day and 28-day compressive strength respectively. A strength improvement of 110% was observed by comparing the 2-day and 28-day compressive strength. The modulus of elasticity is enhanced by 29% between the ages of 2 days and 28 days. The inclusion of steel fibres not only increased the splitting tensile strength by 127%, but significant ductility was also achieved. The splitting tensile behaviour is shown in **Figure 5.13**.

Table 5.3 Properties of UHPC and UHPFRC for determining the effect of concrete cover on bond strength

		2 days	28 days
Compressive strength (MPa)	With fibre	87.5	185.3
	No fibre	83.0	174.1
Modulus of elasticity (GPa)	With fibre	42.8	55.2
	No fibre	41.9	53.2
Splitting tensile strength (MPa)	With fibre	----	13.4
	No fibre	----	5.9

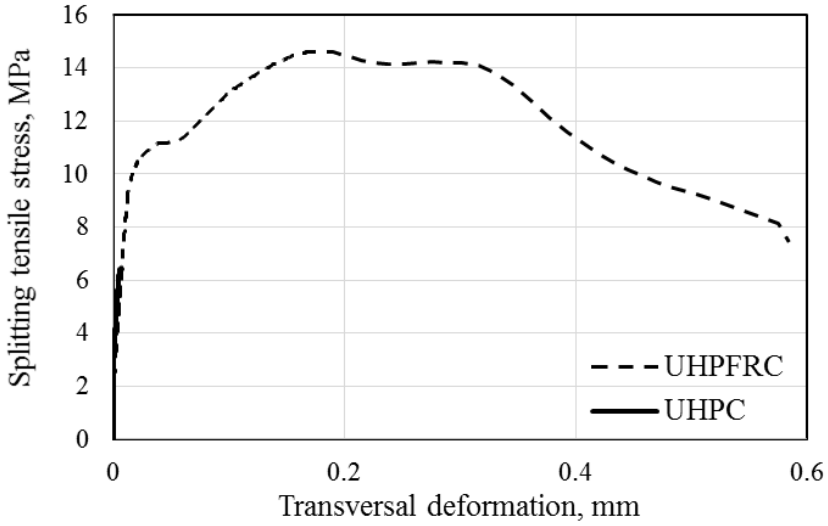

Figure 5.13 Splitting tensile behaviour of UHPC and UHPFRC related to the effect of concrete cover on bond strength

5.5.2 Pull-out test results: Different diameters with identical length

Pull-out test results of this part are presented in **Table 5.4**. Under the "Specimen" column of this table, the following notations were used: P, D, f or nf and d which presents Pull-out, Diameter of specimen in mm, Specimens containing fibre or no fibre, and number of days for aging, respectively. In this section, this notation is used to identify all specimens.

According to **Table 5.4**, two distinct failure modes for bond occurred: (1) wire rupture or (2) slip of the wire from the UHPC, known as bond failure. In all pull-out tests at 2 days, bond failure occurred. This failure showed that the bonding strength is lower than the applied shear stress at the steel-concrete interface; i.e. no strong bond at the steel-concrete interface had developed in 2 days. The results also show that the pull-out load for P-100D-f-2d increased by 13% in comparison with P-100D-nf-2d. It confirms the effect of fibres on the pull-out load enhancement.

This table reveals, in the specimens with 50 mm diameter at 28 days, independent of fibre presence (P-50D-nf-28d, P-50D-f-28d), bond failure was observed. Steel fibres improved the pull-out load from 60.7 kN to 67.2 kN. By increasing the concrete sample diameter from 50 mm to 70 mm, the pull-out load at 28 days improved from 60.7 kN to 65.8 kN in specimens with no fibre. Both failure modes (bond failure and wire rupture) were observed in the specimens with 70 mm diameter in the presence of no fibre (P-70D-nf-28d). The same behaviour occurred in P-100D-nf-28d. In the presence of fibre at 28 days the highest pull-out loads were achieved in P-100D-f-28d. Interestingly, the magnitudes of pull-out loads in the presence of fibre at different lengths (50 mm and 100 mm) are similar (67.3 kN) proving the effect of fibres on bond strength enhancement and crack propagation control.

Table 5.4 Pull-out results for specimens with different diameters but identical length

Specimen	Diameter (mm)	Age (days)	Fibre	Load (kN)	Bond stress (MPa)	Stress in wire (MPa)	Failure mode
P-70D-f-2d	70	2	Yes	60.8	27.65	1580	Bond
P-100D-nf-2d	100	2	No	52.7	23.96	1370	Bond
P-100D-f-2d	100	2	Yes	59.5	27.06	1546	Bond
P-50D-nf-28d	50	28	No	60.7	27.60	1577	Bond
P-50D-f-28d	50	28	Yes	67.2	30.56	1746	Bond
P-70D-nf-28d	70	28	No	65.8	29.92	1710	Bond Rupture
P-100D-nf-28d	100	28	No	63.1 67.8	28.69 30.83	1640 1762	Bond Rupture
P-100D-f-28d	100	28	Yes	67.3	30.60	1749	Rupture

As shown in **Figure 5.14**, in the presence of fibre, there is no major difference in the bond stress for the specimens with the 70 mm and 100 mm diameter at the age of 2 days. In other words, different sample diameters did not affect the bond stress or the failure mode at the age of 2 days.

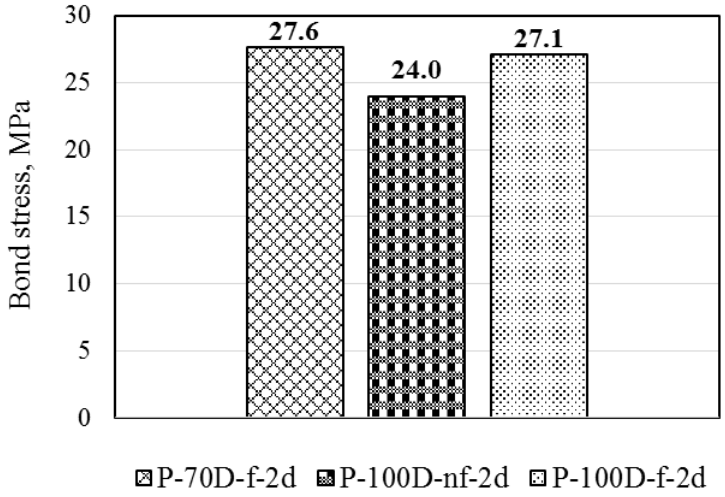

Figure 5.14 Pull-out stress at the age of 2 days in specimens different in diameter

As presented in **Figure 5.15**, the 2 day old fibre reinforced specimens with 70mm and 100mm diameter both exhibited higher slipping in comparison with the specimens without fibre. After the initiation of slipping in P-100D-nf-2d, the bond was lost, leading to slipping with no bond resistance. In contrast, for specimens with fibre, after the initiation of slipping (at 20 MPa), more resistance against slipping can be observed which led to higher bond stresses of 27.6 MPa and 27.1 MPa in P-70D-f-2d and P-100D-f-2d, respectively. After

reaching the capacity, the concrete-steel bond was lost resulting in failure of the specimens due to bond failure.

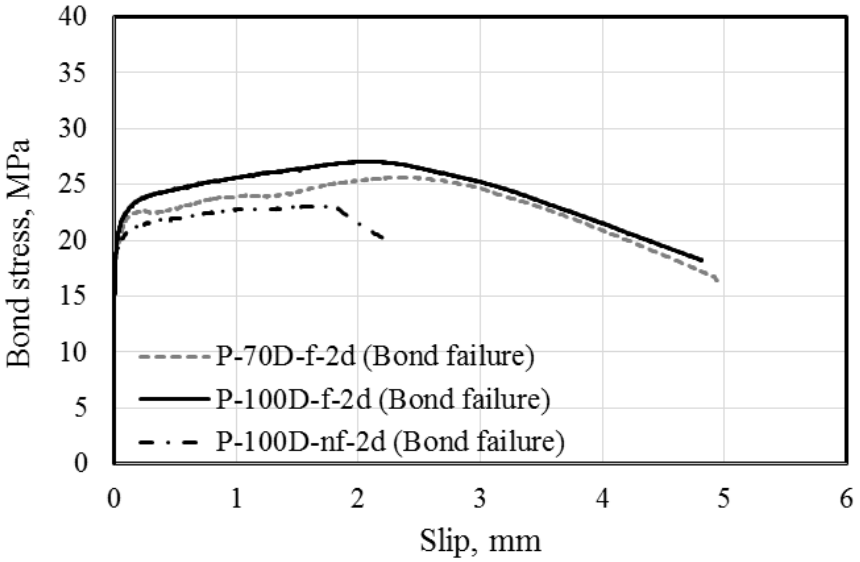

Figure 5.15 Pull-out behaviour in specimens with 70 and 100 mm diameter after 2 days

As shown in **Figure 5.16**, for the specimens with 50 mm diameter at 28 days, an enhancement of 10% was obtained by inclusion of steel fibres. As one can see, in the presence of fibre, the bond strengths for 50 and 100 mm diameter is similar (30.6 MPa) i.e. the maximum capacity of the specimens is unaffected by different diameters in the presence of fibre. These results seem to indicate that concrete cover equivalent to 3 times the wire diameter would be sufficient to prevent loss of bond when reinforcing wires are highly stressed.

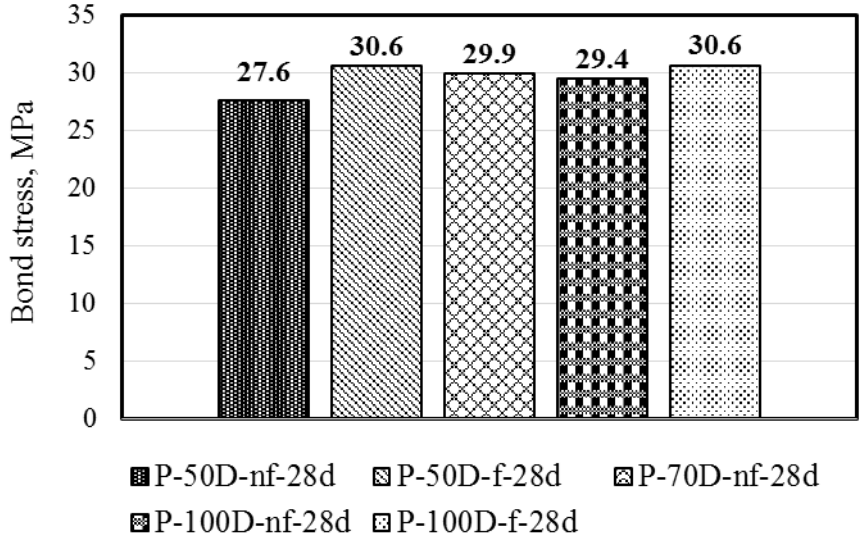

Figure 5.16 Pull-out load at the age of 28 days in specimens different in diameter

The behaviours of 28 day old specimens with 50 mm diameter in pull-out tests are presented in **Figure 5.17**. According to this figure, in the specimens containing fibres (P-50D-f-28d), significant slipping was observed. In all the specimen containing fibres (P-50D-f-28d) bond failure occurred and sliding initiated at higher bond stress (about 27 MPa), while in the specimen with no fibre (P-50D-nf-28d), initial slipping took place at a lower bond stress (about 25 MPa) which is due to lack of fibre enhancing bond between the steel and the concrete.

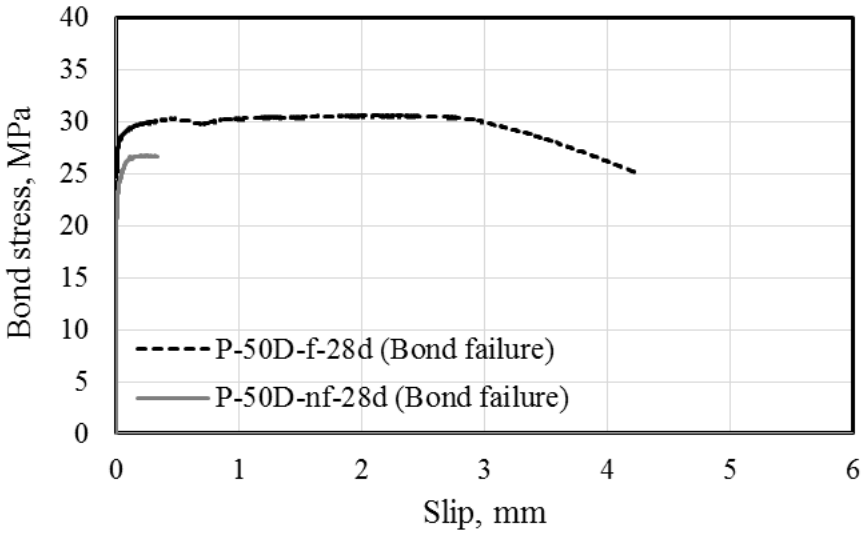

Figure 5.17 Pull-out behaviour in specimens with 50 mm diameter after 28 days

In **Figure 5.18** the behaviour of 70 mm diameter specimens after 2 days and 28 days under the pull-out load are compared. The specimen at 2 days (P-70D-f-2d) started slipping at about a stress of 19 MPa while in the 28 day tests, the sliding was initiated at about 27 MPa. This indicates how much the bond between steel and concrete had improved over time. P-70D-nf-28d showed two different failure modes with both bond failure and wire rupture. This behaviour is due to the strong bond between the steel and concrete that at the time of sliding, the steel wire is about to yield. It depends on how strong the bond is, whether the wire ruptures or the wire to slips. The specimens which failed due to wire rupture showed sudden failure while this behaviour was not observed in the specimens that failed due to bond failure.

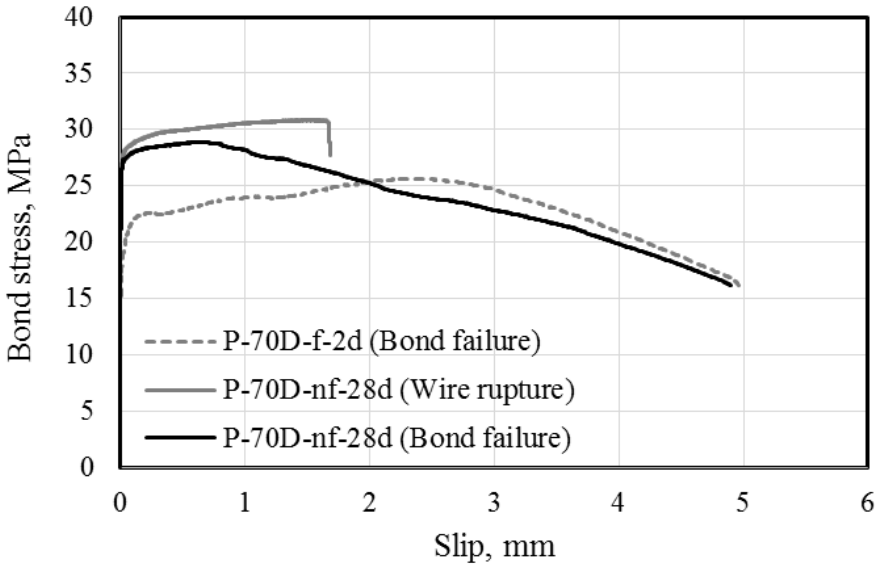

Figure 5.18 Pull-out behaviour of 70 mm diameter specimens after 2 days and 28 days

Figure 5.19 presents the different behaviour of the specimens with 100 mm diameter at the age of 28 days. Specimens in the presence of fibre (P-100D-f-28d) started slipping at about 30 MPa which is approximately 18% higher than specimens with no fibre (P-100D-nf-28d). Due to the strong bond at the steel wire-concrete interface, no slipping occurred before 30 MPa (1663 MPa stress in the wire) which led the wire reaching to its yielding load. Fibres helped to maintain the bond which led to pull-out load enhancement, and failure of specimens due to wire rupture. However, the unpredictable behaviour of specimens with no fibres (P-100D-nf-28d) after slipping initiated, may depend on the behaviour of the concrete surrounding the wire.

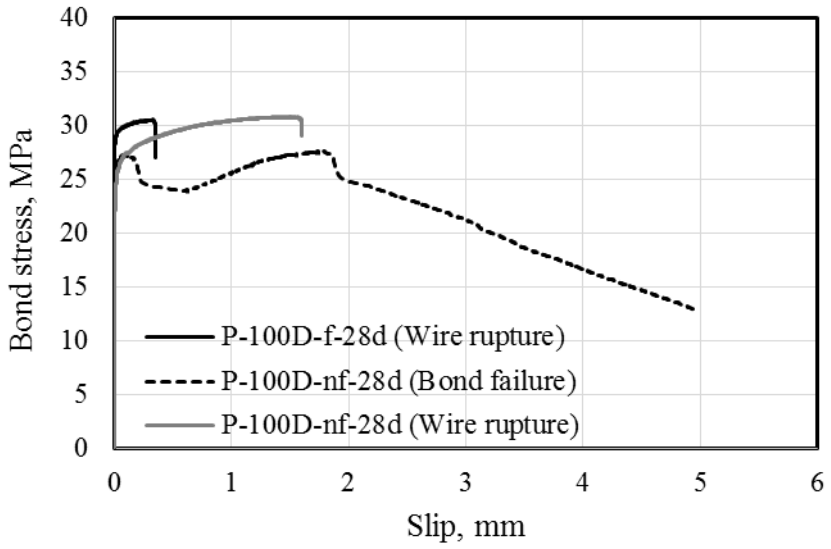

Figure 5.19 Pull-out behaviour of the specimens with 100 mm diameter at the age of 28 days

Pictures of the 28-day specimens after failure were presented in **Appendix C**.

5.6 CONCLUSION

Shrinkage and creep tests were performed for UHPC and UHPFRC. The main conclusions are summarized as follows:

- After 110 days, UHPFRC experiences higher drying shrinkage compared to UHPC (360 με and 250 με, respectively).

- Up to 20 days after loading, creep in UHPC is higher than UHPFRC, while in 110 days similar ultimate creep value was achieved for both specimens. Creep coefficients of 2.4 and 2.3 were achieved for UHPC and UHPFRC, respectively.

Bond performance between concrete and 7 mm steel wires embedded in UHPC and UHPFRC was investigated and the bond performance of UHPC and UHPFRC was evaluated based on pull-out tests performed at different ages. The main conclusions of the first part of study are summarized as follows:

- The bond strength of UHPC for embedment lengths of 75 mm and 100 mm were relatively unpredictable, ranging between 21 and 28 MPa.

- In UHPFRC, no improvement in bond strength was observed after more than 7 days at different embedment lengths. Although the compressive strength of concrete improved marginally between 7 days and 28 days, no enhancement in bond strength was observed.

- Fibres control crack propagation, thus preventing brittle failing. In the presence of fibre after the initiation of slipping, the bond resistance improved significantly.

- The inclusion of fibres change the type of failure from concrete splitting to bond failure for specimens with 75 mm embedment length and from bond failure to wire rupture in specimens with 100 mm embedment length.

- The specimens containing fibre with embedment lengths of 100 mm and more at the age of 7 days and older, experienced wire rupture as a type of failure which indicates

sufficient development length. However, in the specimens without fibre wire rupture occurred at higher embedment lengths of 125 mm and 150 mm.

- Shorter development length is achieved by inclusion of fibres in UHPC.

- Fibres reduced the slip of prestressing steel wires by providing better bond between the concrete and the steel wire.

- By increasing the embedment length, the slip reduces significantly. Therefore, the inclusion of coarse aggregate in prestressed or non-prestressed beams could reduce the slippage of reinforcing wires in tension thus helping to maintain the perfect bond between the pre-stressing steel wire and the concrete.

The main conclusions of the second part of study are summarized as follows:

- Bond strength in UHPFRC is unaffected by sample diameter/size in the presence of fibre.

- UHPFRC specimens with 70mm and 100mm diameter both exhibited increased slipping in comparison with UHPC.

- Concrete cover equivalent to 3 times the wire diameter would be sufficient to prevent loss of bond when reinforcing wires are highly stressed.

- Fibres helped to maintain the bond which led to the pull-out load enhancement, and failure of specimens due to wire rupture. However, the unpredictable behaviour of specimens with no fibres after slip initiation may depend on the behaviour of the concrete surrounding the wire.

- For UHPC with bond failure during the pull-out test, the steel wire was pulled out with a cone of concrete. This confirms that the specimens with no fibre are more prone to concrete damage during the testing, while the specimens containing fibres experienced much less damage.

CHAPTER 6 PRELIMINARY STUDY ON PRESTRESSED BEAMS

6.1 INTRODUCTION

As preliminary study on prestressed beams, in this chapter two 1-m long UHPC and UHPFRC pre-stressed beams were manufactured using single wire tendons. However, for sake of brevity hereafter, wire is used in this document to refer to single wire tendon for prestressed beams.

This chapter was designed to emphasise the effect of fibre on the behaviour of the prestressed beams, and aimed to answer crucial questions that might be encountered in the design of large-scale UHPC and UHPFRC beams. These questions include: Would the embedment length of more than 100 mm be sufficient for pre-stressed beams? What is the influence of fibre on the beam behaviour and the beam failure modes? What is the importance of fibre utilization in UHPC beams? Can the stirrups be eliminated in UHPFRC prestressed beams? What is the effect of fibre in on the controlling of the crack formation at the time of wire releasing in prestressed beams?

This chapter also serves to investigate the probable issues that may occur during prestressing and wire releasing procedures in UHPC and UHPFRC beams containing andesite. Besides, it provides an overall indication of the expected behaviour of UHPC and UHPFRC prestressed beams under flexure. Four-point bending tests were performed on 1-m long UHPC and UHPFRC beams, as a preliminary study. The set-up of the tests, as well as the behaviour of the beams under flexure and the material properties are discussed in this chapter.

6.2 BEAM FABRICATION

Two sets of one-metre long UHPC beams were cast with a mixture containing andesite. One set contained 2% fibre (by volume) and the other was without fibre. The beams were sections of a 6 m beam, which were cut into six 1 m long sections. The beams had a rectangular cross-section of 75 mm x 150 mm and they were prestressed using two 7mm wires in the top and two in bottom of the section. According to the results achieved in the previous chapter,

20 mm concrete cover was considered for both wires in top and bottom. The 7 mm wires were prestressed to 75% of the wire ultimate tensile strength to benefit the most from prestressing and achieve the highest flexural strength in the beams. There is no reinforcement used in the prestressed beams except longitudinal wires. No relevant reinforcement is provided to avoid the formtion of splitting cracks at the time of wire releasing. The prestressing wires were anchored against solid steel blocks at the both ends of the 6 m beam, presented in Figure 6.1. The wire releasing was performed slowly to avoid shocking the concrete while releasing the wires. The wire releasing method is shown in **Figure 6.2**.

After releasing the prestressed wires (2 days after the casting), while taking care to avoid shocking the beams during the release of stress, longitudinal cracks along the wires were formed called spalling cracks. No cracking was however observed in beams containing fibres. The crack formation can be attributed to the fact that the developed splitting tensile strength in the concrete was not enough to resist the prestressed loads and no suitable reinforcement is provided to control the crack formation. However, fibres managed to control the spalling crack formation and propagation even in the absence of suitable reinforcement (stirrups). At the wire releasing time (2 days after the casting), compressive strengths of 64.5 and 64.9 MPa were achieved for UHPC and UHPFRC, respectively. For the next beams, the releasing was performed three days after casting to avoid the crack formation by allowing the concrete splitting tensile strength to increase before the time of releasing. However, the cracks still developed despite the prestressed wires being released three days after casting. The cracking was however much less and less severe. It seems that cracking of UHPC beams is inevitable in the absence of fibre. At the wire releasing time (3 days after the casting), compressive strengths of 85.7 and 80.8 MPa were achieved for UHPC and UHPFRC, respectively. The crack formation after the releasing of prestressed wires are displayed in **Figure 6.3**.

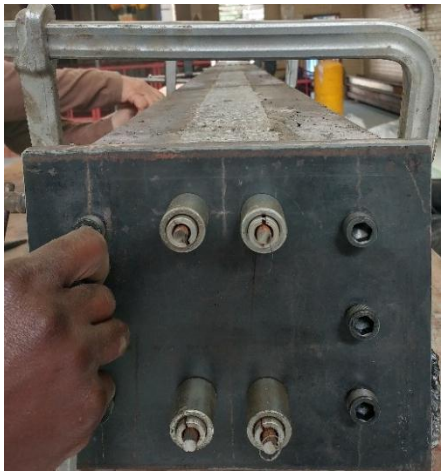

Figure 6.1 The block at the both end of the 6 m beams

Figure 6.2 The process of releasing the prestressing wires

(a)

(b)

Figure 6.3 Cracks development after releasing the prestressing wires in beams containing no fibre (a) two days, (b) three days after casting.

6.3 TEST SET-UP

The beam test was conducted using a closed-loop Material Testing System (MTS) applying displacement at a rate of 0.6 mm/minute. Mid-span deflections were measured by using two LVDTs. The readings were taken at 100 Hz. The load was applied by using two bearing rollers (one of them is a swivelling roller), 150 mm apart, with their center line coinciding with the center of the beam. The supports were 750 mm apart. These settings were applied based on the capacity of available heavy machinery in the laboratory. The test set-up is shown in **Figure 6.4** and **Figure 6.5**.

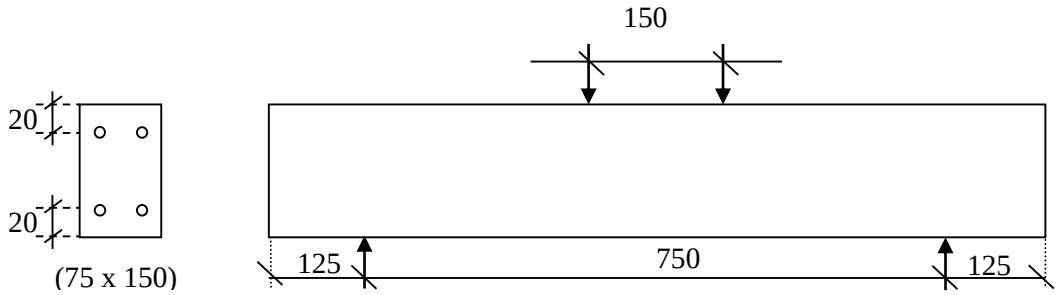

Figure 6.4 Schematic set-up configuration for prestressed beams (Dimensions in mm)

Figure 6.5 Test set-up for prestressed 1m-beam

6.4 MATERIAL PROPERTIES OF PRESTRESSED 1M-BEAMS

Table 6.1 presents the properties of UHPC and UHPFRC of prestressed 1m-beams including compressive strength, modulus of elasticity and splitting tensile strength at 7 and 28 days. The mechanical properties at the time of wire releasing the prestressing wires for both beams are presented, as well. The compressive strength of 158.2 and 168.5 MPa was achieved in the presence of fibres at the ages of 7 days and 28 days, respectively. These results show the enhancement of the compressive strength over the time. However, the same trend was not observed for modulus of elasticity from the ages of 7 days to 28 days for both UHPC and

UHPFRC. The same trend was observed for the splitting tensile strength. While splitting tensile strength for UHPFRC improved over time from 7 days to 28 days, no improvement was observed over time in UHPC splitting tensile strength (9.9 MPa).

Table 6.1 Properties of UHPC and UHPFRC prestressed 1m-beams

		2 days	3 days	7 days	28 days
Compressive strength (MPa)	With fibre	64.9	80.8	158.2	168.5
	No fibre	64.5	85.7	152.1	160.0
Modulus of elasticity (GPa)	With fibre	38.0	42.8	53.7	54.9
	No fibre	40.4	43.7	56.1	56.1
Splitting tensile strength (MPa)	With fibre	----	12.0	16.1	19.0
	No fibre	----	7.4	9.9	9.9

6.5 RESULTS

The behaviour of prestressed beams containing fibre and no fibre at ages of 7 days and 28 days are compared in **Figure 6.6**. In the prestressed beams containing fibre at both 7days and 28days, no cracking was observed up to 60 kN. By the formation of flexural cracks, the beam stiffness decreased gradually, until reaching the peak load. Peak loads of 133 kN and 124 kN were achieved for the pretressed beams with fibre at 7 days and 28 days, respectively. As can be seen, there is a load carrying capacity reduction from 7 days to 28 days which can be due to prestress loss over the time. After reaching the peak load, the load reduced with increasing deflection.

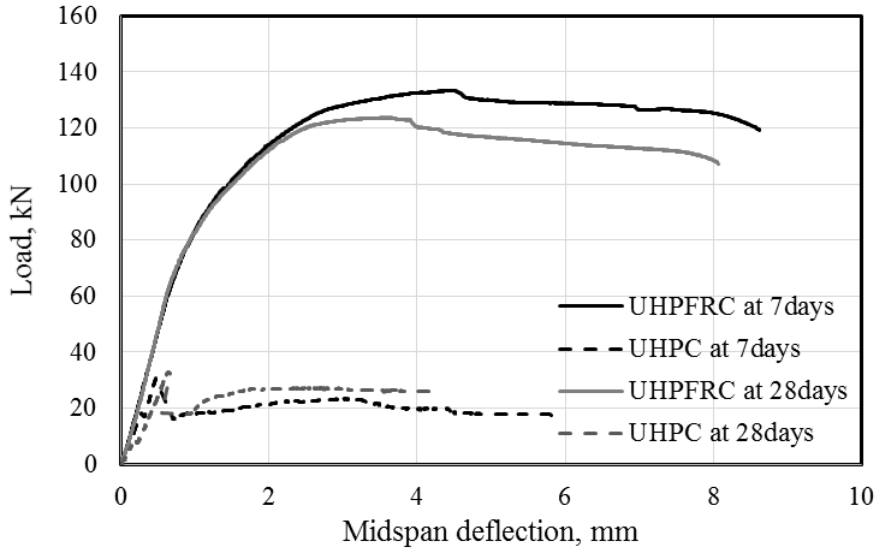

Figure 6.6 Behaviour of UHPC and UHPFRC prestressed 1m-beams under flexure

In the prestressed beams without fibre, the beam stiffness changed before reaching the peak load. The peak loads were 30.5 kN and 33 kN for the beams at the age of 7 days and 28 days, respectively. After reaching the peak load, a sudden drop in load carrying capacity occurred which is attributed to the formation of wide inclined cracks at the level of the prestressing wires. The formation of this crack led to the complete bond loss of the prestressing wires and the concrete along the shear span length. The poor flexural behaviour of the prestressed beam without fibre can be due to the pre-existing cracks along the prestressing wires that developed during the wire releasing procedure (see **Figure 6.7**) which led to a poor development of bond between the concrete and the steel wires. The poor bond development may result in an increase in the loss of prestressing in the beam, causing a significant loss in load carrying capacity. This poor flexural behaviour confirms the necessity of fibres in the UHPC prestressed beams.

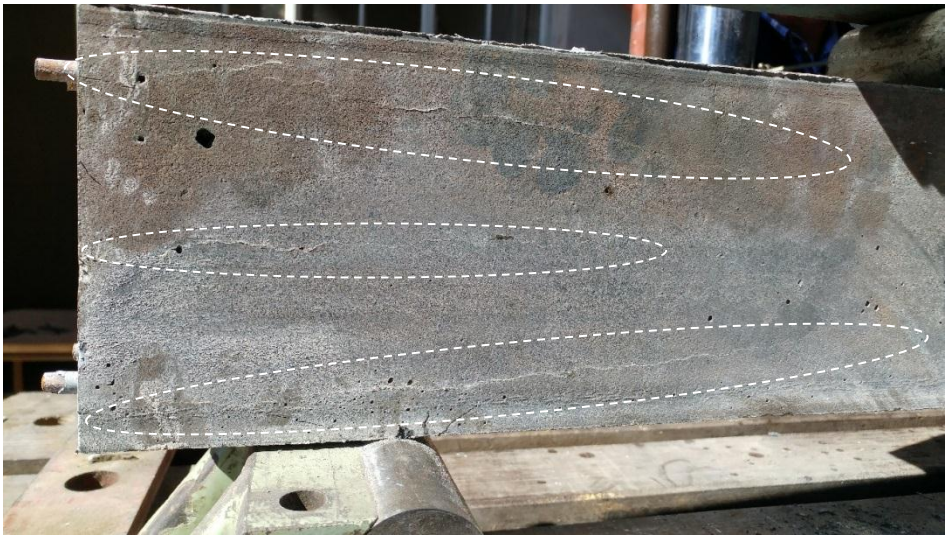

Figure 6.7 Pre-existing cracks due to wire releasing process

For both 7 days and 28 days, the prestressed beams containing fibres showed a considerable enhancement in the load carrying capacity when compared to the prestressed beams without fibre. As mentioned before, the pre-existing cracks in the prestressed beams without fibre (see section 6.2) can be blamed for the low load carrying capacity of beams with no fibre.

The prestressed beams containing no fibre failed due to the formation of inclined tension cracks. These cracks were mostly extensions of initial cracks that formed during wire releasing (see **Figure 6.8**). At the bottom end of the critical inclined crack, cracking propagated along the length of the reinforcing wires, which could be attributed to the

mobilization of a dowel action mechanism in combination with a certain degree of bond failure at the reinforcement level. The inclined cracks spread over the shear span region, as can be seen in **Figure 6.9**.

Figure 6.8 Loading cracks as an extension of pre-existing cracks in UHPC prestressed 1m-beams

Flexural failure in the prestressed beams containing fibre at 28 days can be seen in **Figure 6.10**. Flexural cracks first developed from the bottom surface of the beam in the region below the loading point, where the maximum moment occurred. As the applied load increased, flexural cracks spread toward the loading rollers. The loading was continued till the fracture of the prestressed wires took place.

In the UHPFRC prestressed beam, no slipping of prestressing wires was observed during the tests. This confirmed the sufficiency of the embedment length (125 mm) in UHPFRC prestressed beams.

As final remarks, the results showed the positive effect of fibre even in the presence of very high stress due to wire releasing. In addition, as one may know presence of stirrups makes the fabrication of the beams more complicated with more intensive labour work. Compaction would be an issue as well. According to our observation, a remedy to this issue would be the utilization of fibres in prestressed beams. Fibres utilization reduces the required number of stirrups and additional reinforcements which helps the fabrication of prestressed beams to be more practical with less reinforcement.

Figure 6.9 Shear failure in UHPC prestressed 1m-beams at 28 days

Figure 6.10 Flexural failure in UHPFRC prestressed 1m-beams at 28 days

6.6 CONCLUSION

Flexural behaviour of 1-m long UHPC and UHPFRC prestressed beams was investigated as a preliminary study. The beams were prestressed using 7mm wires prestressed to 75% of the wire ultimate tensile strength. The main conclusions of this chapter are summarized as follows:

- During the wire releasing process, in the beams with no fibre, longitudinal cracks along

the wires were formed called spalling cracks. However, no cracking was observed in beams containing fibres.

- The cracking in UHPC beams is inevitable in the presence of no fibre even by increasing the age of wire releasing.

- In the prestressed beams containing fibre at both 7 days and 28 days, cracking occurred at the same load (60 kN). However, there is a reduction in maximum load carrying capacity from 7 days to 28 days.

- The failure mode in the prestressed beams containing fibre was flexure.

- In the prestressed beams containing fibre for both 7 days and 28 days a considerable enhancement in the load carrying capacity was observed when compared to the prestressed beams without fibre.

- In the prestressed beams containing no fibre, after reaching the peak load, a sudden drop in load carrying capacity occurred due to the formation of wide inclined cracks at the level of the prestressing wires. The formation of these cracks led to the complete bond loss of the prestressing wires and the concrete along the shear span length.

- In the prestressed beams containing no fibre, poor bond development caused significant loss in load carrying capacity which confirms the necessity of using fibres in the UHPC prestressed beams.

- The prestressed beams containing no fibre failed due to the formation of inclined tension cracks. These cracks were mostly extensions of initial cracks that formed during wire releasing.

- In the UHPFRC prestressed beam, no slipping of prestressing wires was occurred during the tests, confirmed the sufficiency of the embedment length (125 mm) in UHPFRC prestressed beams.

CHAPTER 7 PREPARATION OF LARGE-SCALE UHPFRC PRESTRESSED BEAMS

7.1 INTRODUCTION

This chapter contains information on the preparation of large-scale UHPFRC prestressed beams before testing. Based on the results discussed in the previous chapter, no prestressed beam was manufactured without fibre. The preparation of UHPFRC prestressed beams includes the design, construction, and testing method of simply-supported beams subjected to a monotonically-increased, concentrated load. Subsequent sections provide the details of the experimental program.

7.2 BEAM DESIGN

The beam was designed to fail in shear to determine whether I-beams with thin webs are able to resist shear without shear stirrups when fibres are incorporated. In the design process of the beam, capacity and span restriction of available machinery in the laboratory was considered. Therefore, the maximum beam span was set to 3.9 m and other dimensions other dimensions were calculated based on the SANS 51992-1-1:2014 which is presented in Appendix D. **Table 7.1** shows an overview of the beam characteristics including length (L), span (S), total depth (H), effective depth (d), shear span to effective depth ratio (a/d), compressive strength and fibre volume fraction. The beams were 4400 mm in total length having a span of 3900 mm and a total depth of 400 mm. The effective depth was 340 mm. The shear span was 1400 mm, giving a shear-span ratio of a/d = 4.1, for which the direct load transfer to the support by an inclined strut may be regarded not to contribute much to the shear capacity. Since, for beams with an a/d ratio less than approximately 2.5, a direct concrete strut from the loading point to the support is formed, leading to an increase in beam strength compared with slender beams. The web was designed as a thin membrane 50 mm thick. The top flange and the bottom flange were 200 mm wide. The top flange and bottom flange had 50 mm and 100 mm depth, respectively. For prestressed concrete beams, the bottom flange was pretensioned with sixteen 7-mm high strength wires, each with a prestressing force of 50.2 kN (75% ultimate tensile strength of wires). The top flange was pretensioned with two 7-mm high strength wires, each with a prestressing force of 50.2 kN (75% ultimate tensile strength of wires).

To achieve homogeneously distributed fresh mix throughout the whole specimen, the distance between the prestressed wires was fixed at 27 mm, more than the maximum fibre length. The distance between the formwork and the prestressed wires was 30 mm. Schematic beam set-up and cross-section specifications are shown in **Figure 7.1.**

Table 7.1 Specifications of the large-scale prestressed beams

	Length (m)	**Span (m)**	**Total depth (mm)**	**Effective depth (mm)**	**a/d**	**f'_c (MPa)**	**V_f (%)**
Beam	4.4	3.9	400	340	3.9	185	2.5%

7.3 FABRICATING THE BEAM SPECIMENS

The steel mould had a total length of 9 m with a separating section which divided the mould in half (4.4 m). The prestressing wires were arranged according to the cross-section design. The arrangement of steel wires before prestressing is presented in **Figure 7.2**. The wires were prestressed up to 75% of ultimate tensile strength of wires while the wires were anchored against solid steel blocks at both ends of the 8.8 m beam (see **Figure 7.3**). Two mould sections were filled, one with a fresh UHPFRC mixture containing dolomite and the other one with a UHPFRC mixture containing andesite. The beams were compacted using high frequency vibrating pokers. With each beam, cubes for measuring compressive strength, cylinders for determining the modulus of elasticity, splitting tensile strength, creep and shrinkage were cast. The beams and the test specimen were kept in the open environment of the laboratory and covered by plastic sheets followed by a blanket to keep the temperature of the beam at about 24°C. The blanket was used to cover the whole beam and all test specimen for 48 hours (see **Figure 7.4**).

After 48 hours, the compressive strength of cubes that experienced the same curing as the beam were measure to check whether sufficient compressive strength had developed to release the prestressing wires. An average compressive strength of 82 MPa was achieved, which was deemed satisfactory for releasing the prestressing wires. The beams as well as the cylinder and cube specimens were demoulded and then placed in the curing bath. The temperature of the water was initially at 24°C, increasing to 80°C. The beams and other specimens were kept in 80°C water for 2 days. They were taken out of the water when the water had cooled down to 24°C, and placed in a laboratory room. **Figure 7.5** shows the placement of the beams as well as cylindrical and cube specimens in the bath for the heat treatment procedure.

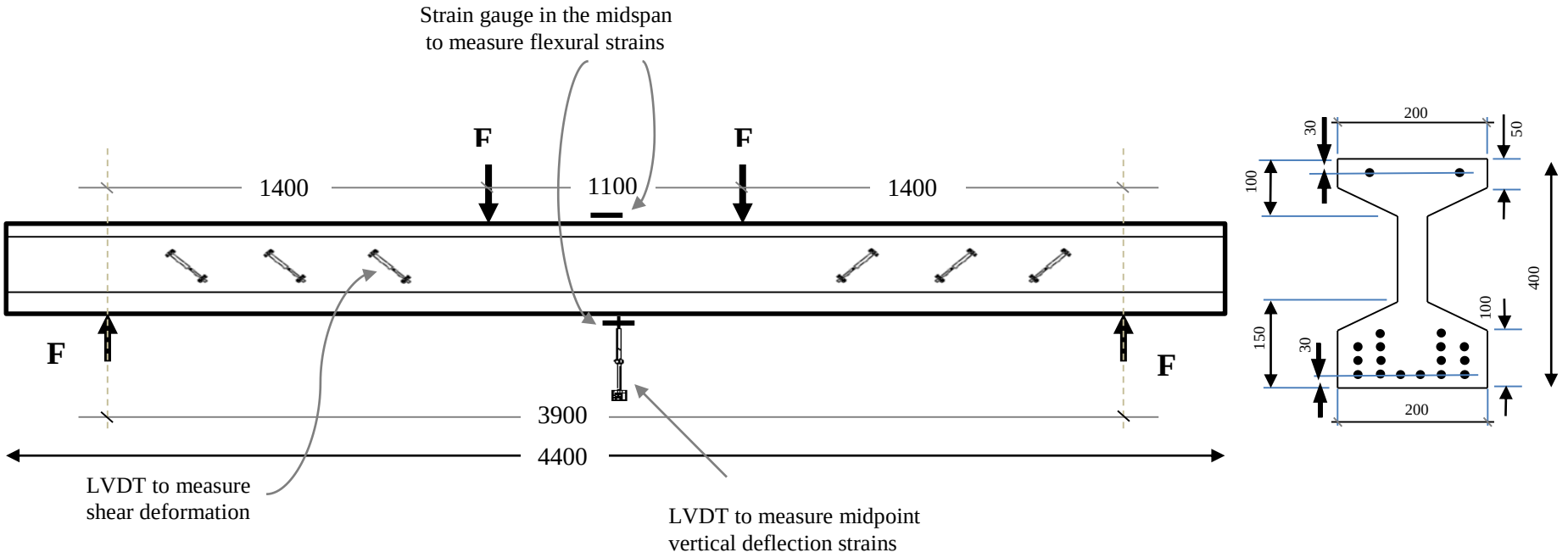

Figure 7.1 Schematic beam set-up and cross-section specifications of large-scale prestressed beams

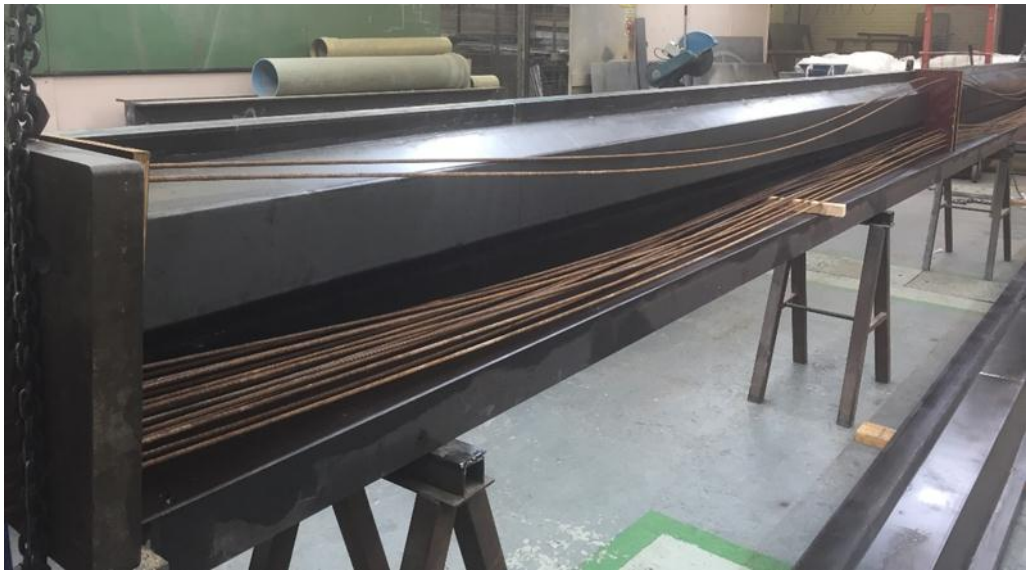

Figure 7.2 Arrangement of steel wires before prestressing in large-scale UHPFRC prestressed beams

Figure 7.3 Procedure of prestressing the steel wires in large-scale UHPFRC prestressed beams

Figure 7.4 Large-scale beams covered by blanket after casting

Figure 7.5 Pretressed beams and the specimens in the bath to apply heat treatment

7.4 FOUR-POINT BENDING TEST SETUP AND INSTRUMENTATION

The four-point load tests were completed using a steel frame designed for flexural beam testing at the University of Pretoria Civil Engineering Laboratory (see **Figure 7.6**). The beams were supported on two steel plates on top of rollers, and a hydraulic actuator was used to apply two point loads, 1100 mm apart, using a spreader beam. All the specimen had a similar experimental setup.

The beams were initially loaded in 10 kN load steps. After the beam began to sustain inelastic damage and exhibit flexural stiffness reduction by formation of inclined shear cracks, the beam was unloaded and reloaded by increment on midspan deflection of 2.5 mm/min until failure. For each increment the gauge data were recorded and the crack pattern was traced.

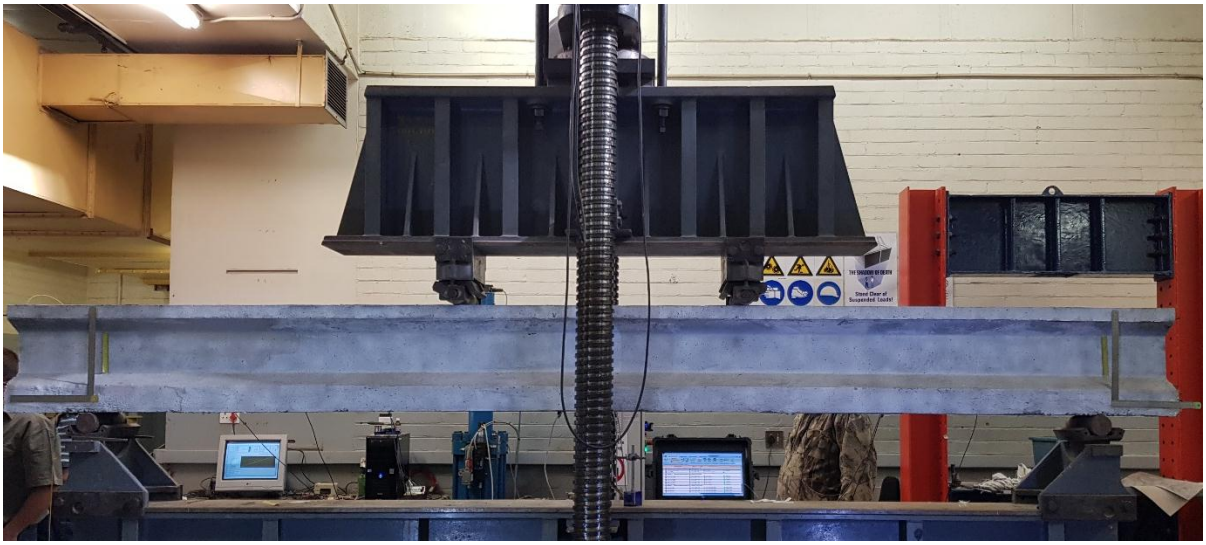

Figure 7.6 Four-point bending test set-up in the large-scale UHPFRC prestressed beams

This research required instrumentation and data acquisition to obtain data required for beam analysis. Each device has a specific function within the scope of the research performed. Individual gauges were used until their readings became unreliable due to cracking of the underlying concrete. A schematic lay-out of LVDTs are presented in **Figure 7.1**. The actual lay-out of instrumentations on the UHPFRC prestressed beams is shown in **Figure 7.7**.

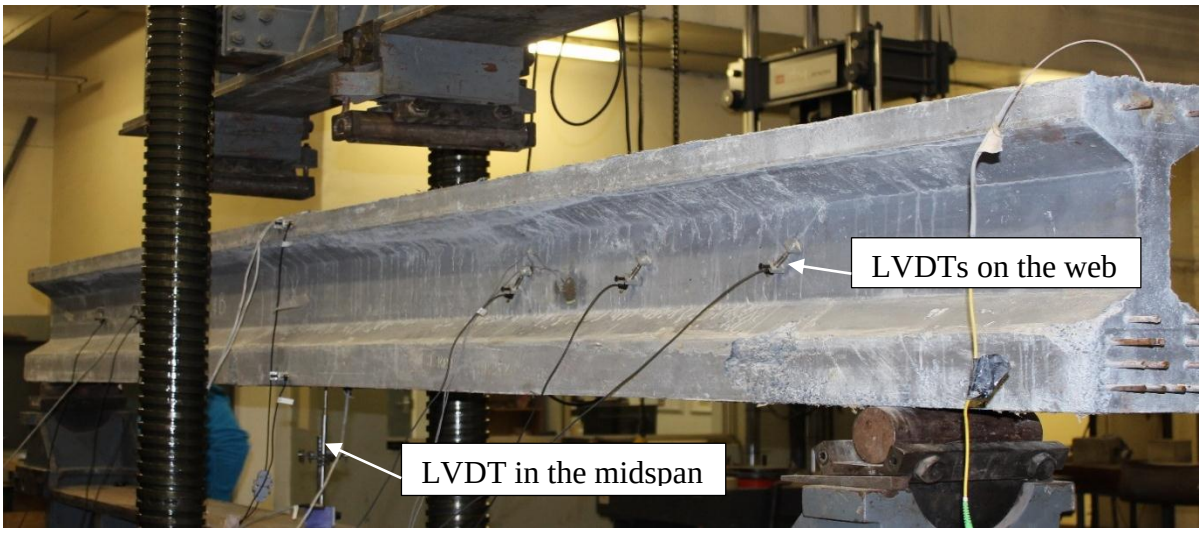

Figure 7.7 Lay-out of LVDTs on UHPFRC prestressed beams

The instrumentations used in this study are as follows:

Strain gauges- this sensor measures compressive and tensile strains caused by forces, pressures, moments, heat, structural changes of the material. For each beam, two strain gauges were glued to the top and bottom fibre of the mid-span measuring the strain during testing in order to create a strain profile over the depth of the beam.

LVDTs- were used in this research to determine the displacement (strain) taking place during the four-point bending test. After being calibrated, the LVDTs were attached as following:

(1) One in the midspan to capture the vertical deflection of the beam,
(2) Six on the web within the shear span to measure the tensile strain and diagonal crack openings.

7.5 DRYING SHRINKAGE AND CREEP SET-UP

Drying shrinkage of UHPFRC containing andesite and dolomite was measured using cylinder specimens (100 mm diameter, 300 mm length). The specimens were cured the same as the beams, then stored in a 24°C laboratory room to measure shrinkage deformation. Deformation was recorded using one LVDT for each specimen.

To measure creep, UHPFRC containing andesite and dolomite were tested. Two cylinder specimens (100 mm diameter, 300 mm length) were used for each UHPFRC mix composition. Two series of curing method were applied. For one series, the creep specimens were loaded after demoulding (2-day age) in a 24°C laboratory room. The other series were stored in an 80°C water bath for 2 days after demoulding. The creep specimens were loaded in a 24°C laboratory room after the specimens were taken out of heat treatment. Deformation was recorded using LVDTs taking reading every 60 seconds for the first 7 days, followed by a reading every 120 seconds for the rest of the duration of testing.

CHAPTER 8 RESULTS AND ANALYSIS OF LARGE-SCALE UHPFRC PRESTRESSED BEAMS

8.1 INTRODUCTION

This chapter provides the experimental results of UHPFRC beams under four-point loading. The mechanical properties of UHPFRC containing dolomite and andesite are presented. Besides, a detailed analysis of the behaviour of the beams are covered. Drying shrinkage and creep performance of both UHPFRCs are presented.

Each beam is analysed separately to fully understand its behaviour, including its load versus deflection relationship, crack pattern, distribution and magnitude of concrete strains in the critical shear span. Finally, the experimental results are compared to values calculated using code provisions. It's noteworthy that DEF may not be an issue since the cement combination (explained in CHAPTER 3) contains fly ash as explained in the literature review section 2.4.4, fly ash restricts the DEF.

8.2 MECHANICAL PROPERTIES OF LARGE-SCALE UHPFRC PRESTRESSED BEAMS

Table 8.1 presents the properties of UHPFRC including compressive strength, modulus of elasticity and splitting tensile strength at different ages (2-day and 120-day). The age of 120 days represents the day of testing. At the time of wire releasing (2 days), the compressive strength of 82 MPa and 81 MPa was achieved for UHPFRC containing dolomite and andesite, respectively. In UHPFRC containing dolomite, at the time of wire releasing, modulus of elasticity and splitting tensile strength of 43 GPa and 10.3 MPa were achieved. However, lower modulus of elasticity and splitting tensile strength were earned for UHPFRC containing andesite. At the testing time of the prestressed beams, higher compressive strength, modulus of elasticity and splitting tensile strength were achieved for UHPFRC containing dolomite.

Table 8.1 Mechanical properties of large-scale UHPFRC prestressed beams

		Dolomite	Andesite
Compressive strength (MPa)	2-day	82.0	81.0
	120-day	186.0	177.0
Modulus of elasticity (GPa)	2-day	43.0	37.7
	120-day	56.5	50.0
Splitting tensile strength (MPa)	2-day	10.3	11.2
	120-day	22.5	21.5

8.3 DRYING SHRINKAGE AND CREEP RESULTS

The results for early-age and long-term drying shrinkage of UHPFRC specimens exposed to heat treatment are presented in **Figure 8.1** and **Figure 8.2**, respectively. The early-age drying shrinkage was measured for the first 24 hours after the specimen was cooled down in water after the heat treatment. The results revealed that UHPFRC containing andesite experiences higher early-age drying shrinkage compared to UHPFRC containing dolomite. The 24 hrs early-age shrinkage of 39.0 με and 13.4 με were achieved for UHPFRC containing andesite and UHPFRC containing dolomite respectively.

After 110 days, the same trend was observed, such that UHPFRC containing andesite underwent higher drying shrinkage than UHPFRC containing dolomite (see **Figure 8.2**). As seen in the figure, descending trends are observed in drying shrinkage over time for both UHPFRC specimens which resulted in the drying shrinkage of 6.7 με and 17.5 με for UHPFRC containing dolomite and andesite, respectively. These values for long-term drying shrinkage are relatively small and can be ignored or taken as zero, which is the same value recommended by AFGC (2002) and JSCE (2006).

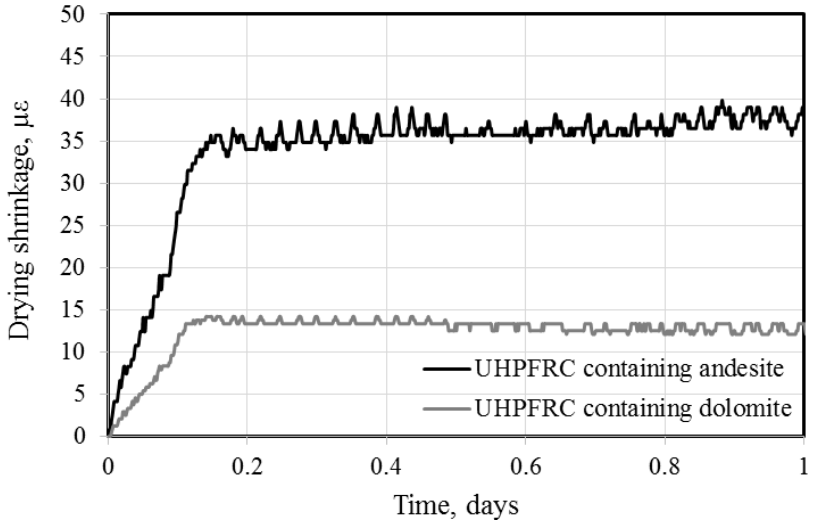

Figure 8.1 Early-age drying shrinkage of UHPFRC that experienced heat treatment

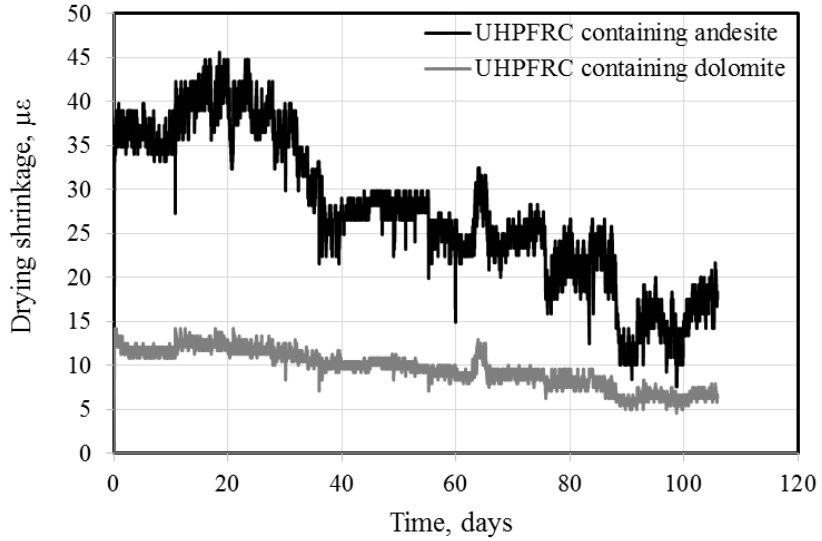

Figure 8.2 Drying shrinkage of UHPFRC that experienced heat treatment

The creep performance of UHPFRC specimens that experienced no heat treatment is presented in **Figure 8.3**. More creep developed for UHPFRC containing andesite over time. Creep coefficient (ratio of the ultimate creep strain to the elastic strain) of 1.46 and 1.50 was achieved for UHPFRC containing dolomite and andesite, respectively when specimens experienced no heat treatment. These values are higher than the value of 0.8 recommended by AFGC (2002) and JSCE (2006). This can be due to different material properties used in UHPFRC developed in this research.

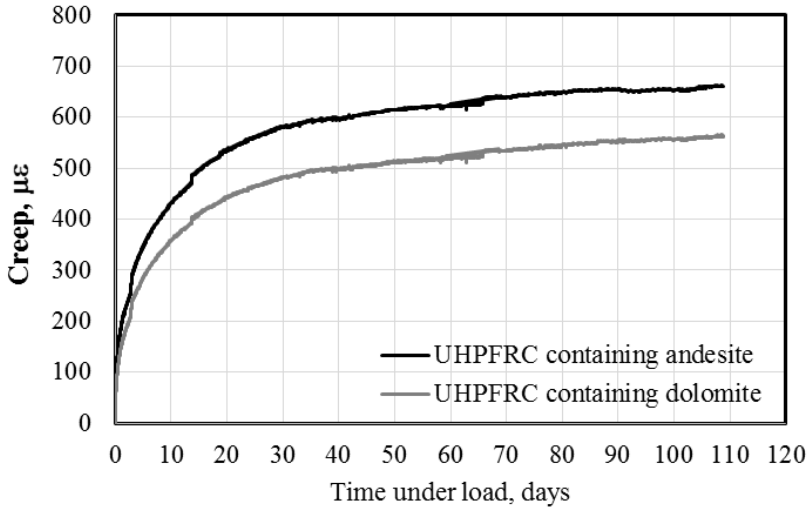

Figure 8.3 Creep in UHPFRC that experienced no heat treatment

Figure 8.4 shows the creep performance of UHPFRC specimens experienced heat treatment. Higher creep developed in UHPFRC containing dolomite over time. Creep coefficient of 0.2 and 0.18 was achieved for UHPFRC containing dolomite and andesite, respectively for specimens that experienced heat treatment. These values are similar to value for creep coefficient recommended by AFGC (2002) and JSCE (2006). It seems that by applying heat treatment, the creep coefficient would be reduced to about 0.2 as recommended by AFGC (2002) and JSCE (2006).

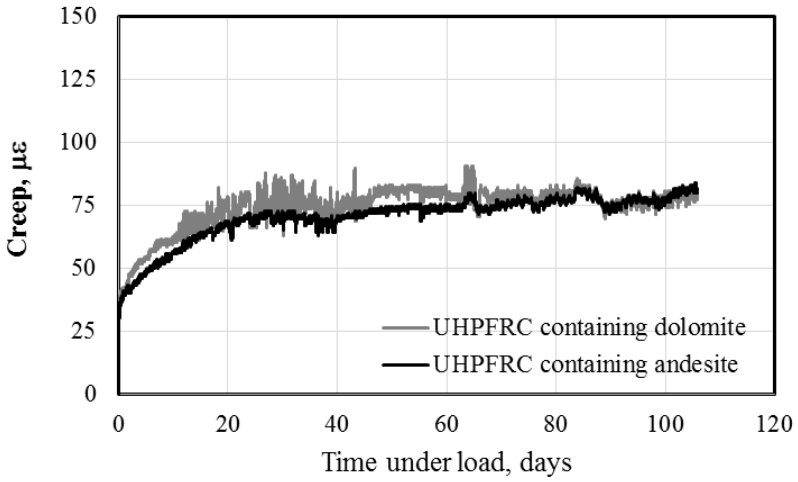

Figure 8.4 Creep in UHPFRC that experienced heat treatment

8.4 RESULTS AND ANALYSIS OF UHPFRC PRESTRESSED BEAM

8.4.1 Dolomite beam

Figure 8.5 shows the load- midspan deflection response of the dolomite beam for both load cycles. In the initial load application, the beam behaviour was linear up to 200 kN prior to the flexural cracks formation in the midspan region. Then, the beam behaviour began to soften at 200 kN of applied load and the deflection of approximately 4.5 mm in the midspan. The clear formation of diagonal shear cracks took place at 345 kN with a corresponding deflection of 11 mm.

By applying the final load application (displacement control), the linear behaviour of the beam reached up to approximately 200 kN, which was the same behaviour as observed in the initial load application. The beam exhibited significant additional load-carrying capacity after initial shear cracking, which can be attributed to the fibre presence. After the formation of diagonal cracks in the web at 200 kN, the beam was able to sustain higher loads up to 423.4 kN with a corresponding midpsan deflection of 16.7 mm. The beam owes this ductile behaviour to the fibres that managed to bridge cracks and helped to avoid brittle behaviour.

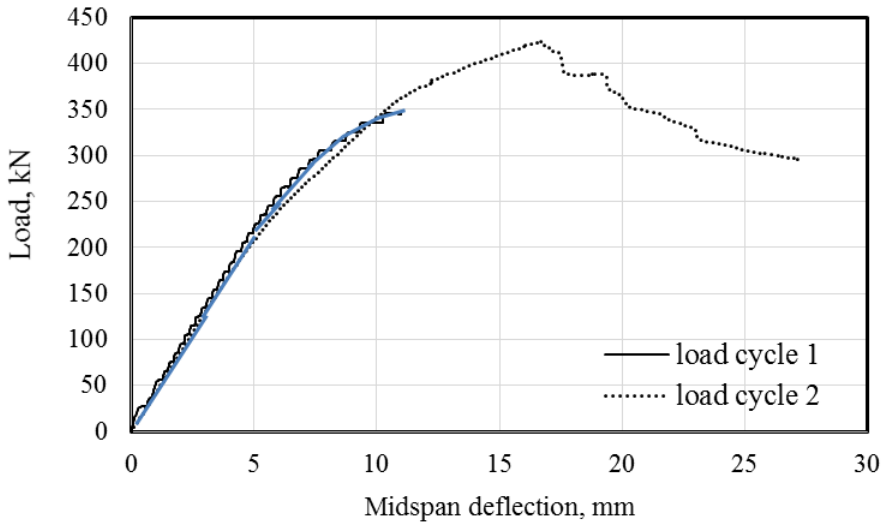

Figure 8.5 Load-deflection response of UHPFRC prestressed beams containing dolomite

8.4.2 Andesite beam

Figure 8.6 presents the load- midspan deflection response of the andesite beam for both load cycles. In the initial loading, the beam behaviour was linear up to 145 kN prior to the beam softening. The beam behaviour began to soften by formation of flexural cracks at 145 kN at a

midspan deflection of 3.7 mm. The clear formation of diagonal shear cracks took place at 175 kN and a corresponding deflection of 4.8 mm.

By applying the final load application (displacement control), the linear behaviour of the beam reached up to approximately 150 kN which was the same as in the initial load application. The beam exhibited significant additional load-carrying after initial cracking, due to the presence of fibres. The peak load of 239 kN at a corresponding deflection of 18.6 mm was achieved. This ductile behaviour is due to presence of fibres managed to transfer stress to the surrounding concrete and avoid a brittle failure.

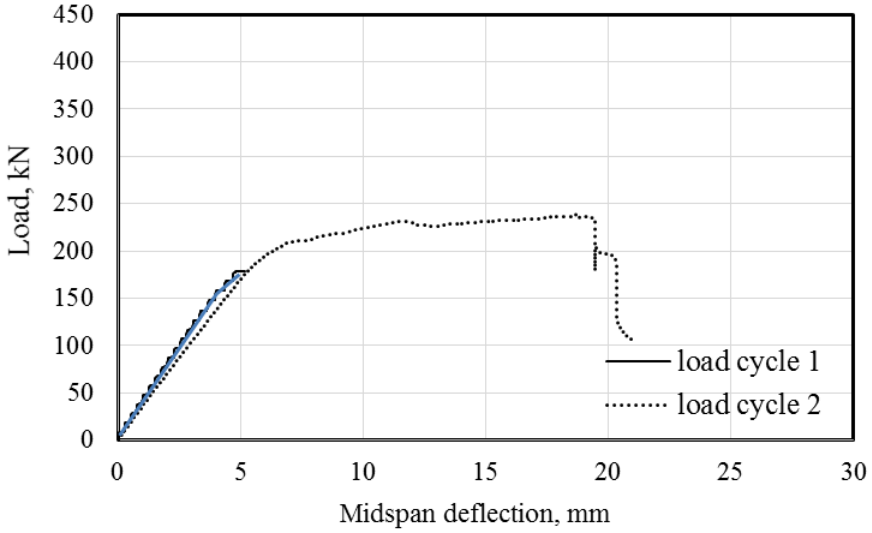

Figure 8.6 Load-deflection response of UHPFRC prestressed beams containing andesite

8.5 FAILURE AND CRACK PATTERNS

8.5.1 Dolomite beam

Figure 8.7 presents the crack patterns in UHPFRC prestressed beam containing dolomite. The first flexural cracks in the midspan region occurred at 200 kN (47% of peak load) where the beam began to behave nonlinear. At a load of 306 kN (72% of peak load), the diagonal shear cracking initiated in the web regions of the right shear span. The initial rigidity decreased due to occurrence of the diagonal crack. As the loading was increased the diagonal cracks then multiplied and propagated toward the top flange and smeared across the spans. Despite of the appearance of the diagonal cracks, the specimen exhibited significant load-carrying capacity either due to compressive strut action or presence of fibre. No crushing of diagonal struts was observed which can be due to the very high compressive strength of the

concrete (186 MPa). Fibres managed to bridge cracks and transfer the stress to the concrete leading to formation of multiple cracks. At the peak load of 423 kN, a major diagonal crack formed in the right span. After the peak load, the diagonal crack opened considerably and the load reduced. **Figure 8.8** was taken at a post peak load of 423 kN with all fibres being pulled out along the crack plane. The figure also shows that the top flange of the beam is rotated at two distinct locations.

The left shear span showed several inclined cracks occurrence due to several concrete compressive struts that intersected at the loading point (see **Figure 8.9**). The multiple crack formation around the inclined cracks can be attributed to the effect of fibre which helped to transfer stress to the surrounding concrete, thus avoiding the opening of the main inclined cracks. Finally, failure resulted from tensile fracture across a single dominant crack in the right shear span. Diagonal tension can be considered as the failure mode. In the right shear span, the angles of the critical inclined cracks with respect to the beam longitudinal axis was 40°. In the left shear span, the angles of inclined cracks was ranging from 40° to 45°.

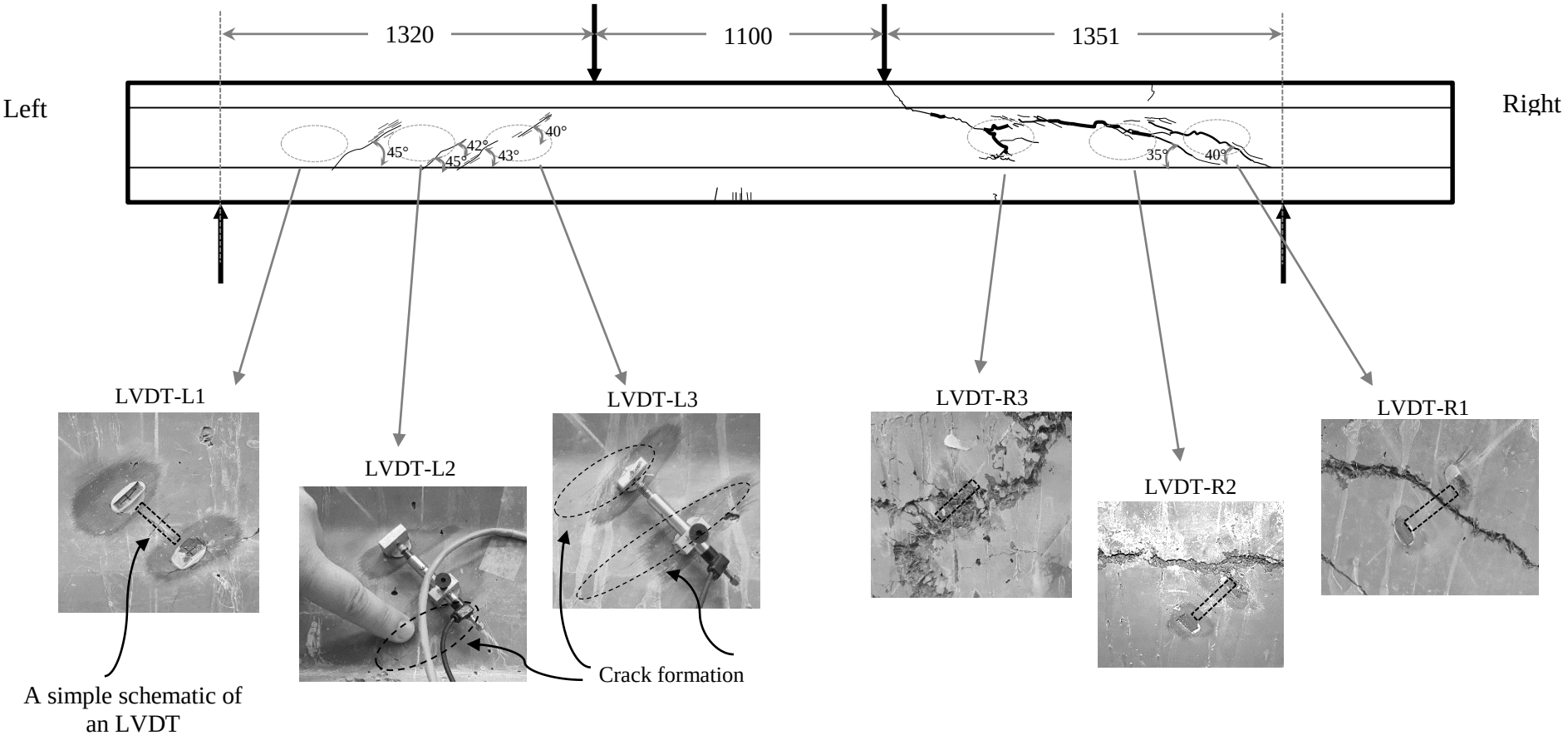

Figure 8.7 Crack patterns in UHPFRC prestressed beam containing dolomite

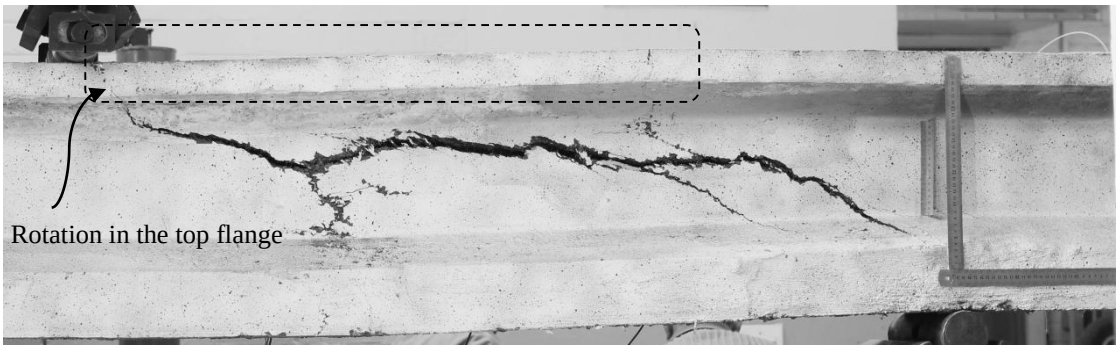

Figure 8.8 UHPFRC prestressed beam containing dolomite at the time of failure at the right shear span

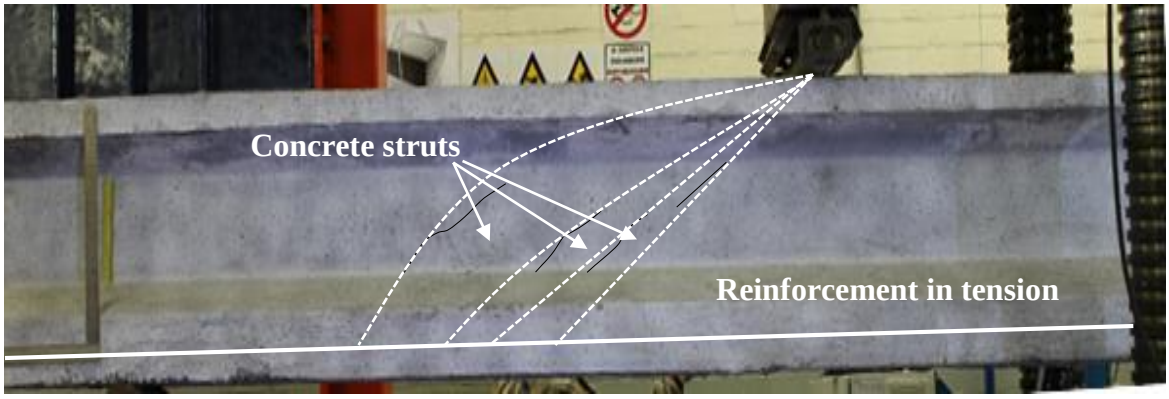

Figure 8.9 Concrete struts at the left shear span UHPFRC prestressed beam containing dolomite

8.5.2 Andesite beam

Figure 8.10 shows the crack patterns in UHPFRC prestressed beam containing andesite. In the Andesite beam, the first flexural cracks in the midspan region occurred at 145 kN (61% of peak load) where the beam began to behave nonlinear. The first diagonal shear cracking was observed at the load of 175 kN (73% of peak load) in the web regions of right shear spans. The diagonal cracks then multiplied and propagated toward the top flange and smeared across the spans with increasing load due to the presence of fibre. The diagonal cracks was observed in web region of the left shear span. At the peak load of 239 kN a major diagonal crack formed in the right span. After the peak load, the diagonal crack opened considerably and the load reduced. Finally, failure resulted from tensile fracture across a single dominant crack in the right shear span. **Figure 8.11** was taken at a post peak load of 239 kN with all fibres being pulled out along the crack plane. The figure also shows that the top flange of the girder is rotated at two distinct locations.

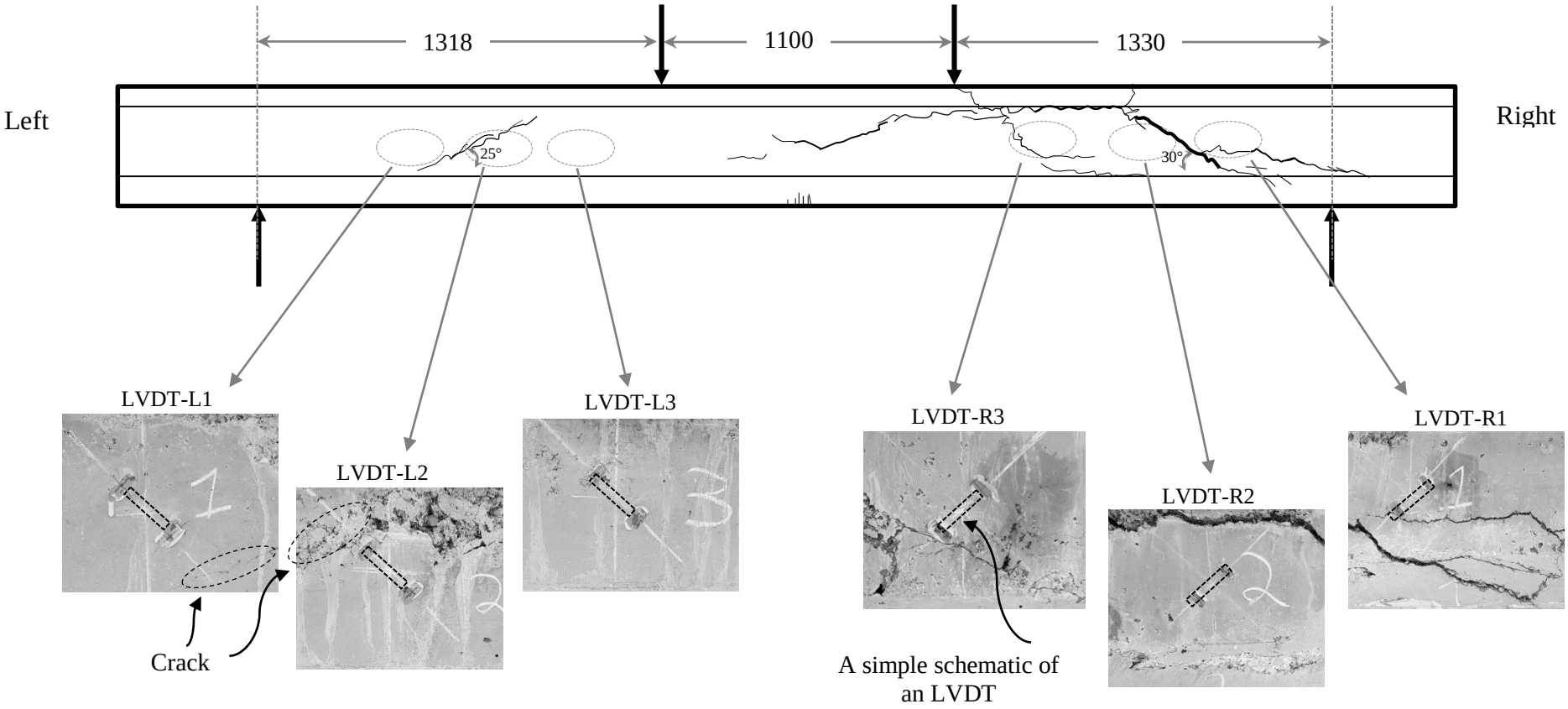

Figure 8.10 Crack patterns in UHPFRC prestressed beam containing andesite

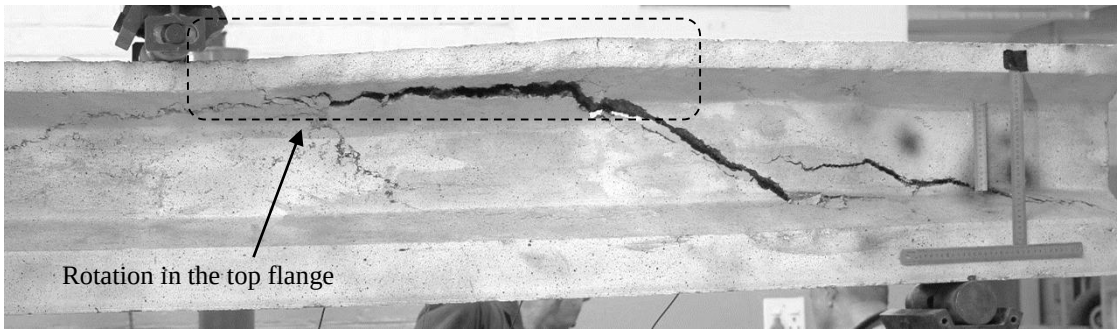

Figure 8.11 UHPFRC prestressed beam containing andesite at the time of failure at the right shear span

Comparing the flexural behaviour of UHPFRC prestressed beams showed the higher load-carrying capacity for UHPFRC prestressed beam containing dolomite than UHPFRC prestressed beam containing andesite. One reason can be attributed to the higher prestress loss occurred in the andesite beam due to the lower early-age modulus of elasticity, the higher early-age shrinkage of UHPFRC containing andesite in comparison with UHPFRC containing dolomite. Besides, more voids in the andesite beam may be present due to the lower workability of the UHPFRC andesite mix.

8.6 STRAIN MEASUREMENTS

8.6.1 Dolomite beam

Figure 8.12 shows the recorded midspan top flange horizontal strain and bottom flange horizontal strain values. Negative strains represent compressive strains while positive strains represent tensile strains. The strain captured by the bottom strain gauge (tensile strain) increased linearly for increasing the midspan deflection up to 4.5 mm where the beam began to behave nonlinear under loading (see **Figure 8.12**). The corresponding tensile strain was 554 μm, equivalent to 31.3 MPa of tensile stress. The maximum tensile strain was observed at 10 mm deflection, followed by strain reduction. It seems that the crack began to close due to the stress re-distribution in the beam. However, the strain captured by the top strain gauge (compressive strain) behaved linear to higher midspan deflection (6 mm). The compressive strain followed the load-midspan pattern and increased up to 1431 μm at 16.7 mm midspan deflection and reduced with the decreasing the load carrying capacity of the beam. The maximum measured compressive strain was 1431 μm which is equivalent to compressive stress of 80.8 MPa. This indicates that crushing of the top flanges was not an issue.

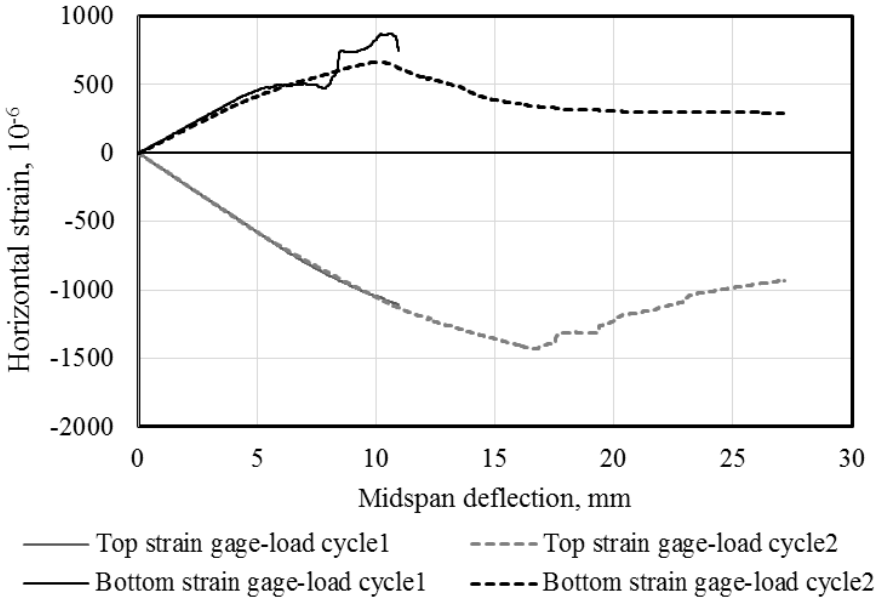

Figure 8.12 Horizontal strain profile results for midspan of UHPFRC prestressed beam containing dolomite

Figure 8.13 to **Figure 8.15** present the recorded tensile strains measured by LVDTs on the web. The strain development in LVDT-R1 and LVDT-L1 which are the ones closest to the supports are shown in **Figure 8.13**. The strain development in both LVDTs was linearly related to increasing midspan deflection up to about 5 mm. At midspan deflections over 8 mm, a diagonal shear crack developed that was captured by LVDT-R1 at a corresponding load of 305.5 kN. The crack occurance can be noticed from the significant jump in the recorded strain. The cracking tensile strength of 9.44 MPa was calculted based on the displacements recorded by LVDT-R1. The crack width of 87.22 µm was measured for the first load cycle based on the LVDT displacement. It is noteworthy that the inclined crack angle of 40° was measured for the angle captured by LVDT-R1. So, the tensile strength and crack width was calculated perpendecular to the LVDT. In the second load cycle, LVDT-R1 captured the crack opening up to the point that the LVDT was out of range.

As discussed by Baby et al. (2013), crack localization can be identified through LVDT under the recognition that localization corresponds to the beginning of a decreasing elongation value measured by LVDTs. Crack localization was identified by LVDT-R2 and LVDT-L2 as seen in **Figure 8.14**.

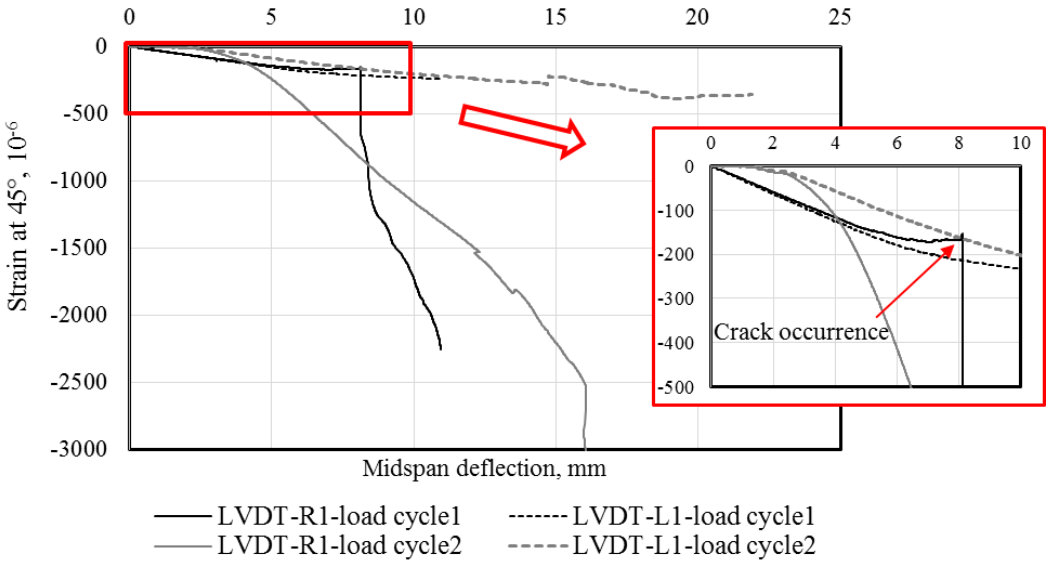

Figure 8.13 Strain calculated from the displacement recorded by LVDT-R1 and LVDT-L1 in the dolomite beam

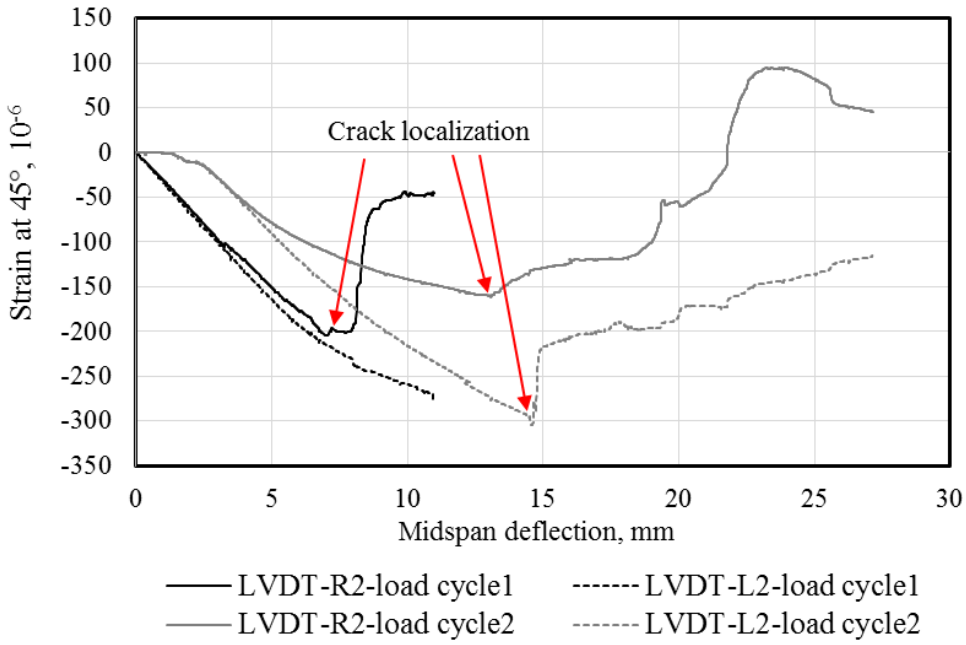

Figure 8.14 Strain calculated from the displacement recorded by LVDT-R2 and LVDT-L2 in the dolomite beam

Figure 8.15 presents the strain calculated from the displacement recorded by LVDT-R3 and LVDT-L3 installed at 45°. During the first load cycle, strain increased linearly with increasing the midspan deflection. No cracking was detected during the first load cycle. During the last load cycle, LVDT-L3 detected crack formations which can be recognised by

the sudden jump in the recorded displacement shown in the figure. Besides, crack localization was identified by LVDT-R3 resulting in reduced strain at increased deflections.

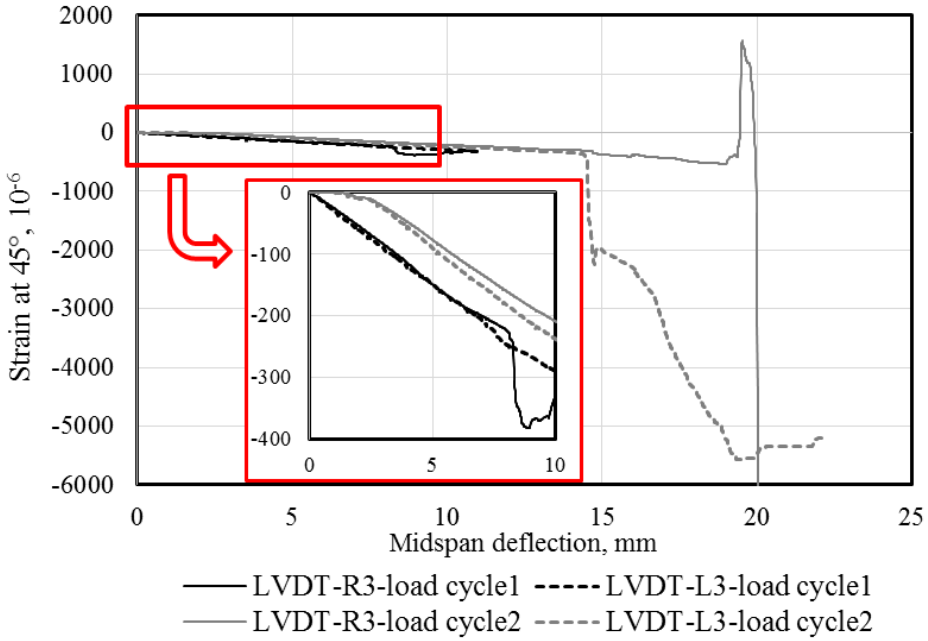

Figure 8.15 Strain calculated from the displacement recorded by LVDT-R3 and LVDT-L3 in the dolomite beam

8.6.2 Andesite beam

Figure 8.16 shows the recorded midspan top flange horizontal strain and bottom flange horizontal strain values in the andesite beam. Negative strains represent tensile strains while positive strains represent compressive strains. The tensile strain increased linearly with increasing midspan deflection up to 3.7 mm. With the formation of a flexural crack, a sudden jump in the recorded strain was noticed which indicates the formation of flexural cracks in the bottom of the beam at the midspan. The tensile strain before cracking was 477 µm which is equivalent to a tensile stress of 23.86 MPa. By increasing the midspan deflection up to 5 mm, the crack opened further.

During the final loading, the tensile strain was increasing nonlinear, since the closed crack began to open up again in the final stage of loading. At 8 mm deflection in the midspan, the strain gauge got out of range and could not measure the crack opening further. However, the compressive strain was increasing up to the beam failure. The maximum compressive strain increased up to 849 µm at 18.8 mm midspan deflection which is equivalent to compressive stress of 42.4 MPa. This indicates that crushing of the top flanges was not an issue.

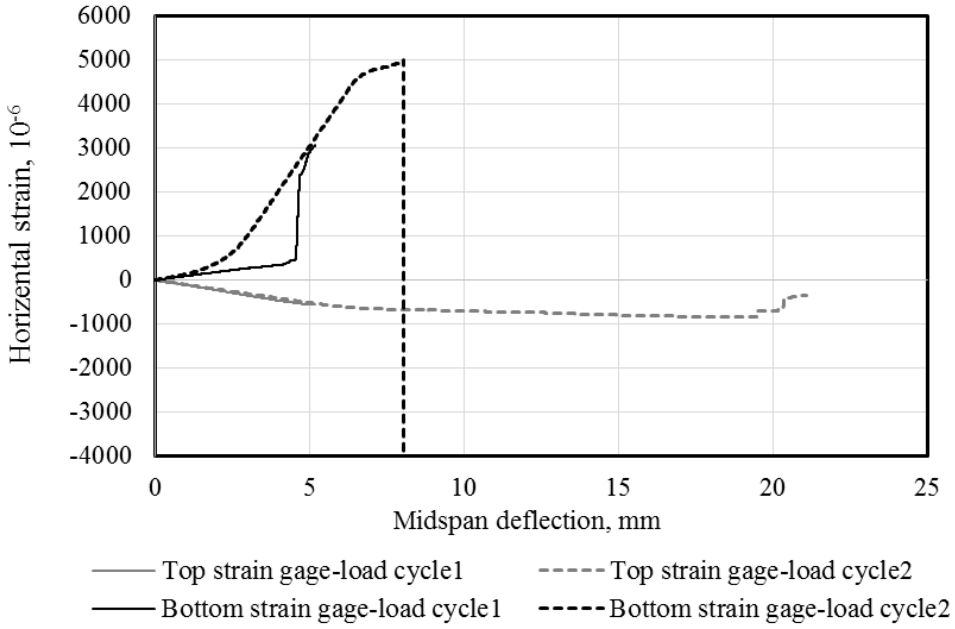

Figure 8.16 Horizontal strain profile results for midspan of UHPFRC prestressed beam containing andesite

Figure 8.17 presents the strain calculated from the displacements recorded by LVDT-R1 and LVDT-L1installed at 45° on the web of the andesite beam. The strain development in LVDT-R1-1 and LVDT-L1-1 was linearly related to the increasing the midspan deflection.

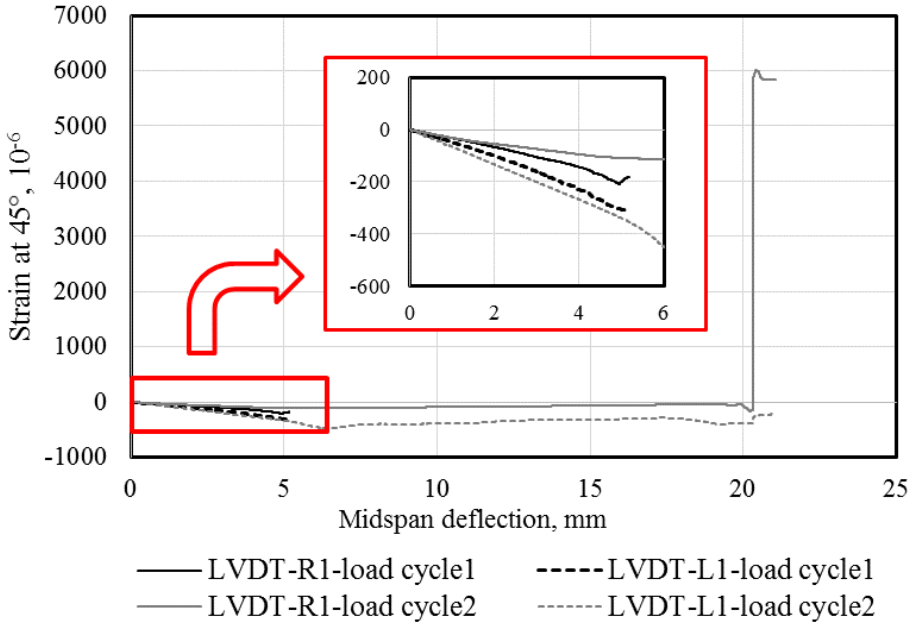

Figure 8.17 Strain calculated from the displacement recorded by LVDT-R1 and LVDT-L1 in the andesite beam

Figure 8.18 presents the strain recorded in LVDT-R2 and LVDT-L2 fixed at 45°. As shown in the figure, the crack localization was captured by both LVDTs during the first cycle load.

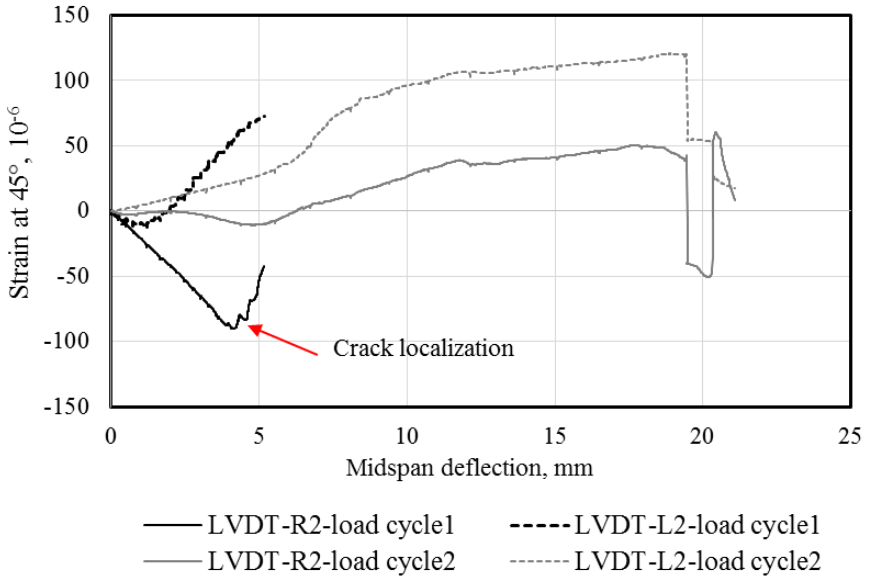

Figure 8.18 Strain calculated from the displacement recorded by LVDT-R2 and LVDT-L2 in the andesite beam

Figure 8.19 presents the strain calculated from the displacement recorded by LVDT-R3 and LVDT-L3 installed at 45°. No cracking was detected by LVDTs during the first load cycle. However, formation of a diagonal crack was captured by LVDT-R3 during the last load cycle.

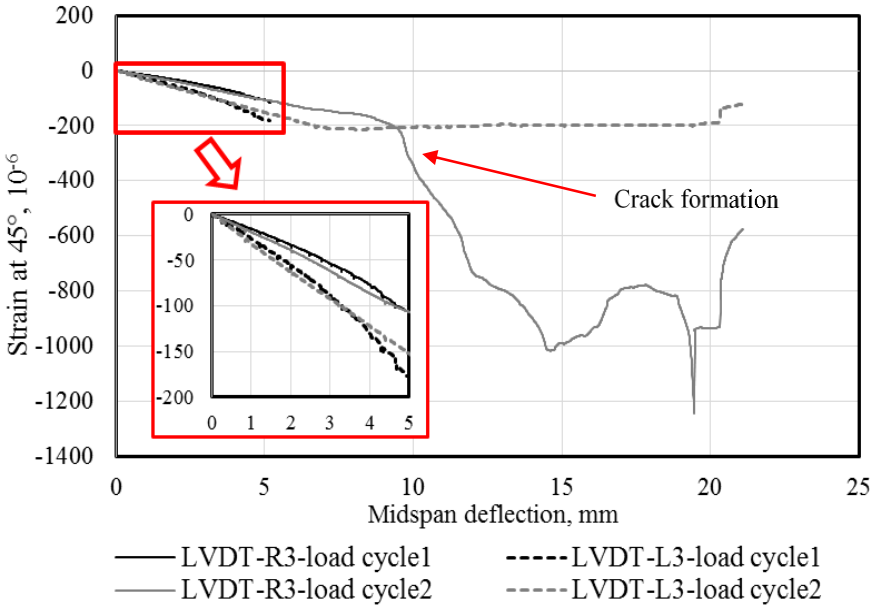

Figure 8.19 Strain calculated from the displacement recorded by LVDT-R3 and LVDT-L3 in the andesite beam

8.7 COMPARISON OF THE RESULTS WITH CODES

The ultimate shear capacities were predicted by several design codes including: ACI 318-11 and Eurocode 2. The experimental results are compared to the predicted results by the aforementioned design codes. The ultimate shear capacities calculated from these codes are of nominal values, not considering the strength reduction factor or safety factor for loads and materials. Besides, average material strength properties are used.

Provisions regarding to shear strength predictions recommended by Eurocode 2 and ACI 318-11 are presented as follows:

Eurocode 2

The shear capacity of a structural concrete member without shear reinforcement is to be determined using Eq. (8.1) or Eq. (8.2) for sections uncracked, respectively cracked in bending.

$$\boldsymbol{V_{Rd} = \frac{I b_w}{Z_t} \sqrt{f_{ctd}{}^2 + \alpha_1 \sigma_{cp} f_{ctd}}} \quad \text{Eq. (8.1)}$$

$$\boldsymbol{V_{Rd} = \left[\frac{0.18}{\gamma_c}\left(1 + \sqrt{\frac{200}{d}}\right)(100\rho_1 f_{ck})^{1/3} + 0.15\sigma_{cp}\right] b_w d} \quad \text{Eq. (8.2)}$$

$$\boldsymbol{V_{min} = \left[0.035\left(1 + \sqrt{\frac{200}{d}}\right)^{3/2} f_{ck}^{1/2} + 0.15\sigma_{cp}\right] b_w d} \quad \text{Eq. (8.3)}$$

Where

$\rho_1 = \frac{A_{s1}}{b_w d} \leq 0.02$

ACI 318-11

The shear strength of members without shear reinforcement is predicted by Eq. (8.4) and Eq. (8.5) which is for members subject to axial compression in addition to shear and flexure.

$$\boldsymbol{V_c = \left(0.16\sqrt{f'_c} + 17\rho_w \frac{V_u d}{M_m}\right) b_w d \leq 0.29\sqrt{f'_c} b_w d} \quad \text{Eq. (8.4)}$$

$$\boldsymbol{M_m = M_u - N_u\left(\frac{4h-d}{8}\right)} \quad \text{Eq. (8.5)}$$

Where

$\rho_w = \frac{A_s}{b_w d}$

Table 8.2 Diagonal cracking load and measured and calculated ultimate shear capacity according to various code provisions

	Calculated, kN		**Measured, kN**		**Measured/ Calculated**	
	Shear strength		**Diagonal cracking**	**Shear strength**	**Shear strength**	
	V_{ACI}	V_{EC2}	V_{cr}	V_{test}	V_{test}/ V_{ACI}	V_{test}/ V_{EC2}
Dolomite beam	46.6	46.7	146.8	207.2	4.45	4.44
Andesite beam	45.6	45.5	85	119.5	2.62	2.63

The results of these calculations are summarized in **Table 8.2** and compared to the experimental failure load. Comparing the measured shear strength versus the calculated ones based on the codes, confirms the significant contribution of fibres in shear resistance. The shear capacities provided by UHPFRC were much higher when compared to the shear strength estimated by both codes. In the UHPFRC prestressed beam containing dolomite, the shear strength achieved in the tests were 4 times higher than the shear strength predicted by ACI 318-11 and Eurocode 2. These results confirm that fibres can act as shear reinforcing, thus making it possible to eliminate shear stirrups and limit the web thickness. It is noteworthy that the designed beam are only an example of UHPFRC beams confirming the effect of fibre on the shear strength. In order to achieve UHPFRC beams resisting higher flexural and shear strength by the help of fibres, finite element modelling will be required.

8.8 COST COMPARISON BETWEEN UHPFRC AND NSC PRESTRESSED BEAMS

To compare the manufacturing cost of UHPFRC and NSC prestressed beams, the following investigation was carried out.

A NSC beam was designed to have the same structural performance as the UHPFRC prestressed beam (introduced in Section 7.2). The NSC beam had the same length and depth as UHPFRC beam while only the width differed. NSC beams were designed to fail in shear by providing less than the required number of shear stirrups. The required end block reinforcement was designed, since no failure and cracking took place in the end block region of the UHPFRC prestressed beams. The design was done based on SANS 51992-1-1:2014, the same code used to design the UHPC prestressed beam. The ultimate compressive strength of 60 MPa was used in the NSC beam calculations. **Table 8.3** introduces the mix design considered for NSC.

Table 8.3 Mix design for NSC with 60 MPa compressive strength

Material	**Amount (kg/m^3)**
Cement (CEM II/ A 42.5R)	478
Dolomite sand (Max: 4.75 mm)	872
Dolomite stone (Max: 9.5 mm)	890
Water	215

The possible options for NSC prestressed beams are presented in **Table 8.4**. The ratios of concrete volume for NSC prestressed beams to UHPFRC prestresses beams can be seen in this table (as Beam volume/ Ref volume). It can be inferred from the data presented in the table, that an increase in compressive strength from 60 MPa to 185 MPa produces a significant reduction in the volume of concrete (up to 244%). This reduction in the volume of concrete required for construction would result in reduced carbon dioxide emissions, which is favourable in terms of environmental impact on global warming. Besides, less reinforcement volume is required.

For more clarification, it is recommended that NSC prestressed beams should be cast to confirm that the prestressed beams would behave the same than the UHPFRC prestressed beams under flexure.

Table 8.4 NSC prestressed beam having the same structural performance as UHPFRC

Beams	Width (mm)	Height (mm)	Length (m)	No. bottom bars	No. top bars	No. shear links	Beam volume/ Ref* volume
NSC beam 1	450	400	4.4	24	10	10	3.4

*UHPFRC prestressed beam

For cost analysis only the material costs including the concrete and the longitudinal and shear reinforcement, the labour costs for cutting, placing and connecting of the reinforcement bars in the concrete beam, the labour costs for concreting the beam, the labour costs for curing the concrete and power consumption were considered. In the cost analysis, neither transportation costs for UHPFRC beams to move sections from precast works to the construction site nor transportation cost for transporting normal-strength fresh mix to the construction site was considered. Casting NSC beams would however require more vehicles to the construction site due to much higher volume of concrete (see **Table 8.4**).

The manufacturing cost of the member is defined as the sum of material, labour costs and power consumption required for the fabrication (Merta, et al., 2010). The manufacturing costs of RC rectangular beam was calculated assuming:

$$Cost = C_{M\ ,c,r} + C_{L,r} + C_{L,c} + C_{L,v} \quad \text{Eq. (8.6)}$$

Where the variable Cost (ZAR) represents the manufacturing costs of the beam, the notations $C_{M,\ldots}$ and $C_{L,\ldots}$ represent the calculated material and labour costs.

The material costs of the concrete and the longitudinal and shear reinforcement was calculated using Equation 8.7:

$$C_{M,c,r} = c_{M\ ,c} \cdot V_c + c_{M,r} \cdot \rho s \cdot (V_{s,l} + V_{sw}) \quad \text{Eq. (8.7)}$$

Where $c_{M,c}$ (ZAR/m^3) and $c_{M,r}$ (ZAR/kg) are the prices of the concrete and reinforcement; V_c, $V_{s,l}$ and V_{sw} in (m^3) represent the volumes of concrete, longitudinal and shear reinforcement respectively; ρ_s (kg/m^3) is the unit mass of steel.

The labour costs for cutting, placing and connecting of the reinforcement bars in the concrete beam was calculated as follows:

$$C_{L,r} = c_L \cdot T_r \cdot \rho_s \cdot (V_{s,l} + V_{sw}) \quad \text{Eq. (8.8)}$$

Where c_L (ZAR/h) denotes the labour costs per working hour; T_r (h/kg) is the time required for cutting, placing and connecting the reinforcement; $V_{s,l,}$ and V_{sw} (m^3) represent the volumes of longitudinal and shear reinforcement respectively; ρ_s (kg/m^3) is the unit mass of steel.

The labour costs for concreting the beam and consolidating the concrete were calculated using Eq. (3.1) and Eq. (3.2), respectively.

The material and labour cost parameters including the price of the concrete and reinforcing tendons as well as labour cost are presented in **Table 8.5**. It is noteworthy that the price for UHPFRC includes material cost as well as the cost of its heat treatment curing. In **Table 8.6** fabrication time parameters used for the cost calculations are listed.

Table 8.5 Material and labour cost parameters

Material and labour cost parameters	**Price**
$c_{M,c}$ **Price of the concrete 60 MPa**	1244 ZAR/m^3
$c_{M,c}$ **Price of the concrete 180 MPa**	(7905 + 165) ZAR/m^3
$c_{M,r}$ **Price of the reinforcing steel**	50 ZAR/kg
c_L **Labour costs**	150 ZAR/h

Table 8.6 Fabrication time parameters

Fabrication time parameters	**Time**
T_r **Time for cutting, placing and connecting of the reinforcement**	0.03 h/kg
T_c **Time of concreting in NSC beams**	1.00 h/m^3
T_c **Time of concreting in UHPFRC beams**	2.00 h/m^3
T_v **Time for consolidation of NSC beams**	0.20 h/m^2
T_v **Time for consolidation of UHPFRC beams**	0.30 h/m^2

The fabrication cost for both NSC and UHPFRC prestressed beams were calculated and compared in **Table 8.7**. Although the initial cost (material and curing costs) for UHPFRC is significantly higher than the material cost of NSC, the total cost for manufacturing UHPFRC prestressed beams is less. This is due to the fact that by requiring less concrete and reinforcement, the labour cost and time required for cutting, placing and connecting the reinforcement are reduced. Labour cost for consolidating the concrete is reduced when less volume of concrete is vibrated even if the vibration time for the UHPFRC beam was assumed to be twice the vibration time required for the NSC beam. In addition, end block reinforcement would not be necessary when UHPFRC is used to produce prestressed beams.

Table 8.7 Fabrication cost comparison between NSC and UHPFRC prestressed beams

Cost (ZAR)	**NSC beam**	**UHPFRC**
$C_{M,c,r}$	3816.2	3045.3
$C_{L,r}$	169.8	107.0
$C_{L,c}$	118.8	69.0
$C_{L,v}$	59.4	39.6
Total	4164.3	3260.9

Several aspects should be taken into account during the economic comparison and these aspects include:

- Durability- the cost of rehabilitation during the lifetime of a structure should be added to the initial construction cost and this can significantly affect the project cost. Utilizing high-strength concrete with superior durability characteristics would result in savings due to reduced rehabilitation cost.

- Reduction in self-weight - member size is reduced by utilizing high-strength concrete especially in bridges and high-rise building. By reducing the member size (less volume of concrete) the size of foundation could be reduced.

- Increase in rentable space- which is beneficial in high-rise buildings.

- Reduction in construction time, in the case of precast member utilization.
- Reduction in formwork, in the case of precast member utilization.
- Reduction in number of supports and the supporting foundation due to the increase in spans.
- Lower number of skilled labours are required in the site.

Despite the advantage of precast construction in terms of saving cost and less emission of carbon dioxide, there are issues of structural design when using precast members. Assembling of the precast members is one of important consideration for ensuring strong structural behaviour. Supervision is necessary for connections between precast structural members that must be done properly to ensure the intended behaviour of the connection such as simple, semi-rigid or rigid connections. Besides, faulty connections may lead to water leakage and lack of sound insulation.

8.9 CONCLUSION

Mechanical properties including compressive strength, modulus of elasticity and splitting tensile strength are measured for both UHPFRC containing andesite and dolomite. Besides, shrinkage and creep tests were performed. The main conclusions are summarized as follows:

- Higher compressive strength, modulus of elasticity and splitting tensile strength were achieved for UHPFRC containing dolomite.
- For specimens experienced no heat treatment, creep coefficient of 1.46 and 1.5 was achieved for UHPFRC containing dolomite and andesite, respectively. These values are higher than those recommended AFGC (2002) and JSCE (2006) which can be due to different material properties used in UHPFRC developed in this research.
- For specimens experienced heat treatment, creep coefficient of 0.2 and 0.18 was achieved for UHPFRC containing dolomite and andesite, respectively. These values are similar to the value for creep coefficient recommended by AFGC (2002) and

JSCE (2006). It seems by applying heat treatment, the UHPFRC creep coefficient would be close to 0.2 (recommended by AFGC (2002) and JSCE (2006)) regardless of exact mix composition.

- For specimens experienced heat treatment, long-term drying shrinkage of 6.7 με and 17.5 με were achieved for UHPFRC containing dolomite and andesite, respectively. These values for long-term drying shrinkage are relatively small and can be consider to be negligible or zero which is the same value recommended by AFGC (2002) and JSCE (2006).

Flexural behaviour of large-scale UHPFRC prestressed beams under four-point loading was investigated. The beams were 4400 mm in total length having a span of 3900 mm and a total depth of 400 mm. The beams were prestressed by sixteen 7mm wires in the bottom flange, two 7mm wires in the top flange prestressed to 75% of the wire ultimate tensile strength. The main conclusions of this chapter are summarized as follows:

- In the UHPFRC prestressed beam containing dolomite, the formation of flexural cracks in the midspan region occurred at a load 47% of peak load. The diagonal shear cracking initiated in the web region at a load 72% of peak load. Despite of the appearance of the diagonal cracks, the specimen exhibited significant load-carrying capacity either due to compressive strut action or presence of fibre. No crushing of diagonal struts was observed which can be due to the very high compressive strength of the concrete (186 MPa). Failure resulted from tensile fracture across an inclined crack in the right shear span.

- In the UHPFRC prestressed beam containing dolomite, the beam behaved ductile under loading, since fibres managed to bridge cracks and helped to avoid a brittle behaviour.

- In the UHPFRC prestressed beam containing dolomite, the bottom flange horizontal strain (tensile strain) increased linearly with increasing midspan deflection up to 4.5 mm, where the beam began to behave nonlinear with the corresponding tensile strain of 554 μm, equivalent to 31.3 MPa of tensile stress.

- In the UHPFRC prestressed beam containing dolomite, the midspan top flange horizontal strain (compressive strain) followed midspan load pattern (increased to 1430 μm at 16.7 mm midspan deflection and reduced with decreasing the load carrying capacity of the beam). The maximum measured compressive strain was 1431 μm which is equivalent to compressive stress of 80.8 MPa. This indicates that crushing of the top flanges was not an issue.

- In the UHPFRC prestressed beam containing dolomite, based on the diagonal shear crack captured by an LVDT, the cracking tensile strength of 9.44 MPa and the crack width of 87.22 μm for a diagonal crack in the web were calculated.

- In the UHPFRC prestressed beam containing andesite, the first flexural cracks in the midspan region occurred at a load 61% of peak load. The first diagonal shear cracking was observed at a load 73% of peak load in the web regions of the shear spans. Despite the appearance of diagonal cracks, the beam had significant load-carrying capacity either due to compressive strut action or presence of fibre. No crushing of diagonal struts was observed which can be due to the very high compressive strength of the concrete (186 MPa). Failure resulted from tensile fracture across an inclined crack in the right shear span.

- In the UHPFRC prestressed beam containing andesite, the tensile strain before cracking was 477 μm which is equivalent to a tensile stress of 23.86 MPa. The maximum top strain (compressive strain) increased up to 849 μm at 18.8 mm midspan deflection which is equivalent to compressive stress of 42.4 MPa. This indicates that crushing of the top flanges was not an issue.

- The UHPFRC prestressed beam containing dolomite showed higher load-carrying capacity than the UHPFRC prestressed beam containing andesite. One reason can be attributed to the higher prestress loss that occurred in the andesite beam due to the lower early-age modulus of elasticity, the higher early-age shrinkage of UHPFRC containing andesite in comparison with UHPFRC containing dolomite. Besides, more voids may be present in the andesite beam due to the lower workability of UHPFRC andesite mix.

- Comparing the measured shear strength with the calculated values based on ACI 318-11and Eurocode 2 confirms the significant contribution of fibres in shear resistance.

- Having the same performance, comparing UHPFRC prestressed beams with 185 MPa compressive strength with NSC prestressed beams with 60 MPa compressive strength, resulted in a significant reduction in the volume of concrete required (up to 244%).

- The manufacturing cost of a UHPFRC prestressed beam is about half of the manufacturing cost of a NSC prestressed beams with the same performance, despite the initial high material cost of UHPFRC. This is due to less reinforcement, labour and time required for cutting, placing and connecting the reinforcement and less concrete to cast and vibrate.

CHAPTER 9 CONCLUSIONS AND RECOMMENDATIONS

9.1 INTRODUCTION

A comprehensive study was conducted on the development of an economical and practical UHPC to promote UHPC utilization. So, development of an economical and practical mix design by using local materials was investigated by considering different aggregate types, cementitious material combinations, aggregate contents and sizes. Development of practical curing regimes was studied by considering the effect of different water temperatures for heat treatment, time that samples were cured in the heat treatment and curing regime after the heat treatment. Further study was conducted on curing regime considering the effect of heat gradient in the curing process on the compressive strength of UHPC.

Manufacturing UHPC prestressed beams aiming to promote UHPC utilization in large-scale applications led to the investigation of bond performance between UHPC and high strength prestressing wires. Pull-out tests were conducted to evaluate embedment lengths thus avoiding bond failure. The effect of embedment length, concrete cover, age of UHPC and fibre content was studied.

UHPFRC prestressed I-beams (containing either dolomite or andesite) were tested under flexure to determine whether shear fibres can act as shear reinforcing, thus making it possible to eliminate shear stirrups and limit the web thickness.

9.2 CONCLUSIONS

The following conclusions were drawn from the results of the investigations on mix design:

- Economical and practical UHPC can be manufactured to be suitable in large-scale applications. This accomplishment is possible as a results of several modifications to the typical UHPC mix design. These modifications include:
  -

- Increasing the aggregate content to an aggregate to cement ratio (by mass) of 2.5, thus reducing the cement content to 593 kg/m3.
- Increasing the aggregate size of andesite with a maximum particle size of 4.75mm and 6.7mm was as a fine aggregate and coarse aggregate, respectively. Dolomite with the same grading can be an alternative. No sieving was done for aggregates and they were used in the mix as they were supplied from the quarry.
- Utilizing Portland cement (CEM II/A 42.5R and CEM II/A 52.5N), silica fume and Ground Granulated Blast Furnace Slag as cementitious materials.
- Utilizing local straight steel fibre with 13mm length and 0.26 diameter to reinforce UHPC.

- Development of an economical UHPC is successfully achieved by increasing the aggregate content and sizes, using supplementary cementitious materials beside cement. The unit costs per compressive strength for the proposed mix design was significantly reduced from 109 ZAR/m^3/MPa for the typical mix design to 28.0 ZAR/m^3/MPa.

- The ultimate compressive strength of UHPFRC is not affected significantly by fibre tensile strengths. However, their effect can be observed on the post-cracking ductile behaviour of concrete.

- Direct tensile strengths of 10 MPa and 9.85 MPa were obtained for UHPC containing hook-ended fibre (Type II) (3000 MPa tensile strength) and micro fibres (2500 MPa tensile strength) respectively with standard curing regime (24°C water).

- Fibres had a significant effect on the post-cracking behaviour and the ultimate splitting tensile strength of UHPFRC. The increase in the strength of UHPFRC after the first cracking can be noted as 42% and 38% for hook-ended fibre (Type II) and micro fibres, respectively. UHPC containing hook-ended fibre (Type II) showed more ductility in the splitting tensile behaviour.

The mechanical properties of UHPC and UHPFRC are summarized in **Table 9.1**.

The following conclusions were summarised from the results of the investigations on curing regime:

- It seems that heat treatment has a negative effect on the stiffness of UHPFRC and the elastic modulus obtained from cylinders that experienced standard curing is higher than those cured for 72 hrs in 85°C. This effect is more considerable in samples with no fibres.

- It is worth mentioning that the reduction in compressive strength was not significantly affected by the different heat gradients and did not continue at older ages as the 90-day compressive strengths exceeded the 7-day strengths.

- Storing UHPC in water after the heat treatment eliminates the self-desiccation phenomena, thermal shocking of samples should be avoided.

- UHPC reinforced with locally available fibres containing dolomite showed higher workability than the same UHPFRC containing andesite.

The following conclusions were drawn from the results of the investigations on creep, shrinkage and bond behaviour:

- For UHPFRC experienced no heat treatment, creep coefficient of 1.46 and 1.5 was achieved for UHPFRC containing dolomite and andesite, respectively. These values are higher than those recommended AFGC (2002) and JSCE (2006) which can be due to different material properties used in UHPFRC developed in this research as well as the probable LDVT drift occurrence.

- For UHPFRC experienced heat treatment, creep coefficient of 0.2 and 0.18 was achieved for UHPFRC containing dolomite and andesite, respectively. These values are similar to the value for creep coefficient recommended by AFGC (2002) and JSCE (2006). It seems by applying heat treatment, the UHPFRC creep coefficient would be close to 0.2 (recommended by AFGC (2002) and JSCE (2006)) regardless of mix composition.

- For UHPFRC experienced heat treatment, long-term drying shrinkage of 6.7 με and 17.5 με were achieved for UHPFRC containing dolomite and andesite, respectively. These values for long-term drying shrinkage are relatively small and can be consider to be negligible or zero which is the same value recommended by AFGC (2002) and JSCE (2006).

- Fibres control crack propagation, thus preventing brittle failing. In the presence of fibre after the initiation of slipping, the bond resistance improved significantly.

- In UHPFRC, no improvement in bond strength was observed after more than 7 days at different embedment lengths.

- The inclusion of fibres change the type of failure from concrete splitting to bond failure for specimens with 75 mm embedment length and from bond failure to wire rupture in specimens with 100 mm embedment length.

- The specimens containing fibre with embedment lengths of 100 mm and more at the age of 7 days and older, experienced wire rupture as a type of failure which indicates sufficient development length. However, in the specimens without fibre wire rupture occurred at higher embedment lengths of 125 mm and 150 mm.

- Shorter development length is achieved by inclusion of fibres in UHPC.

- By increasing the embedment length, the slip reduces significantly.

The main conclusions of the results of the investigations on the large-scale UHPFRC prestressed beams are as follows:

- In the UHPFRC prestressed beams, flexural cracks occurred, followed by diagonal shear cracking in the web. Despite the appearance of the diagonal cracks, the specimen exhibited significant load-carrying capacity either due to compressive strut action or presence of fibre. No crushing of diagonal struts was observed which can be due to the very high compressive strength of the concrete (186 MPa). Failure resulted from tensile fracture across an inclined crack in the shear span.

- In the UHPFRC prestressed beam containing dolomite, the beam behaved ductile under loading, since fibres managed to bridge cracks and helped to avoid a brittle behaviour.

- In the UHPFRC prestressed beam containing dolomite, the midspan top flange horizontal strain (compressive strain) of 1431 μm was achieved, which is equivalent

to compressive stress of 80.8 MPa. This indicates that crushing of the top flanges was not an issue.

- In the UHPFRC prestressed beam containing dolomite, the cracking tensile strength of 9.44 MPa and the crack width of 87.22 µm for a diagonal crack in the web were calculated.

- In the UHPFRC prestressed beam containing andesite, the tensile strain before cracking was 477 µm which is equivalent to a tensile stress of 23.86 MPa. The maximum top strain (compressive strain) increased up to 849 µm at 18.8 mm midspan deflection, which is equivalent to compressive stress of 42.4 MPa. This indicates that crushing of the top flanges was not an issue.

- Comparing the measured shear strength with the calculated values based on ACI 318-11 and Eurocode 2, confirms the significant contribution of fibres in shear resistance.

- Having the same performance, comparing UHPFRC prestressed beams with 185 MPa compressive strength with NSC prestressed beams with 60 MPa compressive strength, resulted in a significant reduction in the volume of concrete required (up to 244%).

- The manufacturing cost of a UHPFRC prestressed beam is about half of the manufacturing cost of a NSC prestressed beams with the same performance, despite the initial high material cost of UHPFRC. This is due to less reinforcement, labour and time required for cutting, placing and connecting the reinforcement and less concrete to cast and vibrate.

Table 9.1 Summary of the properties of UHPC and UHPFRC

	UHPC	**UHPFRC**	
	Andesite	**Andesite**	**Dolomite**
Compressive strength at 28 days, MPa	174.1	185.3	183.5
Modulus of elasticity at 28 days, GPa	53.2	52.0	56.5
Splitting tensile strength at 28 days, MPa	5.9	18.3	19.1
Drying shrinkage after 110 days, microstrain	250	17.5*	6.7*
Creep after 110 days, microstrain	936	661	562
Unit cost per 7-day compressive strength , ZAR/m^3/MPa	10.5	42.5	42.5

*Heat treated

9.3 RECOMMENDATIONS

- Further investigations on durability of UHPC and UHPFRC need to be conducted including water sorptivity, chloride conductivity and etc.
- Further investigations on fire resistance of UHPC and UHPFRC need to be conducted.
- Study on the phenomenon of DEF requires further investigations.
- Study on Carbonation and freeze /thaw of UHPC and UHPFRC needs to be carried out.
- Further investigations on actual performance of UHPC and UHPFRC structures need to be conducted.
- Study on microstructural analysis of UHPC and UHPFRC need to be carried out including comparative SEM images, porosity and permeation data, degree of hydration, given the wide range of materials and curing temperature.
- Further investigations are needed on UHPFRC beams to achieve beams with higher flexural and shear strength confirming the elimination of shear reinforcing.
- Finite element modelling is needed to design UHPC and UHPFRC beams to investigate the effect of fibre on the flexural behaviour of beams.
- Further experimental investigation of normally and heavily loaded NSC and UHPFRC prestressed beams to study the structural behaviour along with the economic feasibility of UHPFRC.

CHAPTER 10 REFERENCES

Abbas, S., Soliman, A., & Nehdi, M. (2015). Exploring mechanical and durability properties of ultra-high performance concrete incorporating various steel fiber lengths and dosages. *Construction and Building Materials*, 75, 429–441.

Abid, M., Hou, X., Zheng, W., & Hussain, R. R. (2017). High temperature and residual properties of reactive powder concrete–A review. *Construction and Building Materials*, 147, 339-351.

Abrams, D. A. (1913). *Tests of bond between concrete and steel*. *Bulletin* No. 71, University of Illinois at Urbana Champaign, College of Engineering. Engineering Experiment Station.

Abu-Lebdeh, T., Hamoush, S., Heard, W., & Zornig, B. (2011). Effect of matrix strength on pullout behavior of steel fiber reinforced very-high strength concrete composites. *Construction and Building Materials*, 25(1), 39-46.

ACI Committee 209 (2002). Report on Factors Affecting Shrinkage and Creep of hardened Concrete. *American Concrete Institute,* Farmington Hills, Michigan.

ACI Committee 318 (2011). Building code requirements for structural concrete. *American Concrete Institute, & International Organization for Standardization*.

ACI Committee 408 (2003). Bond and Development of Straight Reinforcing Bars in Tension (ACI 408R-03). *American Concrete Institute, Detroit, Michigan, US*, 49.

ACI Committee 544 (1988a). Design Considerations for Steel Fiber Reinforced Concrete," *ACI Structural Journal*, 85 (5), 563-580.

ACI Committee 544 (1988b), Measurement of Properties of Fiber Reinforced Concrete. *ACI Materials Journal,* 85 (6), 583-593.

Ahlborn, T. M., Misson, D. L., Peuse, E. J., & Gilbertson, C. G. (2008). Durability and strength characterization of ultra-high performance concrete under variable curing regimes. In *Proceedings of the Second International Symposium on Ultra High Performance Concrete, Kassel, Germany*, 197-204.

Alexander, M. G. & Mindess, S. (2005). *Aggregates in Concrete: Modern Concrete Technology Series*. Taylor & Francis.

Andreasen, A. H. M & Andersen, J. (1930). Über die Beziehung zwischen Kornabstufung und Zwischenraum in Produkten aus losen Körnern (mit einigen Experimenten). *Kolloid-Zeitschrift*, 50(3), 217-228.

Arowojolu, O., Ibrahim, A., & Taha, M. R. (2018). Parametric Study on the Performance of UHPC and Nano-modified Polymer Concrete (NMPC) Composite Wall Panels for Protective

Structures. In International Congress on Polymers in Concrete (pp. 683-688). Springer, Cham.

Ashour, S. A., Hasanain, G. S., & Wafa, F. F. (1992). Shear behavior of high-strength fiber reinforced concrete beams. *Structural Journal*, 89(2), 176-184.

Askar, L. K., Tayeh, B. A., Bakar, B. A., & Zeyad, A. M. (2017). Properties of Ultra-High Performance Fiber Concrete (UHPFC) Under Different Curing Regimes. International Journal of Civil Engineering and Technology, 8(4).

ASTM C1856 / C1856M (2017). Standard Practice for Fabricating and Testing Specimens of Ultra-High Performance Concrete. The American Society for Testing and Materials, USA.

ASTM C469 / C469M-14 (2014). Standard Test Method for Static Modulus of Elasticity and Poisson's Ratio of Concrete in Compression, ASTM International, West Conshohocken, PA.

ASTM C496 / C496M-17 (2017). Standard Test Method for Splitting Tensile Strength of Cylindrical Concrete Specimens, ASTM International, West Conshohocken, PA.

Association Française de Génie Civil (AFGC) (2002). *Ultra High Performance Fibre-Reinforced Concretes—Interim Recommendations,* Paris, France.

Ay, L. (2004). Curing tests on ultra high strength plain and steel fibrous cement based composites. In *Proceedings of the International Symposium on Ultra High Performance Concrete, Kassel, Germany*, 15, 695-701.

Azmee, N. M., & Shafiq, N. (2018). Ultra-high performance concrete: From fundamental to applications. Case Studies in Construction Materials, 9, e00197.

Azizinamini, A., Chisala, M., & Ghosh, S. K. (1995). Tension development length of reinforcing bars embedded in high-strength concrete. *Engineering Structures*, 17(7), 512-522.

Azizinamini, A., Stark, M., Roller, J. J., & Ghosh, S. K. (1993). Bond performance of reinforcing bars embedded in high-strength concrete. *Structural Journal*, 90(5), 554-561.

Baby, F., Marchand, P., & Toutlemonde, F. (2013). Shear behavior of ultrahigh performance fiber-reinforced concrete beams. I: Experimental investigation. *Journal of structural engineering*, 140(5), 04013111.

Bandyopadhyay. J.N. (2008). *Design of Concrete Structures*. Prentice Hall of India Pvt. Ltd., New Delhi.

Banthia, N. (1990). A study of some factors affecting the fiber–matrix bond in steel fiber reinforced concrete. *Canadian Journal of Civil Engineering*, 17(4), 610-620.

Barnes, R. W., Grove, J. W., & Burns, N. H. (2003). Experimental assessment of factors affecting transfer length. *Structural Journal*, 100(6), 740-748.

Barros, J. A., Cunha, V. M., Ribeiro, A. F., & Antunes, J. A. B. (2005). Post-cracking behaviour of steel fibre reinforced concrete. *Materials and Structures*, 38(1), 47-56.

Batson, G., Jenkins, E., & Spatney, R. (1972). Steel Fibers as Shear Reinforcement in Beams. *ACI Journal*, 69 (10), 640-644.

Beglarigale, A., & Yazıcı, H. (2015). Pull-out behavior of steel fiber embedded in flowable RPC and ordinary mortar. *Construction and building materials*, 75, 255-265.

Bentz, D. P., Stutzman, P. E., & Garboczi, E. J. (1992). Experimental and simulation studies of the interfacial zone in concrete. *Cement and concrete research*, 22(5), 891-902.

Blais, P. Y., & Couture, M. (1999). Precast, prestressed pedestrian bridge-world's first reactive powder concrete structure. *PCI journal*, 44, 60-71.

Cairns, J., & Jones, K. (1995). Influence of rib geometry on strength of lapped joints: an experimental and analytical study. *Magazine of Concrete Research*, 47(172), 253-262.

Chan, Y. W., Chen, Y. G., & Liu, Y. S. (2003). Effect of consolidation on bond of reinforcement in concrete of different workabilities. *Materials Journal*, 100(4), 294-301.

Chao, S. H., Naaman, A. E., & Parra-Montesinos, G. J. (2009). Bond behavior of reinforcing bars in tensile strain-hardening fiber-reinforced cement composites. *ACI Structural Journal*, *106*(6), 897.

Charron, J. P., Denarié, E., & Brühwiler, E. (2004). Permeability of UHPFRC under high stresses. In *International RILEM Symposium on Concrete Science and Engineering: A Tribute to Arnon Bentur*. RILEM Publications SARL.

Chen, G., Yen, P. W., Buckle, I., Allen, T., Alzamora, D., Ger, J., & Arias, J. G. (2010). Chile Earthquake implications to the seismic design of bridges. In *Proceedings of the 26th US-Japan Bridge Engineering Workshop*, 203-216.

Chen, Y., Yu, R., Wang, X., Chen, J., & Shui, Z. (2018a). Evaluation and optimization of Ultra-High Performance Concrete (UHPC) subjected to harsh ocean environment: Towards an application of Layered Double Hydroxides (LDHs). Construction and Building Materials, 177, 51-62.

Chen, T., Gao, X., & Ren, M. (2018b). Effects of autoclave curing and fly ash on mechanical properties of ultra-high performance concrete. *Construction and Building Materials*, 158, 864-872.

Chen, T., Gu, X. L., Qi, M., & Yu, Q. Q. (2018c). Experimental Study on Fatigue Behavior of Cracked Rectangular Hollow-Section Steel Beams Repaired with Prestressed CFRP Plates. *Journal of Composites for Construction*, 22(5), 04018034.

Chung, D. D. L. (2002). Improving cement-based materials by using silica fume. *Journal of Materials Science*, 37(4), 673-682.

Chunxiang, Q., & Patnaikuni, I. (1999). Properties of high-strength steel fiber-reinforced concrete beams in bending. *Cement and Concrete Composites*, 21(1), 73-81.

Collepardi, M. (2003). A state-of-the-art review on delayed ettringite attack on concrete. *Cement and Concrete Composites*, *25*(4-5), 401-407.

Cousins, T. E., Johnsone, D. W., & Zia, P. (1990). Transfer length of epoxy-coated prestressing strand. *Materials Journal*, 87(3), 193-203.

Dancygier, A. N., Katz, A., & Wexler, U. (2010). Bond between deformed reinforcement and normal and high-strength concrete with and without fibers. *Materials and Structures*, 43(6), 839-856.

Daniel, L., & Loukili, A. (2002). Behavior of high strength fiber-reinforced concrete beams under cyclic loading. *Structural Journal*, 99(3), 248-256.

De Larrard, F., & Sedran, T. (1994). Optimization of ultra-high-performance concrete by the use of a packing model. *Cement and Concrete Research*, 24(6), 997-1009.

Deatherage, J. H., Burdette, E. G., & Chew, C. K. (1994). Development length and lateral spacing requirements of prestressing strand for prestressed concrete bridge girders. *PCI Journal*, 39(1).

Dhonde, H. (2006). *Steel fibers and self-consolidating concrete in prestressed concrete beams*. Doctoral dissertation, Department of Civil and Environmental Engineering, University of Houston, TX.

Dinh, H. H. (2009). *Shear behavior of steel fiber reinforced concrete beams without stirrup reinforcement*. Doctoral dissertation, University of Michigan.

Dolan, C. W., & Hamilton, H. T. (2019). Prestressed Concrete. Springer, Cham.

Eligehausen, R., Popov, E. P., & Bertero, V. V. (1982). Local bond stress-slip relationships of deformed bars under generalized excitations. *R.No.UCB/EERC-83/23,EERC*, Berkeley.

Elsaigh, W. A., & Kearsley, E. P. (2002). Effect of Steel Fibre Content on Properties of Concrete. *Journal of Concrete/Beton, South Africa*, 102, 8-12.

EN1992, B. S. (2004). 1-1: 2004. *Eurocode 2: Design of concrete structures–Part 1-1: General Rules for buildings*.

Eren, Ö., & Celik, T. (1997). Effect of silica fume and steel fibers on some properties of high-strength concrete. *Construction and Building Materials*, 11(7-8), 373-382.

Escadeillas, G., Aubert, J. E., Segerer, M., & Prince, W. (2007). Some factors affecting delayed ettringite formation in heat-cured mortars. *Cement and Concrete Research*, *37*(10), 1445-1452.

Evans, R. H., & Hosny, A. H. H. (1958). The shear strength of posttensioned prestressed concrete beams. In *Third Congress of the Federation Internationale de la Precontrainte. Berlin*, 112-132.

Evans, R. H., & Schumacher, E. G. (1963). Shear strength of prestressed beams without web reinforcement. In *Journal Proceedings*, 60(11), 1621-1642.

Ezeldin, A., & Balaguru, P. (1989). Bond behavior of normal and high-strength fiber reinforced concrete. *Materials Journal*, 86(5), 515-524.

Fanella, D. A., & Naaman, A. E. (1985). Stress-Strain Properties of Fiber Reinforced Mortar in Compression. *ACI Journal Proceedings*, 82(4), 475-483.

Fehling, E., & Lorenz, P. (2013). Characterization of rebars anchorage in UHPC. In *Proceedings of RILEM-fib-AFGC international symposium on UHPFRC, Marseille, France*, 587-596.

Ferguson, P. M., & Thompson, J. N. (1953). Diagonal Tension in T-Bemas Without Stirrups. In *Journal Proceedings*, 49(3), 665-675.

Filippou, F. C., Bertero, V. V., & Popov, E. P. (1983). Effects of bond deterioration on hysteretic behavior of reinforced concrete joints. *Report* No. UCB/EERC-83/19, University of California, Berkeley, 184.

Fu, Y., Ding, J., & Beaudoin, J. J. (1997). Expansion of Portland cement mortar due to internal sulfate attack. *Cement and Concrete Research*, *27*(9), 1299-1306

Funk, JE & Dinger DR (1994) *Predictive Process Control of Crowded Particulate Suspensions, Applied to Ceramic Manufacturing*. Kluwer Academic Publishers, Boston, the United States.

Garas, V. Y., Kurtis, K. E., & Kahn, L. F. (2012). Creep of UHPC in tension and compression: effect of thermal treatment. *Cement and Concrete Composites*, 34(4), 493-502.

Grattan-Bellew, P. E., Beaudoin, J. J., & Vallée, V. G. (1998). Effect of aggregate particle size and composition on expansion of mortar bars due to delayed ettringite formation. *Cement and concrete research*, *28*(8), 1147-1156.

Graybeal, B. A. (2006). *Material property characterization of ultra-high performance concrete* (No. FHWA-HRT-06-103).

Graybeal, B., & Davis, M. (2008). Cylinder or cube: strength testing of 80 to 200 MPa (11.6 to 29 ksi) ultra-high-performance fiber-reinforced concrete. *Materials Journal*, 105(6), 603-609.

Goto, Y. (1971). Cracks formed in concrete around deformed tension bars. In *Journal Proceedings*, 68(4), 244-251.

Habel, K. (2004). *Structural behaviour of elements combining ultra-high performance fibre reinforced concretes (UHPFRC) and reinforced concrete*. Doctoral dissertation, Swiss Federal Institute of Technology Lausanne, Switzerland.

Habel, K., & Gauvreau, P. (2008). Response of ultra-high performance fiber reinforced concrete (UHPFRC) to impact and static loading. *Cement and Concrete Composites*, 30(10), 938-946.

Hamad, B. S., & Itani, M. S. (1998). Bond strength of reinforcement in high performance concrete: role of silica fume, casting position, and superplasticizer dosage. *Materials Journal*, *95*(5), 499-511.

Hamad, B. S., Harajli, M. H., & Jumaa, G. (2001). Effect of fiber reinforcement on bond strength of tension lap splices in high-strength concrete. *ACI Structural Journal*, 98(5), 638-647.

Hanson, N. W., & Kaar, P. H. (1959). Flexural bond tests of pretensioned prestressed beams. In *Journal Proceedings*, 55(1), 783-802.

Harajli, M. H. (1994). Development/splice strength of reinforcing bars embedded in plain and fiber reinforced concrete. *Structural Journal*, 91(5), 511-520.

Harajli, M., Hamad, B., & Karam, K. (2002). Bond-slip response of reinforcing bars embedded in plain and fiber concrete. *Journal of Materials in Civil Engineering*, 14(6), 503-511.

Harajli, M. H., & Salloukh, K. A. (1997). Effect of fibers on development/splice strength of reinforcing bars in tension. *Materials Journal*, 94(4), 317-324.

Hassan, A. M. T., Jones, S. W., & Mahmud, G. H. (2012). Experimental test methods to determine the uniaxial tensile and compressive behaviour of ultra high performance fibre reinforced concrete (UHPFRC). *Construction and building materials*, 37, 874-882.

Heinz, D., Ludwig, U., & Rüdiger, I. (1989). Delayed ettringite formation in heat treated mortars and concretes. *Concrete Precasting Plant and Technology*, *11*, 56-61.

Holschemacher, K., Weiße, D., & Klotz, S. (2005). Bond of reinforcement in ultra high-strength concrete. *Special Publication*, 228, 513-528.

Horiguchi, T., Saeki, N., & Fujita, Y. (1988). Evaluation of Pullout Test for Estimating Shear, Fexural, and Compressive Strength of Fber Reinforced Silica Fume Concrete. *Materials Journal*, 85(2), 126-132.

Hsu, L. S., & Hsu, C. T. (1994). Stress-strain behavior of steel-fiber high-strength concrete under compression. *Structural Journal*, 91(4), 448-457.

Hsu, T. T. (2017). Unified theory of reinforced concrete. Routledge.

Huang, H., Huang, S. S., & Pilakoutas, K. (2018). Modeling for Assessment of Long-Term Behavior of Prestressed Concrete Box-Girder Bridges. Journal of Bridge Engineering, 23(3), 04018002.

Hung, C. C., Hu, F. Y., & Yen, C. H. (2018). Behavior of slender UHPC columns under eccentric loading. Engineering Structures, 174, 701-711.

Hurst, M. K. (1988). *Prestressed concrete design*. Chapman and hall, London.

Janney, J. R. (1954, May). Nature of bond in pre-tensioned prestressed concrete. In *Journal Proceedings*, 50(5), 717-736.

Japan Concrete Institute (JCI) (1983). *Method of Test for Flexural Strength and Flexural Toughness of Fiber Reinforced Concrete*, 45-51.

Japanese Society of Civil Engineers (JSCE) (2006). *Recommendations for Design and Construction of Ultra High Strength Fiber Reinforced Concrete Structures (Draft)*. Subcommittee on Research of Ultra High Strength Fiber Reinforced Concrete-Japan Society of Civil Engineers. Tokyo, Japan.

Jensen, O. M., & Hansen, P. F. (1999). Influence of temperature on autogenous deformation and relative humidity change in hardening cement paste. *Cement and concrete research*, 29(4), 567-575.

Johnston, C.D. (1985). Toughness of Steel Fibre Reinforced Concrete. *Proceedings of the Steel Fibre Concrete US-Sweden Joint Seminar (NSF-STU), Swedish Cement and Concrete Research Institute, Stockholm / Sweden*, 333-360.

Johnston, C.D., & Zemp, W.R. (1991). Flexural Fatigue Performance of Steel Fibre Reinforced Concrete: Influence of Fibre Content, Aspect Ratio, and Type. *American Concrete Institute, Material Journal*, 88(4), 374-383.

Johnson, R. P. (2018). Composite Structures of Steel and Concrete: beams, slabs, columns and frames for buildings. John Wiley & Sons.

Kang, S. T., & Kim, J. K. (2011). The relation between fiber orientation and tensile behavior in an Ultra High Performance Fiber Reinforced Cementitious Composites (UHPFRCC). *Cement and Concrete Research*, 41(10), 1001-1014.

Kang, S. H., Lee, J. H., Hong, S. G., & Moon, J. (2017). Microstructural investigation of heat-treated ultra-high performance concrete for optimum production. Materials, 10(9), 1106.

Kani, G. (1967, March). How safe are our large reinforced concrete beams?. In *Journal Proceedings*, 64(3), 128-141.

Kazemi, S., & Lubell, A. S. (2012). Influence of Specimen Size and Fiber Content on Mechanical Properties of Ultra-High-Performance Fiber-Reinforced Concrete. *ACI materials Journal*, 109(6), 675-684.

Khaloo, A. R., & Kim, N. (1996). Mechanical Properties of Normal to High-Strength Steel Fiber-Reinforced Concrete. *Cement, Concrete and Aggregates*, 18(2), 92-97.

Khandaker, M., & Hossain, A. (2008). Bond characteristics of plain and deformed bars in lightweight pumice concrete. Construction and Building Materials, 22(7), 1491–1499.

Koutný, O., Snoeck, D., Van Der Vurst, F., & De Belie, N. (2018). Rheological behaviour of ultra-high performance cementitious composites containing high amounts of silica fume. *Cement and Concrete Composites*, 88, 29-40.

Kwak, Y. K., Eberhard, M. O., Kim, W. S., & Kim, J. (2002). Shear strength of steel fiber-reinforced concrete beams without stirrups. *ACI Structural Journal*, 99(4), 530-538.

Lane, S. N. (1998). *A new development length equation for pretensioned strands in bridge beams and piles* (No. FHWA-RD-98-116,).

Langsford, R. P., Lloyd, N., & Sarker, P. K. (2007). Shear strength of steel fibre reinforced prestressed concrete beam. In *Proceedings of the 4th International Structural Engineering and Construction Conference (ISEC-4)—Innovations in Structural Engineering and Construction, Melbourne, Australia*: Taylor & Francis/Balkema, 441-446.

Lappa, E. S. (2007). High Strength Fibre Reinforced Concrete: Static and fatigue behaviour in bending. *Technische Universiteit Darmstadt*, PhD Thesis.

Leonhardt, F., & Walther, R. (1961). The Stuttgart shear tests. *Cement & Concrete Association Library*, 111, 49-54.

Li, V. C., Ward, R., & Hamza, A. M. (1992). Steel and synthetic fibers as shear reinforcement. *ACI Materials Journal*, 89(5), 499-508.

Li, W., & Leung, C. K. (2017). Effect of shear span-depth ratio on mechanical performance of RC beams strengthened in shear with U-wrapping FRP strips. *Composite Structures*, 177, 141-157.

Li, W., Huang, Z., Hu, G., Duan, W. H., & Shah, S. P. (2017). Early-age shrinkage development of ultra-high-performance concrete under heat curing treatment. Construction and Building Materials, 131, 767-774.

Lim, T. Y., Paramasivam, P., & Lee, S. L. (1987). Shear and moment capacity of reinforced steel-fibre-concrete beams. *Magazine of concrete research*, 39(140), 148-160.

Logan, D. R. (1997). Acceptance criteria for bond quality of strand for pretensioned prestressed concrete applications. *PCI journal*, 42(2).

Loukili, A., Richard, P., & Lamirault, J. (1998). A study on delayed deformations of an ultra high strength cementitious material. *Special Publication*, 179, 929-950.

Löfgren, I. (2005). *Fibre-reinforced Concrete for Industrial Construction-a fracture mechanics approach to material testing and structural analysis*. Doctoral dissertation, Chalmers University of Technology, Sweden.

Lutz, L. A.; Gergely, P.; & Winter, G. (1966). The Mechanics of Bond and Slip of Deformed Reinforcing Bars in Concrete. *Report* No. 324, Department of Structural Engineering, Cornell University, Ithaca, N.Y, 711-721.

Lutz, L. A., & Gergely, P. (1967). Mechanics of bond and slip of deformed bars in concrete. In *Journal Proceedings*, 64(11), 711-721.

Ma, J., Orgass, M., Dehn, F., Schmidt, D., & Tue, N. V. (2004). Comparative investigations on ultra-high performance concrete with and without coarse aggregates. In *Proceedings of international symposium on ultra high performance concrete, Germany*, 205-212.

MacGregor, J. G., & Wight, J. K. (2005). *Reinforced Concrete: Mechanics and Design 4th Edition*. Pearson Prentice Hall, New Jersey.

MacGregor, JG., & JK. Wight. (2009). *Reinforced Concrete: Mechanics and Design*. Upper Saddle River, NJ: Prentice Hall.

Malier, Y. (Ed.). (2018). High performance concrete: from material to structure. CRC Press.

Mansur, M. A., Ong, K. C. G., & Paramasivam, P. (1986). Shear strength of fibrous concrete beams without stirrups. *Journal of structural engineering*, 112(9), 2066-2079.

Momeni, A. F., Peterman, R. J., & Beck, B. T. (2018). Prediction Model for Development Length of Indented Prestressing Wires. ACI Structural Journal, 115(2), 525-534.

Machinery enterprises. (2019, January 18). Retrieved from http://www.machineryenterprises.com/en/products/concrete-mixers/small-concrete-mixer 300-ltr/.

Marar, K., Eren, Ö., & Celik, T. (2001). Relationship between impact energy and compression toughness energy of high-strength fiber-reinforced concrete. *Materials letters*, 47(4-5), 297-304.

Marchand, P., Baby, F., Khadour, A., Battesti, T., Rivillon, P., Quiertant, M., ... & Toutlemonde, F. (2016). Bond behaviour of reinforcing bars in UHPFRC. *Materials and structures*, 49(5), 1979-1995.

Marshall, V. & Robberts, J.M. (1996). *Prestressed concrete design and practice*. Prestressed Concrete Division, Concrete Society of Southern Africa.

Mathey, R.G. & Watstein, D. (1961). Investigation of bond in beam and pull-out specimens with high-yield-strength deformed bars. In *Journal Proceedings*, 57(3), 1071-1090.

Meda, A., Minelli, F., Plizzari, G. A., & Riva, P. (2005). Shear behaviour of steel fibre reinforced concrete beams. *Materials and structures*, 38(3), 343-351.

Mehta, PK., & PJM. Montiero. (2006). *Concrete: Microstructure, Properties, and Materials.* 3rd. New York: McGraw-Hill.

Meng, W. (2017). *Design and performance of cost-effective ultra-high performance concrete for prefabricated elements*, Doctoral dissertation, Missouri University of Science and Technology, United states.

Merta, I., Kolbitch, A. and Kravanja, S. (2010). Cost optimization of reinforced concrete beams. *Sixth International Conference Concrete under Severe Conditions Environment & Loading*, Mexico.

Mitchell, D., Cook, W. D., Khan, A. A., & Tham, T. (1993). Influence of high strength concrete on transfer and development length of pretensioning strand. *PCI Journal*, 38(3), 52-66.

Mohammed, H. (2015). *Mechanical Properties of Ultra High Strength Fiber Reinforced Concrete*, Doctoral dissertation, University of Akron, United states.

Monfore, G. E. (1968), A Review of Fiber Reinforcement of Portland Cement Paste, Mortar, and Concrete, *Journal of the PCA Research and Development Laboratories*, 10 (3), 43-49.

Mosley, W. H., Hulse, R., & Bungey, J. H. (2012). *Reinforced concrete design: to Eurocode 2*. Macmillan International Higher Education.

Murty, D. S. R., & Venkatacharyulu, T. (1987). Fibre Reinforced Concrete Beams Subjected to Shear Force. *International Symposium on Fibre Reinforced Concrete, Madras, India*, 1, 1.125-1.132.

Naaman, A. E. (1985). Fiber Reinforcement for Concrete. *Concrete International*, 7(3), 21-25.

Naaman, A. E., & Najm, H. (1991). Bond-slip mechanisms of steel fibers in concrete. *Materials Journal*, 88(2), 135-145.

Narayanan, R., & Darwish, I. Y. S. (1987). Use of steel fibers as shear reinforcement. *Structural Journal*, 84(3), 216-227.

National Precast Concrete Association (2018). Ultra high performance concrete (UHPC), guide to manufacturing architectural precast uhpc elements. Retrieved Dec 8, 2018, from https://precast.org/wp-content/uploads/2015/02/UHPC-White-Paper.pdf.

Nawy G. E. (2009). *Prestressd Concrete - A Fundamental Approach – Fifth Edition*. Pearson. Upper Saddle River, NJ.

Neville, A. M., Dilger, W. H., & Brooks, J. J. (1983). *Creep of Plain and Structural Concrete*, Construction Press, London.\

Nguyen, V. H., Leklou, N., Aubert, J. E., & Mounanga, P. (2013). The effect of natural pozzolan on delayed ettringite formation of the heat-cured mortars. *Construction and Building Materials*, *48*, 479-484.

Nicolaides, D., Kanellopoulos, A., Petrou, M., Savva, P., & Mina, A. (2015). Development of a new Ultra High Performance Fibre Reinforced Cementitious Composite (UHPFRCC) for impact and blast protection of structures. *Construction and Building Materials*, 95, 667-674.

Nilson, A. H. (1987). *Design of Prestressed Concrete – Second Edition*. John Wiley and Sons. New York, NY.

ONR 23303 (2010). Test methods for concrete – national application of testing standards for concrete and its source materials. *Austrian Standards Institute*.

Orangun, C. O., Jirsa, J. O., & Breen, J. E. (1975). *The strength of anchored bars: a reevaluation of test data on development length and splices*. Center for Highway Research, University of Texas at Austin.

Padmarajaiah, S. K., & Ramaswamy, A. (2001). Behavior of fiber-reinforced prestressed and reinforced high-strength concrete beams subjected to shear. *ACI Structural Journal*, 98(5), 752-761.

Páez, P. M., & Sensale, B. (2018). Improved prediction of long-term prestress loss in unbonded prestressed concrete members. *Engineering Structures*, 174, 111-125.

Palmquist, S. M., & Jansen, D. C. (2001). Postpeak strain-stress relationship for concrete in compression. *Materials Journal*, 98(3), 213-219.

Park, J. J., Kang, S. T., Koh, K. T., & Kim, S. W. (2008). Influence of the ingredients on the compressive strength of UHPC as a fundamental study to optimize the mixing proportion. In *Second International Symposium on Ultra High Performance Concrete, Kasse, Germany*, 105-112.

Pavoine, A., Brunetaud, X., & Divet, L. (2012). The impact of cement parameters on Delayed Ettringite Formation. *Cement and Concrete Composites*, *34*(4), 521-528.

Peng, G. F., Niu, X. J., Shang, Y. J., Zhang, D. P., Chen, X. W., & Ding, H. (2018). Combined curing as a novel approach to improve resistance of ultra-high performance concrete to explosive spalling under high temperature and its mechanical properties. *Cement and Concrete Research*, 109, 147-158.

Pillai, S.U., Menon, D. (2003). *Reinforced concrete design*. Tata McGraw-Hill Education.
Placas, A., & Regan, P. E. (1971). Shear failure of reinforced concrete beams. In *Journal Proceedings*, 68(10), 763-773.

Plizzari G. A. (1999). Bond and splitting crack development in normal and high strength fiber reinforced concrete. *13th Engrg mechanics division conference—EMD99, Baltimore (MD, USA*), on CD.

Portland Cement Association (2018a). High-strength concert. Retrieved Dec 8, 2018, from https://www.cement.org/cement-concrete-applications/products/high-strength-concrete.

Portland Cement Association (2018b). Ultra high performance concert. Retrieved Dec 8, 2018, from https://www.cement.org/learn/concrete-technology/concrete-design-production/ultra-high-performance-concrete.

Pyo, S., Kim, H. K., & Lee, B. Y. (2017). Effects of coarser fine aggregate on tensile properties of ultra high performance concrete. *Cement and Concrete Composites*, 84, 28-35.

Qi, J., Wu, Z., Ma, Z. J., & Wang, J. (2018). Pullout behavior of straight and hooked-end steel fibers in UHPC matrix with various embedded angles. *Construction and Building Materials*, 191, 764-774.

Raju, P. M., & Sandeep, T. R. (2017). Long term losses in pre-stressed concrete member as per IS 1343: 2012 and IS 1343: 1980. *Indian Concrete Journal*, 48.

Ragalwar, K. A., Nguyen, H., Ranade, R., Heard, W. F., & Williams, B. A. (2017). Influence of Distribution Modulus of Particle Size Distribution on Rheological and Mechanical Properties of Ultra-High-Strength SHCC Matrix. In International Conference on Strain-Hardening Cement-Based Composites (pp. 221-229). Springer, Dordrecht.

Ramakrishnan, V., Brandshaug, T., Coyle, W. V., & Schrader, E. K. (1980). A comparative evaluation of concrete reinforced with straight steel fibers and fibers with deformed ends glued together into bundles. In *Journal Proceedings*, 77(3), 135-143.

Ramirez, J. A., & Russell, B. W. (2008). *Transfer, development, and splice length for strand/reinforcement in high-strength concrete*. Transportation Research Board, 603.

Ramlochan, T., Zacarias, P., Thomas, M. D. A., & Hooton, R. D. (2003). The effect of pozzolans and slag on the expansion of mortars cured at elevated temperature: Part I: Expansive behaviour. *Cement and Concrete Research*, *33*(6), 807-814.

Randl, N., Steiner, T., Ofner, S., Baumgartner, E., & Mészöly, T. (2014). Development of UHPC mixtures from an ecological point of view. *Construction and Building Materials*, 67, 373-378.

Reda, M. M., Shrive, N. G., & Gillott, J. E. (1999). Microstructural investigation of innovative UHPC. *Cement and Concrete Research*, 29(3), 323-329.

Rehm, G. (1961). *Uber die Grundlagen des Verbudzwischen Stahl undBeton*. Heft 138, Deutscher Ausschuss fur Stahlbeton, Berlin, 59.

Richard, P., & Cheyrezy, M. (1995). Composition of reactive powder concretes. *Cement and concrete research*, 25(7), 1501-1511.

Romualdi, J. P., & Batson, G. B. (1963). Mechanics of Crack Arrest in Concrete. *ASCE Journal of the Engineering Mechanics*, 89(3), 147-168.

Romualdi, J. P. & Mandel, J. A. (1964), "Tensile Strength of Concrete Affected by Uniformly Distributed and Closely Spaced Short Lengths of Wire Reinforcement," *ACI Journal*, 61(6), 657-670.

Ronanki, V. S., Aaleti, S., & Valentim, D. B. (2018). Experimental investigation of bond behavior of mild steel reinforcement in UHPC. *Engineering Structures*, 176, 707-718

Rosenbusch J., Teutsch M. (2002). *Trial Beams in Shear, Brite/Euram Project 97-4163*, Final Report, Sub Task 4.2., Technical University of Braunschweig, Germany.

Rossi, P., Arca, A., Parant, E., & Fakhri, P. (2005). Bending and compressive behaviours of a new cement composite. *Cement and Concrete Research*, 35(1), 27-33.

Russell, B. W., & Burns, N. H. (1993). *Design guidelines for transfer, development and debonding of large diameter seven wire strands in pretensioned concrete girders. Final report* (No. FHWA/TX-93+ 1210-5F).

Russell, H. G., & Graybeal, B. A. (2013). *Ultra-High Performance Concrete: A State-of-the-Art Report for the Bridge Community. Final report* (FHWA-HRT-13-060).

Saleem, M. A., Mirmiran, A., Xia, J., & Mackie, K. (2012). Development length of high-strength steel rebar in ultrahigh performance concrete. *Journal of Materials in Civil Engineering*, 25(8), 991-998.

SANS 5863:2006. Concrete tests – Compressive strength of hardened concrete. SABS, Pretoria.

SANS 51992-1-1:2014. Design of concrete structure - General rules and rules for buildings. SABS, Pretoria.

Savic, A., Beck, B. T., Robertson, A. A., Peterman, R. J., Clark, J., & Wu, C. H. J. (2018, April). Effects of Cover, Compressive Strength, and Wire Type on Bond Performance in Prismatic Prestressed Concrete Members. In 2018 Joint Rail Conference (pp. V001T01A007-V001T01A007). American Society of Mechanical Engineers.

Schachinger, I., Hilbig, H., Stengel, T., & Fehling, E. (2008). Effect of curing temperature at an early age on the long-term strength development of UHPC. In *Proceedings of the Second International Symposium on Ultra High Performance Concrete, Kassel, Germany*, 10, 205-213.

Shafieifar, M., Farzad, M., & Azizinamini, A. (2017). Experimental and numerical study on mechanical properties of Ultra High Performance Concrete (UHPC). *Construction and Building Materials*, 156, 402-411.

Shah, S. P. & Rangan, B. V. (1971), Fiber Reinforced Concrete Properties. *ACI Journal*, 68 (2), 126-135.

Skorobogatov, S. M., & Edwards, A. D. (1979, June). The influence of the geometry of deformed steel bars on their bond strength in concrete. In *Institution of Civil Engineers, Proceedings, Pt2*, 67, No. PT2.

Snyder, M. J., & Lankard, D. R. (1972), "Factors Affecting the Flexural Strength of Steel Fibrous Concrete," *ACI Journal*, 69 (2), 96-100.

Singh, M., Sheikh, A. H., Ali, M. M., Visintin, P., & Griffith, M. C. (2017). Experimental and numerical study of the flexural behaviour of ultra-high performance fibre reinforced concrete beams. *Construction and Building Materials*, 138, 12-25.

Song, P. S., & Hwang, S. (2004). Mechanical properties of high-strength steel fiber-reinforced concrete. *Construction and Building Materials*, 18(9), 669-673.

Song, Q., Yu, R., Wang, X., Rao, S., & Shui, Z. (2018). A novel Self-Compacting Ultra-High Performance Fibre Reinforced Concrete (SCUHPFRC) derived from compounded high-active powders. *Construction and Building Materials*, 158, 883-893.

Soroushian, P., & Choi, K. B. (1989). Local bond of deformed bars with different diameters in confined concrete. *Structural Journal*, *86*(2), 217-222.

Soroushian, P., & Bayasi, Z. (1991). Fiber Type Effects on the Performance of Steel Fiber Reinforced Concrete. *ACI Materials Journal*, 88(2), 129-134.

Soutsos, M., & Domone, P. (2018). *Construction Materials: Their Nature and Behaviour*. Boca Raton: CRC Press.

Sozen, M. A., Zwoyer, E. M., & Siess, C. P. (1959). *Investigation of Prestressed Concrete for Highway Bridges: Strength in Shear of Beams Without Web Reinforcement*. Structural Research Laboratory, Department of Civil Engineering, University of Illinois.

Sozen, M. A., & Moehle, J. P. (1990). *Development and Lap-splice Lengths for Deformed Reinforcing Bars in Concrete: A Report to the Portland Cement Association, Skokie, IL, and the Concrete Reinforcing Steel Institute, Schaumburg, IL*. Portland Cement Association.

Spasojevic, A. (2008). *Structural implications of ultra-high performance fibre-reinforced concrete in bridge design*. Doctoral dissertation. École Polytechnique Fédérale de Lausanne, Switzerland.

Swamy, R. N., & Bahia, H. M. (1985). The effectiveness of steel fibers as shear reinforcement. *Concrete International*, 7(3), 35-40.

Swamy, R. N., Jones, R., & Chiam, A. T. (1993). Influence of steel fibers on the shear resistance of lightweight concrete I-beams. *Structural Journal*, 90(1), 103-114.

Tam, C. M., Tam, V. W., & Ng, K. M. (2012). Assessing drying shrinkage and water permeability of reactive powder concrete produced in Hong Kong. *Construction and Building Materials*, 26(1), 79-89.

Tan, K. H., Paramasivam, P., & Murugappan, K. (1995). Steel fibers as shear reinforcement in partially prestressed beams. *Structural Journal*, 92(6), 643-652.

Tastani, S. P., & Pantazopoulou, S. J. (2010). Direct tension pullout bond test: Experimental results. *Journal of Structural Engineering*, 136(6), 731-743.

Taub, J., & Neville, A. M. (1960, December). Resistance to shear of reinforced concrete beams. In *Journal Proceedings*, 57(12), 715-730.

Taylor, H. P. (1972). Shear strength of large beams. *Journal of the Structural Division*, 98(Proc Paper 9329).

Tepfers, R. (1973). *A theory of bond applied to overlapped tensile reinforcement splices for deformed bars*. Chalmers University of Technology.

Thomas, J., & Ramaswamy, A. (2007). Mechanical Properties of Steel Fiber reinforced Concrete. *ASCE Journal of Materials in Civil Engineering*, 19(5), 385-392.

Timoshenko, S. (1930). *Strength of Materials, Part II; Advanced Theory and Problems*. New York: Van Nostrand Reinhold Company.

Tompos, E. J., & Frosch, R. J. (2002). Influence of beam size, longitudinal reinforcement, and stirrup effectiveness on concrete shear strength. *Structural Journal*, 99(5), 559-567.

Tsioulou, O., Lampropoulos, A., & Paschalis, S. (2017). Combined non-destructive testing (NDT) method for the evaluation of the mechanical characteristics of ultra high performance fibre reinforced concrete (UHPFRC). *Construction and Building Materials*, 131, 66-77.

Türkel, S., & Alabas, V. (2005). The effect of excessive steam curing on Portland composite cement concrete. *Cement and Concrete Research*, 35(2), 405-411.

Tuyan, M., & Yazici, H. (2012). Pull-out behavior of single steel fiber from SIFCON matrix. *Construction and Building Materials*, 35, 571-577.

Vatannia, S., Kearsley, E., & Mostert, D. (2016a). The mechanical properties of UHPC reinforced by different types of fiber. *fib Symposium: Performance-based Approaches for Concrete Structures*, Cape Town, South Africa.

Vatannia, S., Kearsley, E., & Mostert, D. (2016b). The effect of curing regime on the compressive strength of ultra high performance concrete. In *Proceedings of the 9th international concrete conference on environment, efficiency and economic challenges for concrete*, Dundee, Scotland.

Vejmelková, E., Koňáková, D., Čáchová, M., Záleská, M., Svora, P., Keppert, M., ... & Černý, R. (2018). High-strength concrete based on ternary binder with high pozzolan content. *Structural Concrete*.

Vejmelková, E., Koňáková, D., Doleželová, M., Scheinherrová, L., Svora, P., Keppert, M., ... & Černý, R. (2018). Effect of calcined Czech claystone on the properties of high performance concrete: Microstructure, strength and durability. *Construction and Building Materials*, 168, 966-974.

Voo, Y. L., Foster, S. J., & Gilbert, R. I. (2006). Shear strength of fiber reinforced reactive powder concrete prestressed girders without stirrups. *Journal of Advanced Concrete Technology*, *4*(1), 123-132.

Wafa, F. F., & Ashour, S. A. (1992). Mechanical Properties of High-strength Fiber Reinforced Concrete. *ACI Materials Journal*, 89(5), 449-455.

Walraven, J. C. (2009). High performance fiber reinforced concrete: progress in knowledge and design codes. *Materials and Structures*, 42, 1247–1260

Wang, C., Yang, C., Liu, F., Wan, C., & Pu, X. (2012). Preparation of ultra-high performance concrete with common technology and materials. *Cement and concrete composites*, 34(4), 538-544.

Wang, R., Gao, X., Huang, H., & Han, G. (2017). Influence of rheological properties of cement mortar on steel fiber distribution in UHPC. Construction and Building Materials, 144, 65-73.

Wight, J. K., & MacGregor, J. G. (2009). *REINFORCED CONCRETE, Mechanics and Design. New Jersey.* Pearson Education, Inc.

Wille, K., Kim, D. J., & Naaman, A. E. (2011). Strain-hardening UHP-FRC with low fiber contents. *Materials and Structures*, 44(3), 583-598

Wille, K., Naaman, A. E., El-Tawil, S., & Parra-Montesinos, G. J. (2012). Ultra-high performance concrete and fiber reinforced concrete: achieving strength and ductility without heat curing. *Materials and structures*, 45(3), 309-324.

Wille, K., El-Tawil, S., & Naaman, A. E. (2014). Properties of strain hardening ultra high performance fiber reinforced concrete (UHP-FRC) under direct tensile loading. *Cement and Concrete Composites*, *48*, 53-66.

Williamson, G. R. (1974). The effect of steel fibers on the compressive strength of concrete. *Special Publication*, 44, 195-208.

Wu, X., & Han, S. M. (2009). First diagonal cracking and ultimate shear of I-shaped reinforced girders of ultra high performance fiber reinforced concrete without stirrup. *International Journal of Concrete Structures and Materials*, 3(1), 47-56.

Wu, Z., Shi, C., He, W., & Wu, L. (2016). Effects of steel fiber content and shape on mechanical properties of ultra high performance concrete. *Construction and Building Materials*, 103, 8-14.

Yang, R., Lawrence, C. D., & Sharp, J. H. (1999). Effect of type of aggregate on delayed ettringite formation. *Advances in cement research*, *11*(3), 119-132.

Yang, S. L., Millard, S. G., Soutsos, M. N., Barnett, S. J., & Le, T. T. (2009). Influence of aggregate and curing regime on the mechanical properties of ultra-high performance fibre reinforced concrete (UHPFRC). *Construction and Building Materials*, 23(6), 2291-2298.

Yang, I. H., Joh, C., & Kim, B. S. (2010). Structural behavior of ultra high performance concrete beams subjected to bending. *Engineering Structures*, 32(11), 3478-3487.

Yang, I. H., Joh, C., & Kim, B. S. (2012). Flexural response predictions for ultra-high-performance fibre-reinforced concrete beams. *Magazine of Concrete Research*, 64(2), 113-127.

Yang, J. M., Kim, J. K., & Yoo, D. Y. (2018). Transfer length in full-scale pretensioned concrete beams with 1.4 m and 2.4 m section depths. *Engineering Structures*, 171, 433-444.

Yazici, H., Yiğiter, H., Karabulut, A. Ş., & Baradan, B. (2008). Utilization of fly ash and ground granulated blast furnace slag as an alternative silica source in reactive powder concrete. *Fuel*, 87(12), 2401-2407.

Yazıcı, H., Yardımcı, M. Y., Aydın, S., & Karabulut, A. Ş. (2009). Mechanical properties of reactive powder concrete containing mineral admixtures under different curing regimes. *Construction and building materials*, 23(3), 1223-1231.

Yazıcı, H., Yardımcı, M. Y., Yiğiter, H., Aydın, S., & Türkel, S. (2010). Mechanical properties of reactive powder concrete containing high volumes of ground granulated blast furnace slag. *Cement and Concrete Composites*, 32(8), 639-648.

Yerex II, L., Wenzel, T. H., & Davies, R. (1985). Bond Strength of Mild Steel in Polypropylene Fiber Reinforced Concrete. In *Journal Proceedings*, 82(1), 40-45.

Yerlici, V. A., & Ozturan, T. (2000). Factors affecting anchorage bond strength in high-performance concrete. *Structural Journal*, 97(3), 499-507.

Yoo, D. Y., Lee, J. H., & Yoon, Y. S. (2013). Effect of fiber content on mechanical and fracture properties of ultra high performance fiber reinforced cementitious composites. *Composite Structures*, 106, 742-753.

Yoo, D. Y., Kang, S. T., & Yoon, Y. S. (2014a). Effect of fiber length and placement method on flexural behavior, tension-softening curve, and fiber distribution characteristics of UHPFRC. *Construction and Building Materials*, 64, 67-81.

Yoo, D. Y., Shin, H. O., Yang, J. M., & Yoon, Y. S. (2014b). Material and bond properties of ultra high performance fiber reinforced concrete with micro steel fibers. *Composites Part B: Engineering*, 58, 122-133.

Yoo, D. Y., & Banthia, N. (2016). Mechanical properties of ultra-high-performance fiber-reinforced concrete: A review. *Cement and Concrete Composites*, 73, 267-280.

Yu, R., Spiesz, P., & Brouwers, H. J. H. (2015a). Development of Ultra-High Performance Fibre Reinforced Concrete (UHPFRC): Towards an efficient utilization of binders and fibres. *Construction and Building Materials*, 79, 273-282.

Yu, R., Spiesz, P., & Brouwers, H. J. H. (2015b). Development of an eco-friendly Ultra-High Performance Concrete (UHPC) with efficient cement and mineral admixtures uses. *Cement and Concrete Composites*, 55, 383-394.

Yuan, J., & Graybeal, B. A. (2014). *Bond behavior of reinforcing steel in ultra-high performance concrete* (No. FHWA-HRT-14-090).

Yuan, J., & Graybeal, B. (2015). Bond of reinforcement in ultra-high-performance concrete. *ACI Structural Journal*, 112(6), 851.

Zagon, R., Matthys, S., & Kiss, Z. (2016). Shear behaviour of SFR-UHPC I-shaped beams. *Construction and building materials*, 124, 258-268.

Zheng, W., Li, H., & Wang, Y. (2012). Compressive behaviour of hybrid fiber-reinforced reactive powder concrete after high temperature. *Materials & Design*, 41, 403-409.

Zhou, B., & Uchida, Y. (2017). Relationship between fiber orientation/distribution and post-cracking behaviour in ultra-high-performance fiber-reinforced concrete (UHPFRC). *Cement and Concrete Composites*, 83, 66-75.

Zhou, M., Lu, W., Song, J., & Lee, G. C. (2018). Application of Ultra-High Performance Concrete in bridge engineering. *Construction and Building Materials*, 186, 1256-1267.

Zia, P., & Mostafa, T. (1977). Development length of prestressing strands. *Precast/prestressed concrete institute Journal*, 22(5), 54-65

APPENDIX A. TYPE OF SHEAR FAILURE

Shear failure in beams without shear reinforcement occurs with the formation of an inclined tension crack due to the stresses caused by a combination of bending moments and shear forces. **Figure A.1** displays an example of shear failure that occurred in the Chada Bridge in Chile.

Figure A.1 Curtain wall shear failure at abutment of Chada Bridge (Chen et al., 2010)

In prestressed concrete beams without shear reinforcement the following types of failure have been observed:

a) Splitting of concrete due to diagonal tension crack. Formation of this type of cracks leads to diagonal tension failure (see **Figure A.2**). In this failure mode, an inclined crack propagates rapidly due to inadequate shear reinforcement.

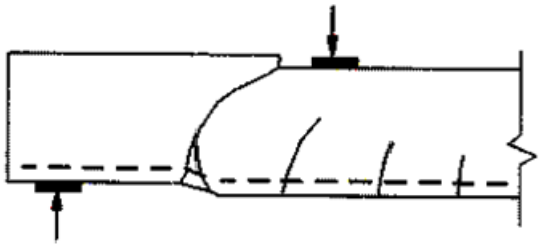

Figure A.2 Shear failure due to diagonal tension crack (Dinh, 2009)

Formation of the crack occurs due to the development of principle tension stresses at the mid-depth level where the beam is subjected to a maximum shear stress. Since this

is a pure shear stress state, the corresponding principal tension and compression stresses have the same magnitude as that of the shear stress. The principal tension stress, often referred to as diagonal tension, is the cause of diagonal cracking at the mid-depth level of the beam.

b) Web crushing under compression due to inadequate web thickness (thin-webbed members such as I−beam). This type of failure as can be seen in **Figure A.3**, is more common in beams with shear reinforcement. When the amount of shear reinforcement is excessive, the concrete in the web portion between the inclined cracks would crush prior to the yielding of shear steel, resulting in a brittle failure.

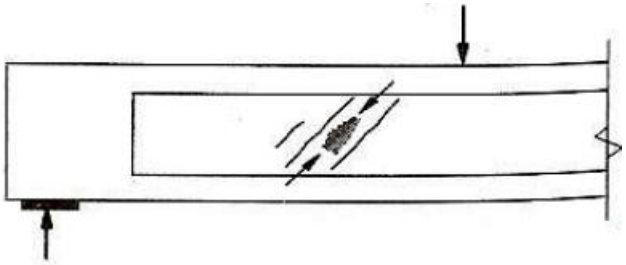

Figure A.3 Shear failure due to web crushing (Pillai and Menon, 2003)

c) Splitting or crushing of concrete in the compressive zone due to compression and shear actions. Failure occurring due to the formation of this type of crack, is called shear compression failure. There is crushing of the concrete near the compression flange above the tip of the inclined crack (see **Figure A.4**).

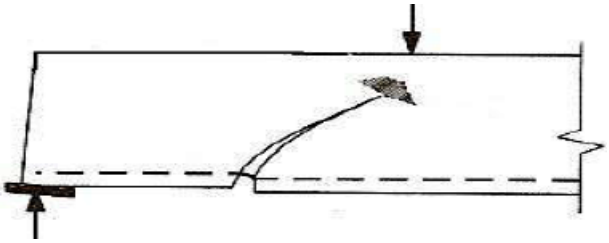

Figure A.4 Shear compression failure (Dinh, 2009)

d) Splitting of concrete along the longitudinal reinforcement following the formation of the inclined tension crack (see **Figure A.5**), which is due to inadequate anchorage of the longitudinal bars.

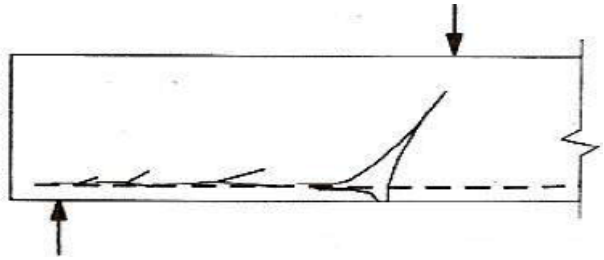

Figure A.5 Shear tension failure (Dinh, 2009)

APPENDIX B. COMPRESSIVE STRENGTH OF UHPC REINFORCED WITH DIFFERENT TYPES OF FIBRE EXPERIENCED DIFFERENT DURATIONS OF HEAT TREATMENT

In the thesis only the compressive strength of UHPFRC that experienced 3 days of 85°C of heat treatment was presented as a sake of brevity. In this appendix, the compressive strength of UHPFRC exposed to 1 day and 6 days of heat treatment is presented.

B.1. HEAT TREATMENT AT 85°C FOR 1 DAY

Figure B.1 presents the 7 days and 28 days compressive strengths of UHPFRC that experienced 1 day of 85°C heat treatment. The highest compressive strengths were achieved in UHPC reinforced with the two types of hooked fibres. Surprisingly, UHPC without fibre showed higher 7-day compressive strength than UHPC containing micro fibre and slit sheet which can be attributed to the higher air content in the mixes. The strength reductions from 7 days to 28 days can be due to the thermal shock occurred in the specimens during the movement of the specimens from the hot bath to standard curing baths.

B.2. HEAT TREATMENT AT 85°C FOR 6 DAYS

According to the **Figure B.2**, 7-day and 28-day compressive strengths of UHPFRCs exceeded 180 MPa when 6 days of heat treatment was applied. The strength reduction of UHPC from 7 days to 28 days can be due to the thermal shock during the curing procedure.

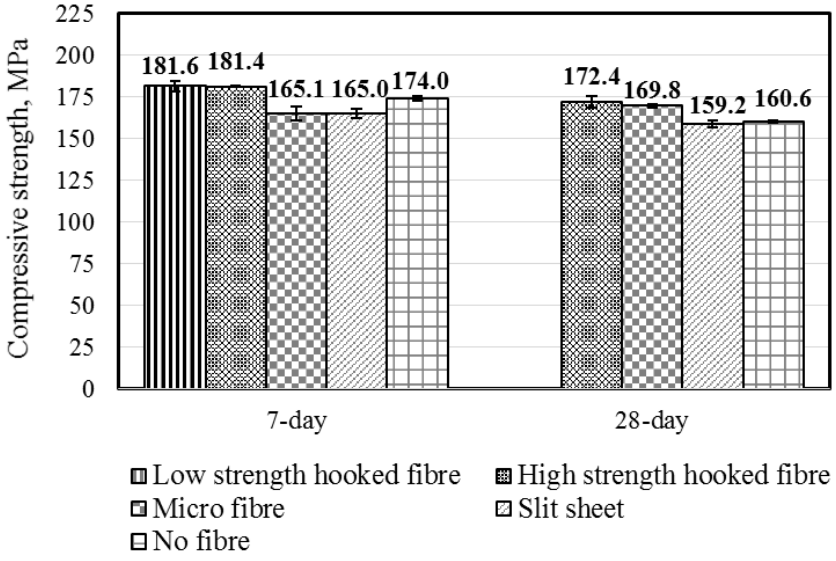

Department of Civil Engineering
University of Pretoria

Figure B.1 Compressive strength of UHPFRC experienced 1 day of heat treatment

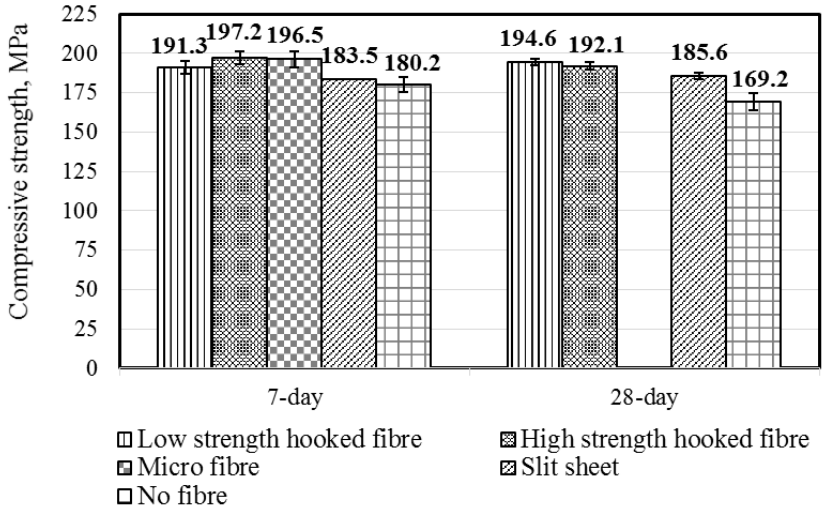

Figure B.2 Compressive strength of UHPFRCs experienced 6 days of heat treatment

B.3. STANDARD CURING REGIME

The compressive strengths of UHPC and UHPFRCs that experienced standard curing are shown in **Figure B.3**. Addition of fibres in UHPC did not enhance the compressive strength when the specimens experienced standard curing. Even different types of fibre did not seem to improve the ultimate compressive strengths. The lowest compressive strength was achieved in UHPC containing high strength hooked fibres (for both 7 days and 28 days of heat curing). The reason may be due to glue used to bind the fibres (hook-ended fibre (Type II)) for easing the mixing process.

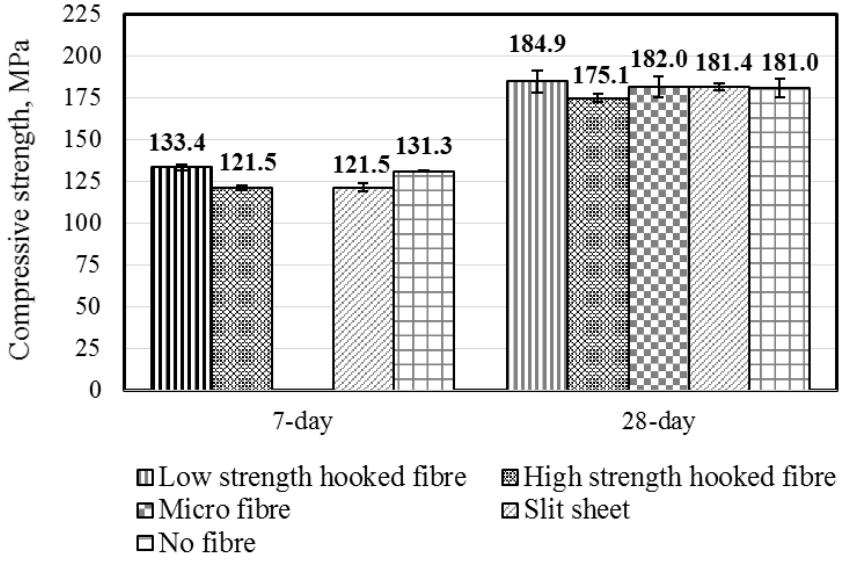

Figure B.3 Compressive strength of UHPC and UHPFRCs experienced standard curing regime

APPENDIX C. PULL-OUT RESULTS

In the thesis, in the first bond study, the results of development length are compared by considering specimen with different lengths but identical diameter. The results of pull-out tests for UHPC and UHPFRC are compared for different ages of 3, 7, 14, 28 and 56 days. The results not presented in CHAPTER 5 are discussed in this Appendix. In the second study, the effect of concrete cover on bond strength is evaluated by considering specimen with different diameters but identical length. The results of pull-out tests for UHPC and UHPFRC are compared for ages of 2 and 28 days. The results not presented in CHAPTER 5 are discussed in this Appendix.

C.1. PULL-OUT RESULTS IN THE FIRST STUDY

C.1.1. Pull-out results after 3 days

Pull-out behaviour of the specimens with 100 mm embedment length after 3 days is shown in **Figure C.**. By comparing the pull-out behaviour of the specimens with and without fibre which failed due to bond loss, no significant difference was observed. These results indicate that the fibres do not improve behaviour within 3 days of casting. The specimens containing no fibre also showed another type of failure. Bond stress dropped significantly due to the formation of cracks in concrete leading to a significant bond loss.

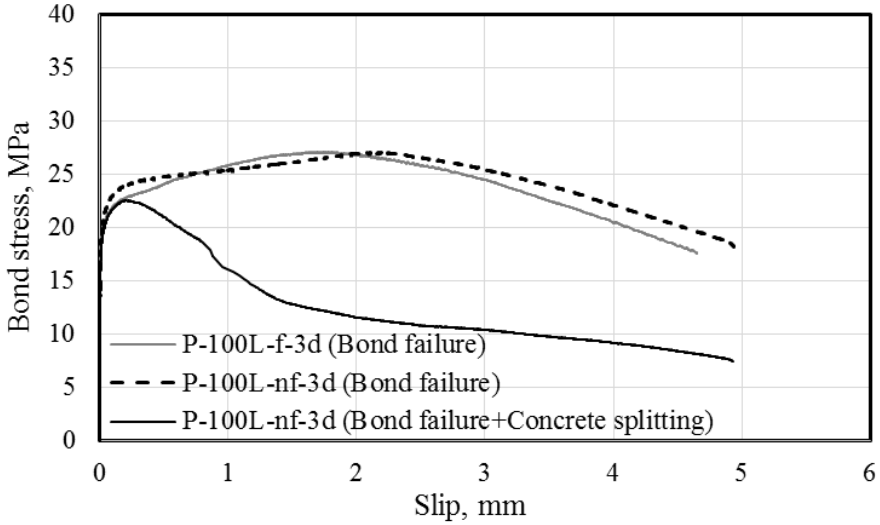

Figure C.1 Pull-out behaviour of the specimens with 100 mm length after 3 days

C.1.2. Pull-out results after 7 days

Figure C.2 displays the results of pull-out test for 100mm-length specimens after 7 days. As shown in this figure, for the specimens containing fibre, slip started at 27.3 MPa. Then the load continuously increased until the tensile stress in the wire reached the yielding point leading to wire rupture. The same failure occurred in 2 out of 3 specimens with no fibre, however,slip initiated at lower stress (about 22.7 MPa). In the third no-fibre specimen, after the initiation of slip, the concrete-steel bond was lost due to the concrete splitting. Two types of failure in specimens with no fibre show the unreliability of UHPC under pull-out load in the absence of fibre. In contrast, by the inclusion of fibre, the behaviour of UHPC, as well as the type of failure, is predictable when the embedment length is 100 mm.

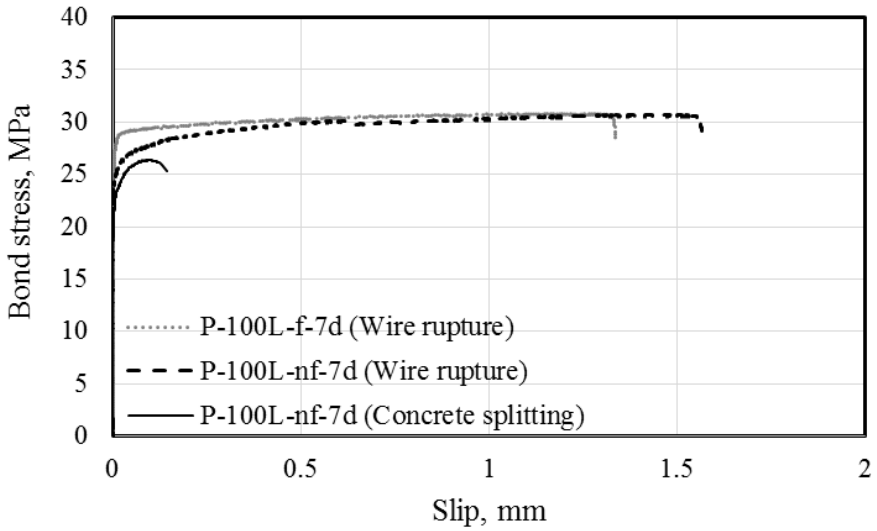

Figure C.2 Pull-out behaviour of the specimens with 100 mm length after 7 days

Pull-out behaviour of the specimens with 125 mm length after 7 days is shown in **Figure C.3**. Both specimens with and without fibre failed by wire rupture. This type of failure showed the sufficiency of the embedment length to provide enough wire anchorage. The specimens with fibre started slipping at higher stress (21.8 MPa) in comparison with the specimens with no fibre. This behaviour confirmed the effect of fibre in controlling slip by providing improved bond between concrete and the steel wire. In the presence of fibre, at about 0.13 mm slip, the steel wire had reached the yielding load that led to rupture. In specimens without fibre, the steel wire ruptured at higher slip (about 0.37 mm). In other words, more slipping took place in the specimens with no fibre.

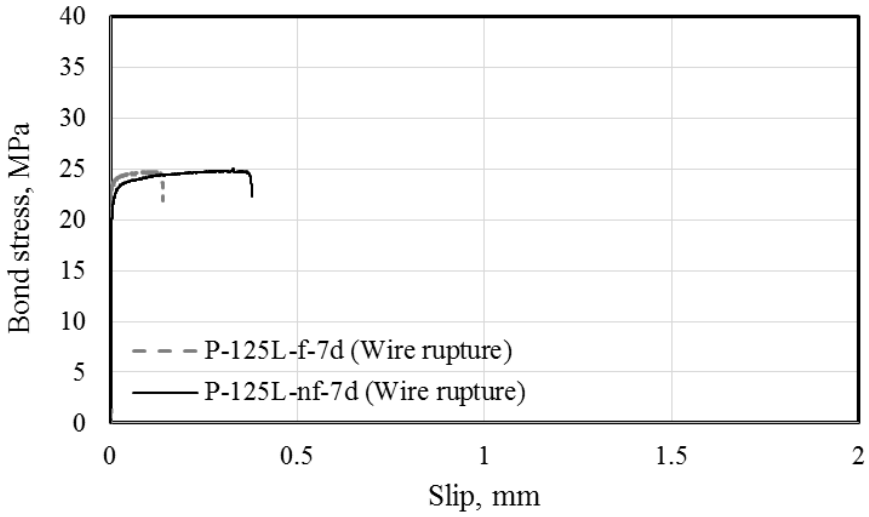

Figure C.3 Pull-out behaviour of the specimens with 125 mm length after 7 days

C.1.3. Pull-out results after 14 days

Figure C.4 presents the behaviour of the specimens with 75 mm length after 14 days under pull-out test. No Slip occurred before 18.2 MPa in both specimens. In the presence of fibre, after slip initiation, bond stress showed a significant increase up to 36.4 MPa (100% enhancement). However, the bond stress for the specimens with no fibre reached only 27.9 MPa before concrete splitting. The results show the positive effect of fibres on controlling the crack propagation and avoiding brittle specimens' failure.

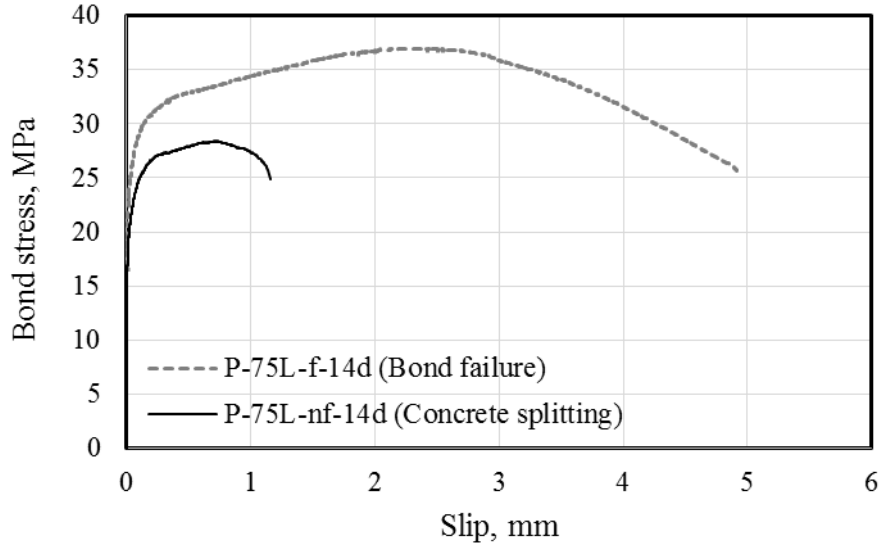

Figure C.4 Pull-out behaviour of the specimens with 75 mm length after 14 days

Pull-out behaviour of the specimens with 100 mm length after 14 days is shown in **Figure C.5**. As mentioned in **Table 5.2**, in 100mm-length specimen with no fibre (P-100L-nf-14d) three different types of failure took place. In two out of three specimens with no fibre,

slip started at about 23.6 MPa. After slip development, one of the specimens experienced bond failure and the other one failed due to wire rupture. These two different behaviours could be due to the slightly different ultimate tensile strength of the wires which led to higher resistance against rupture. In the third specimen with no fibre, slip started at 19.1 MPa and with limited slip, it failed due to the concrete splitting. The 19.1 MPa stress was 19% less than the load of the other no-fibre specimens (23.6 MPa). This behaviour confirms the unpredictability of the no-fibre specimens with 100 mm length. In contrast, for specimens containing fibre just one type of failures was observed. All specimens failed due to the wire rupture.

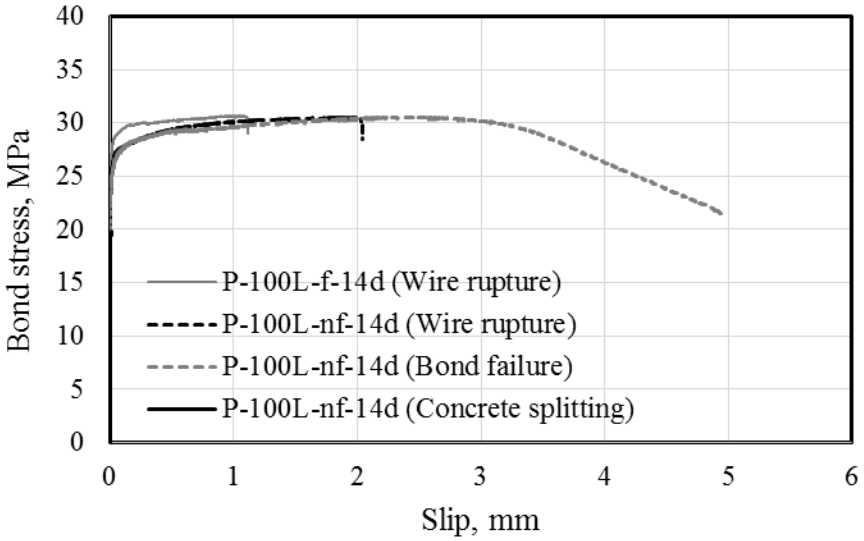

Figure C.5 Pull-out behaviour of the specimens with 100 mm length after 14 days

Figure C.6 presents the pull-out behaviour of the specimens with 125 mm length after 14 days. The specimens with no fibre started slipping earlier, at a lower load, in comparison to the specimens containing fibre. This can be attributed to the effect of fibres in providing improved bond at the steel wire-concrete interface. This also led to the wire reaching its yielding load with less slip. In specimens with no fibre the bond resistance reduced after initial slip, such that more slipping took place before the wire reached yielding load.

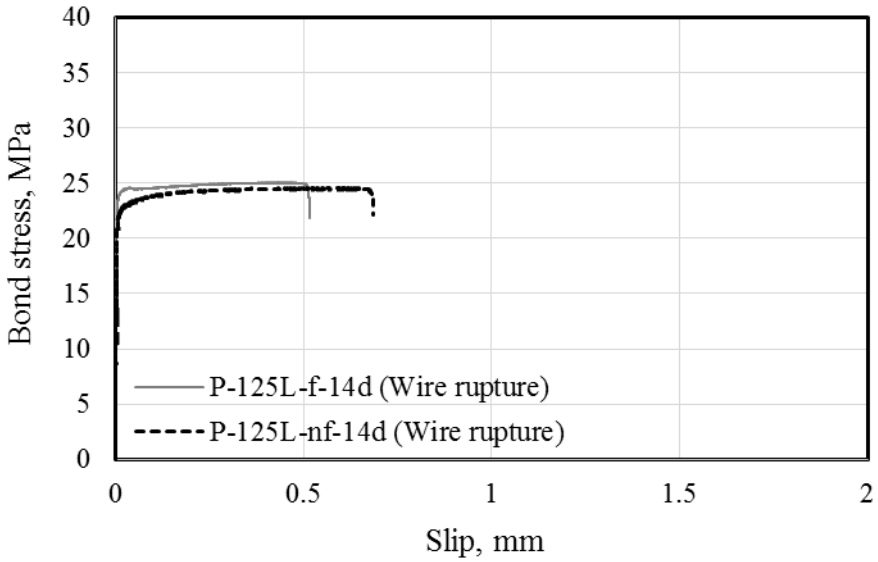

Figure C.6 Pull-out behaviour of the specimens with 125 mm length after 14 days

Figure C.7 compares the pull-out behaviour of specimens with 150 mm length after 14 days. The behaviour was the same as the 125mm-length specimens (see **Figure C.6**). The specimens with no fibre started slipping at a lower load than the ones containing fibre and they also failed after a slipping more than the specimens containing fibre.

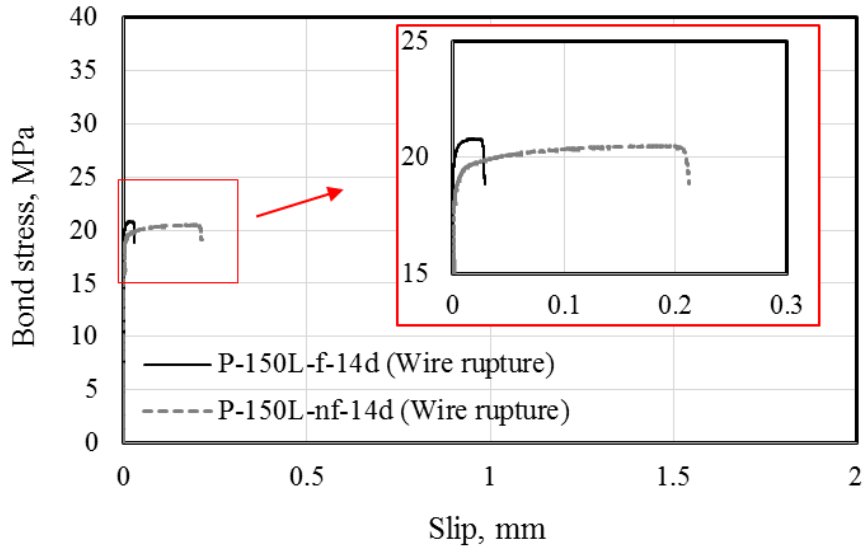

Figure C.7 Pull-out behaviour of the specimens with 150 mm length after 14 days

Figure C.8 presents the14-day specimen failures. In all the 75mm-length specimens with no fibre, failure occurred by the formation of cracks as shown in **Figure C.8.a** while no crack was observed in the specimen with fibre (**Figure C.8.b**), which all failed due to bond failure. In the presence of fibre, increase in the embedment length from 75 mm to 100 mm resulted in a change in the type of the failure to wire rupture (**Figure C.8.b** & **Figure C.8.d**). This trend

was not however observed in the 100 mm-specimens with no fibre (**Figure C.8.c**). Each of these specimens failed differently. E.g. in one specimen that failed due to bond failure, the steel wire was pulled out with a cone of concrete (see the middle specimen in **Figure C.8.c**). By increasing the embedment length of specimens without fibre from 100 mm to 125 mm, the type of failure was changed to wire rupture in all specimens (**Figure C.8.c** and **Figure C.8.e**). This phenomenon was observed at shorter lengths for specimens with fibre (in 100-mm embedment length specimens). Wire rupture was the type of failure in the specimens with 125 mm length, independent of fibre presence (**Figure C.8.e** and **Figure C.8.f**). The difference in the failure behaviour was the formation of a concrete cone at the time of failure. The type of failure that occurred in all the specimens with 150 mm length was wire rupture, independent of fibre presence (**Figure C.8.g** and **Figure C.8.h)**. The main difference between the specimens (with fibre and with no fibre) after the failure was the formation of a concrete cone in P-150L-nf-14d when the wire was pulling out and rupture took place. Formation of a cone of concrete was not observed in P-150L-f-14d.

C.1.4. Pull-out results after 28 days

The behaviours of 150mm length specimens are displayed in **Figure C.9**. As presented in this figure, independent of fibre presence, slipping initiated at about 19.4 MPa. In the specimens with fibre limited slipping (0.008 mm) took place before the steel wire ruptured. However, in the specimens with no fibre the rupture of the wire took place after a more slipping (0.075 mm). This result proves the sufficiency of 150 mm embedment length in order to provide enough steel wire-concrete bond strength at 28 days.

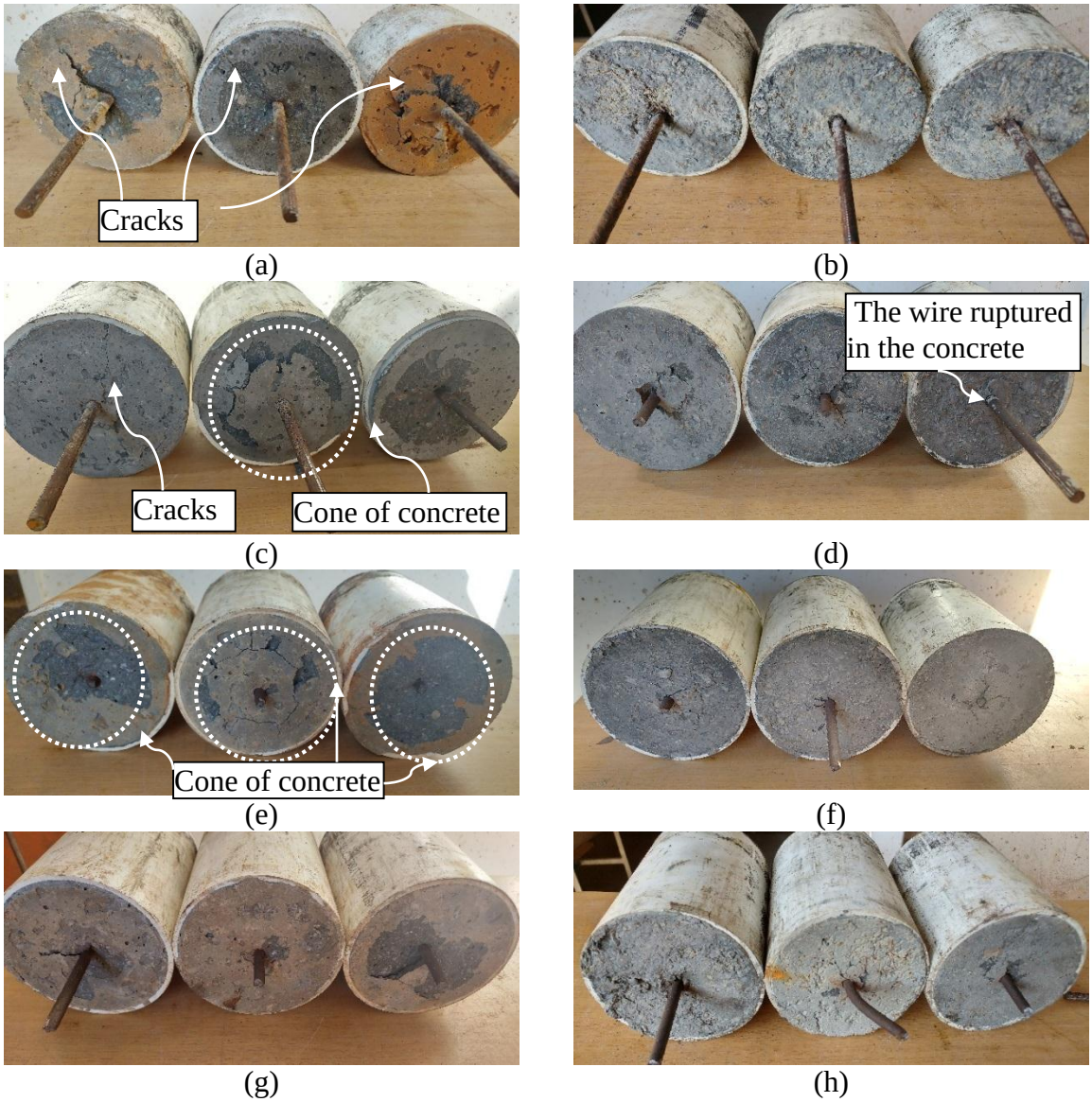

Figure C.8 Specimens after pull-out test after 14-day a) P-75L-nf-14d, b) P-75L-f-14d, c) P-100L-nf-14d, d) P-100L-f-14d, e) P-125L-nf-14d, f) P-125L-f-14d, g) P-150L-nf-14d, h) P-150L-f-14d.

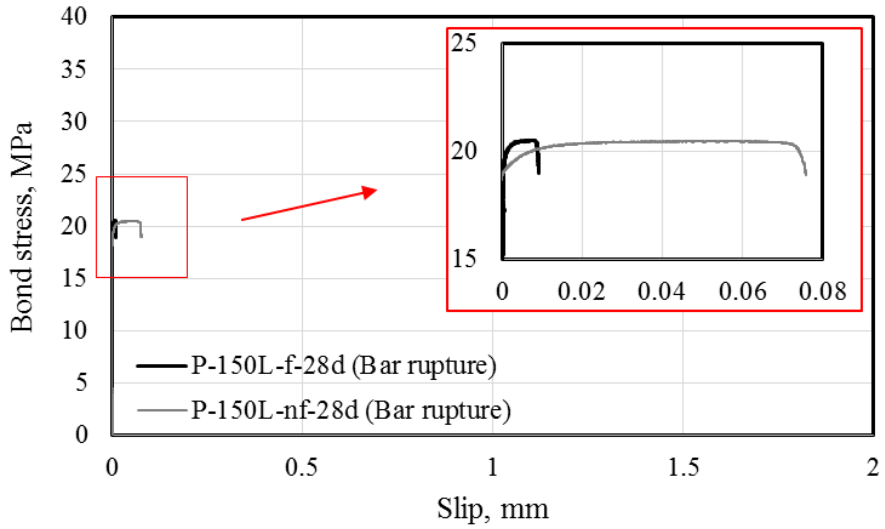

Figure C.9 Pull-out behaviour of the specimens with 150 mm length at 28 days

Figure C.10 shows the failure of 28-day specimens. All the 75 mm-specimens with no fibre **(**Figure C**.10.a**) experienced concrete splitting by the formation of radial cracks due to wedging action. However, in the 75 mm-specimens containing fibre (**Figure C.10.b**), bond failure took place with no visible cracks. Two types of failure occurred in the 100 mm-specimens with no fibre. In one of them, failure occurred due to the formation of cracks (see the left cylinder in **Figure C.10.c**) and the others failed due to the bond failure (see the middle and right cylinders in **Figure C.10.c**).

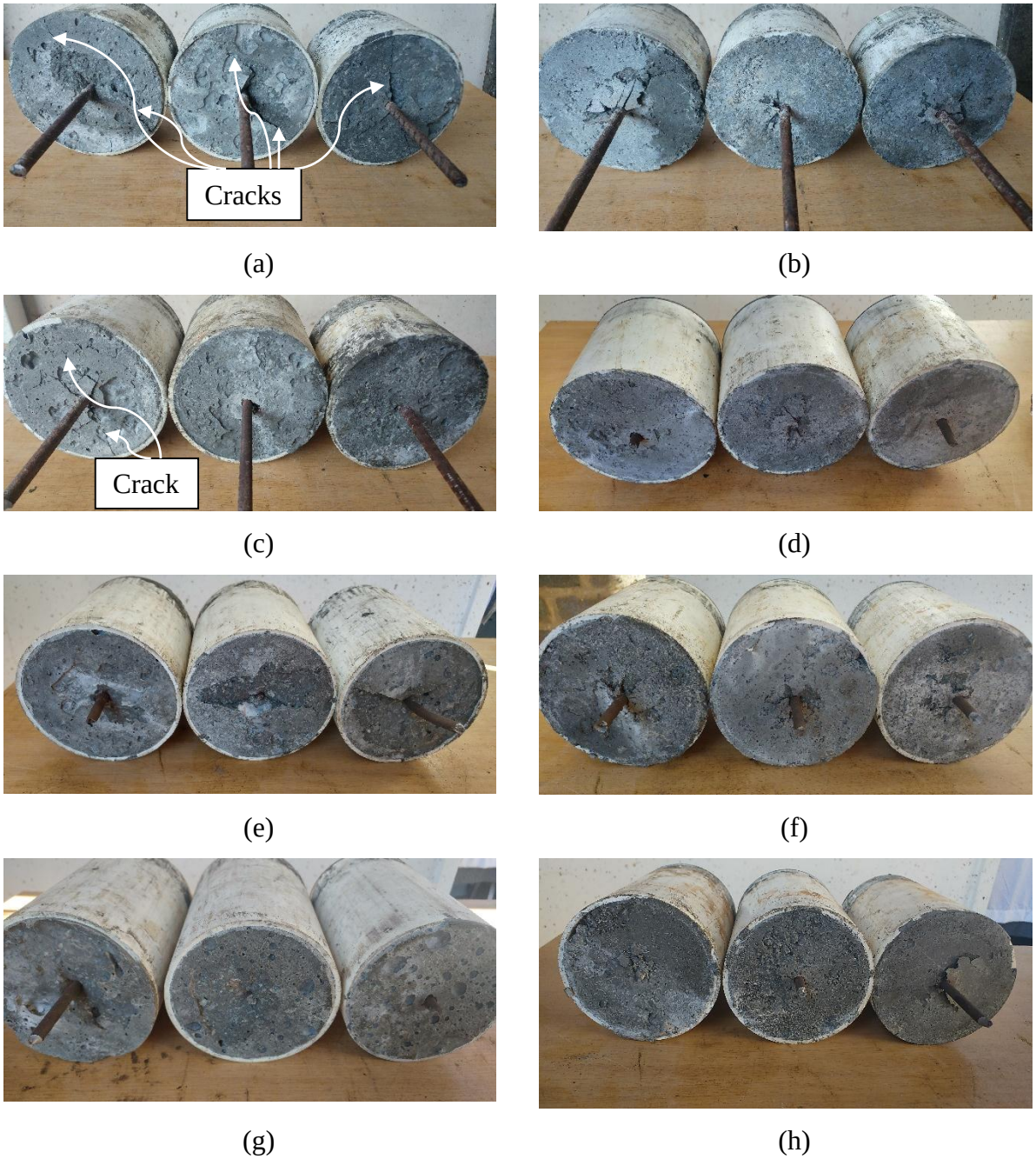

Figure C.10 Specimens after pull-out test at 28-day a) P-75L-nf-28d, b) P-75L-f-28d, c) P-100L-nf-28d, d) P-100L-f-28d, e) P-125L-nf-28d, f) P-125L-f-28d, g) P-150L-nf-28d, h) P-150L-f-28d

All 100 mm-specimens containing fibre, failed due to wire rupture (**Figure C.10.d**). No cracking was observed in these specimens. The specimens with 125 mm and 150 mm length, independent of fibre presence experienced wire rupture (**Figure C.10.e** to **Figure C.10.h**). The only difference was the formation of a concrete cone in some of the specimens with no fibre (**Figure C.10.e**).

C.1.5. Pull-out results after 56 days

Figure C.11 compares the pull-out behaviour of the specimens with 75 mm length after 56 days. No Slipping occurred before 20 MPa in both specimens. In the specimens with no fibre, after the slipping initiated, the sudden formations of cracks led to the complete loss of steel wire-concrete bond. This type of behaviour was not observed in the specimens containing fibre. In these specimens, after the initiation of slipping, the bond was maintained which led to the bond strength enhancement up to 36 MPa. This can be attributed to the presence of fibres at the interface of concrete and the steel wire. After reaching to the maximum capacity of the specimens, they failed due to bond failure.

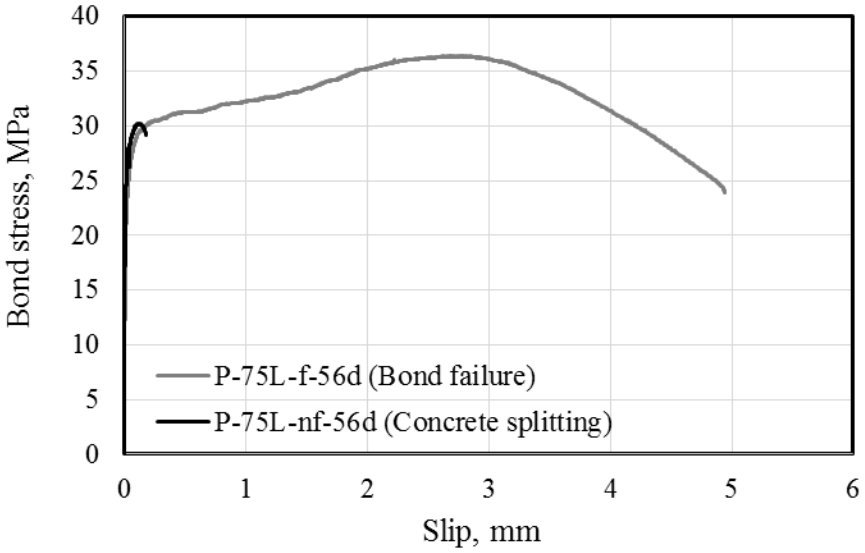

Figure C.11 Pull-out behaviour of the specimens with 75 mm length after 56 days

Figure C.12 displays the results of pull-out test for 100mm-length specimens after 56 days. As shown in this figure, in the specimens containing fibre slipping started at 15 MPa. Then the bond strength continuously increased until the tensile stress in the wire reached the yielding point leading to wire rupture. Two types of failure were observed in the specimen without fibre: concrete splitting and wire rupture. In 2 out of 3 no-fibre specimens, after the

initiation of slipping, the concrete-steel bond was lost due to the concrete splitting. By the inclusion of fibre, UHPFRC exhibited predictable behaviour under pull-out load when the embedment length is 100 mm.

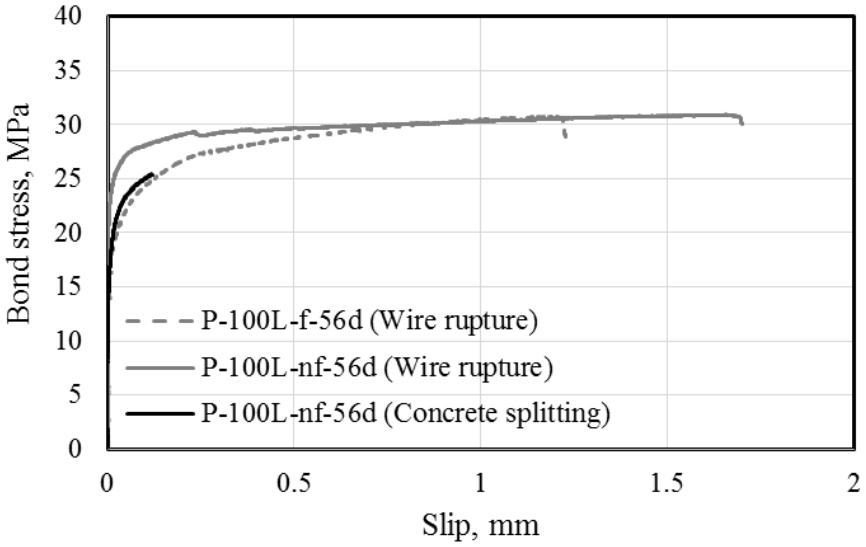

Figure C.12 Pull-out behaviour of the specimens with 100 mm length after 56 days

Pull-out behaviour of the specimens with 125 mm length after 56 days is shown in **Figure C.13.** The specimens with no fibre started sliding earlier at a lower stress in comparison with the specimens with fibre. This is due to the effect of fibres improving bond at the steel wire-concrete interface. This also led to less slipping when the wire reached its yielding stress. In other words, more slipping took place in the specimens with no fibre. In specimens with no fibre, more slipping took place before the wire reached the yielding stress. Both specimens with and without fibre failed by wire rupture. This type of failure showed the sufficiency of the embedment length to provide enough wire anchorage.

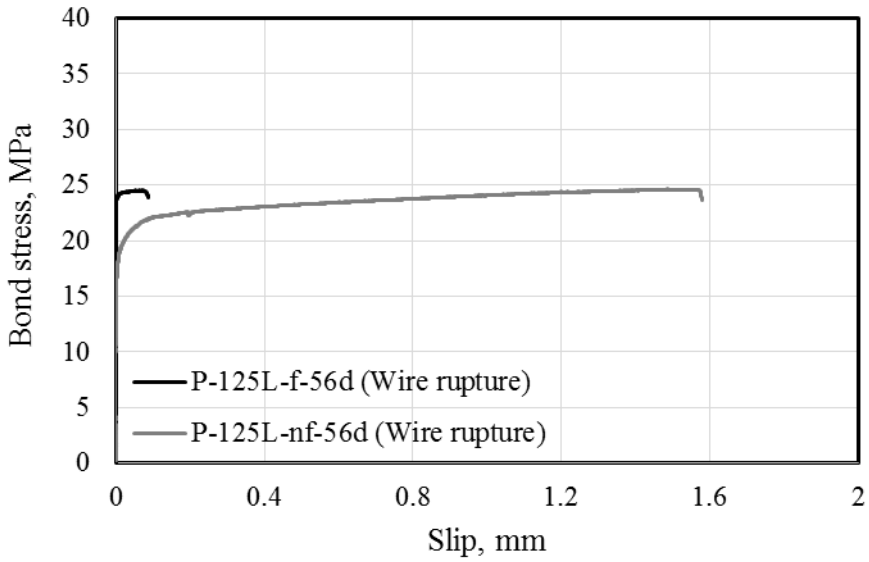

Figure C.13 Pull-out behaviour of the specimens with 125 mm length after 56 days

Figure C.14 displays the results of pull-out tests for 150mm-length after 56 days. As seen in this figure, the specimens with no fibre started slipping at a lower stress than the ones containing fibre (the same as pull-out behaviour of the specimens with 125 mm length (**Figure C.13**)). This confirms the effect of fibres on improving bond at the steel wire-concrete interface. In addition, the presence of fibres helped the steel wire reach yielding load earlier. In the specimens without fibre, the wire ruptured after more slipping occurred in the specimens.

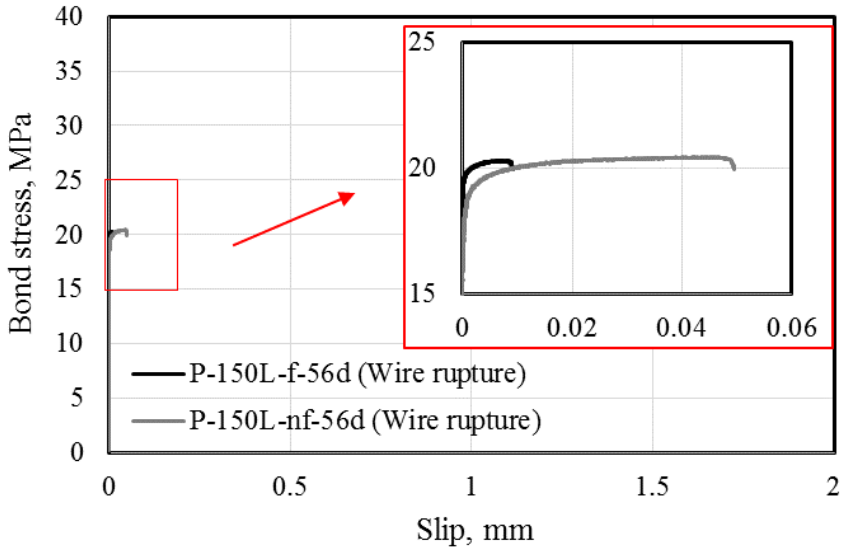

Figure C.14 Pull-out behaviour of the specimens with 150 mm length after 56 days

Figure C.15 presents the 56-day specimen failures. In all the 75mm-length specimens with no fibre, concrete splitting failure occurred by the formation of cracks as shown in **Figure C.15.a**. However, in the 75 mm-specimens containing fibre (**Figure C.15.b**), no crack was observed and all specimen failed due to bond failure. Two types of failure occurred in the 100 mm-specimens with no fibre. In two of them, failure occurred due to the formation of cracks due to wedging action (see the middle and right cylinder in **Figure C.15.c**) and the other one failed due to wire rupture (see the left cylinders in **Figure C.15.c**). All 100 mm-specimens containing fibre, failed due to wire rupture (**Figure C.15.d**). No cracking was observed in these specimens showing that increasing the embedment length from 75 mm to 100 m results in a change in the type of the failure to wire rupture. By increasing the embedment length from 100 mm to 125 mm, all specimens failed due to wire rupture, independent of fibre presence (**Figure C.15.e** & **Figure C.15.f**). This phenomenon was observed at shorter lengths for specimens with fibre (in 100-mm embedment length specimens). The type of failure that occurred in all the specimens with 150 mm length was wire rupture, independent of fibre presence (**Figure C.15.g** & **Figure C.15.h)**.

C.2. PULL-OUT RESULTS AFTER 28 DAYS IN THE SECOND STUDY

Figure C.16 shows pictures of the 28-day specimens after failure. All the 50mm-diameter specimens, both with fibre and without fibre, failed due to bond failure (**Figure C.16.a** & **Figure C.16.b**). The 100mm-diameter specimen with fibre (P-100D-f-28d) failed due to the wire rupture (**Figure C.16.c**) while specimen without fibre had two different types of failure (wire rupture and bond failure) (**Figure C.16.d**).

It can be seen that for the specimens without fibre with bond failure during the pull-out test (**Figure C.16.b** & **Figure C.16.d**), the steel wire was pulled out with a cone of concrete. This confirms that the specimens with no fibre are more prone to concrete damage during the testing, while the specimens containing fibres experienced much less damage due to fibres preventing the specimens from disintegration during the pull-out testing.

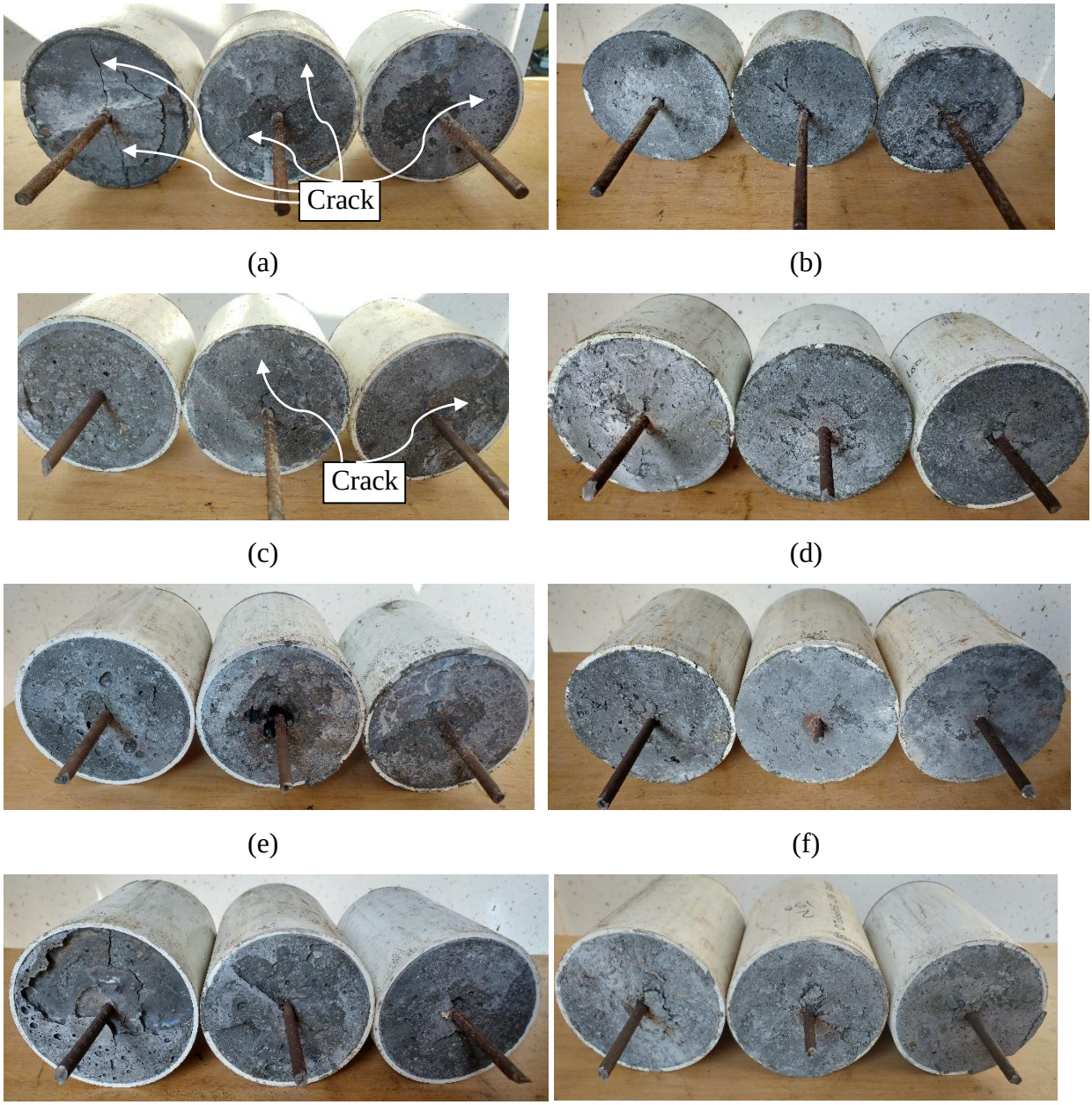

(a) (b)

(c) (d)

(e) (f)

(g) (h)

Figure C.15 Specimens after pull-out test after 56-day a) P-75L-nf-56d, b) P-75L-f-56d, c) P-100L-nf-56d, d) P-100L-f-56d, e) P-125L-nf-56d, f) P-125L-f-56d, g) P-150L-nf-56d, h) P-150L-f-56d

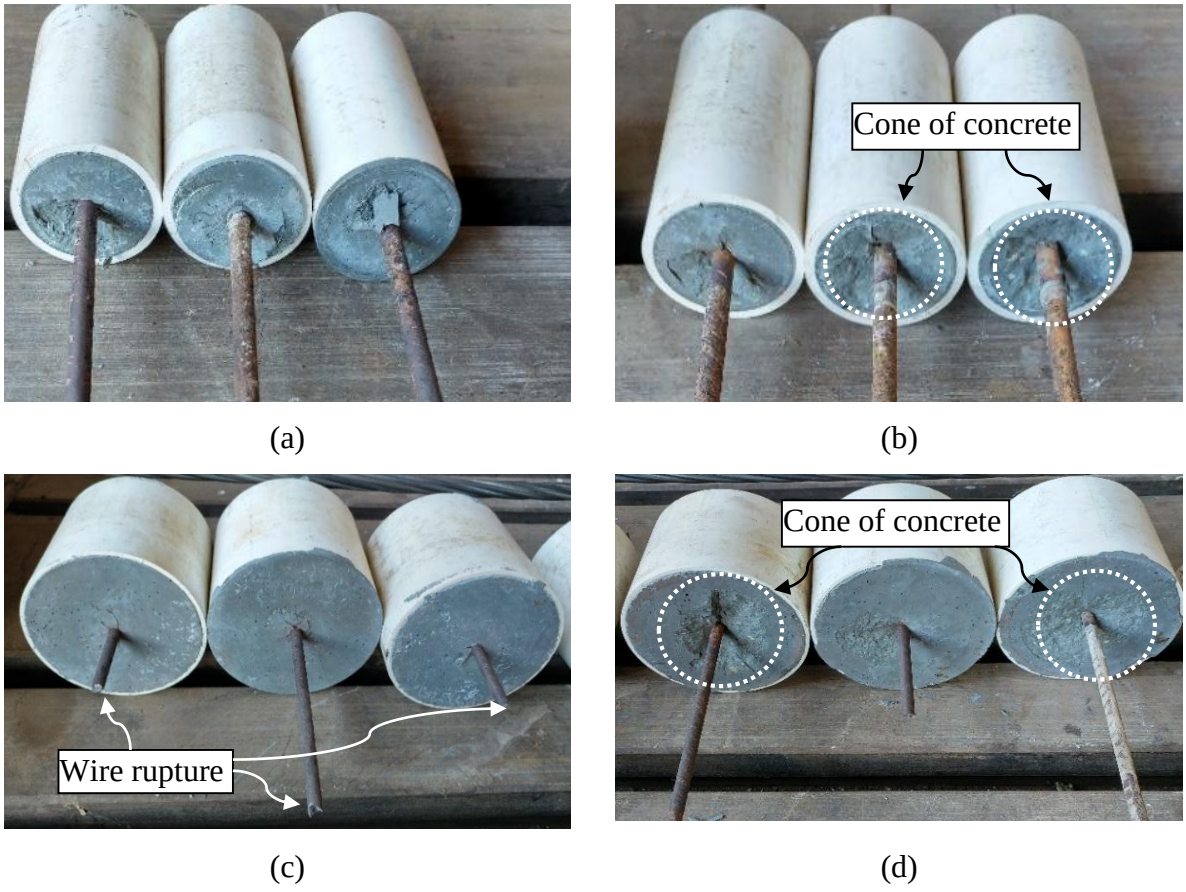

Figure C.16 Type of failure in the specimens with 50 and 100 mm diameter at 28 days, a) P-50D-f-28d, b) P-50D-nf-28d, c) P-100D-f-28d, d) P-100D-nf-28d

APPENDIX D. BEAM DESIGN

The design procedure for the large-scale UHPFRC prestressed beams are covered in this appendix. Firstly, the schematic configuration of the beam (see **Figure D.1**), the initial geometry and the properties required for the beam design (see **Table D.1**) are introduced. Then, the procedure to design a prestressed beam is presented.

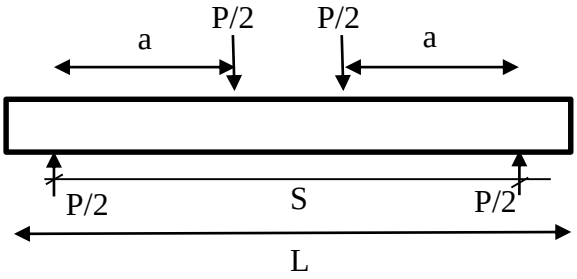

Figure D.1 Schematic sketch of the beam

Table D.1 Loading, initial geometry and material properties

Loading and initial geometry		**Concrete properties**		**Prestressing properties**	
P (kN)	120 ✓	f_c (MPa)	185	D_w (mm)	7
a (m)	1.4 ✓	f_{ci} (MPa)	90	A_w (mm)	38.5
S (m)	3.9	E_{ci} (GPa)	45	f_{pu} (MPa)	1760
L (m)	4.4	E_c (GPa)	54	Pr (%)	75
b (mm)	200	γ (kN/m^3)	25	E_p (GPa)	205

- Calculations

For class 2 members:

Limiting concrete stresses for prestressed members

At transfer	Compression	$f_{ct} = 0.45\, f_{ci} = 40.5$ MPa
	Tension	$f_{tt} = 0.45\sqrt{f_{ci}} = -4.27$ MPa
Serviceability limit state	Compression	$f_{cs} = 0.33\, f_{ci} = 61.05$ MPa
	Tension	$f_{ts} = 0.45\sqrt{f_{ci}} = 6.12$ MPa

Minimum required section properties:

$M_v = \frac{Pa}{2}$ =84 kN.m Eq. (D. 1)

$Z_t \geq \frac{M_v}{(f_{cs} - kf_{tt})}$ = 1303027.401 mm^3 Eq. (D. 2)

$Z_b \geq \frac{M_v}{(kf_{ct} - f_{ts})}$ = 3196427.518 mm^3 Eq. (D. 3)

$Z_{final} = Max\,(Z_b\,, Z_t)$= 3196427.518 mm^3 Eq. (D. 4)

$h = \sqrt{\frac{6\,Z_{final}}{b}}$ = 309.7 mm ➡ h= 400 mm chosen Eq. (D. 5)

Cross-section properties:

A = 51500 mm^2

Y_b = 184.223 mm

Y_t = 215.777 mm

W_D = 1.287 kN/m

M_{max} = 85.958 kN.m

M_{min} = 2.448 kN.m

I = 969681432 mm^4

Z_t = 4493911.699 mm^3

Z_b = 5263619.895 mm^3

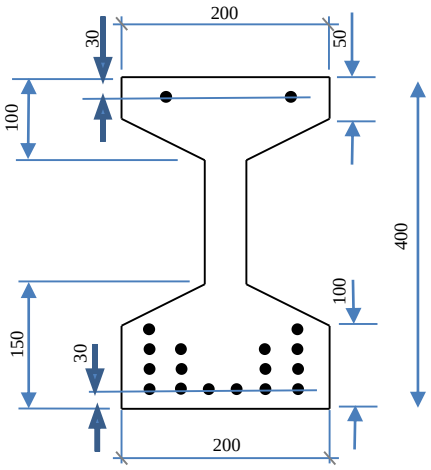

Figure D.2 Cross sectional view of the large-scale UHPFRC prestressed beams

Top wires consideration:

N_{tw}= 2

$P_t = N_{tw} \times Pr \times f_{pu} \times A \times (1 - k)$ = 93.51 kN Eq. (D. 6)

$e_t = Y_t - d'$= 93.51 mm Eq. (D. 7)

d' = 30 mm

Magnel Diagram (see **Figure D.3**):

$\frac{1}{P_0} \geq \frac{k\,(\frac{1}{A} - \frac{e}{Z_t})}{(f_{cs} - \frac{M_{max}}{Z_t} - (\frac{k\,P_t}{A} + \frac{kP_te}{Z_t})}$ Eq. (D. 8)

$\frac{1}{P_0} \leq \frac{k\,(\frac{1}{A} + \frac{e}{Z_b})}{(f_{ts} + \frac{M_{max}}{Z_b} + k(\frac{P_te}{Z_b} - \frac{P_t}{A})}$ Eq. (D. 9)

$\frac{1}{P_0} \geq \frac{(\frac{1}{A} - \frac{e}{Z_t})}{(f_{tt} - \frac{M_{min}}{Z_t} - \left(\frac{P_t}{A} + \frac{P_te}{Z_t}\right))}$ Eq. (D. 10)

$\frac{1}{P_0} \leq \frac{(\frac{1}{A} + \frac{e}{Z_b})}{(f_{ct} + \frac{M_{min}}{Z_b} + (\frac{P_te}{Z_b} - \frac{P_t}{A})}$ Eq. (D. 11)

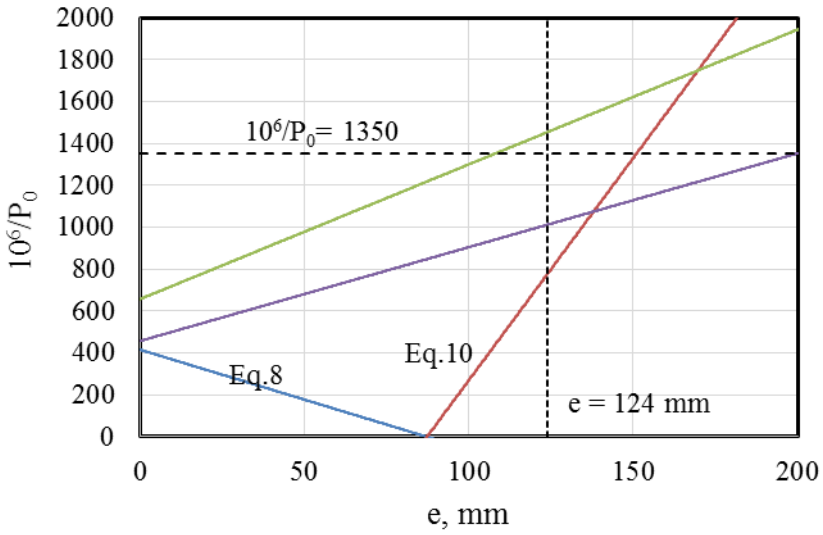

Figure D.3 Magnel diagram

$10^6/P_0 = 1350$ ➡ $P_0 = 740.74$ kN

$$\boldsymbol{P}_{\boldsymbol{per\ wire}} = \boldsymbol{f_{pu}A_w(1-k)} \times \boldsymbol{Pr} = 46.75 \text{ kN} \qquad \text{Eq. (D. 12)}$$

$$\boldsymbol{N_{bw} = 16}$$

$$\boldsymbol{e \leq \frac{Z_t}{A} - \frac{f_{tt}Z_t}{P_0} + \frac{\left(\frac{P_t}{A}+\frac{P_te}{Z_t}\right)Z_t}{P_0} - \frac{M_{min}}{P_0}} \quad \text{at transfer} \quad \boldsymbol{e \leq 148\ mm} \checkmark$$

$$\boldsymbol{e \leq \frac{Z_b}{A} - \frac{f_{ct}Z_b}{P_0} + \frac{\left(\frac{P_te}{Z_b}-\frac{P_t}{A}\right)Z_t}{P_0} - \frac{M_{min}}{P_0}} \quad \text{at transfer} \quad \boldsymbol{e \leq 196\ mm} \checkmark$$

$$\boldsymbol{e \geq \frac{Z_t}{A} - \frac{f_{cs}Z_t}{kP_0} + \frac{\left(\frac{P_t}{A}+\frac{P_te}{Z_t}\right)Z_t}{kP_0} - \frac{M_{max}}{kP_0}} \quad \text{at serviceability} \quad \boldsymbol{e \geq -341\ mm} \checkmark$$

$$\boldsymbol{e \geq \frac{Z_b}{A} - \frac{f_{ts}Z_b}{kP_0} + \frac{\left(\frac{P_te}{Z_b}-\frac{P_t}{A}\right)Z_t}{kP_0} - \frac{M_{max}}{kP_0}} \quad \text{at serviceability} \quad \boldsymbol{e \geq -37\ mm} \checkmark$$

- **Prestressing loss:**

  - Elastic shortening of concrete for bottom wires

Stress in the concrete at the centroid of the steel due to prestressing:

$$\boldsymbol{\sigma_{cp} = \frac{-Pr \times f_{pu} \times N_{bw} \times A_w}{A} + \frac{-Pr \times f_{pu} \times N_{bw} \times A_w \times e^2}{I} + \frac{Pr \times f_{pu} \times N_{tw} \times A_w \times e \times e_t}{I}} \qquad \text{Eq. (D. 13)}$$

Stress in the concrete at the centroid of the steel due to M_{min}: $\frac{M_{min}e}{I}$ Eq. (D. 14)

Loss of prestress due to elastic shortening of the concrete: $\frac{\sigma_{cp}+\frac{M_{min}e}{I}}{\frac{1}{\frac{E_p}{E_{ci}}}-\frac{\sigma_{cp}}{Pr\times f_{pu}}}$ Eq. (D. 15)

- Elastic shortening of concrete for top wires

Stress in the concrete at the centroid of the steel due to prestressing:

$$\boldsymbol{\sigma_{cp}} = \frac{-Pr\times f_{pu}\times N_{tw}\times A_w}{A} + \frac{-Pr\times f_{pu}\times N_{tw}\times A_w\times e_t^2}{I} + \frac{Pr\times f_{pu}\times N_{bw}\times A_w\times e_t\times e}{I}$$ Eq. (D. 16)

Stress in the concrete at the centroid of the steel due to M_{min}: $\frac{M_{min}e_t}{I}$ Eq. (D. 17)

Loss of prestress due to elastic shortening of the concrete: $\frac{\sigma_{cp}+\frac{M_{min}e_t}{I}}{\frac{1}{\frac{E_p}{E_{ci}}}-\frac{\sigma_{cp}}{Pr\times f_{pu}}}$ Eq. (D. 18)

- **Relaxation of steel wires**

With the assumption of the creep plus shrinkage strain less than $500e^{-6}$: 5.8%

- **Shrinkage of concrete**

Shrinkage strain for a relative humidity of 60%: $310e^{-6}$

- **Creep of the concrete**

Maximum compression in the concrete at transfer ($f_{c,max}$): $\frac{-Pr\times f_{pu}\times N_{bw}\times A_w}{A} + \frac{-Pr\times f_{pu}\times N_{bw}\times A_w\times e}{Z_{bot}} + \frac{Pr\times f_{pu}\times N_{tw}\times A_w\times e_t}{Z_{bot}} + \frac{M_{min}}{Z_{bot}}$ Eq. (D. 19)

$f_{c,max}/ f_{ci} < 0.3$ ➡ Creep strain = $48 \times 10^{-6} \times \frac{40}{|f_{ci}|}$

Table D.2 Total loss of prestress

	Elastic shortening		Relaxation of wires	Shrinkage of concrete	Creep of concrete
	Top wires	Bottom wires			
Prestress loss (MPa)	64.14	-108.41	-50.05	-63.55	-114.89

$k_b = \frac{Pr\times f_{pu} - Total\ prestress\ loss\ in\ bottom\ wires}{Pr\times f_{pu}}$ Eq. (D. 20)

$k_t = \frac{\boldsymbol{Pr}\times f_{pu} - Total\ prestress\ loss\ in\ top\ wires}{\boldsymbol{Pr}\times f_{pu}}$ Eq. (D. 21)

$k_b = 0.83$, $k_t = 0.91$

- **Deflection**

$$\boldsymbol{\delta_t} = \frac{\boldsymbol{5W_D L^4}}{\boldsymbol{384E_{ci}I}} - \frac{\boldsymbol{PeL^2}}{\boldsymbol{8E_{ci}I}} + \frac{\boldsymbol{P_t e_t L^2}}{\boldsymbol{8E_{ci}I}} \quad \text{Eq. (D. 22)}$$

$$\boldsymbol{\delta_L} = \frac{{}^{\boldsymbol{P}}/_{\boldsymbol{2}}\times \boldsymbol{aL^2}(\boldsymbol{3-4}\left(\frac{\boldsymbol{a}}{\boldsymbol{L}}\right)^{\boldsymbol{2}})}{\boldsymbol{24E_cI}} \quad \text{Eq. (D. 23)}$$

$$\boldsymbol{\delta_p} = -\frac{\boldsymbol{k_b PeL^2}}{\boldsymbol{8E_cI}} + \frac{\boldsymbol{k_t P_t e_t L^2}}{\boldsymbol{8E_cI}} \quad \text{Eq. (D. 24)}$$

δ_t= -3.99 mm, δ_L = 3.36 mm, δ_p = -2.80 mm

- **Stress calculation**

$$\boldsymbol{\sigma_{top}} = \frac{\boldsymbol{k_b P_0}}{\boldsymbol{A}} + \frac{\boldsymbol{k_t P_t}}{\boldsymbol{A}} - \frac{\boldsymbol{k_b P_0 e}}{\boldsymbol{Z_t}} + \frac{\boldsymbol{k_t P_t e_t}}{\boldsymbol{Z_t}} + \frac{\boldsymbol{Pa}}{\boldsymbol{2Z_t}} \quad \text{Eq. (D. 25)}$$

$$\boldsymbol{\sigma_{bot}} = \frac{\boldsymbol{k_b P_0}}{\boldsymbol{A}} + \frac{\boldsymbol{k_t P_t}}{\boldsymbol{A}} + \frac{\boldsymbol{k_b P_0 e}}{\boldsymbol{Z_t}} - \frac{\boldsymbol{k_t P_t e_t}}{\boldsymbol{Z_t}} - \frac{\boldsymbol{Pa}}{\boldsymbol{2Z_t}} \quad \text{Eq. (D. 26)}$$

$$\boldsymbol{\sigma_{bw1}} = \boldsymbol{Pr}\times \boldsymbol{f_{pu}}(\boldsymbol{1-k_b}) + \frac{\boldsymbol{P_0(Y_b - d')a}}{\boldsymbol{2I}} \quad \text{Eq. (D. 27)}$$

$$\boldsymbol{\sigma_{bw2}} = \boldsymbol{Pr}\times \boldsymbol{f_{pu}}(\boldsymbol{1-k_b}) + \frac{\boldsymbol{P_0(Y_b - d' - 27)a}}{\boldsymbol{2I}} \quad \text{Eq. (D. 28)}$$

$$\boldsymbol{\sigma_{bw3}} = \boldsymbol{Pr}\times \boldsymbol{f_{pu}}(\boldsymbol{1-k_b}) + \frac{\boldsymbol{P_0(Y_b - d' - 2\times 27)a}}{\boldsymbol{2I}} \quad \text{Eq. (D. 29)}$$

$$\boldsymbol{\sigma_{bw4}} = \boldsymbol{Pr}\times \boldsymbol{f_{pu}}(\boldsymbol{1-k_b}) + \frac{\boldsymbol{P_0(Y_b - d' - 3\times 27)a}}{\boldsymbol{2I}} \quad \text{Eq. (D. 30)}$$

Table D.3 Calculation of stress in concrete and prestressing wires

$P_{Loading}$ (kN)	Stress in concrete (MPa)		Strain in concrete (x 10^6)		Stress in prestressing wires (MPa)			
	σ_{top}	σ_{bot}	ε_{top}	ε_{bot}	σ_{bw1}	σ_{bw2}	σ_{bw3}	σ_{bw4}
0	-0.366	25.236	-67.702	4673.410	1214.400	1214.400	1214.400	1214.400
10	1.192	23.907	220.755	4427.130	1215.477	1215.282	1215.087	1214.892
20	2.750	22.577	509.211	4180.860	1216.554	1216.165	1215.775	1215.385
30	4.307	21.247	797.667	3934.580	1217.632	1217.047	1216.462	1215.877
40	5.865	19.917	1086.120	3688.310	1218.709	1217.929	1217.150	1216.370
50	7.423	18.587	1374.580	3442.030	1219.786	1218.812	1217.837	1216.862
60	8.980	17.257	1663.040	3195.760	1220.863	1219.694	1218.524	1217.355
70	10.538	15.927	1951.490	2949.480	1221.941	1220.576	1219.212	1217.847
80	12.096	14.597	2239.950	2703.210	1223.018	1221.459	1219.899	1218.340
90	13.653	13.267	2528.400	2456.930	1224.095	1222.341	1220.587	1218.832
100	15.211	11.938	2816.860	2210.660	1225.172	1223.223	1221.274	1219.325
110	16.769	10.608	3105.320	1964.380	1226.249	1224.105	1221.961	1219.817
120	18.326	9.278	3393.770	1718.110	1227.327	1224.988	1222.649	1220.310
130	19.884	7.948	3682.230	1471.830	1228.404	1225.870	1223.336	1220.802
140	21.442	6.618	3970.680	1225.560	1229.481	1226.752	1224.024	1221.295
150	22.999	5.288	4259.140	979.285	1230.558	1227.635	1224.711	1221.787
160	24.557	3.958	4547.600	733.010	1231.636	1228.517	1225.398	1222.280
170	26.115	2.628	4836.050	486.736	1232.713	1229.399	1226.086	1222.772
180	27.672	1.298	5124.510	240.461	1233.790	1230.282	1226.773	1223.265
190	29.230	-0.031	5412.960	-5.814	1234.867	1231.164	1227.461	1223.757